MATHEMATICAL MODELING AND CONTROL OF MALARIA TRANSMISSION DYNAMICS INCORPORATING VACCINATION, ASYMPTOMATIC CARRIERS, TREATMENT, AND MEDIA AWARENESS

Andualem Tekle Haringo

A Ph.D Dissertation Submitted to the Department of Applied Mathematics,
College of Applied Natural Science

Presented in Partial Fulfillment of the Requirement for the Degree of Doctor of Philosophy in Applied Mathematics

School of Graduate Studies
Adama Science and Technology University

December, 2025
Adama, Ethiopia

Mathematical Modeling and Control of Malaria Transmission Dynamics Incorporating Vaccination, Asymptomatic Carriers, Treatment, and Media Awareness

Andualem Tekle Haringo
Supervisor: Dr. Legesse Lemecha Obsu (PhD)
Co-Supervisor: Dr. Feyissa Kebede Bushu (PhD)

A Dissertation Submitted to the Department of Applied Mathematics
College of Applied Natural Science

Presented in Partial Fulfillment of the Requirement for the Degree of Doctor of Philosophy in Applied Mathematics

School of Graduate Studies
Adama Science and Technology University

December, 2025
Adama, Ethiopia

APPROVAL PAGE

We hereby certify that the recommendations and suggestions made by the board of examiners are appropriately incorporated into the final version of the dissertation entitled "**Mathematical modeling and control of malaria transmission dynamics incorporating vaccination, asymptomatic carriers, treatment, and media awareness**" by **Andualem Tekle Haringo**.

Supervisor	Signature	Date
Co-Supervisor	Signature	Date

We, the undersigned, members of the Board of Examiners of the dissertation open defense by **Andualem Tekle Haringo** have read and evaluated the dissertation entitled "**Mathematical modeling and control of malaria transmission dynamics incorporating vaccination, asymptomatic carriers, treatment, and media awareness**" and examined the candidate during open defense. This is, therefore, to certify that the dissertation is accepted for partial fulfillment of the requirement of the degree of Doctor of Philosophy in Applied Mathematics.

Chairperson	Signature	Date
External Examiner 1	Signature	Date
External Examiner 2	Signature	Date
Internal Examiner 1	Signature	Date
Internal Examiner 2	Signature	Date

Finally, approval and acceptance of the dissertation is contingent upon submission of its final copy to the Office of Postgraduate Studies (OPGS) through the candidate ' s Department Graduate Council (DGC) and School Graduate Committee (SGC).

Department Head	Signature	Date
College Dean	Signature	Date
School of Postgraduate Studies, Dean	Signature	Date

DECLARATION

I hereby declare that this Dissertation entitled "**Mathematical modeling and control of malaria transmission dynamics incorporating vaccination, asymptomatic carriers, treatment, and media awareness**" is my original work. That is, it has not been submitted for the award of any academic degree, diploma or certificate in any other university. All sources of materials used for this dissertation have been duly acknowledged through appropriate citations.

Name	Signature	Date

RECOMMENDATION OF SUPERVISORS

We, the supervisors of this dissertation, hereby certify that we have read and revised the dissertation entitled "**Mathematical modeling and control of malaria transmission dynamics incorporating vaccination, asymptomatic carriers, treatment, and media awareness**" prepared under our guidance by **Andualem Tekle Haringo** submitted in partial fulfillment of the requirements for the degree of Doctor of Philosophy in Applied Mathematics. Therefore, we recommend the submission of the dissertation to the department for further review and defense.

Supervisor	Signature	Date
Co-Supervisor	Signature	Date

ACKNOWLEDGMENTS

I am deeply grateful to God for His mercy through Jesus Christ, guidance, strength, and inspiration throughout my journey. His presence has been a constant source of comfort and motivation.

Special thanks goes to my supervisor, Dr. Legesse Lemecha Obsu, for his dedicated support, insightful guidance, and invaluable encouragement throughout my dissertation journey. His commitment and understanding, particularly during periods of personal challenges, were unforgettable and instrumental in the successful completion of this study. I am grateful to my co-supervisor, Dr. Feyissa Kebede Bushu, for his constructive feedback and valuable insights during the review of my articles, which contributed to the successful organization of this dissertation.

I am thankful to Adama Science and Technology University and Bonga University for their support and commitment in facilitating the Ph.D. program.

I also extend my heartfelt gratitude goes to my wife, Sosina Wondimu, and our children, Afomia Andualem and Efrata Andualem, whose love, support, and encouragement have been my greatest source of strength.

Finally, and most importantly, I extend my sincere gratitude to my family: my father, mother, brothers, sisters as well as my friends and colleagues for their prayer, moral encouragement, constructive ideas, and material support throughout my academic journey.

TABLE OF CONTENTS

List of Tables

List of Figures

ABBREVIATIONS AND ACRONYMS

ACER	Average cost-effectiveness ratio
ICER	Incremental Cost-Effectiveness Ratio
COVID-19	Coronavirus Disease
EPHI	Ethiopian Public Health Institute
GAVI	Global Alliance for Vaccines and Immunization
GDP	Gross Domestic Product
ITN	Insecticide-Treated Net
IRS	Indoor Residual Spraying
LLITNs	Long Lasting Insecticide Treated Nets
ODEs	Ordinary Differential Equations
RTS,S	RTS,S/AS01 Malaria Vaccine
R21	R21/Matrix-M malaria vaccine
UNICEF	United Nations Children's Fund
WHO	World Health Organization

ABSTRACT

Malaria remains a significant global health concern with severe socioeconomic implications particularly in endemic regions. A comprehensive understanding of malaria transmission dynamics is essential for designing effective control strategies, improving prevention, and supporting eradication efforts. This dissertation develops and analyzes a set of novel, data-driven mathematical models to evaluate malaria interventions, integrating optimal control analysis and cost-effectiveness assessments. For each model, key mathematical properties such as positivity, boundedness, and the existence and stability of equilibria are established. Parameter estimation and curve fitting were performed using Ethiopian malaria incidence data, and numerical simulations were conducted to support the analytical findings. Sensitivity analysis further identified the parameters with the greatest influence on transmission. The first model inventively examines the role of media-driven awareness in promoting insecticide utilization alongside treatment interventions. Results conclude that combining awareness-based mosquito control with effective treatment significantly enhances the potential for malaria elimination. The second model evaluates personal protection, expanded treatment capacity, and mosquito breeding site destruction. The findings confirm that the implementation of any single strategy, or a combination of strategies, yields substantial impact. In addition, qualitative insights from the cost-effectiveness analysis suggest that integrating optimal combination of personal protective measures and mosquito breeding site destruction is the most economically efficient approach, maximizing effectiveness while optimizing resource use. The third model emphasizes the contribution of asymptomatic infections, showing that they account for nearly 30 percent of total malaria cases and play a major role in sustaining transmission. The fourth model introduces age-structured vaccination strategies within human–mosquito interactions. Both analytical and numerical results demonstrate that integrating vaccination, treatment, and insecticide-based mosquito control can reduce malaria transmission to near zero, with potential for complete eradication. In conclusion, integrating enhanced malaria treatment, awareness-based mosquito control, childhood vaccination, and effective management of asymptomatic cases can substantially reduce malaria transmission. These findings provide valuable insights for policymakers in Ethiopia and other malaria-endemic regions, informing to the design of more effective control strategies and guiding efforts toward eventual eradication.

KEY WORDS: Mathematical modeling, Media awareness, Transmission dynamics, Control strategies, Asymptomatic infection, Age-structured vaccination, Treatment intervention, Cost-effectiveness analysis, Bifurcation analysis

CHAPTER 1

INTRODUCTION

This chapter offers important background information on malaria infection. Also, it defines the research problem, outlines the objectives of the study, underscores significance, and specifies delimitation of the study which indicates scope and boundaries of the dissertation. Finally, the chapter presents the organization of the dissertation, offering a concise overview of the contents and focus of the subsequent chapters.

1.1 Background

Malaria is one of the oldest known infectious diseases, with a history spanning thousands of years (Jones, 1907). The term ”malaria” originated from Medieval Italian ”mal aria” meaning ”bad air,” as the disease was initially associated with swamps and marshland (Jarcho, 1970). It is a severe and potentially fatal infection caused by protozoan parasites of the *Plasmodium genus*, primarily transmitted by the bites of infected female *Anopheles* mosquitoes. There are five distinct species of *Plasmodium* responsible for causing malaria: *P. falciparum* (the most deadly), *P. vivax*, *P. ovale*, *P. malariae*, and *P. knowlesi* (Sabbatani et al., 2010)

Malaria continues a serious public health challenge in tropical and subtropical regions, with notable social, economic, and health impacts. It ranks as the fifth deadliest infectious disease, following respiratory infections, HIV/AIDS, diarrheal diseases, and tuberculosis (Pierre-Louis et al., 2010). The data from the WHO reveal that around 2.2 billion cases of malaria and 12.7 million deaths have been averted since 2000, but the disease remains a serious global health threat, particularly in the WHO African Region (Adepoju, 2024). According to WHO’s latest World malaria report, there were an estimated 263 million cases and 597 000 malaria deaths worldwide in 2023. This represents about 11 million more cases in 2023 compared to 2022, and nearly the same number of deaths. As highlighted in this report, the WHO African Region accounted for approximately 94% of all malaria cases and 95% of related deaths. In 2023, children under the age of five represented about 76% of all malaria deaths compared with 91% in 2000 (WHO, 2023b). Moreover, a United Nations Children’s Fund (UNICEF) report reveals that nearly one child under five dies of malaria every minute, resulting in a daily toll of over 1,000 fatalities (Badmos et al., 2021; UNICEF, 2024). Additionally, more than 12.7 million pregnancies in the WHO African region are exposed to malaria, leading to fetal loss, low birth weights, and various complications (Mukala et al., 2024).

The economic impact of malaria is considerably important. In countries with endemic malaria, the annual loss of economic growth is estimated to be as high as 1.3% per year, with an estimated US$12 billion of productivity lost in Africa (Samba, 2001). Moreover, an analysis of data from 180 countries between 2000 and 2017 showed that each 10% reduction in malaria incidence was associated with an average rise of 0.3% in per capita gross domestic product (GDP) growth and a 0.11 percentage point faster per annum capita GDP growth (Sarma et al., 2019). Further, the WHO reported in (WHO, 2020b) that the economic impact of malaria disproportionately affects the poor and the cost of treatment for a single case of severe malaria can impose severe financial challenges for a family.

Ethiopia is one of the countries in Sub-Sahara Africa (SSA). In this country, among the four species that infect humans, *P. falciparum* and *P. vivax* are the most dominant malaria parasites. *P. falciparum* accounts for approximately 65-75% of total reported malaria cases (WHO, 2024a). In the country, malaria poses a significant public health challenge covering around 75% of the country's landmass, and around 69% of the population residing in these areas facing the risk of infection where periodic outbreaks contribute more than 20% of deaths among children under the age of five. Over 7.3 million malaria cases and 1157 deaths were reported in Ethiopia, the highest number of annual cases recorded in the last seven years WHO et al. (n.d.). Notably, of the total cases reported in 2024, majority 95% were laboratory-confirmed, with P. falciparum accounting for more than two-thirds of the cases. By contrast, in 2023, 4.1 million malaria cases including 527 deaths were reported, of which P. falciparum accounted for approximately 70% of all reported cases. Also, reports indicate that more than 7.03% of pregnant women in Ethiopia are affected by asymptomatic malaria infections (Kassie et al., 2024). In year 2020, Ethiopia comprised on average two malaria cases per house holds with a prevalence of 32%. The average annual income of households was US$626.7. The mean annual cost of malaria illness to households was US$16, and most of this cost 78% was contributed by the indirect costs. In every household, on average, patients and companions or caregivers lost 3.4 productive workdays due to malaria illness (Tefera et al., 2020).

1.1.1 The malaria parasite life cycle

The life cycle of the malaria parasite, primarily Plasmodium species, involves complex interactions between the parasite and its hosts, which include humans and female *Anopheles* mosquitoes. The report by WHO (2022a) indicates that malaria infection starts when an infected female *Anopheles* mosquito bites and injects *P. parasites* as sporozoites into the human bloodstream (1) as depicted in Figure (1.1).

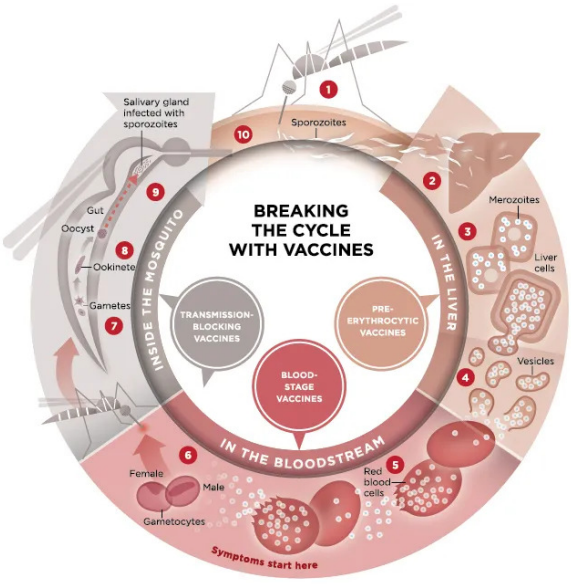

Figure 1.1: Brief malaria life cycle adopted from WHO (2022a).

The incubation period of malaria appears to vary according to the type of parasites. For instance, in non-immune individuals, the incubation period for P. falciparum infection until the appearance of symptoms generally lasts between 8 and 14 days. For those with some level of immunity, this period may be prolonged (WHO, 2022b). It is also detailed in the report that the most common symptoms of malaria infection includes: fever, headache, chills, nausea and vomiting. In more severe case the symptoms are very high fever, severe headache generalized convulsion, kidney failure, seizures, delirium, impaired consciousness and coma. Severe malaria occurs when the parasite affects important organs or parts of the body and may possibly leading to death. Malaria is a preventable and curable disease. The high-risk groups include young children, pregnant women, and non-immune travelers to malarious regions

The prevalence of malaria is intensifying in Sub-Saharan African countries, resulting in elevated morbidity and mortality rates. This trend significantly affects both health outcomes and economic systems in the region (Adugna et al., 2022). In these endemic areas, malaria parasite transmission occurs throughout the year with seasonal increases primarily influenced by rainfall patterns. In particular, the report given in WHO (2022b) shows that the intensity of malaria transmission generally varies as a function of parasite prevalence in the human population and the feeding habits, density, and survival rates of the mosquitoes. These in turn are strongly influenced by temperature and humidity, mosquito species composition and mosquito control measures. Because variations in ecological, climatic, and mosquito control factors influence the abundance of mosquito breeding sites and the survival of mosquitoes. According to this

report, the efficiency of the mosquito in transmitting malaria from one person to another, poor housing conditions resulting in increased exposure to mosquito bites, and weak health systems with limited access to quality prevention and treatment services are among the major factors contributing to the burden of malaria in sub-Saharan Africa.

1.2 Malaria prevention and control strategies

Malaria management utilizes integrated interventions against the parasite and vector. Prevention aims to interrupt transmission and minimize bites, while control focuses on drug treatment, and mosquito control to reduce morbidity and mortality.

1.2.1 Mosquito control

mosquito control is a vital component of malaria control and its elimination strategies (WHO, 2015). Since malaria is transmitted by *Anopheles* mosquitoes, mosquito control aims to reduce mosquito density and transmission capacity. This intervention either eliminates mosquitoes or reduces their survival, thereby disrupting transmission (Smith Gueye et al., 2016). Various mosquito control tools target reducing different life stages of mosquitoes, representing the most scalable strategy to disrupt transmission (WHO, 2015). The primary interventions include long-lasting insecticidal nets (LLINs), indoor residual spraying (IRS), larval source management (LSM), and integrated mosquito management (IVM) (Fillinger & Lindsay, 2011). A study by Lengeler (2004) revealed that insecticide-treated nets (ITNs) decrease the risk of uncomplicated malaria by 50% and unstable malaria by 62% in regions with moderate to high transmission. Additionally, ITNs have been shown to reduce the incidence of severe malaria by 45%. The findings indicate that the use of ITNs could prevent approximately 5.5 out of every 1,000 children from being saved from malaria each year, highlighting their crucial role in malaria control efforts (Lengeler, 2004). However, ITNs offer protection only when individuals sleep under the nets, and their effectiveness is depends upon proper adherence. ITNs do not protect against outdoor mosquito bites and typically require re-treatment every 6 to 12 months following washing. In comparison, LLINs demonstrate greater efficacy, remaining effective for up to 3 years without the need for retreatment, even after washing (CDC, 2024b).

Furthermore, IRS is another effective mosquito control strategy. It involves applying insecticides to walls and ceilings to kill mosquitoes that come into contact with treated surfaces (Irish et al., 2024). Hemingway et al. (2016) demonstrated that IRS reduced the risk of clinical malaria by 31% and severe malaria by 38% in regions with moderate to high transmission areas. However, IRS is often costly and logistically challenging to implement, and its effectiveness is reduced in the presence of insecticide resistance (WHO, 2013). Both ITNs and IRS

interventions are particularly effective against indoor biting and resting mosquitoes and can be supplemented with larval source management (LSM), which targets larvae before they mature into adult mosquitoes (WHO, 2015). Additional mosquito control strategies encompass house screening, space and swarm spraying, attractive sugar baits, auto-dissemination of larvicides, and the use of genetically modified mosquitoes. These combined approaches enhance the overall effectiveness of mosquito control efforts (Bonds et al., 2018; Marcombe et al., 2020; Sabet & Goddard, 2022; Zembere, 2024). However, insufficient use of insecticides as the result of low community knowledge poses a significant threat to mosquito control progress. Addressing these challenges is essential for enhancing the efficacy of malaria mosquito control strategies.

1.2.2 Drug treatment interventions

Malaria is a preventable and treatable disease (Basu & Sahi, 2017). The main goal of malaria treatment is to quickly and completely eliminate *P. parasites* from the bloodstream, curing the infection and preventing uncomplicated malaria from progressing to severe disease or death. Effective treatment also reduces transmission and minimizes the emergence of resistance to antimalarial drugs (WHO, 2015). However, malaria treatment depends on the illness severity, infecting species, drug resistance, and previous antimalarial medications. Using the same prophylactic drug for treatment is not recommended Arrow et al. (2004); WHO (2023c). The cornerstone of current treatment strategies is artemisinin-based combination therapies (ACTs), which have proven highly effective against P. falciparum and P. vivax, the most prevalent malaria-causing parasites Alghamdi et al. (2024). In particular, Chloroquine is used for uncomplicated *vivax* malaria while artemisinin based combination therapy (ACTs) is used for uncomplicated falciparum malaria Basu & Sahi (2017). In addition, patients with complicated malaria, intravenous IV artesunate is the drug of choice irrespective of the *Plasmodium* species CDC (2024a).

Currently, the WHO recommends alternative and novel drug base prevention strategies to reduce malaria transmission among high-risk populations. The most common approaches include Mass Drug Administration (MDA) and Mass Screening and Treatment (MSaT) Poirot et al. (2013). Mass Drug Administration (MDA) involves treating the entire at-risk population with antimalarial drugs, regardless of symptom presence or positive diagnosis. The aim is to reduce the parasite reservoir, thereby interrupting transmission potential and decreasing malaria incidence. However, the efficacy of MDA varies based on factors such as local epidemiology, drug effectiveness, and coverage levels. On the other hand, mass screening and testing (MSaT) strategy involves testing all malaria high-risk individuals within a specific area, regardless of symptoms, to identify and treat malaria infections. It has proven effective in reducing transmission in low- to moderate-prevalence settings, but its success relies on accurate diagnostics,

effective antimalarial drugs, and strong community engagement. Implementation requires substantial resources and infrastructure, and effectiveness may be constrained by poor treatment adherence and the emergence of drug resistance.

1.3 The Role media-awareness

Health education and promotion are crucial components of public health, as they help individuals and communities make informed decisions about their health and well-being. By empowering individuals with knowledge and skills, public health professionals can help prevent diseases, reduce the burden of chronic illnesses, and promote healthy lifestyles (Bauch et al., 2013; Sahay, 2024). Malaria awareness campaigns substantially contributed to health promotion by enhancing knowledge about the disease, fostering positive health-related behaviors, and strengthening both inter-sectoral collaboration and community support systems (Mboera et al., 2007). Implementing targeted information, education, and communication (IEC) strategies, along with behavioral change communication (BCC) interventions is critical to enhancing ITN uptake (Yirsaw et al., 2021). Extensive dissemination of malaria-related messages enhances awareness of prevention, treatment, and control measures (Mwebesa et al., 2024). These messages are conveyed through various media outlets, including television, radio, billboards, and posters, as well as through interpersonal communication during community events and by village health teams (Yaya et al., 2018). Disseminating these messages and accurate information has a crucial importance to brought behavioral change, reduce infection risk, and influence the trajectory of future epidemics (Elzubier et al., 1997; Mensah et al., 2024). The use of mass media in promoting the use of bed nets is effective. A study by Ankomah et al. (2014) demonstrated individuals who knew that sleeping under ITNs prevents malaria were 3.2 times more likely to sleep under a net. Those who listened to the radio are about 1.6 times more likely to use ITN, while individuals who had heard of a specific monitored radio campaign on ITN are 1.53 times more likely to use a bed net. Additionally, exposure to radio broadcasts correlates with a 1.6 times greater likelihood of ITN use. Furthermore, awareness of a specific monitored radio campaign promoting ITNs increases the likelihood of bed net usage by 1.53 times. Similarly, a study by Bamou et al. (2022) found that approximately 86.56% of heads of households demonstrated good knowledge of malaria and its control measures, with a high ownership rate of long-lasting insecticidal nets (LLINs) at 96.8%. More than two-thirds of households owned at least one LLIN for two people, and 85.40% of heads of households reported visiting hospitals or clinics for suspected malaria cases. On the hand the public adherence to persistent misconceptions about malaria causes and transmission hinder effective disease control, resulting in inadequate prevention practices (Basir et al., 2021). These misconceptions are linked to household demographics, residential environments, and perceived barriers, highlighting the

need for awareness-raising initiatives. Furthermore, the integration of media-based educational campaigns with existing malaria prevention and mosquito control strategies has not been evaluated and requires further investigation.

1.4 Effect asymptomatic malaria

Asymptomatic malaria infections frequently go undetected, providing a silent natural reservoir that serves as a major source of gametocytes. The presence of asymptomatic carriers poses substantial challenges for malaria control and elimination efforts, as many individuals remain unaware of their infection status (Gupta et al., 1999). Asymptomatic malaria infections exhibite variation across different locations and age groups. P. falciparum was the predominant parasite species; however, the presence of P. malariae and P. ovale was also noted. This diversity may influence the selection and implementation of diagnostic tools. Recent studies demonstrate a high prevalence of asymptomatic malaria in high-transmission regions, including Uganda, Nigeria, Ethiopia, and Cameroon. Specifically, in Northern Uganda, 34.7% of children aged 2 to 10 are found to be asymptomatically infected (Agaba et al., 2022). In Ethiopia, the prevalence of asymptomatic malaria among pregnant women is significantly high, particularly among those who do not use insecticide-treated bed nets, receive inadequate health education during antenatal care, and live near stagnant water. Overall, asymptomatic cases constitute 6.7% of the general population, while the rates among pregnant women vary between 2.83% and 11.2% (Balcha et al., 2023). A study in Nigeria investigated the prevalence and determinants of asymptomatic P. falciparum infection in individuals aged 40 and above. The findings revealed that the overall prevalence of asymptomatic P. falciparum infection in this age group was 19.0% Ibrahim et al. (2023). On the other hand, asymptomatic malaria is prevalent among children, with variations linked to age and gender. Identified risk factors include proximity to swamps, non-use of insecticide-treated nets (ITNs), a family history of malaria, open eaves or gaps in walls, and lack of indoor residual spraying (IRS). To mitigate prevalence in Cameroon, active case detection is recommended to identify and treat asymptomatic carriers (Kaghou et al., 2024).

1.5 Age, immunity and malaria vaccine

Immunity refers to the state in which the body possesses sufficient defenses to resist disease or other harmful invasions, with multiple biological processes influencing malaria transmission and prevalence (Ermert, 2010). During birth, children are partially protected from malaria due to the pass of antibodies from their mother (Feeney, 2020). This immunity wanes after a few months, leaving them vulnerable to infections. However, following the loss of maternal immunity, they rapidly develop protection against non-severe malaria (Gupta et al., 1999). In addition,

age may impact vaccine-induced immunity, which may elucidate the reduced effectiveness of the currently available malaria vaccine in children from malaria-endemic regions compared to the higher efficacy observed in malaria-naive adults (MESA, 2023). Moreover, the younger age groups are especially vulnerable to severe malaria due to their immature immune systems and also act as reservoirs for malaria transmission, often harboring high parasite densities and asymptomatic infections (Oshagbemi et al., 2023; Ranjha et al., 2023).

Complementing other recommended malaria interventions with malaria vaccinations have the potential to significantly reduce morbidity and mortality associated with the disease. Despite decades of research, developing effective vaccines has proven challenging due to the complex, multi-stage lifecycle of *P. parasites* and their ability to evade immune detection. In October 2021, the WHO recommended the first made vaccine for RTS,S/AS01, was updated in October 2023 to include a second malaria vaccine, R21/Matrix-M (CDC, 2024; Gavi, 2023; PATH, 2023). These vaccines are WHO pre-qualified, confirming their safety, efficacy, and quality, and are eligible for procurement by UNICEF, with financial backing from Global Alliance for Vaccines and Immunization (GAVI), the Vaccine Alliance. In January 2024, Cameroon became the first country to introduce the first shipment of 331,200 doses of RTS,S vaccine. Later over 30 countries have shown interest in integrating malaria vaccines into their routine immunization programs, with more than 20 approved for GAVI support. This rapid adoption highlights strong demand, projected at 40 to 60 million doses annually by 2026 and 80 to 100 million doses by 2030 (PATH, 2024). R21 has not yet been rolled out widely, although in areas where malaria transmission is highly seasonal (limited to four to five months per year), the R21 vaccine reduced malaria cases by 75%. According to WHO, "This high efficacy is similar to the efficacy demonstrated when RTS,S is given seasonally (Joi, 2024).

Malaria vaccination strategies consider the unique immune responses and exposure risks associated with different age groups (Moturi et al., 2023). The RTS,S/AS01 malaria vaccine was introduced in Ghana, Malawi and Kenya in 2019, as part of routine childhood immunization, in a large-scale pilot scheme, with doses at 6,7, 9 and 24 months of age in Ghana and Kenya, and at 5,6,7 and 22 months in Malawi enhance the efficacy of malaria control programs and improve health outcomes in endemic regions (Milligan & Fogelson, 2024). The research cited in (Sauboin et al., 2015) demonstrates that RTS,S vaccination significantly reduces the incidence of clinical malaria, severe cases, hospitalizations, and deaths across 42 countries in sub-Saharan Africa. Moreover, in the multicenter phase 3 trial, children aged 5–17 months who received three doses of the RTS,S/AS01E malaria vaccine experienced a 56% reduction in clinical malaria incidence and a 47% reduction in severe malaria incidence over one year. For those receiving a fourth dose, clinical malaria incidence decreased by 39% and severe malaria incidence by 32%

over four years. Additionally, trials of seasonal vaccination demonstrated a vaccine efficacy of 63% against clinical malaria, 70% against severe malaria hospital admissions, and 73% against malaria-related deaths over three years in children receiving seasonal malaria chemoprevention (Asante et al., 2024).

1.6 Mathematical models of infectious diseases

Modeling infectious diseases is an abstract representation of epidemic dynamics using equations to capture disease behavior, assess influencing factors, and predict epidemic duration, magnitude of an epidemic, and case numbers (Van et al., 2017). The study of epidemiological mathematical models dates back to the 18th century, with Daniel Bernoulli's 1760 used deterministic mathematical models for smallpox (Bernoulli & Chapelle, 2023). In 1906, Hamer introduced a discrete-time model to study measles transmission. Five years later, Ross (1910) employed differential equations to describe malaria transmission between humans and mosquitoes, demonstrating the existence of a threshold mosquito population below which malaria could be controlled. Subsequently, McKendrick and Kermack developed the seminal SIR (susceptible–infectious–recovered) compartmental model, which successfully explained epidemic patterns such as the black death in London and the plague outbreak in Mumbai (Kermack & McKendrick, 1927). In recent years, significant progress has been made in mathematical modeling, with numerous models developed to study a wide range of infectious diseases, spanning from highly theoretical and general frameworks to disease-specific applications. General epidemic dynamical models were developed to study disease dynamics by Bailey (1975); Brauer et al. (2012); Burnet & White (1972); O. Diekmann & Heesterbeek (2000); Van den Driessche & Watmough (2002); Waltman (2013). More specific models have also been developed based on the etiological categories of diseases, such as vector-borne infections (Aldila & Angelina, 2021; Collins & Duffy, 2022; Herdicho et al., 2021; Okosun et al., 2013; Ross, 1910), airborne infections (Castillo-Chavez & Song, 2004; David et al., 2020; Edwards et al., 2023; Salpeter & Salpeter, 1998), and sexually transmitted diseases, including gonorrhea disease (Adamu et al., 2018; Bozkurt & Peker, 2014; Cassels et al., 2008; Olopade et al., 2024; Omondi et al., 2018). Additional studies have examined the dynamics of hepatitis B and C (Ayobami, 2020; S. Zhao et al., 2000), as well as co-infections (Batu & Obsu, 2025; Tchoumi et al., 2021). Building on the foundational model by Ross (Ross, 1910), numerous researchers have developed mathematical models to analyze the transmission dynamics of infectious diseases and evaluate control measures (Agusto et al., 2013; Aldila & Angelina, 2021; Basir & Abraha, 2023; Herdicho et al., 2021; Ngonghala et al., 2020; Shi et al., 2024; Srivastav & Ghosh, 2021; Xue et al., 2023). These studies cover various aspects of malaria transmission dynamics, but have not examined the combination of vaccination, asymptomatic cases, and media awareness in a mathematical model.

Additionally, the effectiveness of malaria vaccination for children under five is not reported in the literature. This study aims to fill these gaps.

1.6.1 Optimal control and cost-effectiveness analysis

Mathematical models with optimal control analysis has become an important tool in order to understand the dynamics of disease transmission and decision making processes regarding intervention programs for the disease control (Igoe et al., 2023; Tilahun & Alemneh, 2021). Several researchers have proposed different optimal control models to inform effective public health benefits and cost-effective interventions. Applications include COVID-19 (Aldila et al., 2022), HIV/AIDS (Cheneke, 2023), influenza infection (Wang & Cai, 2025), tuberculosis (Yusuf & Abidemi, 2023), Zika virus (Yue et al., 2025), Hepatitis B virus (HBV) (Alrabaiah et al., 2020), Hepatitis C virus (HCV) (Okosun & Makinde, 2014), malaria (Okosun et al., 2013), Ebola virus (Bonyah et al., 2016) and cholera (Abubakar & Ibrahim, 2022).

Notable contributions include (Bakare & Hoskova-Mayerova, 2023), who developed an optimal control model with five time-dependent interventions: treated bed nets, treatment, educational campaigns, indoor residual spraying, and mosquito breeding site destruction; Herdicho et al. (2021) proposed and analyzed a mathematical and optimal control model incorporating three control variables: insecticide, prevention, and treatment; (Febiriana et al., 2024) proposed an optimal control and cost-effectiveness analysis that considers mosquito repellent and hospitalization as control strategies; and (Wako et al., 2025) conducted an optimal control analysis of malaria and its associated complications, focusing on three control efforts: outpatient treatment, supportive care, and insecticide spraying. In a related avenue, authors in Mojeeb et al. (2018) developed an optimal control mode considering four control strategies: long-lasting insecticide-treated nets (LLITNs), drug treatment, insecticide spraying, and indoor residual spraying (IRS) and found LLITNs and drug treatment most effective in reducing malaria transmission. Similarly, Abioye et al. (2020) considered four intervention strategies: bed nets, treatment, sterile mosquito release, and reduction of neonatal and maternal mortality and showed that implementation of their combination can substantially mitigate the disease. Further, the authors in (Basir & Abraha, 2023) proposed an advanced optimal control model that incorporates awareness interventions while accounting for the costs of treatment, insecticides, and awareness campaigns, and their finding suggests that administering optimal media awareness is the less costly and more effective approach in curbing malaria. Collectively, prior studies have examined malaria interventions, but the integration of optimal control and cost-effectiveness analysis, incorporating media awareness alongside preventive measures: personal protection, enhanced drug treatment, and mosquito breeding site destruction remains unexplored. Addressing this gap is crucial for designing effective intervention strategies.

1.7 Statement of the Problem

Malaria remains a major public health threat in tropical and subtropical regions, imposing significant social, economic, and health burdens. According to the WHO report WHO (2022b), it continues to cause high morbidity and mortality in many developing countries despite ongoing prevention and control efforts. Global malaria cases increased by five million between 2021 and 2022, reaching 249 million in 2023 (WHO, 2023a). The WHO African Region accounts for 94% of cases and 95% of deaths, with infections rising from 204 million in 2000 to 246 million in 2023 (WHO, 2024b). In Ethiopia, malaria remains a major public health and socioeconomic challenge. In 2024, over 7.3 million cases and 1,157 deaths were reported the highest incidence in seven years (WHO, 2024b). Four regions Oromia (44% of cases; 667 deaths), Amhara (18% of cases; 56 deaths), Southwest (12% of cases; 250 deaths), and South Ethiopia (7% of cases; 45 deaths) accounted for 81% of cases and 89% of health facility deaths (WHO, 2024a).

Economically, malaria substantially reduces productivity and growth. As noted by Consortium (2007), malaria related morbidity results in annual losses of approximately 1.3% of GDP, equivalent to about $12 billion in Africa. Evidence from 180 countries shows that a 10% reduction in malaria incidence is associated with a 0.3% increase in per capita GDP, reaching nearly 2% in high-burden, low-income countries (Sarma et al., 2019). On the other hand, eliminating malaria could increase Africa's GDP by an estimated $127 billion by 2030 (Alliance, 2024; Malaria, 2020).

Mathematical models provide a valuable framework for analyzing malaria transmission dynamics, simulate various scenarios and assess the effectiveness of different control strategies. Incorporating optimal control strategies into these models provides a systematic framework to implement interventions that are both effective and efficient. This comprehensive modeling approach deepens our understanding of malaria transmission dynamics and informs the development of more effective intervention strategies. Building on the first malaria mathematical model by Ronald Ross (Bacaër, 2011b), subsequent researchers have extended his model by incorporating factors related to potential control interventions, including heterogeneous mixing, environmental factors, demographic variables, optimal control strategies, age-dependent susceptibility, and awareness interventions (Abubakar & Ibrahim, 2022; Basir & Abraha, 2023; Ibrahim et al., 2020; Tchoumi et al., 2021; White et al., 2015).

In the study by Basir & Abraha (2023), a mathematical and optimal control model was developed to explore the influence of awareness-based control measures on malaria transmission dynamics. The model conceptualizes level of media awareness as a distinct population, allowing for the differentiation between aware and unaware susceptible individuals. As individuals gain

awareness, they adopt preventive measures, such as using mosquito nets and applying insecticides. The findings suggest that social media awareness campaigns, combined with an optimal control strategy, offer a cost-effective approach to malaria management. However, the model does not account for the synergistic effects of treatment combined with media-induced insecticide application, nor does it include a recovery epidemiological compartment, which may affect the accuracy of long-term transmission predictions.

Current literature on malaria epidemiology reveals a significant gap in understanding asymptomatic malaria transmission, which remains under-explored despite its prevalence (Ibrahim et al., 2023). Asymptomatic infections contribute significantly to transmission dynamics, as individuals may unknowingly harbor the parasite while exhibiting no symptoms. This lack of clinical symptoms complicates detection and treatment efforts, hindering effective control measures (Bassinga et al., 2024). Despite the significant gap in understanding asymptomatic malaria transmission, Shi et al. (2024) and Xue et al. (2023) developed a compartmental mathematical model to analyze the dynamic effects of asymptomatic carriers on malaria transmission. However, these models have several limitations as they neglect waning immunity, exclude treatment effects, disregard the progression of asymptomatic carriers, and screening followed by asymptomatic treatment. Recently, age-structured vaccination has gained significant attention in modeling malaria transmission. Tchoumi, Dongmo, et al. (2022) proposed a compartmental mathematical model incorporating a two-group structure. Their findings indicate that interventions reducing contact between mosquitoes and children under five years old have a substantially greater impact on overall endemicity than similar measures targeting older individuals. This highlights the importance of intensifying malaria control efforts among children under five to effectively reduce transmission. However, the model does not incorporate under-five age-structured vaccination, recovery classes for this age group, treatment compartments, or mosquito insecticide application.

Collectively, previous mathematical models have significantly advanced our understanding of malaria transmission dynamics and control strategies. Nonetheless, these models are constrained by several critical limitations, including insufficient representation of asymptomatic carriers, lack of integration between awareness-driven preventive behaviors and treatment interventions, omission of age-structured vaccination and recovery dynamics, neglect of waning immunity and insecticide-based vector control. These gaps limit the models' ability to fully capture the complexity of malaria transmission and to inform optimal, cost-effective control strategies. To address these gaps, this study develops and analyzes malaria transmission models incorporating media awareness, treatment, asymptomatic infections, and age-structured vaccination for children under five, extending the analysis to optimal control and cost-effectiveness.

1.8 Objectives of the study

1.8.1 General objective

The general objective of this study is to develop mathematical models with optimal control strategies that capture the transmission dynamics of malaria, accounting for age-structured vaccination, asymptomatic carriers, drug treatment, and awareness intervention.

1.8.2 Specific objectives

The specific objectives of the study are to:

1. formulate and analyze a mathematical model of malaria transmission that incorporates the dynamics of infection with media awareness and treatment interventions
2. construct and analyze an age-structured mathematical model of malaria transmission incorporating vaccination and other interventions
3. develop and analyze a mathematical model of malaria infection that quantifies the impact of asymptomatic carriers on transmission dynamics
4. formulate and analyze optimal control strategies that are used to minimize the spread of malaria disease with optimal implementation cost
5. predict the long-term trends of the malaria epidemic in Ethiopia and recommend evidence based mitigation strategies to policymakers

1.9 Significance of the study

Mathematical models play a crucial role in elucidating malaria transmission dynamics and informing effective intervention strategies. The formulation and analysis of these dynamical model provide valuable framework for quantifying key mechanisms of infection such as determining the threshold conditions, and determining stability properties of equilibria. Such mathematical insights enable systematic evaluation of prevention and control measures, clarify the contributions of host–vector interactions, and highlight parameters that drive transmission. By capturing these dynamics analytically and numerically, our models support the design of prevention and control strategies, ultimately contributing to improved public health outcomes in malaria-affected regions.

A mathematical model incorporating media awareness and treatment interventions enhances understanding of their combined impact on malaria transmission. By linking media-driven

awareness to increased insecticide use and improved treatment interventions, the model demonstrates how these interventions jointly reduce infection levels and support malaria elimination efforts. The mathematical analysis provides a quantitative framework for evaluating intervention effectiveness and identifying threshold conditions necessary for disease control. These findings are valuable for designing more effective and integrated strategies to reduce malaria burden and accelerate progress toward elimination goals.

The study on the impact of asymptomatic infections on malaria transmission plays a crucial role in evaluating prevention and control strategies for malaria. The findings indicate that asymptomatic cases significantly contribute to the persistence of malaria infections within communities. This highlights the necessity of a comprehensive approach to malaria control, emphasizing that effective interventions must target both asymptomatic and symptomatic infections. The findings of this study supports evidence-based public health planning.

The study demonstrates that asymptomatic infections significantly contribute to the persistence of malaria within communities, underscoring the need for control strategies that target both asymptomatic and symptomatic cases. The model further reveals the possibility of backward bifurcation, indicating that reducing the reproduction number below one may not guarantee elimination without intensified interventions. These findings highlight the importance of comprehensive control measures and support evidence-based public health planning. The development and analysis of an age-structured vaccination model for malaria transmission are crucial for understanding disease dynamics and enhancing control efforts. Integrating effective vaccination with treatment and vector control improves transmission predictions and reduces transmission rates, thereby supporting progress toward malaria eradication. This study provides essential insights into the synergistic effects of combining vaccination with complementary interventions, thereby informing public health planning for sustainable malaria control in endemic regions.

Incorporating optimal control and cost-effectiveness analysis into malaria model facilitates the identification of the most effective combinations of interventions: personal protective measures, treatment capacity, and vector control strategies, aimed at minimizing infection in human and mosquito hosts. The optimal control analysis offers essential guidance for policymakers and healthcare providers by facilitating efficient resource allocation and the implementation of targeted combined intervention strategies. In parallel, cost-effectiveness analysis enhances this process by comparing the costs of possible interventions with their associated health benefits, thereby informing decisions that maximized health outcomes with less costly strategies. Mathematically, the framework offers a rigorous qualitative and quantitative basis for determining optimal intervention pathways and assessing their influence on disease dynamics. The methodologies and analytical tools employed in this study provide a valuable contribution to

the mathematical epidemiology community, offering reproducible techniques and insights that can support future model development and scientific research. Moreover, these analyses enable policymakers to make informed decisions that maximize health benefits while ensuring the wise use of limited resources in the fight against malaria infection.

1.10 Delimitation of the study

Mathematical modeling of malaria transmission provides insights into disease dynamics, informs preparedness, and supports evidence-based control strategies. This study focuses on three objectives: (i) formulate and analyze a model incorporating infection dynamics, media awareness, and treatment, extended to optimal control and cost-effectiveness; (ii) assess the impact of asymptomatic carriers on transmission; and (iii) develop an age-structured model integrating vaccination and other interventions.

This study formulates and analyzes compartmental malaria transmission models using ordinary differential equations (ODEs). Local and global stability analyses were conducted, and optimal control theory was applied to identify effective interventions, with accompanying cost-effectiveness evaluation. Parameter sensitivity was assessed via the forward sensitivity index, and model fitting used least-squares estimation based on Ethiopian malaria incidence data. Reliance on aggregated incidence data may limit parameter precision due to potential gaps and the difficulty of accessing daily or weekly records from the Ethiopian Public Health Institute (EPHI).

1.11 The Organization of the dissertation

This dissertation is made up of eight chapters. Chapter 1 presents the introduction, a literature review on the biological background of malaria, and the study objectives. Chapter 2 provides a review of mathematical models previously formulated and analyzed to gain insights into malaria disease transmission and control. This review focuses on significant findings from selected malaria models and discusses the application of optimal control theory to malaria interventions. The methodology employed in this dissertation is detailed in Chapter 3. Chapter 4 examines the overall dynamics of malaria transmission, taking into account media awareness and treatment interventions. Chapter 5 further extends the model formulated in Chapter 4 to optimal control and cost-effectiveness analysis. In Chapter 6 of this dissertation, we investigate the effects of asymptomatic infections in malaria transmission dynamics. Chapter 7 presents an age-structured mathematical model of malaria vaccination. Finally, Chapter 8 summarizes the study findings, conclusions, and recommendations.

CHAPTER 2

LITERATURE REVIEW

In this chapter, we review existing mathematical models of malaria transmission to summarize relevant literature and identify key gaps addressed in this dissertation. The focus of the review is primarily on deterministic ordinary differential equation (ODE) frameworks based models. Additionally, we provide a brief history of malaria modeling and discuss key assumptions previously employed in formulating models for specific contexts.

2.1 Comprehensive literature review

Mathematical modeling of infectious diseases serves as a crucial tool for analyzing disease transmission dynamics and evaluating the impact of various intervention strategies. This approach provides valuable insights for public health policymakers, guiding the implementation of effective programs to combat infections (Becker, 1979). Daniel Bernoulli roots the first prominent contribution of mathematical modelling in epidemiology in modeling smallpox inoculation in 1760 (Foppa, 2017) . In a significant advancement in mathematical epidemiology, Anderson Gray McKendrick and William Ogilvy Kermack proposed a new compartmental model to examine the transmission dynamics of the bubonic plague epidemic in Mumbai (Kermack & McKendrick, 1927). The Kermack-McKendrick SIR model describes plague transmission dynamics through a system of ODEs governing the transitions between Susceptible, Infectious, and Removed compartments:

$$\begin{aligned} \frac{dS}{dt} &= -\beta SI, \\ \frac{dI}{dt} &= \beta SI - \gamma I, \\ \frac{dR}{dt} &= \alpha I, \end{aligned} \tag{2.1}$$

where the total population is divided into three mutually exclusive epidemiological states, S represents the susceptible population, I is the infectious population, and R is the recovered population. The parameter β denotes the contact rate per unit time, and α is the recovery rate. The model (2.1) assumes a constant population with homogeneous mixing, indicating that all individuals interact uniformly. It overlooks demographic factors such as birth, death, migration, and other important parameters. Over time, researchers have extended and modified the Ker-

mack & McKendrick (1927) SIR model to address these limitations, incorporating additional compartments, stochasticity, spatial structure, and intervention effects. Despite its limitations, their model remains a cornerstone of mathematical epidemiology and a starting point for more complex models (Anderson & May, 1991; Bacaër, 2011a).

2.1.1 Mathematical modelling of malaria

Mathematical models have provided a framework for understanding malaria transmission in humans for over a century (Mandal et al., 2011). The Malaria Eradication Research Agenda (MalERA) recognizes that such models inform policy, guide research, and support malaria elimination efforts from local to global level (malERA, 2011). By integrating modelers into multidisciplinary teams, models can be iteratively updated to meet the needs of researchers, public health specialists, and policymakers. Given malaria's complex intra-host and inter-host dynamics (Savi, 2022), mathematical modeling offers a structured approach to quantify transmission patterns, evaluate interventions, and support evidence-based public health decision-making. This approach not only enhances our understanding of malaria but also supports the design of targeted and efficient control measures. The concept of using mathematical modeling to describe malaria transmission dynamics through individual-based models was began with a pioneering contribution of Ronald Ross. His pioneering malaria model is comprised of two coupled differential equations that capture the interactions between human and mosquito populations:

$$\begin{aligned} \frac{dI_h}{dt} &= bp' I_m \frac{N_h - I_h}{N_h} - aI_h, \\ \frac{dI_m}{dt} &= bp(N_m - I_m)\frac{I_h}{N_h} - mI_m, \end{aligned} \tag{2.2}$$

In these equations, N_h and N_m represent the total populations of humans and mosquitoes, respectively, while I_h and I_m denote the number of infected individuals within each population. The parameters are defined as follows: b is the biting frequency of mosquitoes; p and p' are the probabilities of malaria transmission from humans to mosquitoes and from mosquitoes to humans, respectively, during a bite; a is the recovery rate for humans; and m indicates mosquito mortality.

After the transmission from the first infected human to mosquitoes and subsequently from those mosquitoes to other humans, the mean number of newly infected humans can be expressed as the product of the previous two results:

$$\mathfrak{R}_0 = \frac{b^2 pp' n}{amN}$$

This equation, $\mathfrak{R}_0$, represents the number of secondary human cases resulting from a single primary case. The infection process, which occurs continuously over time, can also be analyzed through successive generations. Malaria can only "invade" the population if $\mathfrak{R}_0$, which is equivalent to the condition $N_m > N_m^*$. His work remains a cornerstone of infectious disease modeling, highlighting the importance of mathematical approaches in unraveling complex biological systems and informing public health interventions (Ross, 1910). Fifty years later, MacDonald (1957) extended the Ross (1910) model by integrating biological information of latency in the mosquito and is now popularly known as Ross-Macdonald model. Ross-Macdonald's rationale led to a WHO-coordinated campaign to eliminate malaria transmission by focusing on insecticide dichloro-diphenyl-trichloroethane (DDT) application to kill mosquitoes (Pampana, 1963). Macdonald modified Ross's model by introducing superinfection, reinfection of those who are already infected. Macdonald also used the models to quantitatively synthesize a half-century of malaria epidemiology, which made it possible for the two-way flow of ideas to occur between theory and entomological and epidemiological data (McKenzie et al., 2008). Moreover, Anderson & May (1991) introduced latent infection to the human population in to MacDonald (1957) model. This enhancement allowed for a more nuanced understanding of disease dynamics by accounting for individuals who have been infected but are not yet infectious themselves.

Since then, several extensions have been made by incorporating new variables into the model (Anderson & May, 1991; MacDonald, 1957; Ross, 1910), which have addressed a wide range of problems (Basir & Abraha, 2023; Castillo-Chavez & Song, 2004).

2.2 Mathematical model with media-awareness

An important aspect for the implementation of malaria control strategies is the individual awareness about malaria and their willing to take effective prevention actions to reduce disease transmission. Basir et al. (2021) proposed a mathematical model of malaria, assessing the impact of awareness-based intervention. Their approach, assuming an SIS-type sub-model for humans and an SI-type sub-model for mosquitoes, coupled with awareness as a dispersed population, indicates that amplifying awareness through available media can effectively reduce the mosquito population and consequently facilitate disease control. Furthermore, the study presented in (Basir & Abraha, 2023) proposed and analyzed a mathematical model that explains the dynamics of malaria transmission. This model considered the influence of control strategies based on awareness. The findings of this study reveals that awareness campaigns through media and optimal control methods are the most cost-effective strategy to manage malaria. Ibrahim et al. (2020) proposed a non-linear mathematical model that incorporates the interplay between disease transmission, awareness campaigns, and population dynamics, highlighting the impor-

tance of awareness in reducing disease spread. Their model categorizes infected populations into two sub-populations: those aware of infection and those unaware. They considered the cumulative density of awareness programs driven in the region at a time as a separate population. In addition, their model assumed that increasing awareness programs are proportionally linked to the total number of individuals unaware of infection. Finally, the authors assume that aware, infected humans would actively avoid contact with mosquitoes, driven by the impact of heightened awareness. Thus, the spread of this illness could be prevented through effective awareness strategies in regions with rapid spread.

2.3 Asymptomatic malaria model

Xue et al. (2023) formulated a malaria dynamical model incorporating asymptomatic humans, where exposed humans may progress to either asymptomatic or symptomatic infection. However, the model does not account for waning immunity in recovered individuals, which increases susceptibility to reinfection. Similarly, Shi et al. (2024) developed a compartmental model including asymptomatic carriers who can infect mosquitoes without symptoms, but their model neglected waning immunity and the possible progression of asymptomatic cases to symptomatic infection. Cai et al. (2017) introduced a model with asymptomatic infection and super-infection to evaluate prevention strategies, yet excluded waning immunity in recovered individuals and disease dynamics in treated populations. Likewise, Chitnis et al. (2008) analyzed models with exposed humans and mosquitoes to assess parameter effects on transmission, validating results through numerical simulations. Formulating and analyzing asymptomatic malaria models is crucial for guiding effective control and elimination strategies. Since, asymptomatic carriers acts as a key reservoir for parasites, yet it has received less attention (Bassinga et al., 2024; Ibrahim et al., 2023).

2.4 Age-structure and age-structured vaccination malaria models

Olutimo et al. (2024) developed a mathematical model of malaria transmission to examine the role of environmental immunity in humans. Their findings indicate that increased environmental immunity in recovered individuals significantly reduces the number of infected humans, which in turn lowers the number of infected mosquitoes due to fewer transmission opportunities. A sensitivity analysis study that incorporates relapse dynamics and unaware infected individuals, is proposed in (Haile et al., 2025). The findings demonstrate that mosquito protection measures are significantly more effective than treatment alone in reducing disease spread. Zhao & Mohammed-Awel (2014) proposed mathematical model accounting mosquito-stage transmission-blocking vaccines. Their finding indicate that increasing vaccination cover-

age can significantly reduce, and potentially even eliminate, the disease. However, if vaccination rates remain insufficient, the disease may continue to persist. Additionally, it has been observed that the decline in infections among vectors occurs more rapidly than in humans. This discrepancy could be directly attributed to the transition-blocking vaccine, which is designed to target vectors rather than human hosts. In (White et al., 2015), authors formulated a malaria transmission dynamics considering hypothetical vaccination for general population. The finding reveals that malaria eradication is possible by maintaining reproduction number below unity. Banasiak et al. (2023) developed a malaria transmission model to assess demographic growth and transmission-blocking drugs. Findings show that a specific growth pattern markedly increased disease burden. However, the elimination of malaria is succeeded when the high-level treatment and transmission-blocking vaccines administration are implemented simultaneously. Ducrot et al. (2009) developed a two-species malaria model that considers the susceptibility, exposure, and infectivity of human hosts. This model identifies two distinct types of hosts within the human population: non-immune and semi-immune individuals. Non-immune individuals are particularly vulnerable to malaria, as they have never developed any immunity to the disease. In contrast, semi-immune individuals have experienced at least one episode of malaria, allowing them to acquire some level of immunity throughout their lives. A deterministic analysis of an age-sex-structured model of malaria transmission proposed and studied for the Rwanda case (Uwineza et al., 2024). This study highlights the need for women to increase awareness and implement preventive measures, such as educating older children on safe play areas and ensuring younger ones use bed nets. The study recommends enhancing outdoor spraying effectiveness and expanding the model to include climatic factors like temperature, rainfall, and humidity, which impact malaria transmission. In more related way, Tchoumi, Dongmo, et al. (2022) proposed a malaria transmission dynamics considering two-group structures. This study analysis demonstrates that interventions aimed at reducing contact between mosquitoes and individuals under five years old have a significantly greater positive effect on overall endemicity levels than similar measures targeting individuals over five. This finding emphasizes the critical public health implication that efforts to combat malaria should be intensified among children under five to effectively mitigate its spread throughout the population. Forouzannia & Gumel (2014) examined a deterministic mathematical model to assess the impact of age structure on malaria transmission in a community without vaccination or treatment interventions. Their findings indicated that the cumulative incidence of new infections and malaria-related mortality increases with rising average mosquito lifespan and birth rate. Recently, Glèlè Kakaï & Djomatin (2025) proposed an age-structured model to evaluate the impact of vaccination on malaria transmission. The model stratifies humans: unvaccinated, primary doses only, and booster recipients and incorporates the synergistic effects of long-lasting insecticidal nets (LLINs). Calibrated

with demographic and epidemiological data from low (Ethiopia) and high transmission (Nigeria) settings. The study demonstrates that combining vaccination with existing interventions can substantially reduce incidence and mortality. However, the model does not consider treatment for asymptomatic and uncomplicated malaria.

Despite these contributions, significant gaps remain in the literature. Few studies have systematically investigated age-structured vaccination and its integration with LLINs. Moreover, the combined effects of age-structured vaccination strategies with insecticide application and drug treatment on malaria infection remain underexplored

2.5 Optimal control malaria models

Optimal control theory is a powerful tool for designing effective infectious disease interventions (Sharomi & Malik, 2017), enhancing understanding of disease dynamics and guiding control strategies. Several mathematical model and optimal control studies have applied this approach to malaria: Olaniyi et al. (2023) developed a deterministic model incorporating blood transfusion transmission and saturated treatment, demonstrating that combined ITNs, blood screening, improved treatment, and IRS can substantially reduce malaria. Basir & Abraha (2023) showed that optimal media awareness is a cost-effective strategy for malaria control. Aldila & Angelina (2021) applied optimal control to a model with mosquito bias, permanent immunity, and saturated treatment, finding that drug treatment and fumigation efficiently suppress transmission at minimal cost. Bakare & Hoskova-Mayerova (2023) evaluated educational campaigns, treatment, IRS, ITNs, and mosquito habitat management, recommending combined interventions in high-incidence areas and treatment-only strategies in resource-limited settings. The authors in (Mojeeb et al., 2018) developed a SEIR-SEI optimal control model with LLINs, drug treatment, insecticide spraying, and IRS, finding LLINs and treatment particularly effective. Abioye et al. (2020) proposed an optimal control model by considering interventions: usage of insecticide-treated bednets, vector, sterile mosquitoes, and reducing neonatal and maternity deaths. They suggested that curbing the disease is possible when the implemented controls are well managed. Abioye et al. (2020) developed an optimal control model that integrates four intervention strategies: the use of insecticide-treated bed nets, killing mosquitoes, deployment of sterile mosquitoes, and reduction of neonatal and maternal mortality. They concluded that effective management of these interventions can significantly mitigate the disease.

2.6 Synthesis of the Literature

The reviewed literature highlights the pivotal role of mathematical modeling in understanding and managing malaria transmission dynamics. Foundational models such as the SIR model

and the Ross-MacDonald framework have served as the cornerstone of epidemiological modeling, offering simplified yet powerful insights into the spread and control of infectious diseases. These models assume homogeneous mixing and constant population size, which, while mathematically convenient, limit their applicability in diverse and heterogeneous real-world settings. Over time, the literature reflects a clear evolution toward more nuanced and realistic models. Researchers have addressed key limitations of classical frameworks by incorporating demographic factors, stochastic processes, environmental variables, age structure, optimal control strategies, and increasingly, behavioral components such as awareness and media-driven interventions. These advancements allow models to capture the complex interplay between human hosts, mosquito vectors, intervention strategies, and societal behavior. Particular attention has been given to the inclusion of asymptomatic carriers, which play a significant but often underrepresented role in sustaining transmission. Several studies recognize the need to account for waning immunity and reinfection, which are critical for accurate long-term projections, especially in endemic regions. Nonetheless, existing models often fall short in addressing these elements simultaneously or in integrating them with empirical data for real-world validation. Another recurring theme is the importance of optimal control theory in designing cost-effective intervention strategies. Models that incorporate intervention optimization, such as ITNs, IRS, treatment coverage, and media campaigns, demonstrate the potential for mathematics to guide policy decisions. However, the literature also reveals a trade-off between model complexity and practical applicability, especially when data are scarce. Despite the advancements, certain gaps persist. There remains a need for:

- better integration of asymptomatic dynamics with immunity considerations;
- age-structured models to reflect localized transmission patterns;
- validation and calibration using real-world data, particularly in high-burden settings;
- interdisciplinary collaboration between modelers, epidemiologists, and public health practitioners to ensure models are both theoretically sound and practically useful.

In summary, the literature underscores the transformative potential of mathematical models in malaria control but also signals the need for continued refinement. Future research should aim to build data-informed, context-sensitive, and policy-relevant models that bridge the gap between theoretical analysis and field implementation. This synthesis informs the motivation and direction of the current study, which seeks to address existing gaps by developing an extended model that integrates asymptomatic transmission, waning immunity, and awareness-based interventions using data from Ethiopia.

CHAPTER 3

RESEARCH METHODOLOGY

In this chapter, we outline the research methodologies employed to achieve the intended general and specific objectives stated in Chapter 1. We provide a concise discussion of the data analysis methods, data sources, study approach, and mathematical procedures utilized in this dissertation.

3.1 Models formulation

In this study, four population-level mathematical models are developed to describe the interaction between humans and mosquitoes. The modeling process begins by partitioning both populations according to their infection status. Each model is governed by a system of nonlinear ordinary differential equations (ODEs). The first model formulates malaria transmission dynamics incorporating media awareness and treatment interventions. It follows an $SITRS$ structure for the human population and an SI structure for the mosquito population, with media awareness represented as an additional compartment.

Building on the first model, the second is designed to assess optimal control strategies and cost-effectiveness analysis. It extends the first model by introducing three time-dependent control variables aimed at strengthening malaria control and accelerating elimination efforts.

The third model, formulates a compartmental mathematical model of malaria to portray the effect of asymptomatic infection on the transmission dynamics of infection. It employs an $S-E-A-I-T-R-S$ compartmental structure for the human population and an SI structure for the mosquito population

Finally, an age-structured vaccination model is formulated to further strengthen malaria control and advance elimination goals. This model assumes that host susceptibility and infectivity depend on age, dividing the human population into two groups: individuals under five years of age and those aged five and above.

3.2 Model analysis

The formulated models are analyzed both qualitatively and quantitatively using appropriate methods.

3.2.1 Qualitative analysis

The proposed mathematical models are analyzed using various mathematical tools, theories, and theorems suitable for systems of ODEs. The fundamental models' property, including mathematical well-posedness and biological feasibility, are proven by demonstrating the non-negativity and boundedness of the solutions. Subsequently, the equilibrium points of the models: malaria-free equilibrium (MFE) point and the malaria-endemic equilibrium point (MEE) are determined. The MFE is obtained by setting the infectious compartments of both human and mosquito populations to zero, while the MEEP represents the persistence of infection within the population.

Descartes' Rule of Signs, or the geometric approach, was utilized to establish the existence of a positive steady state characterized by malaria persistence. The basic reproduction number $\mathfrak{R}_0$ was derived using the next-generation matrix approach. To assess the stability of the steady states, the methodologies such as: the eigenvalue analysis, the Routh-Hurwitz stability criterion, the Castillo-Chavez and Song theorem, bifurcation analysis, and analytical sensitivity analysis were employed. Furthermore, the Pontryagin Maximum Principle was applied to the optimal control problem. This comprehensive approach ensures a robust analysis of the model's dynamics and control strategies.

3.2.2 Numerical analysis

To validate and complement the analytical findings, numerical analyses were performed using various numerical methods. Python was employed for implementation, with the GEKKO optimization package applied to the optimal control model. Parameter estimation was first conducted by fitting the models to Ethiopian epidemiological data using the least squares method. Building on this, sensitivity analysis was applied to assess how variations in parameters influenced the basic reproduction number. Subsequently, numerical simulations with the Runge–Kutta method were performed to explore infection trajectories, evaluate intervention effectiveness, and predict outbreak dynamics. Collectively, these steps established a coherent and rigorous framework for analyzing and managing malaria transmission.

3.2.3 Source of data

The data used for the analysis in this study was obtained from secondary sources, which were carefully taken to enhance our understanding of disease dynamics. These sources included published articles and WHO situation case reports. All data sources used in this research have been meticulously cited to ensure integrity and credibility.

CHAPTER 4

A MATHEMATICAL MODEL OF MALARIA TRANSMISSION WITH MEDIA-AWARENESS AND TREATMENT INTERVENTIONS

In this chapter, we formulate a mathematical model for malaria transmission that incorporates media awareness and treatment interventions. We establish its biological relevance and mathematical well-posedness, then analyze the model through the basic reproduction number $\mathfrak{R}_0$, equilibria stability, and numerical simulations to interpret the disease dynamics.

4.1 Model formulation

To describe malaria transmission dynamics, we develop an eight-compartment model governed by a nonlinear system of ODEs, incorporating human and mosquito populations, as well as the level of media awareness. The model includes two biological populations: humans and mosquitoes. The media awareness compartment is not a biological population but a behavioral factor that modulates transitions between compartments and influences mosquito mortality. Both human and mosquito populations are variable: the human population changes due to natural births, deaths, and disease-induced mortality, while the mosquito population varies due to natural mortality and control interventions. Consequently, population sizes fluctuate in response to disease prevalence, vector control measures, and awareness levels. The model follows susceptible-infected-treated-recovered-susceptible (S-I-T-R-S) structure for human population, and susceptible-infected (S-I) for mosquito population. The human population is categorized into five distinct classes: susceptible aware humans S_{ah}, susceptible unaware humans S_{uh}, infected humans I_h, treated humans T_h, and recovered humans R_h. The total human population is represented by N_h as

$$N_h(t) = S_{ah}(t) + S_{uh}(t) + I_h(t) + T_h(t) + R_h(t).$$

Susceptible humans are recruited into the S_{ah} and S_{uh} classes at rates $b\Pi_h$ and $(1-b)\Pi_h$, respectively. Unaware susceptibles become aware at rate κ, whereas aware susceptible revert to unawareness at rate d, influenced by the awareness level $M_a(t)$ through the term $\frac{dS_{ah}}{1+M_a}$. The infection rates for susceptible humans are denoted by β_i $(i = 1,2)$. As reported by Ibrahim et al. (2020), awareness campaigns reduce human–mosquito contact, so unaware susceptible are more likely to become infected than aware individuals, implying $\beta_2 > \beta_1$. Recovered individuals acquire temporary immunity, which wanes over time, returning them to the aware susceptible

class at rate ε. Infected individuals receive treatment at rate ρ. Treatment failure results in persistent infection, potentially causing recurrent malaria episodes, prolonged illness, increased disease burden, and a higher risk of complications (Egwu et al., 2023). Thus, during treatment, a rate φ of treated individuals experience treatment failure death. Each human compartment is subject to natural mortality at rate μ_h, while recovered and infected classes experience recovery and disease-induced death at rates δ and η, respectively. In contrast, the mosquito population is divided into susceptible (S_m) and infected (I_m) classes, with no recovered class due to their short lifespan. Therefore, the total mosquito population, denoted as N_m at a given time t, is expressed as:

$$N_m(t) = S_m(t) + I_m(t).$$

The susceptible mosquito population is recruited at a constant rate Π_m. Susceptible mosquitoes S_m acquire infection from biting infected humans at rate β_3, thereby moving to the infected class. Mosquito mortality occurs through natural death at rate μ_m and insecticide-induced death given by $\frac{\gamma M_a}{1+M_a}$. The compartment M_a represents media awareness, which increases at constant rate π due to external and global media influences and at rate ξ through awareness campaigns, while declining at rate ϑ owing to inefficiency and fading memory. The schematic flow diagrams illustrating the human and mosquito components of the model are presented in Figure 4.1.

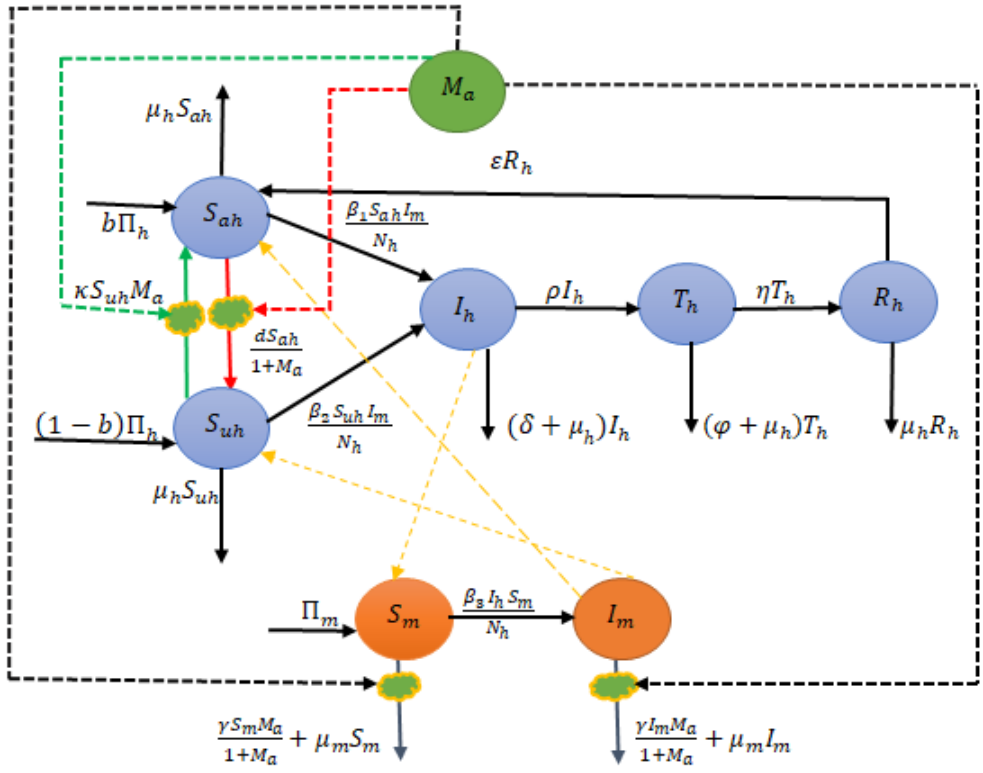

Figure 4.1: Flow diagram for malaria dynamical model (4.1) .

Based on the above assumptions and the interaction between susceptible humans and infected vectors, the governing system of ODEs is derived as follows:

$$\begin{cases} \frac{dS_{ah}}{dt} = b\Pi_h + \kappa S_{uh} M_a - \frac{dS_{ah}}{1+M_a} - \frac{\beta_1 S_{ah} I_m}{N_h} + \varepsilon R_h - \mu_h S_{ah}, \\ \frac{dS_{uh}}{dt} = (1-b)\Pi_h + \frac{dS_{ah}}{1+M_a} - \kappa S_{uh} M_a - \frac{\beta_2 S_{uh} I_m}{N_h} - \mu_h S_{uh}, \\ \frac{dI_h}{dt} = \frac{\beta_1 S_{ah} I_m}{N_h} + \frac{\beta_2 S_{uh} I_m}{N_h} - (\rho + \delta + \mu_h) I_h, \\ \frac{dT_h}{dt} = \rho I_h - (\eta + \varphi + \mu_h) T_h, \\ \frac{dR_h}{dt} = \eta T_h - (\mu_h + \varepsilon) R_h, \\ \frac{dS_m}{dt} = \Pi_m - \frac{\beta_3 I_h S_m}{N_h} - \frac{\gamma S_m M_a}{1+M_a} - \mu_m S_m, \\ \frac{dI_m}{dt} = \frac{\beta_3 I_h S_m}{N_h} - \frac{\gamma I_m M_a}{1+M_a} - \mu_m I_m, \\ \frac{dM_a}{dt} = \pi + \xi I_h - \vartheta M_a, \end{cases} \tag{4.1}$$

subjected to the initial conditions,

$$S_{ah0} > 0, S_{uh0} \geq 0, I_{h0} \geq 0, T_{h0} \geq 0, R_{h0} \geq 0, S_{m0} > 0, I_{m0} \geq 0, M_{a0} \geq 0. \tag{4.2}$$

Increasing media-awareness promotes insecticide application for mosquito control which is modeled by the terms $\frac{\gamma M_a S_m}{1+M_a}$ and $\frac{\gamma M_a I_m}{1+M_a}$. Initially, insecticide application is low due to limited media-awareness contribution, but it approaches maximum application rate γ as awareness saturates. At full awareness, insecticide application reaches its maximum, removing $-\gamma S_m$ and $-\gamma I_m$ from the mosquito population, consistent with the spraying strategy described in (Basir et al., 2018).

Remark 1. *All state variables and parameters listed in Table 4.1 adhere to the conditions stipulated in the model (4.1). It is assumed that all parameters are non-negative.*

4.2 Model analysis

This section examines key properties of the model, including solution positivity and boundedness, the existence of equilibrium points, and their local and global stability.

4.2.1 Existence and Uniqueness of Solutions

Theorem 4.2.1 (Existence and Uniqueness)**.** *Consider the initial value problem (4.1) for the malaria transmission model defined by the system:*

$$\frac{d\mathbf{X}}{dt} = \mathbf{F}(\mathbf{X}), \quad \mathbf{X}(0) = \mathbf{X}_0,$$

where

Table 4.1: Model parameters, state variables, and their biological meanings.

Parameters	Descriptions	unit
Π_h	recruitment rate to susceptible humans	day^{-1}
ε	rate of immunity loss	day^{-1}
b	a constant proportion of newly recruited susceptible humans	unit-less
κ	rate of unaware susceptible become aware susceptible	day^{-1}
d	rate of aware susceptible become unaware susceptible	day^{-1}
β_1	transmission rate from $I_m(t)$ to $S_{ah}(t)$	day^{-1}
β_2	transmission rate from $I_m(t)$ to $S_{uh}(t)$	day^{-1}
μ_h	natural death rate of humans	day^{-1}
ρ	infectious treatment rate	day^{-1}
δ	malaria-induced death rate	day^{-1}
η	treated humans recovery rate	day^{-1}
φ	treatment failure death rate	day^{-1}
Π_m	mosquitoes constant recruitment rate	day^{-1}
γ	insecticide usage rate	day^{-1}
β_3	transmission rate from $I_h(t)$ to $S_m(t)$	day^{-1}
μ_m	natural death rate of mosquitoes	day^{-1}
π	rise of awareness level	day^{-1}
ξ	progress of awareness due to media awareness efficacy	day^{-1}
ϑ	fading of memory of awareness	day^{-1}

$$\mathbf{X}(t) = \begin{pmatrix} S_{ah} \\ S_{uh} \\ I_h \\ T_h \\ R_h \\ S_m \\ I_m \\ M_a \end{pmatrix}, \qquad \mathbf{F}(\mathbf{X}) = \begin{pmatrix} b\Pi_h + \kappa S_{uh} M_a - \dfrac{dS_{ah}}{1+M_a} - \dfrac{\beta_1 S_{ah} I_m}{N_h} + \varepsilon R_h - \mu_h S_{ah} \\ (1-b)\Pi_h + \dfrac{dS_{ah}}{1+M_a} - \kappa S_{uh} M_a - \dfrac{\beta_2 S_{uh} I_m}{N_h} - \mu_h S_{uh} \\ \dfrac{\beta_1 S_{ah} I_m}{N_h} + \dfrac{\beta_2 S_{uh} I_m}{N_h} - (\rho + \delta + \mu_h) I_h \\ \rho I_h - (\eta + \varphi + \mu_h) T_h \\ \eta T_h - (\mu_h + \varepsilon) R_h \\ \Pi_m - \dfrac{\beta_3 I_h S_m}{N_h} - \dfrac{\gamma S_m M_a}{1+M_a} - \mu_m S_m \\ \dfrac{\beta_3 I_h S_m}{N_h} - \dfrac{\gamma I_m M_a}{1+M_a} - \mu_m I_m \\ \pi + \xi I_h - \vartheta M_a \end{pmatrix}$$

with $N_h = S_{ah} + S_{uh} + I_h + T_h + R_h$, $N_m = S_m + I_m$, *and initial conditions satisfying* $\mathbf{X}_0 \in \mathbb{R}^8_+$.

Assume that all the parameters are positive constants and the initial conditions satisfy $\mathbf{X}_0 \in$

Ω, *where* Ω *is the biologically feasible region defined by:*

$$\Omega = \left\{ \left(S_{ah}, S_{uh}, I_h, T_h, R_h, S_m, I_m, M_a\right) \in R_+^8 : 0 \leq N_h \leq \frac{\Pi_h}{\mu_h}, 0 \leq N_m \leq \frac{\Pi_m}{\mu_m}, 0 \leq M_a \leq \frac{\pi\mu_h + \xi\Pi_h}{\mu_h \vartheta} \right\}.$$

Then the governing model (4.1) *admits a unique, nonnegative, and bounded solution* $\mathbf{X}(t)$ *that exists for all time* $t \geq 0$ *and remains in the region* Ω.

Proof. We establish the result as follows. Note that the function $\mathbf{F}(\mathbf{X})$ is continuously differentiable with respect to all state variables in $\mathbb{R}_+^8$, provided $N_h > 0$. Since $\mathbf{F}$ and its Jacobian matrix are continuous on the closed, bounded set Ω, they satisfy a Lipschitz condition inside Ω. By the Picard-Lindelöf theorem (Coddington et al., 1956), there exists a unique local solution $\mathbf{X}(t)$ on some maximal interval of existence $[0, t_{\max})$. The derivative of the vector field $\mathbf{F}$ is also nonnegative, for each state variable, when it approaches zero. That is,

$$\left.\frac{dS_{ah}}{dt}\right|_{S_{ah}=0} = (1-\sigma)\Pi_h + \frac{dS_{ah}}{1+M_a} > 0, \quad \left.\frac{dS_{uh}}{dt}\right|_{S_{uh}=0} = (1-b)\Pi_h + \frac{dS_{ah}}{1+M_a} \geq 0,$$

and similarly for other compartments. Thus, by the invariance principle for cooperative systems (Salle, 1966), solutions starting in the nonnegative orthant $\mathbb{R}_+^8$ remain nonnegative for all $t \geq 0$.

Next, define the total human population $N_h(t) = S_{ah}(t) + S_{uh}(t) + I_h(t) + T_h(t) + R_h(t)$. Adding the first five equations yields:

$$\frac{dN_h}{dt} = \Pi_h - \mu_h N_h - \delta I_h - \varphi T_h, \tag{4.3}$$

Since $I_h > 0$ and $T_h > 0$, we have

$$\frac{dN_h}{dt} \leq \Pi_h - \mu_h N_h.$$

Solving the inequality yields,

$$N_h(t) \leq N_h(0)\exp(-\mu_h t) + \frac{\Pi_h}{\mu_h}\left(1 - \exp(-\mu_h t)\right)$$

This implies,

$$\limsup_{t\to\infty} N_h(t) \leq \frac{\Pi_h}{\mu_h}.$$

Consequently, we have

$$0 \leq +N_h \leq \frac{\Pi_h}{\mu_h}. \tag{4.4}$$

Similarly, the total mosquito population as $N_m = S_m + I_m$. The time derivative of N_m gives

$$\frac{dN_m}{dt} = \Pi_m - \Big(\frac{\gamma M_a}{1+M_a} + \mu_m\Big)N_m. \tag{4.5}$$

$$\frac{dN_m}{dt} \leq \Pi_m - \mu_m N_m. \tag{4.6}$$

From this inequality, we deduce that,

$$\limsup_{t\to\infty} N_m(t) \leq \frac{\Pi_m}{\mu_m}.$$

Consequently, we have

$$0 \leq S_m + I_m \leq \frac{\Pi_m}{\mu_m}. \tag{4.7}$$

Following the same procedure, it is evident that

$$0 \leq M_a \leq \frac{\pi\mu_h + \xi\Pi_h}{\mu_h\vartheta}. \tag{4.8}$$

Thus, all state variables remain uniformly bounded on any finite time interval. Since the right-hand side $\mathbf{F}$ is Lipschitz continuous on Ω and solutions remain bounded, by the continuation theorem for ordinary differential equations (Hirsch, 1974), the local solution can be extended to all $t \geq 0$. Specifically, the boundedness of solutions prevents finite-time blow-up, ensuring global existence.

From the bounds derived above, it follows directly that if $\mathbf{X}(0) \in \Omega$, then $\mathbf{X}(t) \in \Omega$ for all $t \geq 0$. Thus, Ω is positively invariant (Hale, 2009). Therefore, by combining the Picard-Lindelöf theorem, and the continuation principle, we conclude that the model equations (4.1) has a unique, nonnegative, bounded solution that exists globally in time and remains within the biologically feasible region Ω. □

4.2.2 Malaria-free equilibrium (MFE)

A malaria-free equilibrium (MFE), denoted by $\mathcal{E}_0$, is a steady-state solution in which malaria transmission is completely absent from both the human and mosquito populations. To determine $\mathcal{E}_0$, we set $I_h = I_m = 0$ and solve the remaining model equations in (4.1) by equating them to

zero.

$$
\begin{aligned}
&b\Pi_h + \kappa S_{uh} M_a - \frac{dS_{ah}}{1+M_a} - \frac{\beta_1 S_{ah} I_m}{N_h} + \varepsilon R_h - \mu_h S_{ah} = 0 \\
&(1-b)\Pi_h + \frac{dS_{ah}}{1+M_a} - \kappa S_{uh} M_a - \frac{\beta_2 S_{uh} I_m}{N_h} - \mu_h S_{uh} = 0 \\
&\frac{\beta_1 S_{ah} I_m}{N_h} + \frac{\beta_2 S_{uh} I_m}{N_h} - (\rho + \delta + \mu_h) I_h = 0 \\
&\rho I_h - (\eta + \varphi + \mu_h) T_h = 0 \\
&\eta T_h - (\mu_h + \varepsilon) R_h = 0 \\
&\Pi_m - \frac{\beta_3 I_h S_m}{N_h} - \frac{\gamma S_m M_a}{1+M_a} - \mu_m S_m = 0 \\
&\frac{\beta_3 I_h S_m}{N_h} - \frac{\gamma I_m M_a}{1+M_a} - \mu_m I_m = 0 \\
&\pi + \xi I_h - \vartheta M_a = 0
\end{aligned}
$$

Solving the resulting steady-state system yields:

$$
\mathcal{E}_0 = \left(S_{ah}^0, S_{uh}^0, 0, 0, 0, S_m^0, 0, M_a^0 \right), \tag{4.9}
$$

where

$$
\begin{aligned}
&S_{ah}^0 = \frac{(\pi+\vartheta)(\pi\kappa + b\vartheta\mu_h)\Pi_h}{\mu_h(d\vartheta^2 + \pi(\pi+\vartheta)\kappa + \theta(\pi+\vartheta)\mu_h}, \quad S_{uh}^0 = \frac{\vartheta(d\vartheta + (1-b)(\vartheta+\pi)\mu_h)\Pi_h}{\mu_h(d\vartheta^2 + \pi(\pi+\vartheta)\kappa + \theta(\pi+\vartheta)\mu_h)}, \\
&S_m^0 = \frac{\Pi_m}{\gamma + \mu_m} \quad \text{and} \quad M_a^0 = \frac{\pi}{\vartheta}.
\end{aligned} \tag{4.10}
$$

4.2.3 Basic reproduction number

The basic reproduction number, $\mathfrak{R}_0$, is a key threshold parameter in epidemiological modeling, representing the average number of secondary infections generated by a single infectious individual in a wholly susceptible population (Heesterbeek & Dietz, 1996; Heffernan et al., 2005). To compute $\mathfrak{R}_0$ for model (4.1), we apply the next-generation matrix method (Van den Driessche & Watmough, 2002) with infected compartments I_h and I_m. Accordingly, the new infection vector is denoted by $\mathcal{F}$ and the transition vector by $\mathcal{V}$

$$
\mathcal{F} = \begin{pmatrix} \frac{\beta_1 S_{ah} I_m}{N_h} + \frac{\beta_2 S_{uh} I_m}{N_h} \\ \frac{\beta_3 I_h S_m}{N_h} \end{pmatrix}, \mathcal{V} = \begin{pmatrix} (\rho + \delta + \mu_h) I_h \\ \gamma I_m + \mu_m I_m \end{pmatrix}. \tag{4.11}
$$

The corresponding Jacobian matrices of vectors $\mathcal{F}$ and $\mathcal{V}$ at MFE respectively become F and V as

$$F=\left[\frac{\partial \mathcal{F}_i(\mathcal{E}_0)}{\partial(I_h,I_m)}\right]=\begin{pmatrix} 0 & \frac{\beta_1 S^0_{ah}}{S^0_{ah}+S^0_{uh}}+\frac{\beta_2 S^0_{uh}}{S^0_{ah}+S^0_{uh}} \\ \frac{\beta_3 S^0_m}{S^0_{ah}+S^0_{uh}} & 0 \end{pmatrix}, \text{ and } V=\left[\frac{\partial \mathcal{V}_i(\mathcal{E}_0)}{\partial(I_h,I_m)}\right]=\begin{pmatrix} \rho+\delta+\mu_h & 0 \\ 0 & \mu_m+\gamma \end{pmatrix}.$$

Thus, we can show that

$$FV^{-1}=\begin{pmatrix} 0 & \frac{\beta_1 S^0_{ah}+\beta_2 S^0_{uh}}{(\mu_m+\gamma)(S^0_{ah}+S^0_{uh})} \\ \frac{\beta_3 S^0_m}{(\rho+\delta+\mu_h)\left(S^0_{ah}+S^0_{uh}\right)} & 0 \end{pmatrix}. \tag{4.12}$$

Therefore, the basic reproduction number $\mathfrak{R}_0$ of system (4.1) is given by the dominating eigenvalue of the matrix FV^{-1}. Thus, we obtain,

$$\mathfrak{R}_0=\sqrt{\frac{\beta_1\mu_h(\pi+\vartheta)(\pi\kappa+b\vartheta\mu_h)+\mu_h\vartheta\beta_2(d\vartheta+(1-b)(\pi+\vartheta)\mu_h)}{(\rho+\delta+\mu_h)\left(d\vartheta^2+\pi(\pi+\vartheta)\kappa+\vartheta(\pi+\vartheta)\mu_h\right)\Pi_h}}\sqrt{\frac{\beta_3\Pi_v}{(\gamma+\mu_m)^2}}=\sqrt{\mathfrak{R}_h}\sqrt{\mathfrak{R}_v}, \tag{4.13}$$

where

$$\mathfrak{R}_h=\frac{\beta_1\mu_h(\pi+\vartheta)(\pi\kappa+b\vartheta\mu_h)+\mu_h\vartheta\beta_2(d\vartheta+(1-b)(\pi+\vartheta)\mu_h)}{(\rho+\delta+\mu_h)\left(d\vartheta^2+\pi\kappa(\pi+\vartheta)+\vartheta(\pi+\vartheta)\mu_h\right)\Pi_h} \quad \textit{and} \quad \mathfrak{R}_v=\frac{\beta_3\Pi_v}{(\gamma+\mu_m)^2}.$$

Here, $\mathfrak{R}_0$ is expressed as a geometric mean because malaria transmission proceeds through two sequential stages-human-to-mosquito and mosquito-to-human. Each stage contributes its own reproduction factor, and a complete transmission cycle requires the successful occurrence of both. The term $\mathfrak{R}_h$ denotes the average number of humans infected by a single infectious mosquito, assuming full human susceptibility, while $\mathfrak{R}_v$ denotes the average number of mosquitoes infected by a single infectious human, assuming full mosquito susceptibility.

In equation (4.13), the expressions $\frac{1}{\rho+\delta+\mu_h}$ and $\frac{1}{\gamma+\mu_m}$ correspond to the average infectious period of humans and mosquitoes, respectively. The terms $\frac{\beta_1}{\alpha_0}$ and $\frac{\vartheta\beta_2}{\alpha_0}$, where $\alpha_0=\frac{\mu_h}{d\vartheta^2+\pi(\pi+\vartheta)\kappa+\vartheta(\pi+\vartheta)\mu_h}$, respectively indicate the probabilities of typical aware and unaware susceptible individuals coming into contact with infected mosquitoes. Additionally, the term $\frac{\beta_3}{\gamma+\mu_m}$ represents the probability that a typical susceptible mosquito contacts infected humans.

4.2.4 Local Stability of the malaria-free equilibrium point

The Jacobian matrix evaluated at an equilibrium point $\mathcal{E} = \left(S_{ah}^*, S_{uh}^*, I_h^*, T_h^*, R_h^*, S_m^*, I_m^*, M_a^*\right)$ is given by

$$J(\mathcal{E}) = \left[J_{ij}\right]_{8\times 8} \tag{4.14}$$

from which each entries are listed below

$$J_{11} = -\left(\mu_h + \frac{d}{1+M_a}\right) + J_{13} - \frac{\beta_1 I_m}{N_h}, \qquad J_{12} = \kappa M_a + J_{13} J_{13} = J_{14} = \frac{\beta_1 S_{ah} I_m}{N_h^2},$$

$$J_{15} = \varepsilon + J_{13}, \quad J_{16} = 0, \quad J_{17} = -\frac{\beta_1 S_{ah}}{N_h}, \quad J_{18} = \kappa S_{uh} + \frac{d S_{ah}}{(1+M_a)^2}, \quad J_{21} = \frac{d}{(1+M_a)^2} + J_{23},$$

$$J_{22} = -(\kappa M_a + \mu_h) + J_{23} - \frac{\beta_2 I_m}{N_h}, \quad J_{23} = J_{24} = J_{25} = \frac{\beta_2 S_{uh} I_m}{N_h^2}, \quad J_{26} = 0, \quad J_{27} = -\frac{\beta_2 S_{uh}}{N_h},$$

$$J_{28} = -\kappa S_{uh} - \frac{d S_{ah}}{(1+M_a)^2}, \quad J_{31} = J_{32} = -J_{13} + \frac{\beta_1 I_m}{N_h} - J_{23}, \quad J_{33} = -(\rho + \delta + \mu_h) - (J_{13+J_{23}}),$$

$$J_{34} = J_{35} = -(J_{13} + J_{23}), \quad J_{36} = 0, \quad J_{37} = \frac{\beta_1 S_{ah}}{N_h} + \frac{\beta_2 S_{uh}}{N_h}, \quad J_{38} = 0, \quad J_{41} = J_{42} = 0,$$

$$J_{43} = \rho, \quad J_{44} = -(\eta + \varphi + \mu_h), \quad J_{45} = J_{46} = J_{47} = J_{48} = 0, \quad J_{51} = J_{52} = J_{53} = 0,$$

$$J_{54} = \eta, \quad J_{55} = -(\varepsilon + \mu_h), \quad J_{56} = J_{57} = J_{58} = 0, \quad J_{61} = J_{62} = J_{64} = J_{65} = \frac{\beta_3 S_m I_h}{N_h^2},$$

$$J_{63} = J_{61} - \frac{\beta_1 S_m}{N_h}, \quad J_{66} = -(\gamma + \mu_m) - \frac{\beta_3 I_h}{N_h}, \quad J_{67} = J_{68} = 0, \quad J_{71} = J_{72} = J_{74} = J_{75} = -J_{61},$$

$$J_{73} = -J_{61} + \frac{\beta_3 S_m}{N_h} = -J_{63}, \quad J_{76} = \frac{\beta_3 I_m}{N_h}, \quad J_{77} = -(\gamma + \mu_m), \quad J_{78} = 0, \quad J_{81} = J_{82} = 0,$$

$$J_{83} = \xi, \quad J_{84} = J_{85} = J_{86} = J_{87} = 0, \quad J_{88} = -\vartheta.$$

Theorem 4.2.2. *The MFE point of the system (4.1) is locally asymptotically stable in* Ω *if* $\mathfrak{R}_0 < 1$ *and unstable if* $\mathfrak{R}_0 > 1$.

Proof. We investigate the local stability of the system (4.1) at $\mathcal{E}_0$ by using the Jacobian matrix approach. At the malaria-free equilibrium point $\mathcal{E}_0$, the Jacobean matrix $J(\mathcal{E}_0)$ of (4.1) is

provided as follows:

$$\begin{pmatrix} -\frac{d}{1+M_a^0}-\mu_h & \kappa M_a^0 & 0 & 0 & \varepsilon & 0 & -\frac{\beta_1 S_{ah}^0}{N_h^0} & \frac{d\kappa S_{uh}^0}{(1+M_a^0)^2}+\kappa S_{uh}^0 \\ \frac{d}{1+M_a^0} & -\kappa M_a^0-\mu_h & 0 & 0 & 0 & 0 & -\frac{\beta_2 S_{ah}^0}{N_h^0} & -\frac{d\kappa S_{uh}^0}{(1+M_a^0)^2}-\kappa S_{uh}^0 \\ 0 & 0 & -\rho-\delta-\mu_h & 0 & 0 & 0 & \frac{\beta_1 S_{ah}^0+\beta_2 S_{uh}^0}{N_h^0} & 0 \\ 0 & 0 & \rho & -\eta-\varphi-\mu_h & 0 & 0 & 0 & 0 \\ 0 & 0 & 0 & \eta & -\varepsilon-\mu_h & 0 & 0 & 0 \\ 0 & 0 & -\frac{\beta_3 S_m^0}{N_h^0} & 0 & 0 & -\gamma-\mu_m & 0 & 0 \\ 0 & 0 & \frac{\beta_3 S_m^0}{N_h^0} & 0 & 0 & 0 & -\gamma-\mu_m & 0 \\ 0 & 0 & \xi & 0 & 0 & 0 & 0 & -\vartheta \end{pmatrix},$$

where values for $S_{uh}^0, S_{uh}^0, S_m^0$ and M_a^0 are given in Section (4.2.2). We want to show that each the eigenvalues of matrix $J(\mathcal{E}_0)$ has negative sign. The matrix $J(\mathcal{E}_0)$ is an upper triangular block diagonal matrix. Its eigenvalues are the eigenvalues of first and fourth block sub-matrices. Here, λ_1 and λ_2 are the eigenvalues obtained from the first block matrix denoted by sub matrix $J_1(\mathcal{E}_0)$ and the remaining eigenvalues $\lambda_i, i = 3,4,5,6,7,8$ can be easily obtained from the fourth block sub matrix $J_4(\mathcal{E}_0)$. Sign of λ_1 and λ_2 is determined by the sign analysis of trace (Tr) and determinant (Det) of $J_1(\mathcal{E}_0)$.

$$J_1(\mathcal{E}_0) = \begin{pmatrix} -\frac{d}{1+M_a^0}-\mu_h & \kappa M_a^0 \\ \frac{d}{1+M_a^0} & -\kappa M_a^0-\mu_h \end{pmatrix}. \tag{4.15}$$

That is, $Tr\big(J_1(\mathcal{E}_0)\big) = -(\frac{d}{1+M_a^0}+\kappa M_a^0+\mu_h) < 0$, and $Det\big(J_1(\mathcal{E}_0)\big) = \mu_h(\frac{d}{1+M_a^0}+\kappa M_a^0+\mu_h) > 0$. Hence, the eigenvalues $\lambda_1 < 0$ and $\lambda_2 < 0$. From sub-matrix $J_4(\mathcal{E}_0)$, we have $\lambda_4 = -(\varphi+\eta+\mu_h) < 0, \lambda_5 = -(\varepsilon+\mu_h) < 0, \lambda_6 = -(\gamma+\mu_m) < 0, \lambda_8 = -\vartheta$ and the remaining eigenvalues λ_3 and λ_7 are the eigenvalues sub block diagonal matrix of the $J_4(\mathcal{E}_0)$ which is denoted by matrix B such that

$$B = \begin{pmatrix} -(\rho+\delta+\mu_h) & \frac{\beta_1 S_{ah}^0+\beta_2 S_{uh}^0}{N_h^0} \\ \frac{\beta_3 S_m^0}{N_h^0} & -(\gamma+\mu_m) \end{pmatrix}. \tag{4.16}$$

Similarly, we have $Tr(B) = -(\rho+\delta+\mu_h+\gamma+\mu_m) < 0$ and

$$det(B) = (\rho+\delta+\mu_h)(\gamma+\mu_h) - \Big(\frac{\beta_1 S_{ah}^0+\beta_2 S_{uh}^0}{N_h^0}\Big)\frac{\beta_3 S_m^0}{N_h^0} = (\rho+\delta+\mu_h)(\gamma+\mu_m)(1-\mathfrak{R}_0^2).$$

Clearly, $\det(B) > 0$ for $\mathfrak{R}_0 < 1$. This implies that λ_3 and $\lambda_7 < 0$. For this reason, all the eigenvalues of the Jacobian matrix $J(\mathcal{E}_0)$ have negative real parts and the $\mathcal{E}_0$ is locally asymptotically stable in Ω if $\mathfrak{R}_0 < 1$. □

Remark 2. *From an epidemiological perspective, malaria can be eliminated from a community when* $\mathfrak{R}_0 < 1$. *If* $\mathfrak{R}_0 < 1$, *it implies that, on average, a single infected individual generates fewer than one new infected individual over its infectious period, leading to the eventual extinction of the infection.*

4.2.5 Global stability of malaria free equilibrium Point

In this subsection we adopt the method described by Castillo-Chavez & Song (2004); Kanyi et al. (2021) to show the global asymptotically stability (GAS) of the MFE. The malaria model (4.1) is then rewritten as follows:

$$\begin{cases} \frac{dH}{dt} = F(H,Z) \\ \frac{dZ}{dt} = G(H,Z), \quad G(H,0) = 0 \end{cases} \tag{4.17}$$

in which $H = (S_{ah}, S_{uh}, R_h, S_m, M_a) \in \mathbb{R}^{+5}$ and $Z = (I_h, T_h, I_m) \in \mathbb{R}^{+3}$ stand for non-infected and infected compartments, respectively. Furthermore, $\mathcal{E}^0 = (H^0, 0) = \left(S^0_{ah}, S^0_{uh}, 0, S^0_m, M^0_a, 0, 0, 0\right)$ denotes the malaria free equilibrium of the new system. Assume that

(H_1) $\frac{dH}{dt} = F(H,0)$, $\quad H^0$ is globally asymptotically stable.

(H_2) $G(H,Z) = AZ^T - \hat{G}(H,Z)$, $\quad \hat{G}(H,Z) \geq 0$ for all $(H,Z) \in \Omega$ where the off-diagonal entries of the community matrix A is non-negative (A is a Metzler-matrix) and the model makes biological sense in Ω. Then $\mathcal{E}_0$ is globally asymptotically stable on the assumption that $\mathfrak{R}_0 < 1$.

Based on the aforementioned finding, we can derive the following theorem for the model (4.1).

Theorem 4.2.3. *The malaria-free equilibrium point* $\mathcal{E}_0$ *of the model (4.1) is a globally asymptotic stable (G.A.S.) if* $\mathfrak{R}_0 < 1$ *and that assumptions* (H_l) *and* (H_2) *hold true.*

Proof. To show that malaria-free equilibrium point $\mathcal{E}_0$ is GAS when $\mathfrak{R}_0 < 1$, we have to verify the condition H_1 and H_2 holds true. Now the two vector-valued functions $F(H,Z)$ and $G(H,Z)$ are given as:

$$F(H,Z) = \begin{pmatrix} b\Pi_h + \kappa S_{uh} M_a - \frac{dS_{ah}}{1+M_a} - \frac{\beta_1 S_{ah} I_m}{N_h} + \varepsilon R_h - \mu_h S_{ah} \\ (1-b)\Pi_h - \kappa S_{uh} M_a + \frac{dS_{ah}}{1+M_a} - \frac{\beta_2 S_{uh} I_m}{N_h} - \mu_h S_{uh} \\ \rho I_h - (\eta + \varphi + \mu_h) T_h \\ \eta T_h - (\mu_h + \varepsilon) R_h \\ \Pi_m - \frac{\beta_3 I_h S_m}{N_h} - \frac{\gamma S_m M_a}{1+M_a} - \mu_m S_m \\ \pi + \xi I_h - \vartheta M_a, \end{pmatrix}, G(H,Z) = \begin{pmatrix} \frac{\beta_1 S_{ah} I_m}{N_h} + \frac{\beta_2 S_{uh} I_m}{N_h} - (\rho + \delta + \mu_h) I_h \\ \frac{\beta_3 I_h S_m}{N_h} - (\gamma + \mu_m) I_m \end{pmatrix}.$$

Now we consider about the reduced systems

$$\frac{dH}{dt} = F(H,0) \iff \begin{cases} \dot{S_{ah}} = b\Pi_h + \kappa S_{uh} M_a - \frac{dS_{ah}}{1+M_a} + \varepsilon R_h - \mu_h S_{ah} \\ \dot{S_{uh}} = (1-b)\Pi_h - \kappa S_{uh} M_a + \frac{dS_{ah}}{1+M_a} - \mu_h S_{uh} \\ \dot{T_h} = -(\eta + \varphi + \mu_h) T_h \\ \dot{R_h} = -(\mu_h + \varepsilon) R_h \\ \dot{S_m} = \Pi_m - (\gamma + \mu_m) S_m \\ \dot{M_a} = \pi - \vartheta M_a, \end{cases} \tag{4.18}$$

has unique equilibrium point $\mathcal{E}^0 = (H^0, 0)$ where,

$$(H^0,0) = \left(\frac{(\pi+\vartheta)(\pi\kappa + b\vartheta\mu_h)\Pi_h}{\mu_h(d\vartheta^2 + \pi(\pi+\vartheta)\kappa + \theta(\pi+\vartheta)\mu_h}, \frac{\vartheta\mu_h(d\vartheta + (1-b)(\vartheta+\pi))\Pi_h}{\mu_h(d\vartheta^2 + \pi(\pi+\vartheta)\kappa + \theta(\pi+\vartheta)\mu_h)}, 0, \frac{\Pi_m}{\mu_m+\gamma}, \frac{\pi}{\vartheta}, 0, 0, 0 \right).$$

It is noted that the third, fourth and the fifth equations of system of ODEs given in equation (4.18) are linear, and their solutions are given by,

$$\begin{cases} T_h(t) = T_{h0} e^{-(\eta+\varphi+\mu_h)t} \\ R_h(t) = R_{h0} e^{-(\mu_h+\varepsilon)t} \\ S_m(t) = S_{v0} e^{-(\gamma+\mu_m)t} + \frac{\Pi_m}{\gamma+\mu_m}\left(1 - e^{-(\gamma+\mu_m)t}\right) \\ M_a(t) = M_{a0} e^{-\vartheta t} + \frac{\pi}{\vartheta}\left(1 - e^{-\vartheta t}\right). \end{cases} \tag{4.19}$$

Now, assume that as time goes to infinity, the solutions of $R_h(t), S_m(t)$ and $M_a(t)$ converges to

$$T_h(t) \to 0, R_h(t) \to 0,\ S_m(t) \to \frac{\Pi_m}{\gamma+\mu_m} \text{ and } M_a(t) \to \frac{\pi}{\vartheta}.$$

Since the first and the second equation of the system $\frac{dH}{dt} = F(H,0)$ are coupled, we can solve them easily by considering solution $R_h(t) = 0$ and $M_a(t) = \frac{\pi}{\vartheta}$. Thus, we can determine the solutions of $S_{ah}(t)$ and $S_{uh}(t)$ as

$$\begin{cases} S_{ah}(t) = S_{ah}(0) e^{-C_1 t} + \frac{(b\mu_h + \kappa M_a)(1+M_a)\Pi_h}{\mu_h((1+M_a)(\kappa M_a + \mu_h) + d)}(1 - e^{-C_1 t}) \\ S_{uh}(t) = S_{uh}(0) e^{-C_2 t} + \frac{(1+M_a)((1-b)\mu_h\Pi_h(1+M_a) + d\Pi_h)}{\mu_h(1+M_a)\left(\kappa M_a(1+M_a) + d + \mu_h(1+M_a)\right)}(1 - e^{-C_2 t}) \\ T_h(t) = T_{h0} e^{-(\eta+\varphi+\mu_h)t} \\ R_h(t) = R_h(t)(0) e^{-(\mu_h+\varepsilon)t} \\ S_m(t) = \frac{\Pi_m}{\gamma+\mu_m}(1 - e^{-(\gamma+\mu_m)t}) \\ M_a(t) = M_{a0} e^{-\vartheta t} + \frac{\pi}{\vartheta}\left(1 - e^{-\vartheta t}\right) \end{cases} \tag{4.20}$$

where $C_2 = \frac{\kappa M_a(1+M_a) + d + \mu_h(1+M_a)}{1+M_a}$, $\quad C_1 = \frac{(1+M_a)(\kappa M_a + \mu_h) + d}{1+M_a}$ and $M_a(t)$ is constant solution and

it takes value $M_a(t) = \frac{\pi}{\vartheta}$. By substituting the constants C_1, C_2, and $M_a(t)$ into equation (4.20), we get

$$\begin{cases} S_{ah}(t) = S_{ah}(0)e^{-C_1 t} + \frac{(\pi+\vartheta)(\pi\kappa+b\vartheta\mu_h)\Pi_h}{\mu_h(d\vartheta^2+\pi(\pi+\vartheta)\kappa+\theta(\pi+\vartheta)\mu_h}(1-e^{-C_1 t}) \\ S_{uh}(t) = S_{uh}(0)e^{-C_2 t} + \frac{\vartheta\mu_h(d\vartheta+(1-b)(\vartheta+\pi))\Pi_h}{\mu_h(d\vartheta^2+\pi(\pi+\vartheta)\kappa+\theta(\pi+\vartheta)\mu_h)}(1-e^{-C_2 t}) \\ T_h(t) = T_{h0}e^{-(\eta+\varphi+\mu_h)t} \\ R_h(t) = R_h(t)(0)e^{-(\mu_h+\varepsilon)t} \\ S_m(t) = \frac{\Pi_m}{\gamma+\mu_m}(1-e^{-(\gamma+\mu_m)t}). \\ M_a(t) = M_{a0}e^{-\vartheta t} + \frac{\pi}{\vartheta}\left(1-e^{-\vartheta t}\right) \end{cases} \tag{4.21}$$

Clearly, the solutions $\left(S_{ah}(t), S_{uh}(t), T_h(t), R_h(t), S_m(t), M_a(t)\right) \to \left(S^0_{ah}, S^0_{uh}, 0, 0, S^0_m, M^0_a\right) = H^0$ as $t \to \infty$. Thus, H^0 is globally asymptotically stable. Hence, MFE is globally asymptotically stable given that $\mathfrak{R}_0 < 1$. First we determine that $G(H,Z) = AZ^T - \hat{G}(H,Z)$. Subsequently, we show that $\hat{G}(H,Z) \geq 0$.

$$A = \frac{\partial G(H_0,0)}{\partial Z} = \begin{pmatrix} -(\rho+\delta+\mu_h) & 0 & \frac{\beta_1 S^0_{ah}+\beta_2 S^0_{uh}}{S^0_{ah}+S^0_{uh}} \\ \frac{\beta_3 S^0_m}{S^0_{ah}+S^0_{uh}} & 0 & -(\gamma+\mu_m) \end{pmatrix}, \tag{4.22}$$

then we have

$$\hat{G}(H,Z) = \begin{pmatrix} -(\rho+\delta+\mu_h) & 0 & \frac{\beta_1 S^0_{ah}+\beta_2 S^0_{uh}}{S^0_{ah}+S^0_{uh}} \\ \frac{\beta_3 S^0_m}{S^0_{ah}+S^0_{uh}} & 0 & -(\gamma+\mu_m) \end{pmatrix} \begin{pmatrix} I_h \\ I_m \end{pmatrix} - \begin{pmatrix} \frac{\beta_1 S_{ah} I_m}{N_h} + \frac{\beta_2 S_{uh} I_m}{N_h} - (\rho+\delta+\mu_h)I_h \\ \frac{\beta_3 I_h S_m}{N_h} - (\gamma+\mu_m)I_m \end{pmatrix},$$

$$= \begin{pmatrix} (\frac{S^0_{ah}}{N^0_0} - \frac{S_{ah}}{N_h})\beta_1 I_m + (\frac{S^0_{uh}}{N^0_h} - \frac{S_{uh}}{N_h})\beta_2 I_m \\ \beta_3 I_h(\frac{S^0_m}{N^0_h} - \frac{S_m}{N_h}) \end{pmatrix}.$$

For the conditions $\frac{S^0_{ah}}{N^0_0} - \frac{S_{ah}}{N_h} \geq 0, \frac{S^0_{uh}}{N^0_h} - \frac{S_{uh}}{N_h} \geq 0$ and $\frac{S^0_m}{N^0_h} - \frac{S_m}{N_h} \geq 0$, vector $\hat{G}(H,Z) \geq 0$ for all $(H,Z) \in \Omega$. Therefore, the malaria-free equilibrium point $\mathcal{E}_0$ is globally asymptotically stable. □

4.2.6 Existence of malaria equilibrium point

In addition to the malaria-free equilibrium point, it was shown that model (4.1) has an malaria equilibrium point denoted by $\mathcal{E}_1$. Malaria equilibrium point is a positive state of steady-state solution where the disease continues to exist within the population.

$$\mathcal{E}_1 = \left(S^*_{ah}, S^*_{uh}, I^*_h, T^*_h, R^*_h, S^*_m, I^*_m, M^*_a\right),$$

each elements of its coordinate should satisfy the condition:
$S^*_{ah} > 0, S^*_{uh} > 0, I^*_h > 0, T^*_h > 0, R^*_h > 0, S^*_m > 0, I^*_m > 0, M^*_a > 0.$

Following the study introduced in (Roy et al., 2020), to determine the conditions for the existence of the malaria equilibrium, we begin by setting the first and third equations of system (4.1) to zero. This yields the following system of equations:

$$\begin{cases} I_m = -\frac{(d+\mu_h+\mu_h M_a)N_h}{\beta_1(1+M_a)} + \frac{(\varepsilon R_h+\kappa M_a S_{uh}+b\Pi_h)N_h}{\beta_1 S_{ah}} = F_1(S_{ah}, S_{uh}), \\ S_{ah} = -\frac{\beta_2 S_{uh}}{\beta_1} + \frac{(\rho+\delta+\mu_h)N_h I_h}{\beta_1 I_m} = F_2(S_{uh}, I_m). \end{cases} \tag{4.23}$$

We assess the solvability of the remaining system by analyzing the intersection of the graphs of the functions $I_m = F_1(S_{ah}, S_{uh})$ and $S_{ah} = F_2(S_{uh}, I_m)$ in the coordinate system (S_{ah}, S_{uh}, I_m). Both functions exhibit a clear decreasing and concave pattern, and they also satisfy the following conditions:

$$\begin{aligned} &\lim_{S_{ah}\to 0^+} F_1(S_{ah}, S_{uh}) = +\infty, \quad \lim_{I_m\to 0^+} F_2(S_{uh}, I_m) = +\infty, \\ &\lim_{S_{ah}\to +\infty} F_1(S_{ah}, S_{uh}) = -\infty, \lim_{I_m\to +\infty} F_2(S_{uh}, I_m) = -\beta_2 S_{uh}. \end{aligned} \tag{4.24}$$

We observe that the graphs of these functions intersect at a single point $(S^*_{ah}, S^*_{uh}, I^*_m)$ in the region $S_{ah} > 0, S_{uh} > 0, I_m > 0$ where the point S^*_{uh} is obtained by employing similar procedures to the second and third equations of system (4.1). Continuing this way, we set the six and seventh equations of model (4.1) equal to zero with the given value $I^*_m > 0$. Consequently, we derive $N^*_m = \frac{\Pi_m}{\gamma+\mu_m} > 0$. Since $N^*_m > I^*_m$, it follows that $S^*_m = \frac{\Pi_m}{\gamma+\mu_m} - I^*_m > 0$. By solving the seventh equation of model (4.1), we readily obtain $I^*_h > 0$. Lastly, setting the fourth, fifth, and sixth equations of model (4.1) to zero with values $I^*_m > 0$, we ascertain: $T^*_h = \frac{\rho I^*_h}{\eta+\varphi+\mu_h} > 0, R^*_h = \frac{\eta T^*_h}{\varepsilon+\mu_h} > 0, M^*_a = \frac{\pi+\xi I^*_h}{\vartheta} \geq 0$. Thus, we conclude that the malaria equilibrium

$$\mathcal{E}_1 = \left(S^*_{ah}, S^*_{uh}, I^*_h, T^*_h, R^*_h, S^*_m, I^*_m, M^*_a\right)$$

is positive and unique in the region $S^*_{ah} > 0, S^*_{uh} > 0, I^*_h > 0, T^*_h > 0, R^*_h > 0, S^*_m > 0, I^*_m > 0, M^*_a > 0$.

to the system complexity, the local stability of the malaria-endemic equilibrium $\mathcal{E}_1$ cannot be established analytically using the Jacobian eigenvalues or the Routh-Hurwitz criterion. Instead, the local asymptotic stability of $\mathcal{E}_1$ for $\mathfrak{R}_0 > 1$ is inferred from the forward bifurcation analysis and confirmed numerically for specific parameter values, as illustrated in Figure 4.2.

4.2.7 Bifurcation Analysis

In this subsection, we establish conditions for the parameters using Theorem 4.1 from (Castillo-Chavez & Song, 2004). To implement the center manifold theory, we reassign variables. For this we let
$S_{ah} = x_1, S_{uh} = x_2, I_h = x_3, T_h = x_4, R_h = x_5, S_m = x_6, I_m = x_7$ and $M_a = x_8$, then $N_h = x_1 + x_2 + x_3 + x_4 + x_5$ and $N_m = x_6 + x_7$. Using vector representation
$x = (x_1, x_2, x_3, x_4, x_5, x_6, x_7, x_8)^T$ and system (4.1) can be written compactly in the form

$$\frac{dx}{dt} = (f_1, f_2, f_3, f_4, f_5, f_6, f_7, f_8),$$

with

$$\begin{aligned}
\frac{dx_1}{dt} &= b\Pi_h + \kappa x_2 x_8 - \frac{dx_1}{1+x_8} - \frac{\beta_1 x_1 x_7}{x_1+x_2+x_3+x_4+x_5} + \varepsilon x_5 - \mu_h x_1 = f_1,\\
\frac{dx_2}{dt} &= (1-b)\Pi_h - \kappa x_2 x_8 + \frac{dx_1}{1+x_8} - \frac{\beta_2 x_2 x_7}{x_1+x_2+x_3+x_4+x_5} - \mu_h x_2 = f_2,\\
\frac{dx_3}{dt} &= \frac{\beta_1 x_1 x_7}{x_1+x_2+x_3+x_4+x_5} + \frac{\beta_2 x_2 x_7}{x_1+x_2+x_3+x_4+x_5} - (\rho+\delta+\mu_h)x_3 = f_3,\\
\frac{dx_4}{dt} &= \rho x_3 - (\eta+\varphi+\mu_h)x_4 = f_4,\\
\frac{dx_5}{dt} &= \eta x_4 - (\varepsilon+\mu_h)x_5 = f_5,\\
\frac{dx_6}{dt} &= \Pi_m - \frac{\beta_3 x_6 x_3}{x_1+x_2+x_3+x_4+x_5} - \frac{\gamma x_6 x_8}{1+x_8} - \mu_m x_6 = f_6,\\
\frac{dx_7}{dt} &= \frac{\beta_3 x_6 x_3}{x_1+x_2+x_3+x_4+x_5} - \frac{\gamma x_7 x_8}{1+x_8} - \mu_m x_7 = f_7,\\
\frac{dx_8}{dt} &= \pi + \xi x_3 - \vartheta x_8 = f_8.
\end{aligned} \tag{4.25}$$

We choose the rate of transmission $\beta_1^* = \beta_1$ when $\Re_0 = 1$. Then β_1^* can be determined as

$$\beta_1^* = \frac{(\rho+\delta+\mu_h)\left(d\vartheta^2 + \pi(\pi+\vartheta)\kappa + \vartheta(\pi+\vartheta)\mu_h\right)(\gamma+\mu_m)^2\Pi_h - \vartheta\beta_2\beta_3\mu_h\left(d\vartheta + (1-b)(\pi+\vartheta)\mu_h\right)\Pi_m}{\beta_3\mu_h(\pi+\vartheta)\left(\pi\kappa + b\vartheta\mu_h\right)\Pi_m}$$

Thus, the Jacobian matrix of system (4.1) evaluated at malaria free equilibrium point becomes

$$J(\mathcal{E}_0,\beta_1^*)=\begin{pmatrix} J_1 & J_2 & 0 & 0 & \varepsilon & 0 & J_3 & J_4 \\ J_5 & J_6 & 0 & 0 & 0 & 0 & J_7 & J_8 \\ 0 & 0 & -\rho-\delta-\mu_h & 0 & 0 & 0 & J_9 & 0 \\ 0 & 0 & \rho & -\eta-\varphi-\mu_h & 0 & 0 & 0 & 0 \\ 0 & 0 & 0 & \eta & -\varepsilon-\mu_h & 0 & 0 & 0 \\ 0 & 0 & J_{10} & 0 & 0 & -\gamma-\mu_m & 0 & 0 \\ 0 & 0 & -J_{10} & 0 & 0 & 0 & -\gamma-\mu_m & 0 \\ 0 & 0 & \xi & 0 & 0 & 0 & 0 & -\vartheta \end{pmatrix}, \quad (4.26)$$

where

$$\begin{aligned}
J_1 &= -\Big(\frac{d\vartheta}{\pi+\vartheta}+\mu_h\Big), \quad J_2=\frac{\pi\kappa}{\vartheta}, \quad J_3=-\frac{(\pi+\vartheta)\beta_1(\pi\kappa+b\vartheta\mu_h)}{d\vartheta^2+\pi(\pi+\vartheta)\kappa+\vartheta(\pi+\vartheta)\mu_h}, \\
J_4 &= \frac{\vartheta\left(\pi^2+2\pi\vartheta+(1+d)\vartheta^2\right)\kappa(d\vartheta+(1-b)(\pi+\vartheta)\mu_h)\Pi_h}{(\pi+\vartheta)^2\mu_h(d\vartheta^2+\pi(\pi+\vartheta)\kappa+\vartheta(\pi+\vartheta)\mu_h)}, \quad J_5=\frac{d\vartheta}{\pi+\vartheta}, \\
J_6 &= -\frac{\pi\kappa+\vartheta\mu_h}{\vartheta}, J_7=-\frac{\vartheta\beta_2(d\vartheta+(1-b)(\pi+\vartheta)\mu_h)}{d\vartheta^2+\pi(\pi+\vartheta)\kappa+\vartheta(\pi+\vartheta)\mu_h}, \\
J_8 &= -\frac{\vartheta\left(\pi^2+2\pi\vartheta+(1+d)\vartheta^2\right)\kappa(d\vartheta+(1-b)(\pi+\vartheta)\mu_h)\Pi_h}{(\pi+\vartheta)^2\mu_h(d\vartheta^2+\pi(\pi+\vartheta)\kappa+\vartheta(\pi+\vartheta)\mu_h)}, \\
J_9 &= \frac{(\pi+\vartheta)\beta_1(\pi\kappa+b\vartheta\mu_h)+\vartheta\beta_2(d\vartheta+(1-b)(\pi+\vartheta)\mu_h)}{d\vartheta^2+\pi(\pi+\vartheta)\kappa+\vartheta(\pi+\vartheta)\mu_h}, \\
J_{10} &= -\frac{\beta_3\mu_h\Pi_m}{(\gamma+\mu_m)\Pi_h}, \quad J_{11}=-J_{10}=\frac{\beta_3\mu_h\Pi_m}{(\gamma+\mu_m)\Pi_h}.
\end{aligned}$$

It can be shown that a right eigenvector associated with simple zero eigenvalue is

$Y=(y_1,y_2,y_3,y_4,y_5,y_6,y_7,y_8)^T$, where

$$\begin{aligned}
y_1 &= \frac{\varepsilon\eta(\pi+\vartheta)\rho(\pi\kappa+\vartheta\mu_h)}{\mu_h(\varepsilon+\mu_h)(\eta+\varphi+\mu_h)(d\vartheta^2+\pi(\pi+\vartheta)\kappa+\vartheta(\pi+\vartheta)\mu_h)}y_3>0, \\
y_2 &= -\frac{1}{J_6\xi}\Big(J_8\vartheta+\frac{J_7\xi\beta_3\Pi_m\mu_h}{\Pi_h(\gamma+\mu_m)^2}\Big)y_3>0, \quad y_3=y_3>0, \\
y_4 &= \frac{\rho}{\eta+\varphi+\mu_h}y_3>0, \quad y_5=\frac{\eta\rho}{(\varepsilon+\mu_h)(\eta+\varphi+\mu_h)}y_3>0, \\
y_6 &= -\frac{\beta_3\mu_h\Pi_m}{(\gamma+\mu_m)^2\Pi_h}y_3<0, \quad y_7=\frac{\beta_3\mu_h\Pi_m}{(\gamma+\mu_m)^2\Pi_h}y_3>0, \quad y_8=\frac{\xi}{\vartheta}y_3>0.
\end{aligned}$$

In the same way, the left eigenvector is given as $Z = (z_1, z_2, z_3, z_4, z_5, z_6, z_7, z_8)$ where,

$$
\begin{aligned}
&z_1 = 0, z_2 = 0, z_4 = 0, z_5 = 0, z_6 = 0, z_8 = 0,\\
&z_7 = z_7 > 0, z_3 = \frac{(\pi+\vartheta)\beta_1(\pi\kappa + b\vartheta\mu_h) + \vartheta\beta_2(d\vartheta + (1-b)(\pi+\vartheta)\mu_h)}{(\rho+\delta+\mu_h)\left(d\vartheta^2 + \pi(\pi+\vartheta)\kappa + \vartheta(\pi+\vartheta)\mu_h\right)} z_7 > 0.
\end{aligned}
$$

Next we shall compute the values of a and b. Since $z_1 = 0, z_2 = 0, z_4 = 0, z_5 = 0, z_6 = 0, z_8 = 0$, we only need to compute the partial derivatives of f_3 and f_7 at $\mathcal{E}_0$. For system (4.25) the associated non-zero partial derivative of f_3 and f_7 at $\mathcal{E}_0$ are given by

$$
\begin{aligned}
&\frac{\partial^2 f_3}{\partial x_1 \partial x_7} = \frac{\partial^2 f_3}{\partial x_7 \partial x_1} = \frac{\vartheta(\beta_1{}^* + \beta_2)\mu_h(d\vartheta + (1-b)(\pi+\vartheta)\mu_h)}{(d\vartheta^2 + \pi(\pi+\vartheta)\kappa + \vartheta(\pi+\vartheta)\mu_h)\Pi_h},\\
&\frac{\partial^2 f_3}{\partial x_2 \partial x_7} = \frac{\partial^2 f_3}{\partial x_7 \partial x_2} = \frac{(\pi+\vartheta)(\beta_1{}^* + \beta_2)\mu_h(\pi\kappa + b\vartheta\mu_h)}{(d\vartheta^2 + \pi(\pi+\vartheta)\kappa + \vartheta(\pi+\vartheta)\mu_h)\Pi_h},\\
&\frac{\partial^2 f_3}{\partial x_4 \partial x_x 7} = \frac{\partial^2 f_3}{\partial x_7 \partial x_4} = -\frac{\mu_h(\pi+\vartheta)\beta_1{}^*(\pi\kappa + b\vartheta\mu_h) + \vartheta\beta_2(d\vartheta + (1-b)(\pi+\vartheta)\mu_h))}{(d\vartheta^2 + \pi(\pi+\vartheta)\kappa + \vartheta(\pi+\vartheta)\mu_h)\Pi_h},\\
&\frac{\partial^2 f_3}{\partial x_5 \partial x_x 7} = \frac{\partial^2 f_3}{\partial x_7 \partial x_5} = -\frac{(\pi+\vartheta)\beta_1{}^*\mu_h(\pi\kappa + b\vartheta\mu_h)}{(d\vartheta^2 + \pi(\pi+\vartheta)\kappa + \vartheta(\pi+\vartheta)\mu_h)\Pi_h},\\
&\frac{\partial^2 f_7}{\partial x_1 \partial x_3} = \frac{\partial^2 f_7}{\partial x_3 \partial x_1} = -\frac{\beta_3\mu_h^2\Pi_m}{(\gamma+\mu_m)\Pi_h^2}, \quad \frac{\partial^2 f_7}{\partial x_2^2} = -\frac{\beta_3\mu_h^2\Pi_m}{(\gamma+\mu_m)\Pi_h^2}, \quad \frac{\partial^2 f_7}{\partial x_3^2} = -\frac{2\beta_3\mu_h^2\Pi_m}{(\gamma+\mu_m)\Pi_h^2},\\
&\frac{\partial^2 f_7}{\partial x_3 \partial x_4} = \frac{\partial^2 f_7}{\partial x_4 \partial x_3} = -\frac{\beta_3\mu_h^2\Pi_m}{(\gamma+\mu_m)\Pi_h^2}, \frac{\partial^2 f_7}{\partial x_3 \partial x_5} = \frac{\partial^2 f_7}{\partial x_5 \partial x_3} = -\frac{\beta_3\mu_h^2\Pi_m}{(\gamma+\mu_m)\Pi_h^2},\\
&\frac{\partial^2 f_7}{\partial x_3 \partial x_6} = \frac{\partial^2 f_7}{\partial x_6 \partial x_3} = \frac{\beta_3\mu_h}{\Pi_h}, \quad \frac{\partial^2 f_3}{\partial x_7 \partial \beta_1^*} = \frac{(\pi+\vartheta)(\pi\kappa + b\vartheta\mu_h)}{d\vartheta^2 + \pi(\pi+\vartheta)\kappa + \vartheta(\pi+\vartheta)\mu_h}.
\end{aligned}
$$

It follows that

$$
\begin{aligned}
a &= z_3 \sum_{i,j=1}^{8} y_i y_j \frac{\partial^2 f_3}{\partial x_i \partial x_j} + z_3 \sum_{i,j=1}^{8} y_i y_j \frac{\partial^2 f_7}{\partial x_i \partial x_j}\\
&= z_3\left(y_1 y_7 \frac{\partial^2 f_3}{\partial x_1 \partial x_7} + y_2 y_7 \frac{\partial^2 f_3}{\partial x_2 \partial x_7} + y_4 y_7 \frac{\partial^2 f_3}{\partial x_4 \partial x_7} + y_5 y_7 \frac{\partial^2 f_3}{\partial x_5 \partial x_7}\right) + z_7\left(y_1 y_3 \frac{\partial^2 f_7}{\partial x_1 \partial x_3} + y_2^2 \frac{\partial^2 f_7}{\partial x_2^2}\right.\\
&\left. + y_3^2 \frac{\partial^2 f_7}{\partial x_3^2} + y_3 y_4 \frac{\partial^2 f_7}{\partial x_3 \partial x_4} + y_3 y_5 \frac{\partial^2 f_7}{\partial x_3 \partial x_5} + y_3 y_6 \frac{\partial^2 f_7}{\partial x_3 \partial x_6}\right) < 0.
\end{aligned}
$$

For the sign of b, all partial derivatives of $\frac{\partial^2 f_3}{\partial x_i \partial \beta_1^*}$ are vanishing except $\frac{\partial^2 f_3}{\partial x_7 \partial \beta_1^*}$. Thus, it becomes:

$$
b = z_3 \sum_{i=1}^{8} y_i \frac{\partial^2 f_3}{\partial x_i \partial \beta_1^*} = z_3 y_7 \frac{\partial^2 f_3}{\partial x_7 \partial \beta_1^*} = z_3 y_7 \frac{(\pi+\vartheta)(\pi\kappa + b\vartheta\mu_h)}{d\vartheta^2 + \pi(\pi+\vartheta)\kappa + \vartheta(\pi+\vartheta)\mu_h} > 0.
$$

Due to the condition where a is negative and b is positive, as per Theorem 4.1 outlined in (Castillo-Chavez & Song, 2004), it can be inferred that the system undergoes a forward bifurcation at $\mathfrak{R}_0 = 1$. Thus, the malaria-free equilibrium is stable when $\mathfrak{R}_0 < 1$ and loses stability as $\mathfrak{R}_0$ crosses 1. For $\mathfrak{R}_0 > 1$, a stable endemic equilibrium emerges. This assertion is visually represented in Figure (4.2).

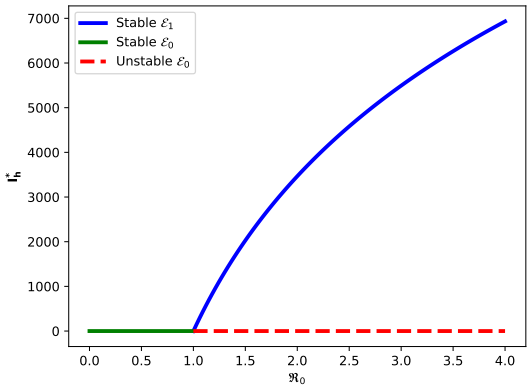

Figure 4.2: Forward bifurcation diagram of I_h versus $\mathfrak{R}_0$, with $\beta 1$ as the bifurcation parameter, other parameters as in Table 4.2

Due to system complexity, the global asymptotic stability of the malaria endemic equilibrium cannot be shown analytically. Instead, a numerical approach is used to demonstrate global convergence, where the malaria equilibrium typically exhibits globally asymptotic stability for various initial conditions and specific parameter values.

4.3 Sensitivity analysis

In this section, we used the approach presented in (Chitnis et al., 2008; Samsuzzoha et al., 2013; Siriprapaiwan et al., 2018) to examine the sensitive parameters for the basic reproductive number of the model. It is important as it can be applied to make a decision about the parameters that are most significant in lowering the level of a disease. The normalized forward sensitivity index for a quantity $\mathfrak{R}_0$ in relation to a parameter σ is defined as:

$$\Upsilon_{\sigma}^{\mathfrak{R}_0} := \frac{\partial \mathfrak{R}_0}{\partial \sigma} \times \frac{\sigma}{\mathfrak{R}_0}. \tag{4.27}$$

We derive an analytical expression for the $\mathfrak{R}_0$ given in equation (4.13) to each of the different basic parameters. For instance, the normalized forward sensitivity indices of $\mathfrak{R}_0$ along β_1, β_3, Π_h

and Π_m do not depend on any parameter

$$\Upsilon_{\beta_3}^{\mathfrak{R}_0} = \Upsilon_{\Pi_m}^{\mathfrak{R}_0} = \frac{1}{2}, \quad \Upsilon_{\Pi_h}^{\mathfrak{R}_0} = -\frac{1}{2}.$$

Similarly, the normalized forward sensitivity indices of $\mathfrak{R}_0$ with respect to the remaining parameters are obtained, and their sensitivity indices are given in Table 4.3.

Table 4.2: Parameters values used for sensitivity analysis and numerical simulations.

Parameters	Values	Source
Π_h	100	Srivastav & Ghosh (2021)
ε	0.005	Herdicho et al. (2021)
b	0.6	assumed
κ	0.001	Basir & Abraha (2023)
d	0.0005	assumed
β_1	0.019	assumed
β_2	0.02	Basir & Abraha (2023)
μ_h	0.002	Basir et al. (2021)
ρ	0.07	Ibrahim et al. (2020)
δ	0.001	Basir et al. (2021)
η	0.025	Basir et al. (2021)
φ	0.0006	assumed
Π_m	10000	Wang et al. (2018)
γ	0.003	Basir & Abraha (2023)
β_3	0.25	Basir & Abraha (2023)
μ_m	0.05	Keno et al. (2022)
π	0.03	Basir et al. (2018)
ξ	0.01	Basir & Abraha (2023)
ϑ	0.016	Basir et al. (2018)

In Table 4.3, we computed and presented sensitivity indices for the basic reproductive number, $\mathfrak{R}_0$, alongside with each basic parameters. The positive or negative signs of forward sensitivity index values in Table 4.3 shows the positive and negative influence, respectively, of the basic parameters on $\mathfrak{R}_0$. Our analysis reveals that parameters $\mu_m, \Pi_h, \rho, \gamma, \pi, \delta, b$ and κ exhibit negative sensitivity indices. Consequently, an increase in the value of these parameters, while holding the remaining factors constant, leads to a decrease in the value of $\mathfrak{R}_0$. For instance, consider, $\Upsilon_{\rho}^{\mathfrak{R}_0} = -0.480$, a 10% decrease (or increase) in drug treatment rate leads to a 4.8%

Table 4.3: Sensitivity index of $\mathfrak{R}_0$ evaluated at the parameter values in Table 4.2.

Parameters	Sensitivity indices	Parameters	Sensitivity indices
γ	-0.0593	β_2	0.00213
ϑ	0.000106	κ	-0.000105
δ	-0.00685	π	-0.00980
ρ	-0.480	b	-0.000159
μ_m	-0.940	μ_h	0.486
β_3	0.5	Π_m	0.5
β_1	0.4978	Π_h	-0.5

increase (or decrease) in $\mathfrak{R}_0$. This signifies that a higher treatment rate diminishes the number of secondary infections by either curing the disease or suppressing the malaria parasite load in human blood. When infected individuals undergo treatment, they are more likely to recover and become non-infectious, thereby reducing the pool of infected individuals in the population. This decrease in the number of infected individuals lowers the chances of susceptible individuals encountering infected ones and acquiring the infection, consequently mitigating the spread of the disease.

On the contrary, parameters $\Pi_m, \beta_1, \beta_2, \beta_3, \mu_h$ and ϑ exhibit positive sensitivity indices, indicating that an increase in their values, while keeping other parameters constant, contributes to an elevation in the value of $\mathfrak{R}_0$. In both low and high transmission scenarios, exemplified by $\Upsilon_{\beta_3}^{\mathfrak{R}_0} = \Upsilon_{\Pi_m}^{\mathfrak{R}_0} = +0.5$, a 10% decrease (or increase) in the contact rate between infected humans and susceptible mosquitoes, as well as a reduction (or augmentation) in mosquito recruitment by Π_m, leads to a 5% decrease (or increase) in $\mathfrak{R}_0$.

Identifying these pivotal parameters holds significance in devising effective control strategies to combat the spread of malaria. Given the challenge of altering natural death rates of humans and mosquitoes, the most effective approaches to reduce $\mathfrak{R}_0$ involve manipulating the contact rates between humans and mosquitoes (β_1, β_2 and β_3), increasing the recruitment of susceptible humans Π_h, elevating the treatment rate ρ, enhancing the insecticide usage rate γ, reducing the malaria-induced death rate δ, and decreasing the constant growth rate of mosquitoes Π_m. Consequently, our preventive and control strategies should prioritize interventions targeting parameters $\beta_1, \beta_3, \rho, \gamma, \Pi_h, \delta$ and Π_m.

4.4 Numerical simulation and discussion

In this section, we present the numerical solutions for the model (4.1) to substantiate the theoretical findings established in preceding sections. The numerical computations of the model

are executed utilizing the Runge-Kutta method within the Python software, employing parameter values obtained from Table 4.2. While most parameters are sourced from publicly available articles, a few are assumed. Initial values are set as follows: $S_{ah}(0) = 8000, S_{uh}(0) = 2000, I_h(0) = 10, T_h(0) = 10, R_h(0) = 0, S_m(0) = 10000, I_m(0) = 10, M_a(0) = 3$.

The graphical representations of selected numerical solutions are examined, and the outcomes are detailed in Figures (4.3)–(4.11). Notably, (4.3) and (4.4) depict the convergence of solutions under different initial conditions. Figure (4.7) illustrates the impact of insecticide usage, while Figure (4.8) showcases the influence of malaria treatment. Figures (4.9) and (4.11) delve into the effects of transmission rates between mosquitoes and humans, and reciprocally, from humans to the mosquito population.

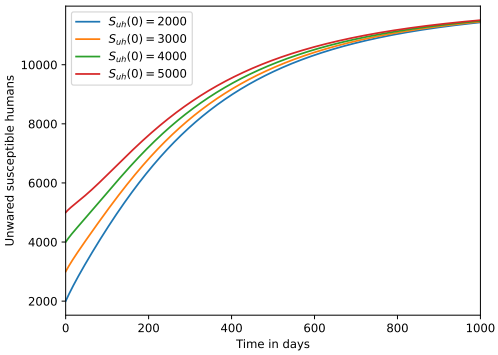

(a) Dynamic of S_{uh} humans

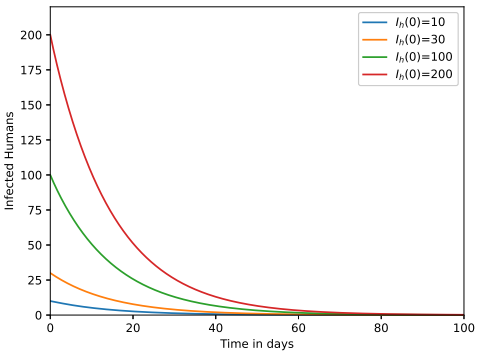

(b) Dynamic of I_h humans

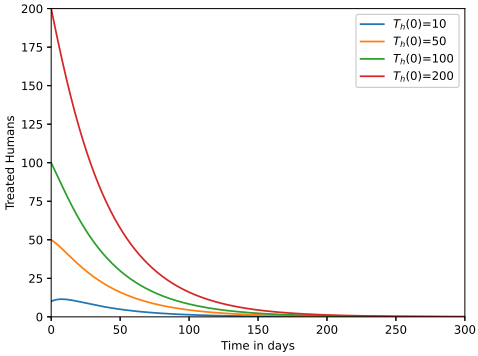

(c) Dynamic of T_h humans

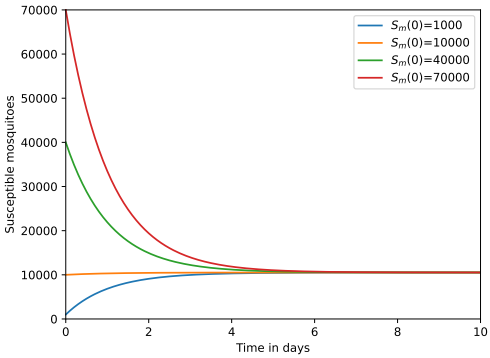

(d) Dynamic of S_m mosquitoes

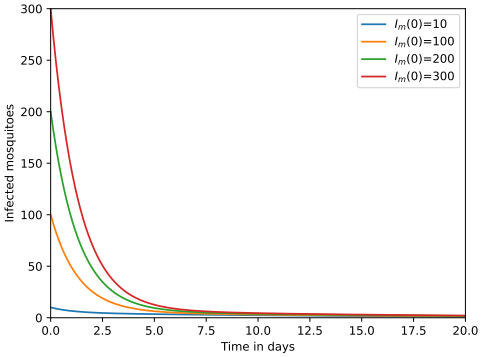

(e) Dynamic of I_m mosquitoes

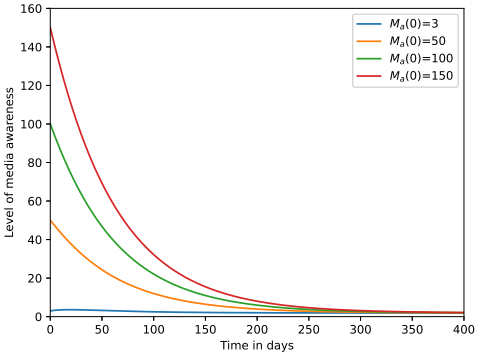

(f) Dynamic of M_a levels

Figure 4.3: Global stability of malaria free equilibrium point (MFE) .

To demonstrate the convergence of the malaria-free equilibrium point MFE $\mathcal{E}_0$ in model (4.1), we employ the parameter values from Table 4.2 while assuming a high insecticide application, specifically $\gamma = 0.9$. Upon substituting these values into equation (4.13), we deter-

mine that $\mathfrak{R}_0 = 0.12$. In this scenario, the model exhibits a malaria-free equilibrium point, $\mathcal{E}_0 = (37973.2, 12026.8, 0, 0, 0, 10552.8, 0, 1.87)$, which is globally asymptotically stable.

Figures (4.3a)-(4.3f) visually depict the convergence of all trajectories of the model to the malaria-free equilibrium point $\mathcal{E}_0$ for various sets of initial values. The biological implication is that the disease gradually diminishes over time, with the number of aware susceptible humans eventually reaching $37,973$ and the number of unaware susceptible humans rising to $12,026$. The mosquito population in each compartment steadily decreases due to awareness-driven insecticide usage. Moreover, the populations of humans in compartments I_h, T_h, and R_h approach zero as the populations in compartments S_{ah} and S_{uh} approach values of $37,973$ and $12,027$, respectively. The infected mosquito population in I_m approaches zero as the susceptible mosquito population S_m reaches $10,553$. Furthermore, Figure (4.3f) indicates that media awareness levels eventually decrease to 1.87 as the population achieves its malaria-free state. This decline is a result of the perception that malaria has been sufficiently mitigated.

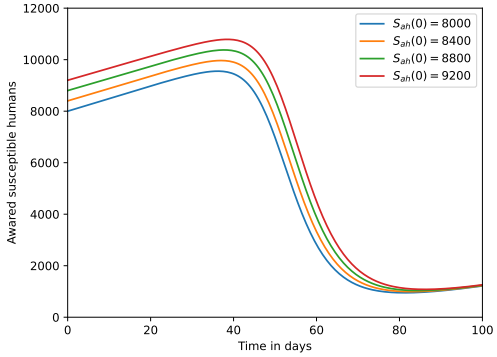

(a) Dynamics of aware susceptible humans

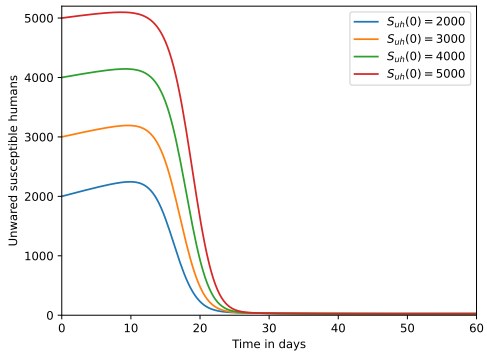

(b) Dynamics of unaware susceptible humans

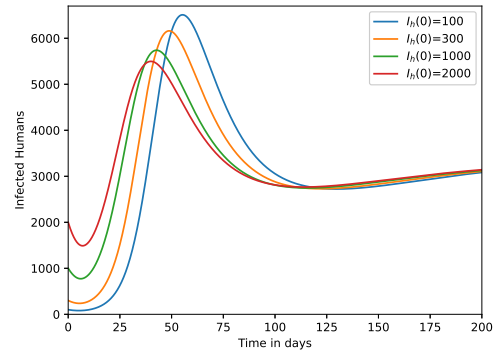

(c) Dynamics of infected humans

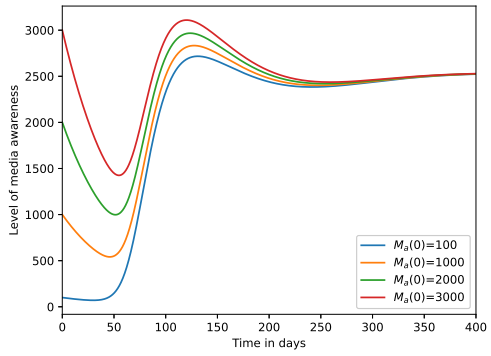

(d) Dynamics of media awareness

Figure 4.4: Global stability of malaria equilibrium point ($\mathcal{E}_1$)

Alternatively, when we set $\gamma = 0.003$ and utilize the parameter values specified in Table 4.2, we ascertain $\Re_0 = 2.25$, indicating a distinct positive malaria equilibrium point, denoted as $\mathcal{E}_1$. This equilibrium point is defined as:

$$\mathcal{E}_1 = \big(1847.28, 17.25, 3474, 8811.4, 31, 469.3, 87427, 101252, 2173.4\big).$$

The dynamic behavior of the malaria equilibrium point in model (4.1) is depicted as globally asymptotically stable, as illustrated in Figure 4.4. Across four distinct sets of initial conditions, the solution trajectories reveal notable patterns. In Figure (4.4a), the trajectories for aware susceptible humans eventually decrease and converge to a value of 1847, while in Figure (4.4b), trajectories for unaware susceptible humans similarly decrease and converge to a value of 17. Conversely, trajectories for malaria-infected humans Figure (4.4c) increase before converging to endemic values of 3474.

Observing Figure (4.4d), it is evident that media awareness levels initially decrease at the onset of the outbreak, followed by a subsequent increase until reaching a stable malaria equilibrium value of 2173.4. This dynamic suggests that at the outset of a malaria outbreak, media campaigns aimed at educating and creating awareness about the infection may experience a decline in activity. However, as the outbreak progresses and the evident risk of infection becomes more pronounced, media campaigns tend to intensify in both frequency and scope. This heightened media attention serves to educate the population about the risks, promote preventive measures, and mobilize resources for affected communities.

Finally, the biological implication of the globally asymptotically stable equilibrium point $\mathcal{E}_1$ is that malaria infection remains constant over time. Therefore, the maintenance of effective control measures becomes imperative to prevent disruptions that could lead to increased transmission.

More interestingly, powerfully supporting numerical observations of globally asymptotically stable equilibrium points $\mathcal{E}_0$ and $\mathcal{E}_1$ are provided in Figures (4.5) and (4.6), respectively. In Figure (4.5a), we have plotted the phase portrait of model (4.1) for malaria-infected humans I_h vs and malaria-treated humans T_h. Here, both state variables I_h and T_h ultimately converge to its malaria-free equilibrium point $\mathcal{E}_0$. Similarly, Figure (4.5b) shows that the vector fields of state variables S_m and I_m converge to the equilibrium point $\mathcal{E}_0$. Lastly, Figures (4.6a) and (4.6b) show that the pairs of state variables (S_{ah}, S_{uh}) and (I_h, M_a) respectively converge to the malaria equilibrium point $\mathcal{E}_1$ and diverge from the equilibrium point $\mathcal{E}_0$.

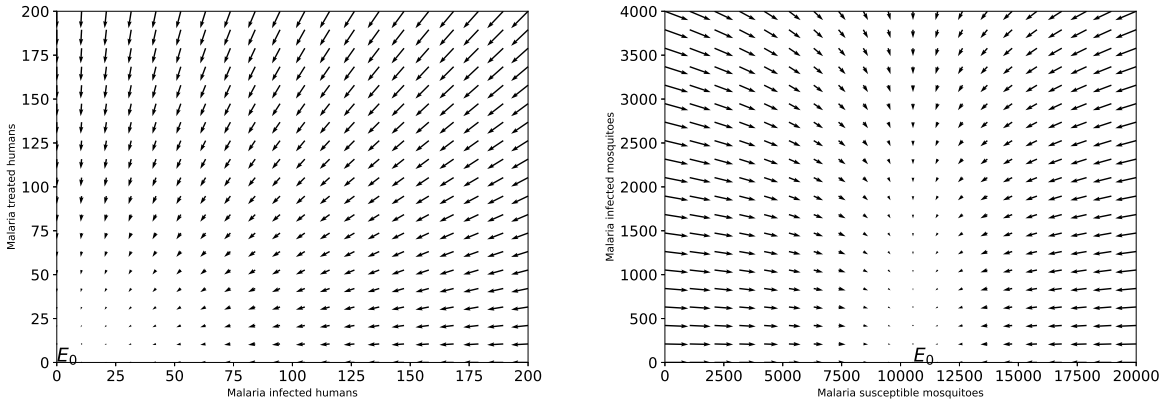

(a) **(b)**

Figure 4.5: Phase portraits illustrating the global stability of $\mathcal{E}_0$ for model (4.1): infected versus treated humans in Figure (4.5a) and susceptible versus infected mosquitoes in Figure (4.5b).

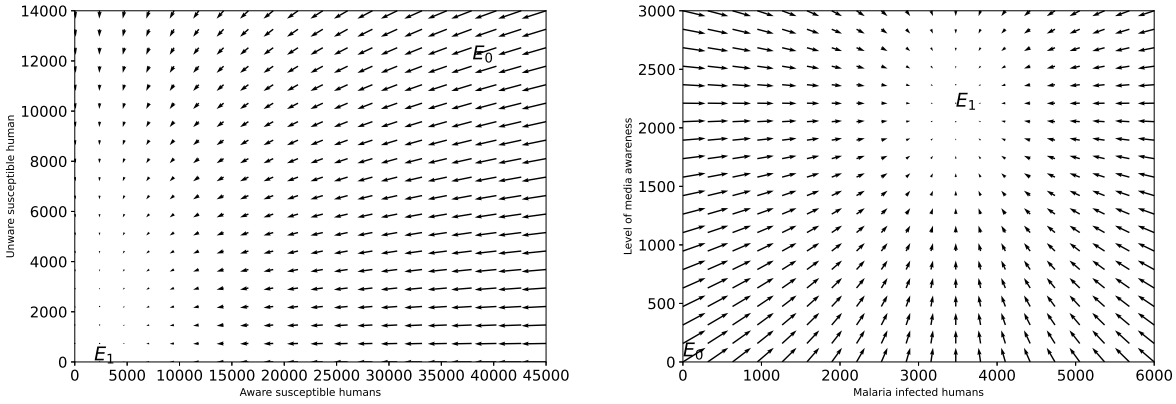

(a) **(b)**

Figure 4.6: Phase portraits illustrating the global stability of both $\mathcal{E}_0$ and $\mathcal{E}_1$ for model (4.1): aware susceptible vs unaware susceptible humans in Figure (4.5a) when $\mathfrak{R}_0 = 0.12$ and susceptible versus infected mosquitoes in Figure (4.6b) when $\mathfrak{R}_0 = 2.25$.

4.4.1 The effect of insecticide use γ

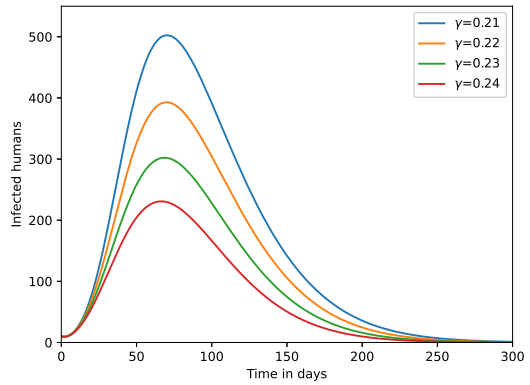

(a) Dynamics of I_h humans

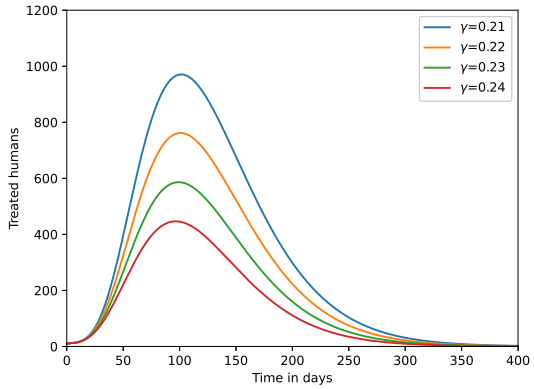

(b) Dynamics of T_h humans

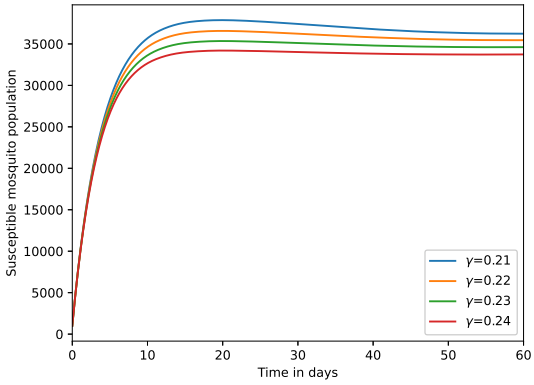

(c) Dynamics of S_m mosquitoes

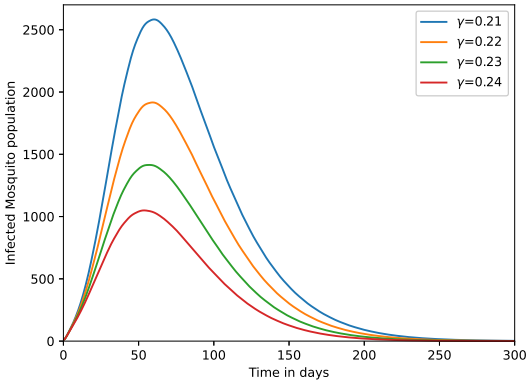

(d) Dynamics of I_m mosquitoes

Figure 4.7: Figures showing the effect of insecticide usage for various γ values

In this section, we examine the efficacy of awareness-based insecticide usage γ with the aim of minimizing the rate of malaria transmission. The results demonstrate that an escalation in insecticide utilization effectively diminishes the risk of transmission between the human and mosquito populations, as illustrated in Figure 4.7. Specifically, Figures (4.7a) and (4.7b) reveal that heightened insecticide use leads to a decrease in the number of malaria-infected and treated humans, thereby significantly impacting the reduction of malaria cases.

Furthermore, Figures (4.7c) and (4.7d) underscore the substantial impact of increased awareness-based insecticide usage on reducing both the numbers of susceptible and infected mosquitoes. This observation emphasizes the crucial role of heightened insecticide awareness in mitigating the transmission of malaria, affecting not only human cases but also targeting the mosquito

population.

4.4.2 The effect of malaria treatment ρ

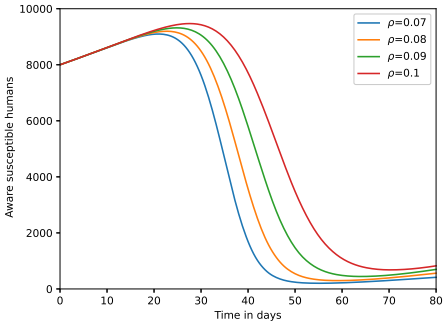

(a) Dynamics of S_{ah} humans

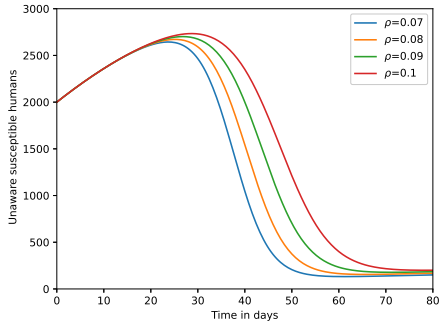

(b) Dynamics of S_{uh} humans

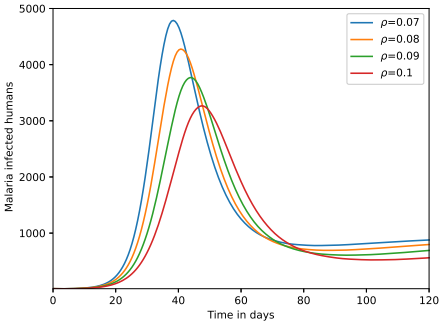

(c) Dynamics of I_h humans

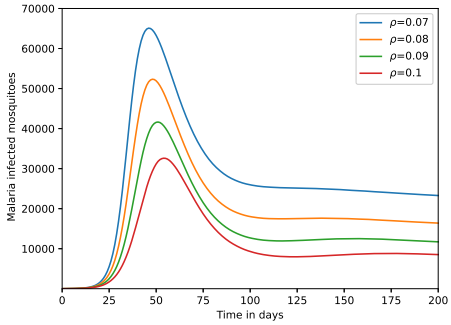

(d) Dynamics of I_m mosquitoes

Figure 4.8: Figures showing the effect of malaria treatment rate for different ρ values.

Figure (4.8) depicts the varied effects of malaria drug treatment on the human population, maintaining the remaining parameters from Table 4.2 constant. Particularly, in Figures (4.8a) and (4.8b), it's apparent that both aware and unaware susceptible humans increase as the treatment rate escalates. Meanwhile, Figures (4.8c) and (4.8d) illustrate a decrease in the number of infectious individuals in both human and mosquito species with a rise in the malaria treatment rate.

4.4.3 The effect of infection rates β_1 and β_3

In our sensitivity analysis, we observe that augmenting (or diminishing) infection rates β_1 and β_3 leads to an increase (or decrease) in the number of secondary infections. Therefore, by reducing the contact rates β_1 and β_3, it is possible to minimize the number of infected humans and mosquitoes. This strategic approach facilitates the implementation of effective preventive

and control strategies.

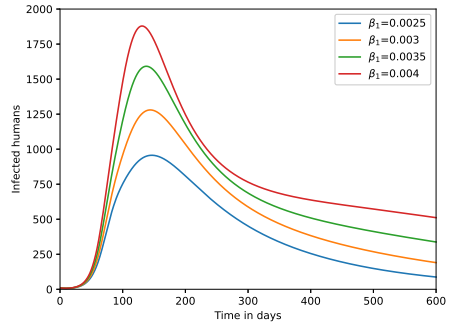

(a) Dynamics of I_h humans

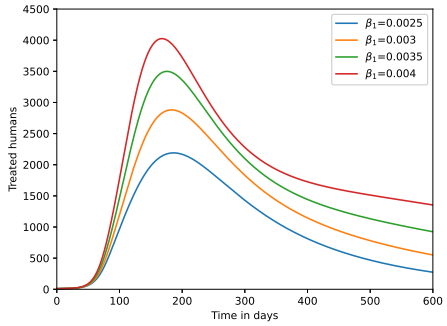

(b) Dynamics of T_h humans

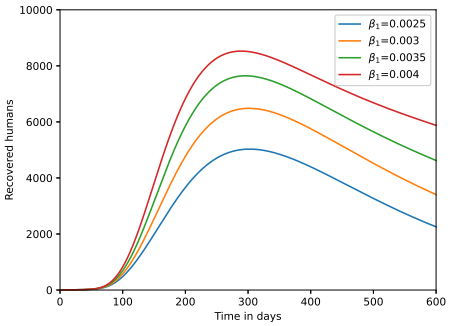

(c) Dynamics of R_h humans

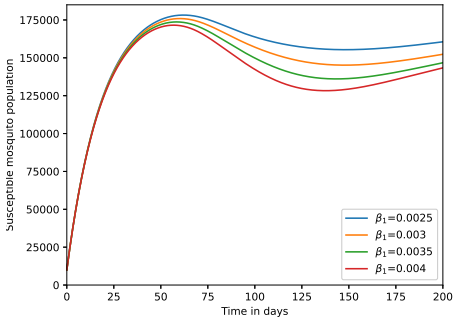

(d) Dynamics of S_m mosquitoes

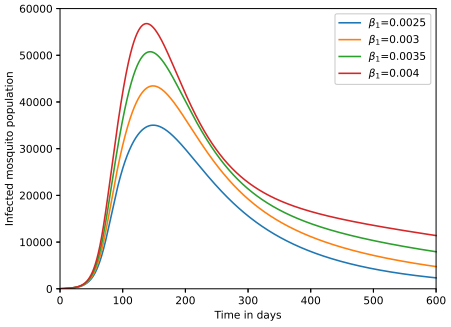

(e) Dynamics of I_m mosquitoes

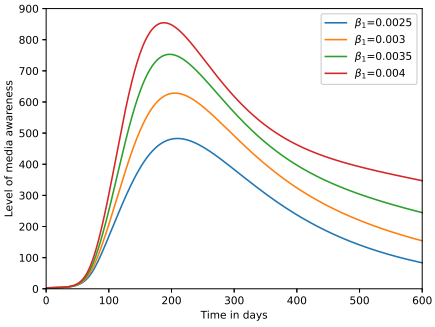

(f) Dynamics of M_a level

Figure 4.9: Figures showing the effect of infection rate from infected mosquitoes to aware susceptible humans using various β_1 values.

Figures (4.9a)-(4.9f) depict the dynamics of various factors in response to changes in the contact rate β_1 between malaria-infected mosquitoes and aware susceptible humans. The illustrations demonstrate that the number of infected humans, malaria-treated humans, malaria-

recovered humans, malaria-infected mosquitoes, and the level of media awareness all increase as the contact rate β_1 decreases. Conversely, the number of susceptible mosquitoes rises as the contact rate between malaria-infected mosquitoes and aware susceptible humans decreases.

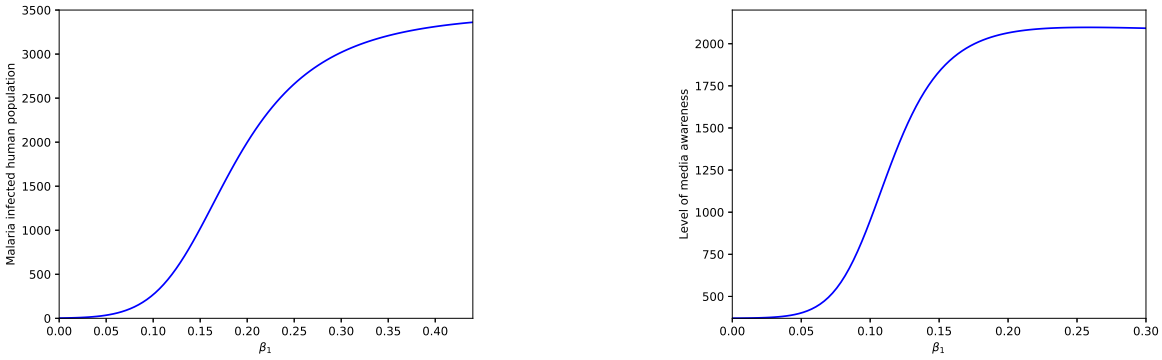

(a) Dynamics of I_h humans

(b) Dynamics of M_a level

Figure 4.10: Figures showing the dynamics of I_h and M_a as β_1 value varies.

In Figure (4.10a), we present the dynamics of I_h as the parameter β_1 varies. When β_1 exceeds 0.04, the number of infected humans converges to the malaria endemic state, indicating that higher transmission rates can sustain the disease within the population. Conversely, when β_1 falls below the value 0.04, the infection declines to a malaria-free state. Similarly, Figure (4.10b), illustrates the dynamics of M_a in relation to variations in β_1. When β_1 exceeds 0.04, media awareness M_a converges to its larger equilibrium state. However, when β_1 is below the value 0.04, M_a declines as the population reaches malaria free state.

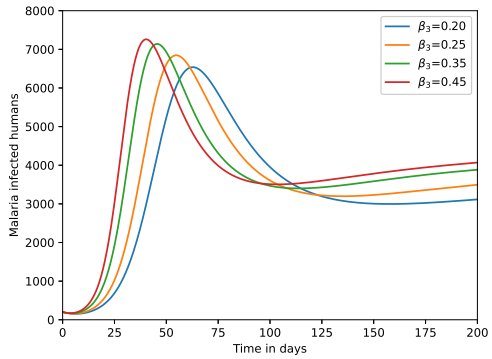

(a) Dynamics of I_h humans

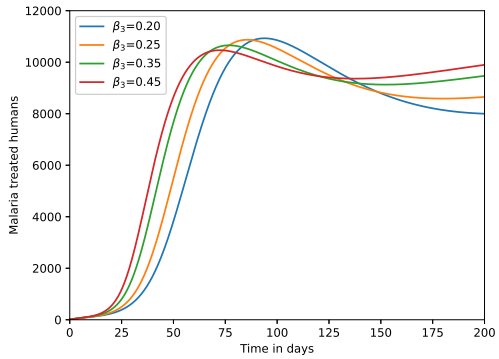

(b) Dynamics of T_h humans

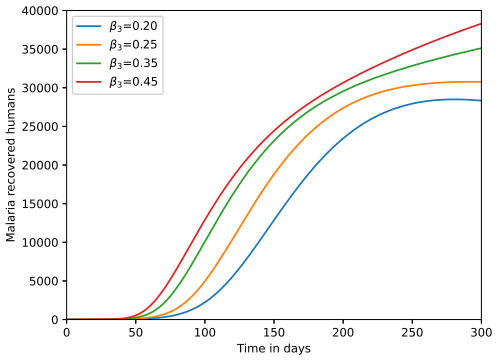

(c) Dynamics of R_h humans

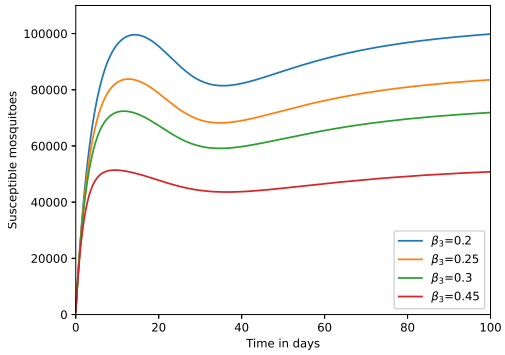

(d) Dynamics of S_m mosquitoes

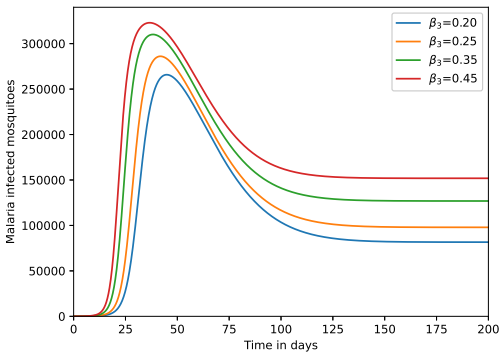

(e) Dynamics of I_m mosquitoes

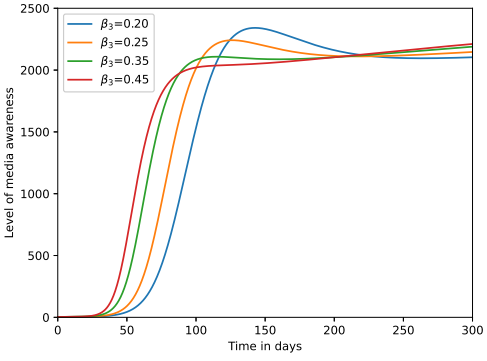

(f) Dynamics of M_a level

Figure 4.11: Figures showing the effect of infection rate from infected humans to susceptible mosquitoes using different β_3 values.

Figure (4.11) illustrates the impact of the infection rate from infected humans on susceptible mosquitoes for various values of β_3. In Figures (4.11a)– (4.11d), it is evident that the endemicity of malaria increases in both human and mosquito populations as the β_3 value rises. However,

Figure (4.11d) highlights that the number of susceptible mosquitoes increases as the contact rate β_3 decreases, and vice versa. Consequently, by minimizing the contact between infected humans and susceptible mosquitoes, the likelihood of mosquitoes transmitting malaria to other individuals is significantly reduced. This, in turn, leads to a decrease in malaria infection rates within the population. Furthermore, Figure (4.11d) reveals that the level of media awareness increases as the contact between infected humans and susceptible mosquitoes intensifies. In the context of a malaria outbreak, heightened media mobilization tends to extend coverage to ensure the population is well-informed and awareness is raised about the situation.

CHAPTER 5

OPTIMAL CONTROL AND COST-EFFECTIVENESS ANALYSIS OF MALARIA TRANSMISSION DYNAMICS

In this chapter, we present an optimal control and cost-effectiveness analysis of the model introduced in Chapter 4. We begin with the computation of the basic reproduction number $\mathfrak{R}_0$, followed by model fitting using Ethiopian malaria incidence data from 2000 to 2022. Subsequently, we perform a sensitivity analysis to identify the key parameters influencing the model dynamics. Pontryagin's Minimum Principle is then applied to establish the necessary and sufficient conditions for optimal control. Finally, the cost-effectiveness of intervention strategies is evaluated using the Average Cost-Effectiveness Ratio (ACER) and the Incremental Cost-Effectiveness Ratio (ICER).

5.1 Formulation of optimal control model

Optimal control theory has been used to develop more effective and efficient malaria control strategies (Engida et al., 2024; Romero-Leiton et al., 2018; J. Zhao, 2022). Epidemiologically, malaria control depends on various parameters and is one of extremely complex tasks. Regarding sensitivity analysis, it is evident that rates of malaria transmission, treatment, and insecticide application are the most sensitive and essential parameters of disease dynamics. By focusing on these sensitive parameters, this study intended to optimize the impact of malaria control efforts and accelerate progress towards elimination. Thus, we extend the our model presented in Chapter 4 to an optimal control model by introducing three time-evolution controls. The control effort $u_1(t)$ represents the use of personal protective measures, such as applying skin repellents, lotions, and electronic devices, to avoid mosquito bites and transmission between humans and mosquitoes during both day and night; the control effort $u_2(t)$ represents improved enhanced treatment capacity, reflecting improved quality of health services and timely case management; and the control effort $u_3(t)$ represents mosquito breeding-site destruction. This intervention is modeled as habitat elimination that indirectly reduces adult mosquito populations by removing critical resting sites, disrupting oviposition behavior, and creating environmental conditions that reduce adult survival. If $u_i(t) = 0$ for $i = 1,2,3$, then no attempt is made to exercise the control at time t, and if $u_i(t) = 1$, then the maximum controlling effort is applied.

Aware and unaware susceptible human populations are decreased by the control-induced incidence terms $(1-u_1)\frac{\beta_1 S_{ah} I_m}{N_h}$ and $(1-u_1)\frac{\beta_2 S_{uh} I_m}{N_h}$ respectively. Infected human is increased by

the control induced incidence term $\left(1-u_1\right)\left(\frac{\beta_1 S_{ah}+\beta_2 S_{uh}}{N_h}\right)I_m$ and reduced by $\left(\rho+au_2+\delta+\mu_h\right)I_h$. Here, we assume that the rate of treatment for infected persons is $\rho+au_2$, where $a\in[0,1]$ represents the treatment monitoring and ρ represents the treatment rate.

Similarly, the susceptible mosquito populations leave their class and relocate to increase infected class with the control-induced incidence term $(1-u_1)\frac{\beta_3 S_m I_h}{N_h}$. Each mosquito population dies either by insecticide application with the term $pu_3+\gamma$ or dies naturally with the rate μ_m. Lastly, we assume all parameters involved in the model positive. Arising the aforementioned details with and model assumptions in Chapter 4 together, we formulate the following control induced mathematical model (5.1) for malaria transmission.

$$\begin{cases} \frac{dS_{ah}}{dt} = \sigma\Pi_h + \kappa S_{uh}M_a - \frac{dS_{ah}}{1+M_a} - (1-u_1)\frac{\beta_1 S_{ah}I_m}{N_h} + \varepsilon R_h - \mu_h S_{ah}, \\ \frac{dS_{uh}}{dt} = (1-\sigma)\Pi_h + \frac{dS_{ah}}{1+M_a} - \kappa S_{uh}M_a - (1-u_1)\frac{\beta_2 S_{uh}I_m}{N_h} - \mu_h S_{uh}, \\ \frac{dI_h}{dt} = (1-u_1)\frac{\beta_1 S_{ah}I_m}{N_h} + (1-u_1)\frac{\beta_2 S_{uh}I_m}{N_h} - (\rho+au_2+\delta+\mu_h)I_h, \\ \frac{dT_h}{dt} = (\rho+au_2)I_h - (\eta+\phi+\mu_h)T_h, \\ \frac{dR_h}{dt} = \eta T_h - (\mu_h+\varepsilon)R_h, \\ \frac{dS_m}{dt} = \Pi_m - (1-u_1)\frac{\beta_3 I_h S_m}{N_h} - (pu_3+\gamma+\mu_m)S_m, \\ \frac{dI_m}{dt} = (1-u_1)\frac{\beta_3 I_h S_m}{N_h} - (pu_3+\gamma+\mu_m)I_m, \\ \frac{dM_a}{dt} = \pi + \xi I_h - \theta M_a, \end{cases} \tag{5.1}$$

subjected to the initial conditions,

$$S_{ah}(0)>0, S_{uh}(0)\geq 0, I_h(0)\geq 0, T_h(0)\geq 0, R_h(0)\geq 0, S_m(0)>0, I_m(0)\geq 0, M_a(0)\geq 0. \tag{5.2}$$

5.1.1 Existence and stability of MFE with constant controls

It is obvious that the malaria-free equilibrium point (MFE) of model (5.1) denote by $\mathcal{E}_0$ is given as

$$\mathcal{E}_0 = \left(S_{ah}^0, S_{uh}^0, 0, 0, 0, S_m^0, 0, M_a^0\right), \tag{5.3}$$

where

$$S_{ah}^0 = \frac{(\pi+\theta)(\pi\kappa+\sigma\theta\mu_h)\Pi_h}{\mu_h(d\theta^2+\pi(\pi+\theta)\kappa+\theta(\pi+\theta)\mu_h}, \; S_{uh}^0 = \frac{\theta(d\theta+(\theta+\pi)(1-\sigma)\mu_h)\Pi_h}{\mu_h(d\theta^2+\pi(\pi+\theta)\kappa+\theta(\pi+\theta)\mu_h)},$$
$$S_m^0 = \frac{\Pi_m}{pu_3+\gamma+\mu_m} \quad \text{and} \quad M_A^0 = \frac{\pi}{\theta}.$$

We compute the basic reproduction number, $\mathfrak{R}_0$, for model (5.1) using the next-generation matrix method described in Section (4.2.3). The resulting expression is given by

$$\mathfrak{R}_0 = \sqrt{\frac{(1-u_1)\beta_1\mu_h(\pi+\theta)(\pi\kappa+\sigma\theta\mu_h)+\mu_h\theta\beta_2(d\theta+(1-\sigma)(\pi+\theta)\mu_h)}{(\rho+au_2+\delta+\mu_h)\big(d\theta^2+\pi(\pi+\theta)\kappa+\theta(\pi+\theta)\mu_h\big)\Pi_h}}\sqrt{\frac{(1-u_1)\beta_3\Pi_m}{(pu_3+\gamma+\mu_m)^2}}. \tag{5.4}$$

5.1.2 Parameter estimation

In this section, we used malaria data from Ethiopia to fit the model and estimate some basic parameters. Since malaria has remained endemic in Ethiopia for a long time, we can predict the dynamics of the disease in the future by fitting the autonomous model of model (5.1) with Ethiopian data. The malaria incidence is here defined as the number of new cases of malaria per 1,000 population at risk in Ethiopia. Ethiopian malaria incidence data was taken from the World Bank from 2000 to 2022 years (WorldBank, 2024), which is depicted in Figure (5.1a).

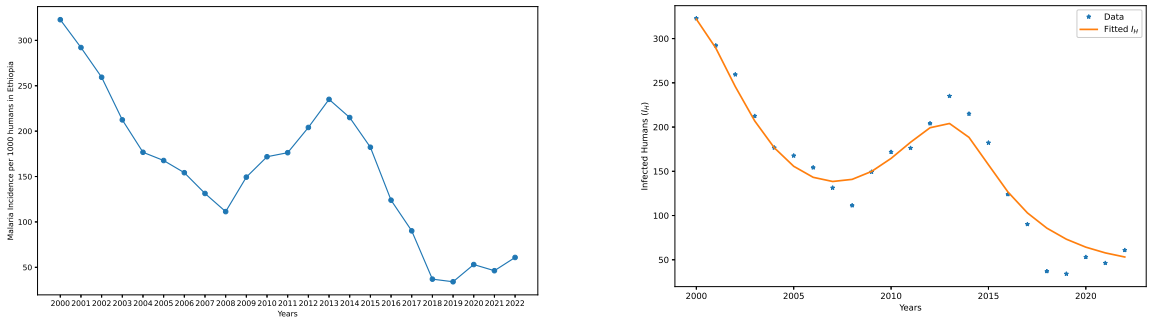

(a) Ethiopian malaria prevalence per 1000 humans

(b) Curve fit

Figure 5.1: Plot depicting Ethiopian malaria incidence data and curve fit

In this work, we employ the least-square method with the help of the "Limited-memory Broyden-Fletcher-Goldfarb-Shanno with Box (L-BFGS-B)" method, which is readily available in Python SciPy, to address the model fit and parameter estimation. This method efficiently minimizes a least-squares objective function measuring the deviation between model output and observed data while respecting bound constraints on parameters l, such that $l_{min} \leq l \leq l_{max}$. The constant recruitment of susceptible humans Π_h and the natural death rate μ_h are estimated from the Ethiopian demography. The natural death rate of humans, μ_h, is obtained from the inverse of the average life expectancy in Ethiopia. The average life expectancy in Ethiopia is 67.8 years (Kifle & Obsu, 2022), therefore, $\mu_h = \frac{1}{67.8}$ per year. The constant recruitment Π_h is calculated as follows: we consider 1000 population at risk as a total population of Ethiopia. Hence, $\Pi_h = 1000 \times \mu_h$.

For the model fitting, the parameters constant recruitment of susceptible humans b, rate of unaware susceptiblebe come aware susceptible κ, rate of unaware susceptiblebe come unaware

susceptible d, treatment failure ϕ, recruitment of mosqutoes Π_m, insecticide application rate γ, natural death rate of mosquitoes μ_m, constant increase media awareness π, progress of awareness due to media awareness efficacy ξ, and fading of memory of awareness θ are fixed during model fitting because they are taken from related studies. The remaining model parameters: transmission rates ($\beta_1, \beta_2,$ and β_3), waning immunity rate of recovered humans ε, treated humans recovery rate η, treatment rate ρ, and disease induced death rate δ are estimated. The initial conditions are chosen to reflect real-world observations. Specifically, $I_h(0) = 322.77$ is set to correspond to the WHO-reported number of infected individuals per thousand humans in the year 2022, ensuring that the model aligns with actual epidemiological data. The remaining human compartments, $S_{ah}(0) = 564.23$, $S_{uh}(0) = 100$, $T_h(0) = 10$, $R_h(0) = 3$, together with the mosquito compartments $S_m(0) = 800$, $I_m(0) = 200$, and the awareness level $M_a(0) = 0.5$, are reasonably assumed for numerical investigation. The result of our model-fit is presented in Figure (5.1b). Its result reveals that the model best fits Ethiopian malaria incidence data from 2000 to 2022. The parameters that are obtained from estimation, the literature, and model fitting are presented in Table 5.1. Also we note that all parameters in the Table 5.1 are given in per year. Having the parameter values, the basic reproductive number is $\mathfrak{R}_0 = 2.36 > 1$.

Table 5.1: Parameters and their respective values.

Parameters	value	Reference
Π_h	15	Calculated
ε	0.1	Fitted
b	0.6	Otieno et al. (2016)
κ	0.07	Assumed
d	0.02	Assumed
β_1	0.124	Fitted
β_2	0.129	Fitted
β_3	0.189	Fitted
μ_h	$\frac{1}{67.8}$	Kifle & Obsu (2022)
ρ	0.06	Fitted
δ	0.24	Fitted
η	0.083	Fitted
ϕ	0.006	Assumed
Π_m	350	Assumed
γ	0.02	Assumed
μ_m	$\frac{1}{21}$	Keno et al. (2022)
π	0.001	Assumed
ξ	0.00003	Assumed
θ	0.016	Basir & Abraha (2023)
$a = p$	0.25	Otieno et al. (2016)

5.1.3 Sensitivity analysis

Following Chitnis et al. (2008), the normalized forward sensitivity index of a variable $\mathfrak{R}_0$ along to parameter P is defined by:

$$\Upsilon_P^{\mathfrak{R}_0} := \frac{\partial \mathfrak{R}_0}{\partial P} \times \frac{P}{\mathfrak{R}_0}. \tag{5.5}$$

It is instructive to mention that if $u_i(t) = 0$, then system (5.1) produces autonomous model whose sensitivity indexes have been presented in Table 5.2. From the sensitivity indexes, it

Table 5.2: The sensitivity indexes of $\mathfrak{R}_0$ along with some basic parameters evaluated at parameter values given in Table 5.1.

Parameters	**Sensitivity indices**
Π_h	-0.5
b	0.0001
κ	-2.5×10^{-7}
d	2.2×10^{-7}
β_1	+0.49
β_2	0.0002
μ_h	+0.476
ρ	-0.100
δ	-0.38
Π_m	+0.5
γ	-0.3
β_3	+0.5
μ_m	-0.7
π	-0.01
θ	$+5 \times 10^{-7}$

can be seen that the natural death rate of mosquitoes μ_m, biting rates of mosquitoes β_1 and β_3, constant recruitment of susceptible humans Π_h, constant recruitment of mosquitoes Π_m, the natural death rate of humans μ_h, insecticide application rate γ and treatment rate ρ are the most sensitive parameters.

In more related development, we analytically compute the forward sensitivity indexes of basic reproduction number of equation (5.4) with respect to constant control u_i for $i = 1, 2, 3$ are given by:

$$\frac{\partial \mathfrak{R}_0}{\partial u_1} \times \frac{u_1}{\mathfrak{R}_0} = -\frac{u_1}{1-u_1} < 0, \frac{\partial \mathfrak{R}_0}{\partial u_2} \times \frac{u_2}{\mathfrak{R}_0} = -\frac{au_2}{\rho + au_1 + \mu_h} < 0, \frac{\partial \mathfrak{R}_0}{\partial u_3} \times \frac{u_3}{\mathfrak{R}_0} = -\frac{pu_3}{pu_3 + \gamma + \mu_h} < 0.$$

The negative sensitivity indexes of $\mathfrak{R}_0$ for each u_i indicated that increasing any control effort reduced the average number of new infections.

5.2 Analysis of the optimal control model

This section provides a detailed qualitative analysis of the malaria model (5.1) by adopting the implementation of Pontryagin's Minimum Principle (Chambers, 1965). The majority of models in the mathematical epidemiology incorporates optimal control theory based on the Pontryagin's Minimum Principle (PMP) (Keno et al., 2022; Olaniyi et al., 2020, 2018). For this specific study, we construct the objective functional denoted by $\mathcal{J}$ in order to minimize the number of infectious humans $I_h(t)$ and the total mosquito population $N_m(t)$ with time-dependent control variables:

$$\mathcal{J} = \int_0^{T_f} \left(A_1 I_h(t) + A_2 N_m(t) + \frac{1}{2} K_1 u_1^2(t) + \frac{1}{2} K_2 u_2^2(t) + \frac{1}{2} K_3 u_3^2(t) \right) dt \rightarrow \text{ Min} \tag{5.6}$$

subject to the model (5.1) with initial condition in (5.2), where A_1 and A_2 are relative costs associated to infected humans and entire mosquitoes population respectively. The weight constants K_1, K_2 and K_3 indicate the relative costs of the interventions associated with the controls $u_1(t), u_2(t)$ and $u_3(t)$, respectively. The time interval $[0, T_f]$ represents the control program to be conducted, while T_f represents the expected final time at which controls to be conducted. The objective functional (5.6) contains the cost control function associated to personal protective measures $\frac{1}{2} K_1 u_1^2(t)$, cost control function associated to improved treatment capability of malaria $\frac{1}{2} K_2 u_2^2(t)$ and cost control function associated with the mosquito breeding site destruction $\frac{1}{2} K_3 u_3^2(t)$. Moreover, the terms $A_1 I_h(t)$ and $A_2 N_m(t)$ quantify the cost imposed due to malaria-infected humans and total mosquitoes population. In this study, we adopt a non-linear quadratic form to the cost of controls as an approximation to the non-linear functional to avoid singular or bang-bang optimal control situations (Fleming & Rishel, 2012; Oke et al., 2018).

Here our primary objective is to determine optimal control $u^*(t) = \left(u_1^*(t), u_2^*(t), u_3^*(t)\right)$ subjected to state trajectories of (5.1) for $t \in [0, T_f]$ and minimize the given cost functional in (5.6). That is,

$$\mathcal{J}(u^*(t)) = min\{\mathcal{J}(u(t)) | u(t) \in U\}, \tag{5.7}$$

subject to the state system (5.1), where

$$U = \{u(t) : u(t) \text{ is a Lebesgue measurable set and } 0 \leq u_i(t) \leq 1,\ i = 1,2,3,\ t \in [0, T_f]\}. \tag{5.8}$$

In the following sub-sections, we present the existence as well as characterization of the optimal control model (5.1).

5.2.1 Existence of an optimal control malaria model

It is important to establish the existence of optimal controls that solves the minimization problem (5.6). To determine the existence and uniqueness of the optimal control, it is better to prove the boundedness of the right-hand side of system (5.1).

Theorem 5.2.1. *For a given objective function $\mathcal{J}$ (5.6), specified on the control set U, and subjected to the state system (5.1) with initial values in (5.2), there exists an optimal control u^* such that $\mathcal{J}(u^*) = min\{\mathcal{J}(u) | u \in U\}$.*

Let $x = \left(S_{ah}, S_{uh}, I_h, T_h, R_h, S_m, I_m, M_a\right)$, $u = \left(u_1, u_2, u_3\right)$ and let $f(t,x,u)$ be the right-hand side of system (5.1), then the following requirements are the foundation for the proof of Theorem 5.2.1.

i. The solutions set of the system (5.1) with associated control functions in (5.8) is non-empty.

ii. Closure and convexity of the control set U.

iii. The right-hand side of system (5.1) is bound by state variables and a linear function in the control.

iv. The integrand of $\mathcal{J}$ in the equation (5.6) is convex along with control functions.

v. There are constants $\alpha_1, \alpha_2 > 0$ and $\alpha_3 > 1$ such that the Lagrangian function is bounded by $\alpha_1 |u|^{\alpha_3} - \alpha_2$.

Proof. i. It is important to verify that the condition (i) hold for the existence of optimal u^*. As established in Section **??**, the state variables in each population remain bounded. Furthermore, the right-hand side of the model (5.1) satisfies the Lipschitz condition with respect to the state variables. Therefore, according to the existence theorem of Picard-Lindelöf stated in (Coddington et al., 1956), the solution of the model (5.1) exists and is non-empty. Consequently, the condition (i) is satisfied.

ii. Let a control set $U = \{u(t) \in [0,1]^3 : 0 \leq u_i(t) \leq 1,\ i = 1,2,3\}$. Then we can conclude that U is closed. Let us pick any arbitrary points $v, w \in U$ such that $v = (v_1, v_2, v_1)$ and $w = (w_1, w_2, w_3)$. Then by referring theory of convex set found in (Niculescu & Persson, 2006), we have

$$\varpi v + (1 - \varpi) w \in [0,1]^{3,}\ \forall \varpi \in [0,1].$$

This implies, $\varpi v + (1 - \varpi) w \in U$. Therefore, U is convex set.

iii. It is possible to rewrite the right hand side of the model (5.1) as follows:

$$f(t,x,u) = g(t,x) + h(t,x)u,$$

where

$$g(t,x) = \begin{pmatrix} \sigma\Pi_h + \kappa S_{uh} M_a - \frac{dS_{ah}}{1+M_a} - \frac{\beta_1 S_{ah} I_m}{N_h} + \varepsilon R_h - \mu_h S_{ah} \\ (1-\sigma)\Pi_h + \frac{dS_{ah}}{1+M_a} - \kappa S_{uh} M_a - \frac{\beta_2 S_{uh} I_m}{N_h} - \mu_h S_{uh} \\ \frac{\beta_1 S_{ah} I_m}{N_h} + \frac{\beta_2 S_{uh} I_m}{N_h} - (\rho + \delta + \mu_h) I_h \\ \rho I_h - (\eta + \phi + \mu_h) T_h \\ \eta T_h - (\mu_h + \varepsilon) R_h \\ \Pi_m - \frac{\beta_3 I_h S_m}{N_h} - (\gamma + \mu_m) S_m \\ \frac{\beta_3 I_h S_m}{N_h} - (\gamma + \mu_m) I_m \\ \pi + \xi I_h - \theta M_a \end{pmatrix}, \tag{5.9}$$

$$h(t,x)u = \begin{pmatrix} \frac{\beta_1 S_{ah} I_m}{N_h} & 0 & 0 \\ \frac{\beta_2 S_{uh} I_m}{N_h} & 0 & 0 \\ -\frac{\beta_1 S_{ah} + \beta_1 S_{ah}}{N_h} I_m & -aI_h & 0 \\ 0 & aI_h & 0 \\ 0 & 0 & 0 \\ \frac{\beta_3 S_m I_h}{N_h} & 0 & -pS_m \\ -\frac{\beta_3 S_m I_h}{N_h} & 0 & -pI_m \\ 0 & 0 & 0 \end{pmatrix} \begin{pmatrix} u_1 \\ u_2 \\ u_3 \end{pmatrix}. \tag{5.10}$$

Thus, from Euclidean matrix norm in (Celebi et al., 2011), we have

$$\begin{aligned} f(t,x,u) &\leq ||g(t,x)|| + ||h(t,x|| \; ||u|| \\ &\leq \beta + \alpha \; ||u||. \end{aligned} \tag{5.11}$$

We find the upper bound square sums of the matrices $g(t,x)$ and $h(t,x)$ in order to verify the inequality (5.11) holds true. We substitute the proper upper bound for each state variable and then find the upper bound square sums of the matrices. In addition to this analogous proof is carried out in (Olaniyi et al., 2018). Now, the upper bound square sums of column entries a_{ij} of matrix $g(t,x)$ is,

$$\sqrt{\sum_{i=1}^{8} |a_{i1}|^2} = a_0 + a_1 \Pi_h^2, + a_2 \Pi_m^2 \tag{5.12}$$

where

$$a_0 = 1 + \frac{2\zeta\Pi_h}{\mu_h}, \; a_1 = \frac{\eta^2}{\mu_h^2} + \frac{\zeta^2}{\mu_h^2} + \frac{(d\theta + (1+\theta)\mu_h + \zeta\Pi_h)^2}{((1+\theta)\mu_h + \zeta\Pi_h)^2} + \frac{(\varepsilon\theta + \kappa)\mu_h + \theta\sigma\mu_h^2 + \zeta\kappa\Pi_h^2}{\theta^2\mu_h^4},$$

$$a_2 = 1 + \frac{(\beta_1 + \beta_2)^2 + \beta_3^2}{(pu_3 + \mu_m)^2}.$$

Taking square root to both sides of equation (5.12), we have

$$\sqrt{\sum_{i=1}^{8}|a_{i1}|^2} = \sqrt{a_0 + a_1\Pi_h^2 + a_2\Pi_m^2}.$$

Having the concept of weighted sum inequality, $ax+by+c \leq \text{Max}\{a,b,c\}(x+y+1)$, we have

$$\sqrt{a_0 + a_1\Pi_h^2 + a_2\Pi_m^2} \leq \sqrt{\text{Max}\{a_0,a_1,a_2\}(1+\Pi_h^2+\Pi_m^2)} = \alpha.$$

Similarly, the square root of upper bound square sums of entries a_{ij} of matrix $h(t,x)$ is given as

$$\sqrt{\sum_{i=1}^{8}\sum_{j=1}^{8}|a_{ij}|^2} = \sqrt{b_1\Pi_h^2 + b_2\Pi_m^2} \leq \sqrt{Max\{b_1,b_2\}(\Pi_h^2+\Pi_m^2)} = \beta, \tag{5.13}$$

where $b_1 = 2(\frac{a}{\mu_h})^2, b_2 = \frac{2(p^2+\beta_1^2+\beta_1\beta_2+\beta_3^2+\beta_1\beta_2)}{(pu_3+\mu_m)^2}$.

iv. The objective functional of (5.6) has an integrand

$$\begin{aligned} L(t,x,u) &= A_1 I_h(t) + A_2 N_m(t) + \sum_{i=1}^{3}\frac{1}{2}K_i u_i^2 \\ &= L_1(t,x) + L_2(t,u). \end{aligned} \tag{5.14}$$

To prove the convexity of integrand function $L(t,x,u)$, it suffices to show that $L_2(t,u) = \sum_{i=1}^{3}\frac{1}{2}K_i u_i^2$ is convex over the control variable u. Notice that $L_2(t,u)$ is a finite non-linear combination of $s_i(u) = \frac{1}{2}u_i^2$ with positive constants K_i. Therefore, it is sufficient to define the function $s(u)$ such that $s(u) = \frac{1}{2}u^2$. By computing the Hessian matrix (second derivative) of $s(u)$ with respect to the control variable u, we have

$$\frac{\partial^2 s(u)}{\partial u_i \partial u_j} = \begin{cases} 1 & \text{if } i = j \\ 0 & \text{if } i \neq j, \end{cases}$$

where $i,j \in \{1,2,3\}$. Hence, the Hessian matrix is positive definite, and as a result, the function $s(u)$ is convex. Therefore, $L_2(t,u)$ is convex, implying that the integrand function $L(t,x,u)$ is convex, which ends the proof of condition (iv).

v. To prove last condition (v), it is evident that, $\frac{K_3 u_3^2}{2} \leq \frac{K_3}{2}$ as $u_3 \in [0,1]$.

$$L(t,x,u) \geq \frac{1}{2}K_1 u_1^2 + \frac{1}{2}K_2 u_2^2 + \frac{1}{2}K_3 u_3^2 \tag{5.15}$$

$$\geq \frac{K_1}{2}u_1^2 + \frac{K_2}{2}u_2^2 + \frac{K_3}{2}u_3^2 - \frac{K_3}{2} \tag{5.16}$$

$$\geq \min\{\frac{K_1}{2}, \frac{K_2}{2}, \frac{K_3}{2}\}|u_1,u_2,u_3|^2 - \frac{K_3}{2}$$

Deciding on $\alpha_1 = \min\{\frac{K_1}{2}, \frac{K_2}{2}, \frac{K_3}{2}\}, \alpha_2 = \frac{K_3}{2} > 0$, we found $L(t,x,u) \geq \alpha_1 |u|^{\alpha_3} - \alpha_2$ with $\alpha_3 = 2$. This ends the proof of condition (v).

□

5.2.2 Characterization of optimal control

In this sub-section, we use the PMP (Kopp, 1962) to provide the necessary conditions for the existence of optimal control. This principle converts equations (5.1), (5.8) and (5.6) into a pointwise minimization of Hamiltonian function $\mathbb{H}$ given as:

$$\mathbb{H} = A_1 I_h(t) + A_2 N_m(t) + \frac{1}{2}K_1 u_1^2(t) + \frac{1}{2}K_2 u_2^2(t) + \frac{1}{2}K_3 u_3^2(t) + \sum_{i=1}^{8} \lambda_i(t) f_i(t,x,u), \tag{5.17}$$

where $f(t,x,u) = \big(f_i(t,x,u)\big)_{i=1}^{8}$, and $\lambda_i, i = 1,2,...,8$ are the adjoint variables which determine the adjoint system.

Theorem 5.2.2. *Let control u_i^* be an optimal triplet with the solution of state system (5.1) that minimizes control problem (5.6), then there exists $\lambda_i(t)$ for $i = 1,2,...,8$ satisfying*

$$
\begin{aligned}
\frac{d\lambda_1}{dt} &= \frac{d(\lambda_1-\lambda_2)}{1+M_a} + \frac{(1-u_1)\beta_1 I_m S_{ah}}{N_h^2}(\lambda_3-\lambda_1) + \frac{(1-u_1)\beta_2 S_{uh} I_m}{N_h^2}(\lambda_3-\lambda_2) \\
&+ \frac{(1-u_1)\beta 3 S_m I_h}{N_h^2}(\lambda_7-\lambda 6) + \frac{(1-u_1)\beta_1 I_m}{N_h}(\lambda_1-\lambda_3) + \mu h\lambda_1, \\
\frac{d\lambda_2}{dt} &= \frac{(1-u_1)\,\beta_1 S_{ah} I_m}{{N_h}^2}(\lambda_3-\lambda_1) + \frac{(1-u_1)\,\beta_2 S_{uh} I_m}{{N_h}^2}(\lambda_3-\lambda_2) \\
&+ \frac{(1-u_1)\,\beta_3 S_m I_h}{{N_h}^2}(\lambda_7-\lambda_6) + \frac{(1-u_1)\,\beta_2 I_m}{N_h}(\lambda_2-\lambda_3) + \kappa M_a\,(\lambda_2-\lambda_1) + \mu_h\lambda_2, \\
\frac{d\lambda_3}{dt} &= \frac{(1-u_1)\beta_1 S_{ah} I_m(\lambda_3-\lambda_1)}{N_h^2} + \frac{(1-u_1)\beta_2 S_{uh} I_m(\lambda 3-\lambda 2)}{N_h^2} + \frac{(1-u_1)\beta_3 S_m I_h(\lambda_7-\lambda_6)}{N_h^2} \\
&+ \frac{(1-u_1)\beta_3 S_m(\lambda_6-\lambda_7)}{N_h} + (\delta+\rho+au_2+\mu_h)\lambda_3 - (\rho+au_2)\lambda_4 - \zeta\lambda_8 - A_1 \\
\frac{d\lambda_4}{dt} &= \frac{(1-u_1)\beta_1 S_{ah} I_m}{N_h^2}(\lambda_3-\lambda_1) + \frac{(1-u_1)\beta_2 S_{uh} I_m}{N_h^2}(\lambda_3-\lambda_2) \\
&+ \frac{(1-u_1)\beta_3 S_m I_h}{N_h^2}(\lambda_7-\lambda_6) + \eta(\lambda_4-\lambda_5) + \lambda_4(\phi+\mu_h), \\
\frac{d\lambda_5}{dt} &= \frac{(1-u_1)\,\beta_1 S_{ah} I_m}{N_h^2}(\lambda_3-\lambda_1) + \frac{(1-u_1)\,\beta_2 S_{uh} I_m}{{N_h}^2}(\lambda_3-\lambda_2) + \frac{(1-u_1)\,\beta_3 S_m I_h}{{N_h}^2}(\lambda_7-\lambda_6) \\
&+ \lambda_5(\varepsilon+\mu_h) - \varepsilon\lambda_1, \\
\frac{d\lambda_6}{dt} &= \frac{(1-u_1)\beta_3 I_h}{N_h}(\lambda_6-\lambda_7) + \lambda_6(\gamma+pu_3+\mu_h) - A_2, \\
\frac{d\lambda_7}{dt} &= \frac{(1-u_1)\beta_1 S_{ah}}{N_h}(\lambda_1-\lambda_3) + \frac{(1-u_1)\beta_2 S_{uh}}{N_h}(\lambda_2-\lambda_3) + \lambda_7(\gamma+u_3+\mu_h) - A_2, \\
\frac{d\lambda_8}{dt} &= \frac{dS_{ah}}{(1+M_a)^2}(\lambda_2-\lambda_1) + \kappa S_{uh}(\lambda_2-\lambda_1) + \theta\lambda_8,
\end{aligned}
\tag{5.18}
$$

with transversality conditions

$$
\lambda_i(T_f) = 0, i = 1,2,...,8. \tag{5.19}
$$

Furthermore, the triple optimal controls $u_i^* = (u_1^*, u_2^*, u_3^*)$, is given by

$$
\begin{aligned}
u_1^*(t) &= \min\left\{\max\left\{0, \frac{\beta_1(\lambda_3-\lambda_1)S_{ah}I_m + \beta_2(\lambda_3-\lambda_2)S_{uh}I_m + \beta_3(\lambda_7-\lambda_6)S_m I_h}{K_1 N_h}\right\}, 1\right\}, \\
u_2^*(t) &= \min\left\{\max\left\{0, \frac{aI_h(\lambda_3-\lambda_4)}{K_2}\right\}, 1\right\}, \\
u_3^*(t) &= \min\left\{\max\left\{0, \frac{pS_m\lambda_6 + pI_m\lambda_7}{K_3}\right\}, 1\right\}.
\end{aligned}
\tag{5.20}
$$

Proof. By differentiating the Hamiltonian function (5.17) with respect to state variables yields

the adjoint equation (5.18). That is,

$$\frac{d\lambda_1}{dt} = -\frac{\partial \mathbb{H}}{\partial S_{ah}}, \quad \frac{d\lambda_2}{dt} = -\frac{\partial \mathbb{H}}{\partial S_{uh}}, \quad \frac{d\lambda_3}{dt} = -\frac{\partial \mathbb{H}}{\partial I_h}, \frac{d\lambda_4}{dt} = -\frac{\partial \mathbb{H}}{\partial T_h}, \tag{5.21}$$
$$\frac{d\lambda_5}{dt} = -\frac{\partial \mathbb{H}}{\partial R_h} \frac{d\lambda_6}{dt} = -\frac{\partial \mathbb{H}}{\partial S_m}, \quad \frac{d\lambda_7}{dt} = -\frac{\partial \mathbb{H}}{\partial I_m}, \quad \frac{d\lambda_8}{dt} = -\frac{\partial \mathbb{H}}{\partial M_a}.$$

Assuming the final state $x(T_f)$ is free at the final time T_f, we obtain the transversality conditions $\lambda(T_f) = 0$ where x represents the state solutions. In addition, the optimal control characterization in equation (5.20) is obtained by solving the next three equations:

$$\frac{\partial \mathbb{H}}{\partial u_1} = 0 \text{ for } u_1^*, \ \frac{\partial \mathbb{H}}{\partial u_2} = 0 \text{ for } u_2^* \text{ and } \frac{\partial \mathbb{H}}{\partial u_3} = 0 \text{ for } u_3^*. \tag{5.22}$$

Depending on the minimality criterion and $0 \leq u_i^* \leq 1$,

$$u_i^* = \begin{cases} 0 \text{ if } \frac{\partial \mathbb{H}}{\partial u_i} > 0 \\ \omega_i^* \text{ if } \frac{\partial \mathbb{H}}{\partial u_i} = 0 \\ 1 \text{ if } \frac{\partial \mathbb{H}}{\partial u_i} < 0 \end{cases}, \begin{cases} \omega_1^* = \frac{\beta_1(\lambda_3-\lambda_1)S_{ah}I_m+\beta_2(\lambda_3-\lambda_2)S_{uh}I_m+\beta_3(\lambda_7-\lambda_6)S_mI_h}{K_1N_h} \\ \omega_2^* = \frac{aI_h(\lambda_3-\lambda_4)}{K_2} \\ \omega_3^* = \frac{pS_m\lambda_6+pI_m\lambda_7}{K_3} \end{cases}, \tag{5.23}$$

where i=1,2,3. To prove optimal control problem described in (5.6) is a problem of minimization, we first calculate the Hessian matrix of the Hamiltonian function with respect to the controls.

$$\mathcal{H} = \begin{pmatrix} K_1 & 0 & 0 \\ 0 & K_2 & 0 \\ 0 & 0 & K_3 \end{pmatrix}. \tag{5.24}$$

Since the weight parameters $K_1, K_2,$ and K_3 are positive constants, then the Hessian matrix $\mathcal{H}$ of the Hamiltonian function is positive definite. Hence, the Hamiltonian function in (5.17) is convex with respect to the control u. Therefore, the optimal control problem described in (5.6) is a problem of minimization. The state system (5.1) is an initial value problem, whereas the adjoint system (5.18) subject to (5.19) is a terminal value problem. Therefore, the optimal control problems stated in Theorem 5.2.2 can be solved numerically with computer assistance. This completes the proof. □

5.3 Numerical simulation

We simulate our optimal control problem (5.1) using Python GEKKO optimization suite. GEKKO, as a dynamic optimization package, aids the differential algebraic equations (DAEs) using inbuilt numerical integration schemes and simplifies its applications with modes of operation and tuning model parameters. GEKKO performs both simultaneous and sequential methods for differential and algebraic systems. Its operation modes include reconciliation of input data, real-time optimisation, dynamic simulation, nonlinear predictive control, and moving horizon estimation. The back-end compiles the model into an efficient low-level format and performs model reduction (Beal et al., 2018). Thus, the optimality system is determined by solving state system (5.1), adjoint system (5.18) and optimal controls (5.20) with Python GEKKO suits. For

the numerical investigation of the optimal control problem, we used parameter values in Table 5.1 and initial data of Ethiopian population at risk of malaria, which were presented in Section 5.1.2. We choose the weighting constants $A_1 = A_2 = K_1 = K_2 = K_3 = 1$ to balance the objective functional, rather than prioritizing between the cost of infections and the cost of controls. This equal-weighting structure is particularly advantageous for cost-effectiveness analysis, as it standardizes the relative contributions of health outcomes and intervention expenses. Consequently, differences between control strategies arise solely from model dynamics and intervention performance rather than from arbitrary parameter scaling, enabling fair comparison and yielding more interpretable cost-effectiveness measures. Global experts and WHO have embraced the goal of malaria eradication by the year 2050 (Feachem, 2014; Mahase, 2019). We decided to use the simulation time from year 2000 to 2050, aiming to assess how control efforts could lead to global malaria eradication by the year 2050. Thus, we take $t \in [0, T_f]$ such that $T_f = 50$ years. In addition, we take the parameter value $a = p = 0.25$ from Otieno et al. (2016). To explore the best disease control and cost-effective strategies, we considered all seven strategies:

Strategy A: Personal protective measures $(u_1 \neq 0, u_2 = u_3 = 0)$,

Strategy B: Improved treatment capability $(u_2 \neq 0, u_1 = u_3 = 0)$,

Strategy C: Mosquito breeding site destruction $(u_3 \neq 0, u_1 = u_2 = 0)$,

Strategy D: Combination of personal protective measures and improved treatment capability $(u_1 \neq 0, u_2 \neq 0, u_3 = 0)$,

Strategy E: Combination of personal protective measures and mosquito breeding site destruction $(u_1 \neq 0, u_3 \neq 0, u_2 = 0)$,

Strategy F: Combination of improved treatment capability and mosquito breeding site destruction $(u_2 \neq 0, u_3 \neq 0, u_1 = 0)$,

Strategy G: Combination of all $(u_1 \neq 0, u_2 \neq 0, u_3 \neq 0)$.

5.3.1 Strategy A: Personal protective measures $(u_1 \neq 0, u_2 = u_3 = 0)$

In this strategy, the cost functional $\mathcal{J}$ is optimized by using personal protective measures u_1 only, while the rest controls $u_2 = u_3 = 0$.

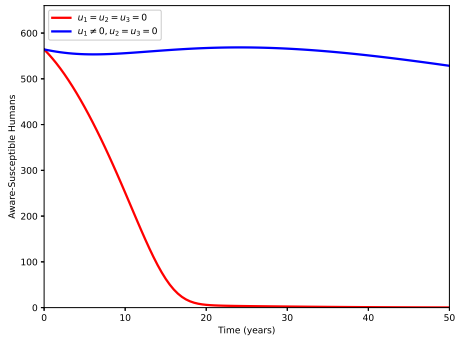

(a) Dynamics of S_{ah}

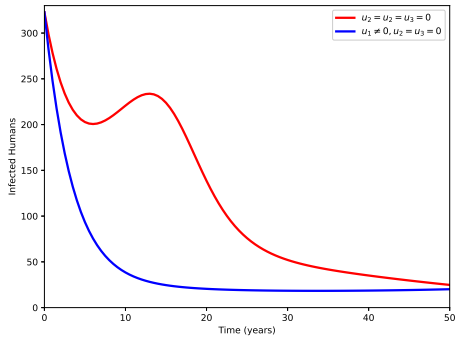

(b) Dynamics of I_h

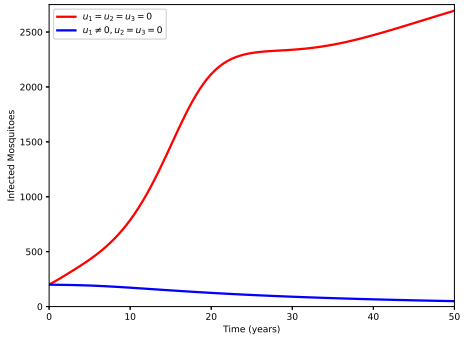

(c) Dynamics of I_m

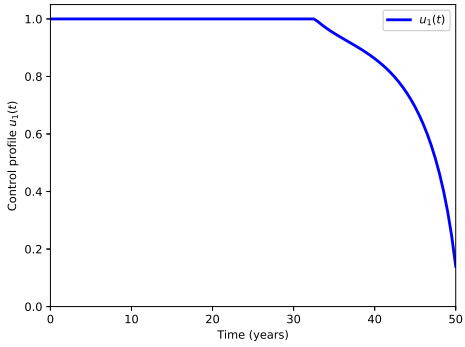

(d) Dynamics of control profile u_1

Figure 5.2: Solution of the system (5.1) depicting the effect of control u_1

Figure (5.2b) demonstrates that the effective use of personal protective measures significantly reduces the number of malaria-infected humans compared to those who do not utilize these measures. Simultaneously, Figure (5.2c) illustrates that the number of malaria-infected mosquitoes decreases to approximately 60 when control measures are consistently implemented over 50 years. In contrast, without these controls, the number of infected mosquitoes rapidly increases to around $6,000$ following the intervention period. Additionally, Figure (5.2a) shows a gradual rise in the number of susceptible humans as personal protective measures are put in place. Finally, the control profile in Figure (5.2d)indicates that the use of personal protective measures should be maintained at 100% until 32 years, after which it gradually declines to 14% by 50 year.

5.3.2 Strategy B: Improved treatment capability $(u_2 \neq 0, u_1 = u_3 = 0)$

In this strategy, control u_2, which focuses solely on improved treatment capability, is utilized to optimize the cost functional $\mathcal{J}$, while the other controls, u_1 and u_3, are set to zero.

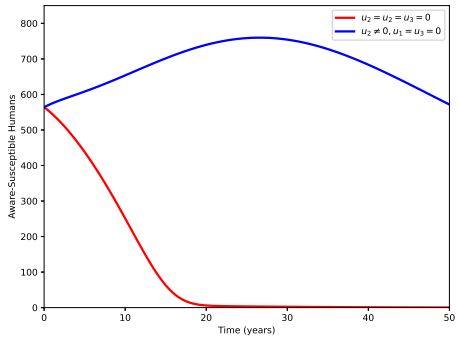

(a) Dynamics of S_{ah}

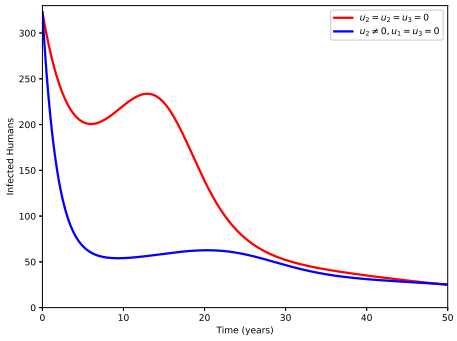

(b) Dynamics of I_h

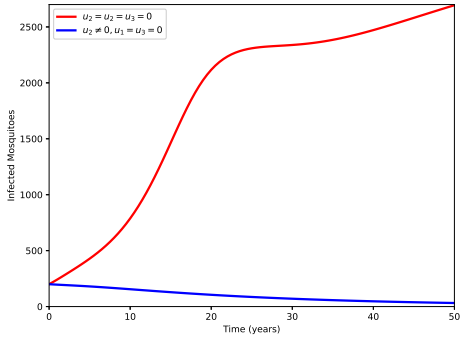

(c) Dynamics of I_m

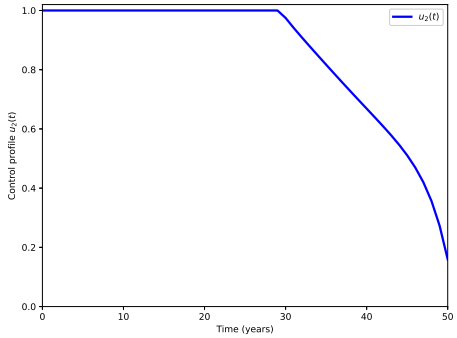

(d) Dynamics of control profile u_2

Figure 5.3: Solution of the system (5.1) depicting the effect of improved treatment capability u_2.

In Figures (5.3b) and (5.3c), there is a notable difference in the numbers of infected humans I_h and infected mosquitoes I_m when improved treatment capability is applied. The infectious populations in both species significantly decline with the implementation of this control. As a consequence, Figure (5.3a) shows applying improved treatment capability increases the number of vulnerable humans from 564 to 750 around year 30. This occurs because effective malaria treatment clears infections in humans, but recovered individuals may subsequently lose their immunity, making them susceptible to future infections. Moreover, the control profile in Figure (5.3d) indicates that the optimal improved treatment capability should be applied at 100% intensity until year 29, after which it should gradually decrease to 15% post year 30.

5.3.3 Strategy C: Mosquito breeding site destruction $(u_3 \neq 0, u_1 = u_2 = 0)$

In this strategy, we implement the use of mosquito breeding site destruction effort u_3 alone to optimize the cost functional $\mathcal{J}$, while the other controls u_1 and u_2 were kept zero, and the simulation results are depicted in Figure 5.4.

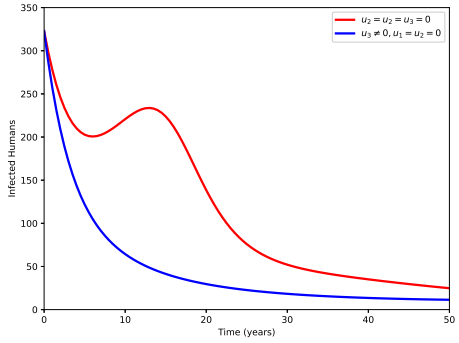

(a) Dynamics of I_h

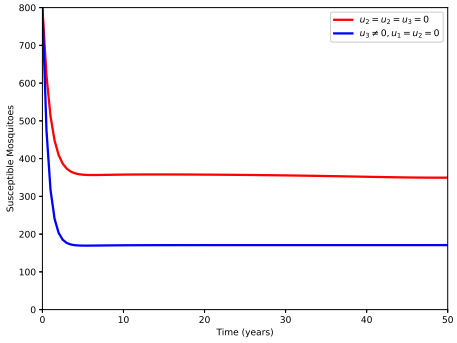

(b) Dynamics of S_m

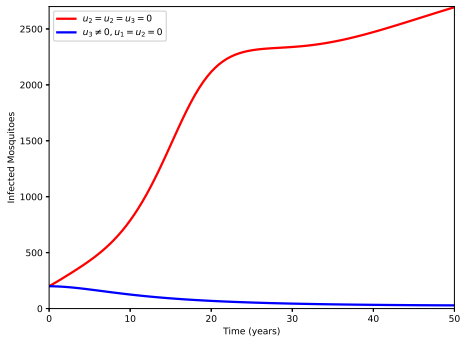

(c) Dynamics of I_m

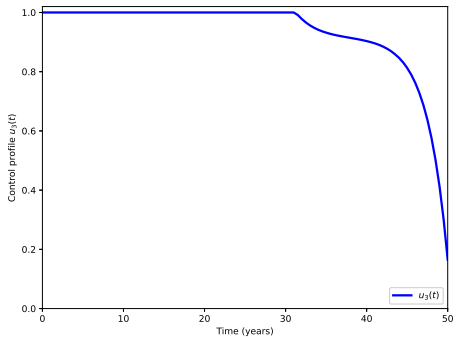

(d) Dynamics of control profile u_3

Figure 5.4: Solution of system (5.1) depicting the effect of mosquito breeding site destruction u_3.

The data presented in Figures (5.4a)- (5.4c) clearly demonstrate that implementing mosquito breeding site destruction u_3 significantly reduces the numbers of infected humans I_h, infected mosquitoes I_m, and susceptible mosquitoes S_m compared to the uncontrolled case. Without this control measure, the number of infected mosquitoes I_m rapidly escalates to approximately $2,700$ around year 50, while the number of susceptible mosquitoes S_m gradually declines due to infection, stabilizing at about 350 after 10 years. In contrast, implementing an optimal mosquito breeding site destruction strategy results in substantial reductions in infected humans, infected mosquitoes, and susceptible mosquitoes, converging to at least $10, 36$, and 175, respectively, after 50 years. Furthermore, Figure (5.4d) indicates that the mosquito breeding site destruction efforts u_3 should be maintained at 100% until year 31, followed by a gradual decrease to 17% by year 50.

5.3.4 Strategy D: Combination of personal protective measures and improved treatment capability $(u_1 \neq 0, u_2 \neq 0, u_3 = 0)$

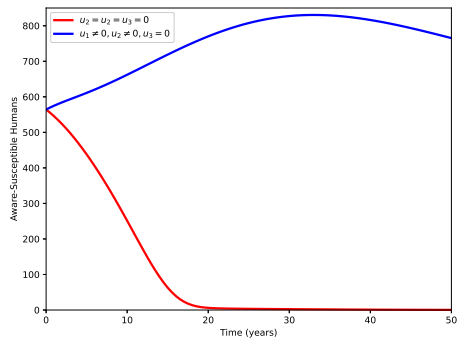

(a) Dynamics of S_{ah}

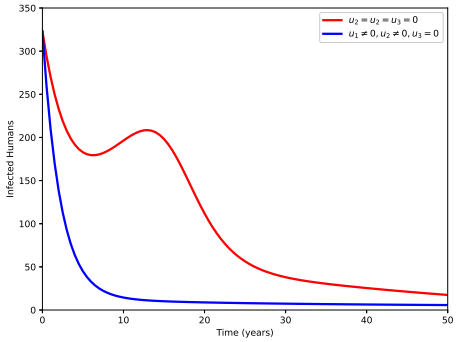

(b) Dynamics of I_h

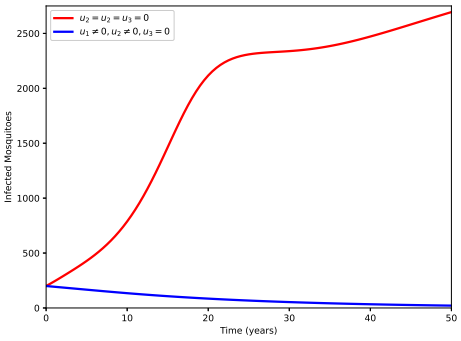

(c) Dynamics of I_m

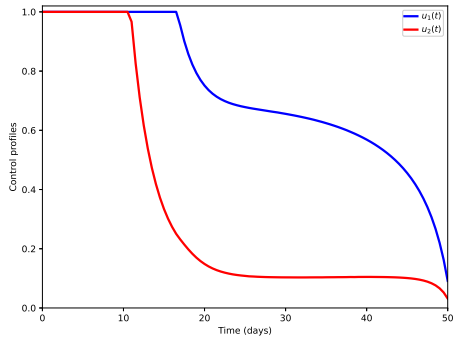

(d) Dynamics of control profiles u_1 and u_2

Figure 5.5: Solution of the system (5.1) depicting the effect of personal protective measures u_1 and improved treatment capability u_2.

The simulation results presented in Figures (5.5b) and (5.5c) illustrate that how the combined use of the considered controls significantly reduce malaria incidence among both human and mosquito populations. This approach shows that both infectious species decrease more rapidly to lower levels compared to strategy without any controls. Consequently, the number of aware-susceptible humans increases from an initial value of 564 to 800 nearly 30 years of optimal implementation. Figure (5.5d) further indicates that the optimal control for personal protective measures u_1 is maintained at 100% for 16 consecutive years, before gradually declining to 9% by 50 year. Meanwhile, the optimal control for improved treatment capability u_2 remains at 100% for 10 years and then decreases to 3% by 50 year.

5.3.5 Strategy E: Personal protective measures and mosquito breeding site destruction $(u_1 \neq 0, u_3 \neq 0, u_2 = 0)$

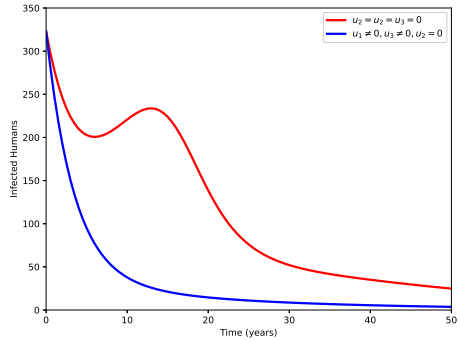

(a) Dynamics of I_h

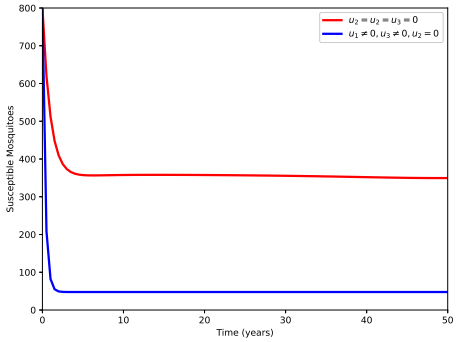

(b) Dynamics of S_m

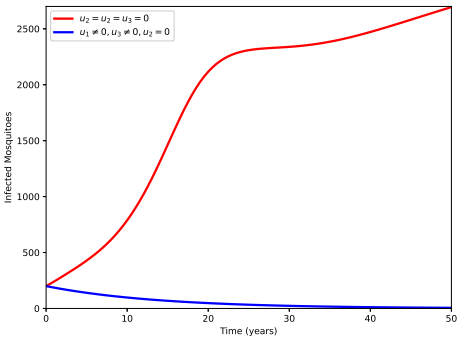

(c) Dynamics of I_m

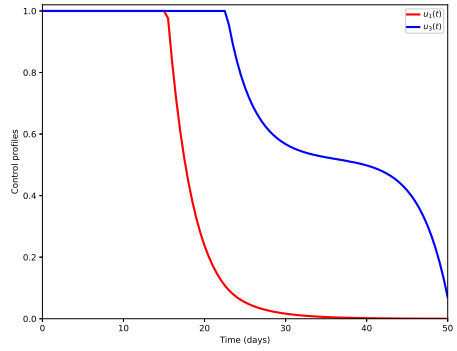

(d) Dynamics of control profiles u_2 and u_3

Figure 5.6: Solution of the system (5.1) depicting the effect of controls u_1 and u_3.

In this strategy, we implement personal protective measures u_1 and mosquito breeding site destruction u_3 to minimize the objective functional $\mathcal{J}$ presented in (5.6). Figures (5.7a)-(5.7c) reveals that the number of infectious humans I_h, infectious mosquitoes I_m, and susceptible mosquitoes S_m decreases when the integrated control measure is applied. As indicated by the control profiles in Figure (5.7d), the optimal personal protective measure control u_1 maintains 100% until $t = 15$ years and then goes down to the lower bound after $t = 35$ years, while the optimal mosquito breeding site destruction control u_3 maintains its 100% for $t = 22$ years and then decreases to maintain 7% in the $t = 50$ year.

5.3.6 Strategy F: Combination of improved treatment capability and mosquito breeding site destruction $(u_2 \neq 0, u_3 \neq 0, u_1 = 0)$

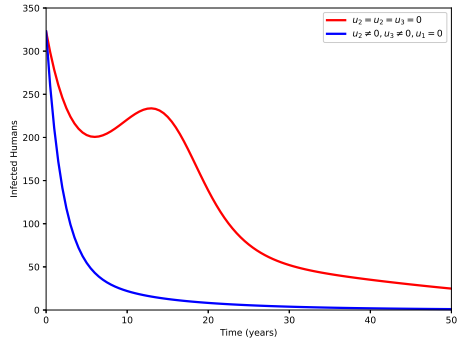

(a) Dynamics of I_h

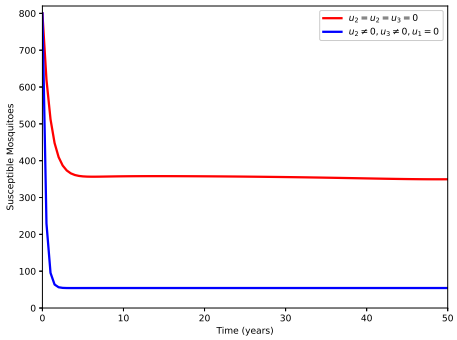

(b) Dynamics of S_m

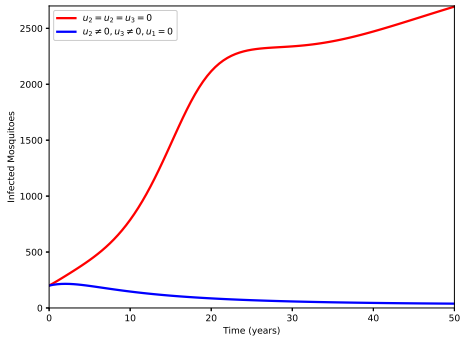

(c) Dynamics of I_m

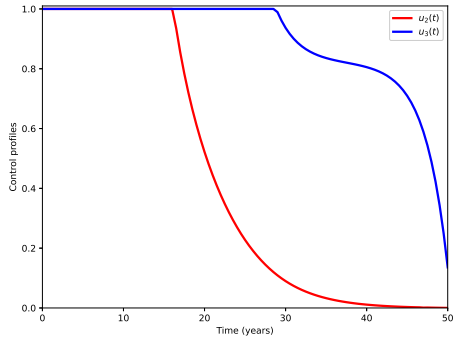

(d) Dynamics of u_2 and u_3

Figure 5.7: Solution of the system (5.1) depicting the effect of controls u_2 and u_3.

In this strategy, improved treatment capability u_2 and mosquito breeding site destruction u_3-were implemented simultaneously to minimize the objective functional $\mathcal{J}$ in (5.6), while control u_1 was set to zero. Figures (5.6a)-(5.6c) illustrate that this combined control strategy effectively reduced the numbers of both infectious humans and mosquitoes compared to uncontrolled scenarios. Figure (5.6d) reveals that the optimal control for improved treatment capability u_2 is maintained at 100% until 20 year, after which it gradually decreases to its lower bound by 40 year. Meanwhile, the optimal control for mosquito breeding site destruction u_3 remains at 100% for 28 years before gradually declining to 14% by 50 year. This indicates that, under this strategy, achieving improved treatment capability required less effort after 40 years.

5.3.7 Strategy G: Combination of all $(u_1 \neq 0, u_2 \neq 0, u_3 \neq 0)$

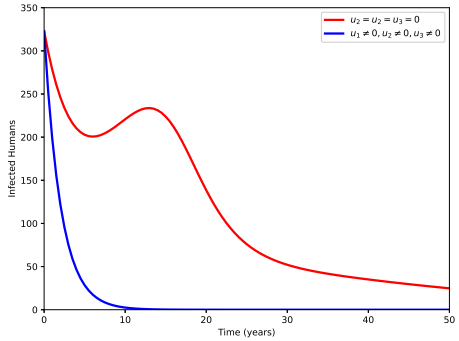

(a) Dynamics of I_h

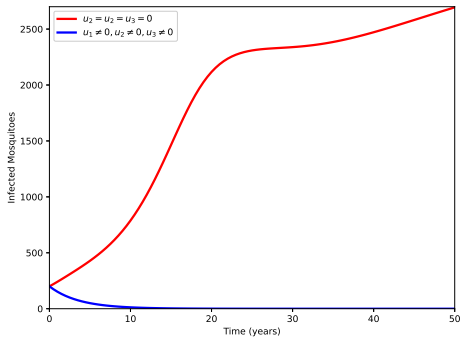

(b) Dynamics of I_m

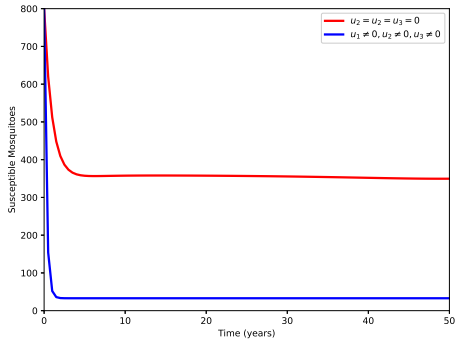

(c) Dynamics of S_m

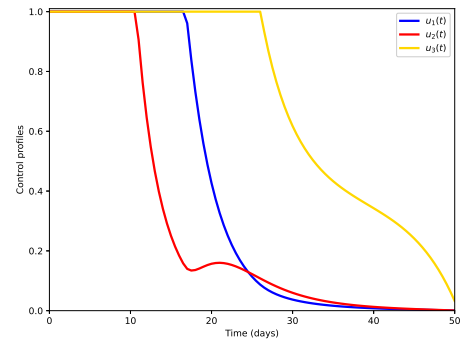

(d) Dynamics of control profiles u_1, u_2 and u_3

Figure 5.8: Solution of the system (5.1) depicting the effect of controls u_1, u_2 and u_3.

In this strategy, we implement all the considered control strategies to optimize the cost functional $\mathcal{J}$ as defined in (5.6). Figures (5.8a) and (5.8b) show that the populations of both infectious humans and mosquitoes decrease to nearly zero around 10 year with the optimal implementation of all considered control measures. Additionally, the population of susceptible mosquitoes drops to 35 after 2 years with the application of this combined control strategy. The control profiles illustrated in Figure (5.8d) indicate that the personal protective measure u_1 is maintained at 100% until year 16, after which it gradually declines to its lower bound by 40 year. Meanwhile, the optimal treatment capability u_2 decreases gradually from its upper bound at year 11 to its lower bound by 42 year. The optimal mosquito breeding site destruction u_3 remains at its upper bound until 26 year, before slowly declining to maintain 5% for the duration of the simulation.

5.4 Cost-effectiveness analysis

Based on the simulation findings in Section 5.3, reveal that each of the intervention strategies substantially reduces malaria transmission. However, these strategies differ markedly in resource requirements, implementation complexity, and associated economic costs. Thus, it is

essential to identify the most cost-effective intervention strategy among the options considered. In this context, we calculate the average cost-effectiveness ratio (ACER) and the incremental cost-effectiveness ratio (ICER), as outlined in (Berhe et al., 2018; Engida et al., 2024; Okosun et al., 2013). The total implementation cost during the simulation period is given by:

$$\mathcal{C}(u_1,u_2,u_3)=\frac{1}{2}\int_0^{T_f}\left(K_1u_1^2(t)+K_2u_2^2(t)+K_3u_3^2(t)\right)dt. \tag{5.25}$$

The ACER of control strategy $\mathcal{S}$ given by the formula:

$$ACER(\mathcal{S})=\frac{\text{Total implementation cost resulted by the strategy } \mathcal{S}}{\text{Total infection averted due to the strategy } \mathcal{S}}. \tag{5.26}$$

The ACER method considers one optimal strategy and compares that strategy against an existing intervention. The overall number of infectious cases averted during the simulation period is determined by subtracting the total number of infected individuals without control from the total number of infected individuals under control implementation. A strategy with the lowest ACER value is the effective and costly-less strategy. Thus, the total number of infection-averted humans during the simulation period denoted by $\mathcal{A}_{I_h}$ is calculated as follows:

$$\mathcal{A}_{I_h}=\int_0^{50}I_h(t)dt-\int_0^{50}I_h^{\star}(t)dt \tag{5.27}$$

where the integrals $\int_0^{50}I_h(t)dt$ and $\int_0^{50}I_h^{\star}(t)dt$ respectively represents the total number infections in humans with and without control over $[0,50]$ years. Having equation (5.25), the overall cost employed by each strategy is given by

$$T_{CA}=\frac{1}{2}\int_0^{50}K_1u_1^2dt,\ T_{CB}=\frac{1}{2}\int_0^{50}K_2u_2^2dt,\ T_{CC}=\frac{1}{2}\int_0^{50}K_3u_3^2dt,\ T_{CD}=\frac{1}{2}\int_0^{50}\left(K_1u_1^2+K_2u_2^2\right)dt,$$
$$T_{CE}=\frac{1}{2}\int_0^{50}\left(K_2u_2^2+K_3u_3^2dt,T_{CF}=\frac{1}{2}\int_0^{50}\left(K_1u_1^2+K_3u_3^2\right)dt,T_{CG}=\frac{1}{2}\int_0^{50}\left(K_1u_1^2+K_2u_2^2+K_3u_3^2\right)dt.$$

Now, using equation (5.26), the ACER values for each strategy are calculated and presented in Table 5.3.

$$ACER(A)=\frac{637.5}{2674.34}=0.238,\ ACER(B)=\frac{279.2}{195.8}=1.43,\ ACER(C)=\frac{637.5}{1948.9}=0.327, \tag{5.28}$$
$$ACER(D)=\frac{644.5}{3162.5}=0.204,\ ACER(E)=\frac{459.28}{2672.7}=0.186, \tag{5.29}$$
$$ACER(F)=\frac{496.7}{2960.85}=0.168,\ ACER(G)=\frac{697.3}{3160.14}=0.22.$$

As shown in Table 5.3, the strategy F is the most economical and has the greatest health benefits than the remaining six strategies. Additionally, the summary of Table 5.3 is portrayed in bar graph (5.9).

Table 5.3: The ACER computation of strategies of Strategies $A, B, C, D, E, F,$ and G.

Strategies	$\mathcal{A}_{I_h}$ **values**	T_C **values**	**ACER values**
A	2674.34	637.5	0.238
B	195.8	279.2	1.43
C	1948.9	637.5	0.327
D	3162.5	644.5	0.204
E	2672.7	459.28	0.186
F	2960.85	496.7	0.167
G	3160.14	697.3	0.22

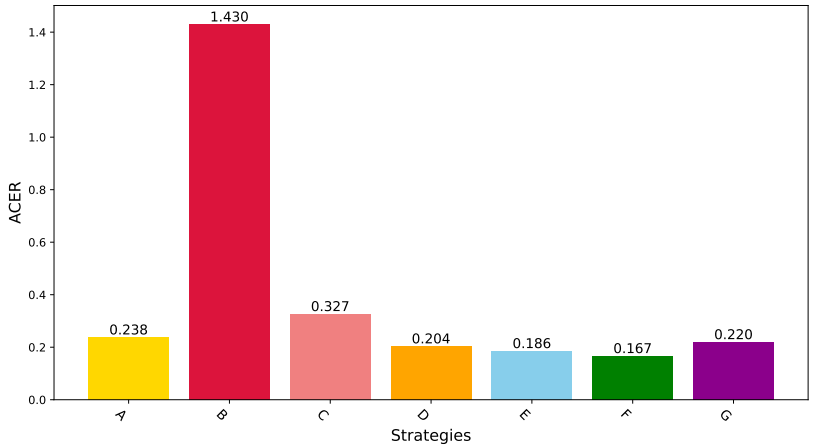

Figure 5.9: The ACER analysis for seven strategies.

Furthermore, for two competing intervention strategies striving for the same resources, the ICER is defined as the difference in costs between the two strategies divided by the difference in their respective outcomes. Economically, this represents the average incremental cost associated with achieving one additional unit of health outcome. When comparing two strategies, the ICER provides an economic perspective on the additional costs required to obtain an extra unit of health benefit from one strategy over the other. Thus, ICER analysis facilitates the ranking of implemented strategies based on their cost-effectiveness. It is calculated using the following mathematical formula:

$$ICER = \frac{\text{Difference between the overall implementation costs of Strategies k and j}}{\text{Difference between the overall infection averted by implementing strategies k and j}}$$

To implement the ICER, we recall a simulation result of the optimal control model provided in Section 5.3 for the seven intervention strategies. Based on these results, our proposed strategies are ranked in ascending order of the total number of infections averted. Thus, we put strategies

$B, C, E, A, F, G,$ and D in their ascending order of number of malaria averted and the corresponding ICER values given in Table 5.4 are calculated as:

$$ICER(B) = \frac{279.2-0}{195.8-0} = 1.43,\ ICER(C) = \frac{637.5-279.2}{1948.9-195.8} = 0.204,$$
$$ICER(E) = \frac{459.28-637.5}{2672.7-1948.9} = -0.246, ICER(A) = \frac{637.5-459.28}{2674.34-2672.7} = 108.67,$$
$$ICER(F) = \frac{496.7-637.5}{2960.85-2674.34} = -0.49, ICER(G) = \frac{697.3-496.7}{2960.85} = 1.0,$$
$$ICER(D) = \frac{644.5-697.3}{3162.5-3160.14} = -22.37.$$

Table 5.4: The ICER values for strategies $A, B, C, D, E, F,$ and G.

Strategies	$\mathcal{A}_{I_h}$ **values**	T_C **values**	**ICER values**
B	195.8	279.2	1.43
C	1948.9	637.5	0.204
E	2672.7	459.28	-0.246
A	2674.34	637.5	108.67
F	2960.85	496.7	-0.49
G	3160.14	697.3	1.0
D	3162.5	644.5	-22.37

From Table 5.4, the strategy A has a higher ICER compared to the rest six strategies. Since, alternative A is most expensive and ineffective one. Thus, we excluded strategy A from further calculation. Having strategies B, C, E, F, G and D, ICERs are recalculated, and their results are given in the Table 5.5.

$$ICER(B) = \frac{279.2-0}{195.8-0} = 1.43,\ ICER(C) = \frac{637.5-279.2}{1948.9-195.8} = 0.204,$$
$$ICER(E) = \frac{459.28-637.5}{2672.7-1948.9} = -0.246, ICER(F) = \frac{496.7-459.28}{2960.85-2672.74} = 0.129,$$
$$ICER(G) = \frac{697.3-496.7}{2960.85} = 1,\ ICER(D) = \frac{644.5-697.3}{3162.5-3160.14} = -22.37.$$

Table 5.5: The ICER values of strategies $B, C, D, E, F,$ and G.

Strategies	$\mathcal{A}_{I_h}$ **values**	T_C **values**	**ICER values**
B	195.8	279.2	1.43
C	1948.9	637.5	0.204
E	2672.7	459.28	-0.246
F	2960.85	496.7	0.129
G	3160.14	697.3	1.0
D	3162.5	644.5	-22.37

The ICER values in Table 5.5 indicate that strategy B is a expensive and ineffective strategy than strategies C, E, F, G and D. It follows that strategy

. Therefore, we exclude strategy G from the list, and ICER values of $C, E, F,$ and D are recalculated, and their results are given in Table 5.6.

$$ICER(C) = \frac{637.5-0}{1948.9-0} = 0.327,\ ICER(E) = \frac{459.28-637.5}{2672.7-1948.9} = -0.246,$$
$$ICER(F) = \frac{496.7-459.28}{2960.85-2672.74} = 0.129, ICER(G) = \frac{697.3-496.7}{2960.85} = 1,$$
$$ICER(D) = \frac{644.5-697.3}{3162.5-3160.14} = -22.37.$$

Table 5.6: The ICER values of strategies $C, D, E, F,$ and G.

Strategies	$\mathcal{A}_{I_h}$ **values**	T_C **values**	**ICER values**
C	1948.9	637.5	0.327
E	2672.7	459.28	-0.246
F	2960.85	496.7	0.129
G	3160.14	697.3	1.0
D	3162.5	644.5	-22.37

With this result, we conclude that strategy G has the highest ICER and therefore is cost ineffective than the rest strategies. Therefore, we exclude strategy G from the list and ICER of C, E, F and D are recalculated and the result given in Table 5.7

$$ICER(C) = \frac{637.5-0}{1948.9-0} = 0.327,\ ICER(E) = \frac{459.28-637.5}{2672.7-1948.9} = -0.246,$$
$$ICER(F) = \frac{496.7-459.28}{2960.85-2672.74} = 0.129, ICER(D) = \frac{644.5-496.7}{3162.5-2960.85} = 0.73.$$

Table 5.7: The ICER values of strategies $C, D, E,$ and F.

Strategies	$\mathcal{A}_{I_h}$ **values**	T_C **values**	**ICER values**
C	1948.9	637.5	0.327
E	2672.7	459.28	-0.246
F	2960.85	496.7	0.129
D	3162.5	644.5	-21.44

The strategy C is significantly dominated and is expensive than strategy E, F and D as then strategy C is excluded from the options. Thus, the ICER of strategies E, F and D are recalculated.

$$ICER(E) = \frac{459.28 - 0}{2672.7 - 0} = 1.72, ICER(F) = \frac{496.7 - 459.28}{2960.85 - 2672.74} = 0.129,$$
$$ICER(D) = \frac{644.5 - 496.7}{3162.5 - 2960.85} = 0.73.$$

Table 5.8: The ICER values of strategies $E, F,$ and D

Strategies	$\mathcal{A}_{I_h}$ **values**	T_C **values**	**ICER values**
E	2672.7	459.28	0.172
F	2960.85	496.7	0.129
D	3162.5	644.5	-21.44

The comparison between strategies E and F shows $ICER(E) > ICER(F)$ shows that strategy E is costly high and ineffective strategy than strategy F. Therefore, strategy E is removed from the list of alternatives. Lastly, the ICER of strategies F and D are recalculated as

$$ICER(F) = \frac{496.7 - 0}{2960.85 - 0} = 0.17, ICER(D) = \frac{644.5 - 496.7}{3162.5 - 2960.85} = -21.44.$$

The results indicate that $ICER(F) = 0.17$ and $ICER(D) = 0.73$. The ICER for Strategy D is negative, with $ICER(F) = 0.17$, indicating that this intervention both reduces total costs and improves health outcomes compared to the strategy F. The negative ICER value signifies that optimal combination of personal protective measures (u_1) and mosquito breeding site destruction (u_3) is dominant, being economically advantageous while more effective in controlling the malaria. This result suggests that implementing Strategy F not only lowers expenditures associated with infections and interventions but also maximizes health benefits, underscoring its efficiency and supporting its prioritization over alternative control measures.

CHAPTER 6

IMPACT OF ASYMPTOMATIC INFECTIONS IN MALARIA TRANSMISSION DYNAMICS

This chapter, we present a deterministic mathematical model of malaria transmission that assess the impact of asymptomatic cases. We establish fundamental mathematical properties, including positivity, boundedness of solutions, and feasibility. Additionally, we derive and analyze the basic reproduction number $\mathfrak{R}_0$, perform stability and bifurcation analysis of equilibrium points. Finally, we provide model validation, estimate key parameters, and present numerical investigations.

6.1 The model formulation

To portray the transmission dynamics of malaria infection, we develop a compartmental mathematical model using a nonlinear system of ODEs. The model entails human and mosquito populations. The model flow is susceptible-exposed-asymptomatic-infected-treated-recovered-susceptible $(S–E–A–I–T–R–S)$ patterns for the human population and the susceptible-infected $(S–I)$ pattern for the mosquito population. The total human population denoted by N_h is sub-divided into six mutually disjoint classes: susceptible human S_h, exposed human E_h, asymptomatic infected human A_h, symptomatic infected human I_h, treated human T_h, and recovered human R_h classes. Therefore, we express the total human population N_h, as:

$$N_h = S_h + E_h + A_h + I_h + T_h + R_h.$$

On the other hand, the mosquito population is sub-divided into two classes: susceptible mosquitoes S_m and infected mosquitoes I_m. The total mosquito population, denoted as N_m, is given by:

$$N_m = S_m + I_m.$$

Individuals who are born or immigrate are assumed to be susceptible, denoted by Λ_h influxed into susceptible class. As mentioned in (Aguilar & Gutierrez, 2020; Zahid et al., 2023), human-mosquito contact rates greatly vary and are dependent on a number of factors, such as the number of susceptible and infectious species present in the particular area. It is also assumed that total population sizes of humans in the community determine the average number of mosquito bites that humans experience. Thus, humans in a susceptible class become infected if they come into contact with infected mosquitoes at the transmission rate β_1 with the force of infection $\frac{\beta_1 S_h I_m}{N_h}$ and then move to the exposed class. We assume that recovery from malaria does not confer lifelong immunity. Therefore, ε rate of recovered humans lose their immunity and return to the susceptible class. Due to the arrival of secondary infections from the susceptible human class, there is an increase in the number of exposed human class by $\frac{\beta_1 S_h I_m}{N_h}$ humans. Exposed humans remain in that class for a mean duration of $\frac{1}{r}$. A proportion σr of exposed humans enter the asymptomatic infected class A_h, while the remaining $(1-\sigma)r$ of exposed humans enter the

symptomatic infected class I_h. We assume that an asymptomatic case serves as a reservoir for transmission and is one of the precursors to symptomatic malaria (Kassie et al., 2024). Without treatment, asymptomatic malaria infections can persist and potentially lead to complications over time, causing chronic health issues such as anemia (Agaba et al., 2022). Thus, we assume a proportion $q\phi$ of asymptomatic infectious individuals are precursors to the symptomatic infected ones, whereas the remaining $(1-q)\phi$ are added to the recovery class due to screening followed by on spot treatment tactic (Singh et al., 2022). It is assumed that symptomatic humans who are treated enter the recovery class at the rate η and die due to treatment failure at a rate φ. The recovery class increases as humans recover from both asymptomatic and treated classes, with rates $(1-q)\phi$ and η respectively. Finally, the human population in each class is decreased by the natural death rate μ_h.

The constant recruitment of mosquitoes into the susceptible mosquitoes class at a rate Λ_m is assumed. When a susceptible mosquito S_m, bites a asymptomatic infectious human at rate β_2, the force of infection is $\frac{\beta_2 S_m A_h}{N_h}$. In similar way, when a susceptible mosquito bites a symptomatic infectious human I_h, at rate β_3, the resulting force of infection is $\frac{\beta_3 S_m I_h}{N_h}$. Consequently, the force of infection resulting from human-to-mosquito transmission is defined as the sum of the force of infections associated with humans in classes A_h and I_h. This is expressed mathematically as: $\frac{\beta_2 S_m A_h}{N_h} + \frac{\beta_3 S_m I_h}{N_h}$. Finally, mosquitoes population in each class is reduced by either the insecticide application at the rate γ or by the natural death at the rate μ_m.

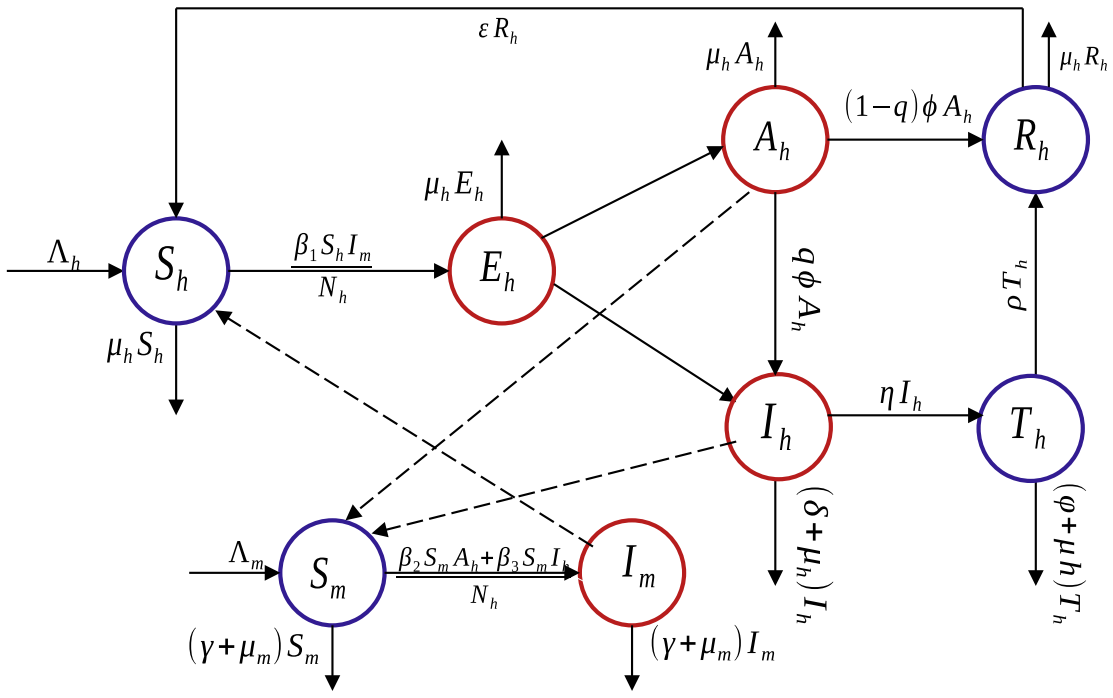

Figure 6.1: Schematic diagram showing dynamic transmission of malaria

Based on the aforementioned assumptions and the interaction between humans and mosquitoes, the governing system of ODEs model is given as

$$\begin{cases} \frac{dS_h}{dt} = \Lambda_h - \frac{\beta_1 S_h I_m}{N_h} + \varepsilon R_h - \mu_h S_h, \\ \frac{dE_h}{dt} = \frac{\beta_1 S_h I_m}{N_h} - (r+\mu_h)E_h, \\ \frac{dA_h}{dt} = \sigma r E_h - (\phi+\mu_h)A_h, \\ \frac{dI_h}{dt} = (1-\sigma)rE_h + q\phi A_h - (\eta+\delta+\mu_h)I_h, \\ \frac{dT_h}{dt} = \eta I_h - (\rho+\varphi+\mu_h)T_h, \\ \frac{R_h}{dt} = (1-q)\phi A_h + \rho T_h - (\varepsilon+\mu_h)R_h, \\ \frac{dS_m}{dt} = \Lambda_m - \frac{\beta_2 S_m A_h}{N_h} - \frac{\beta_3 S_m I_h}{N_h} - (\gamma+\mu_m)S_m, \\ \frac{dI_m}{dt} = \frac{\beta_2 S_m A_h}{N_h} + \frac{\beta_3 S_m I_h}{N_h} - (\gamma+\mu_m)I_m \end{cases} \tag{6.1}$$

subjected to the initial conditions,

$$S_{h0} > 0, E_{h0} \geq 0, A_{h0} \geq 0, I_{h0} \geq 0, T_{h0} \geq 0, R_{h0} \geq 0, S_{m0} \geq 0, I_{m0} \geq 0. \tag{6.2}$$

Table 6.1: Description of parameters involved in the malaria model (6.1).

Parameters	Meanings	Units
Λ_h	Recruitment rate of susceptible humans by birth/immigration	year^{-1}
Λ_m	Recruitment of susceptible mosquitoes	year^{-1}
ε	Rate of waning of immunity	year^{-1}
σ	Constant proportions between 0 and 1 for exposed humans	-
q	Constant proportions between 0 and 1 asymptomatic progression	-
β_1	The rate of transmission from I_m to S_h class	year^{-1}
β_2	The rate of transmission from A_h to S_m class	year^{-1}
β_3	The rate of transmission from I_h to S_m class	year^{-1}
ϕ	The progression rate asymptomatic humans to either I_h or R_h class	year^{-1}
r	The progression rate expose humans to either A_h or I_h class	year^{-1}
μ_h	Natural death rate of humans	year^{-1}
η	Drug treatment rate of symptomatic infected humans	year^{-1}
δ	Malaria-induced death rate of symptomatic infected humans	year^{-1}
ρ	Recovery rate of treated humans	year^{-1}
φ	Death rate due to malaria treatment failure	year^{-1}
γ	Rate of insecticides usage	year^{-1}
μ_m	Natural death rate of mosquitoes	year^{-1}

We assume all state variables and parameters involved in the model are non-negative.

6.2 Model analysis

This section provides mathematical and epidemiological well-posedness, including positivity and boundedness, existence of steady states, computing malaria-reproductive number, stability analysis of steady states, and sensitivity analysis of the malaria model (6.1).

6.2.1 Positivity and boundedness of the model solutions

Theorem 6.2.1. *Every solution of the model (6.1) remains positive for all $t > 0$ given that the initial conditions provided in (6.1) are positive.*

Proof. Define

$$t_1 = sup\{t > 0 : S_h(t) > 0, E_h(t) > 0, A_h(t) > 0, I_h(t) > 0, T_h(t) > 0, R_h(t) > 0, S_m(t) > 0, I_m(t) > 0\}.$$

Given that

$S_h(0) > 0$, $E_h(0) > 0$, $A_h(0) > 0$, $I_h(0) > 0$, $T_h(0) > 0$, $R_h(0) > 0$, $S_m(0) > 0$, and $I_m(0) > 0$. Hence, $t_1 > 0$. If $t_1 < \infty$, then $S_h(t)$, $E_h(t)$, $A_h(t)$, $I_h(t)$, $T_h(t)$, $R_h(t)$, $S_m(t)$ and $I_m(t)$ all take zero at t_1. Accordingly, from the first equation of model (6.1), we have

$$\frac{dS_h}{dt} + \left(\mu_h + \frac{\beta_1 I_m}{N_h}\right) S_h = \Lambda_h + \varepsilon R_h$$

Applying the integrating factor, we obtain

$$S_h(t_1) = S_h(0) e^{-\int_0^{t_1} \left(\mu_h + \frac{\beta_1 I_m(\tau)}{N_h(\tau)}\right) d\tau} + e^{-\int_0^{t_1} \left(\mu_h + \frac{\beta_1 I_m(\tau)}{N_h(\tau)}\right) d\tau} \times \int_0^{t_1} \left[\left(\Lambda_h + \varepsilon R_h(\tau)\right) e^{\int_0^{t} \left(\mu_h + \frac{\beta_1 I_m(\xi)}{N_h(\xi)}\right) d\xi} \right] d\tau > 0.$$

From the second equation of model (6.1), we have

$$\frac{dE_h}{dt} + (r + \mu_h) E_h = \frac{\beta_1 S_h I_m}{N_h}.$$

Applying integrating in the same way, we have

$$E_h(t_1) = E_h(0)\, e^{-\int_0^{t_1} \left(r+\mu_h\right) d\tau} + e^{-\int_0^{t_1} \left(r+\mu_h\right) d\tau} \times \int_0^{t_1} \left[\left(\frac{\beta_1 S_h(\tau) I_m(\tau)}{N_h(\tau)} \right) e^{\int_0^{t} \left(r+\mu_h\right) d\xi} \right] d\tau > 0.$$

Similarly, we can demonstrate that the state variables
$A_h(t) > 0, I_h(t) > 0, T_h(t) > 0, R_h(t) > 0, S_m(t) > 0,$ and $I_m(t) > 0$. □

To ensure the biological relevance of model (6.1), both human and mosquito populations remain bounded for all $t \geq 0$. We now state the following Theorem.

Theorem 6.2.2. *All solution of the system (6.1) with initial data (6.1) are bounded above in a biological viable set Ω.*

$$\Omega = \left\{ \left(S_h, E_h, A_h, I_h, T_h, R_h, S_m, I_m\right) \in R_+^8 : 0 \leq S_h + E_h + A_h + I_h + T_h + R_h \leq \frac{\Lambda_h}{\mu_h}, 0 \leq S_m + I_m \leq \frac{\Lambda_m}{\mu_m} \right\}.$$

Proof. Adding the first six equations of model (6.1) gives the total dynamics of the human host, represented by:

$$\frac{dN_h}{dt} = \Lambda_h - \mu_h N_h - \delta I_h - \varphi T_h \leq \Lambda_h - \mu_h N_h. \tag{6.3}$$

Solving differential inequality (6.3) by using integrating factor method, we get

$$N_h(t) \leq \frac{\Lambda_h}{\mu_h} + \big(N_h(0) - \frac{\Lambda_h}{\mu_h}\big)e^{-\mu_h t}.$$

Now, at $t = 0$, we have $N_h(0) \leq \frac{\Lambda_h}{\mu_h}$. Furthermore, for all $t > 0$, it follows that $N_h(t) \leq \frac{\Lambda_h}{\mu_h}$. Therefore, if $N_h(0)$ is within the set Ω, it can be concluded that $N_h(t)$ remains in Ω for all $t > 0$. Then we can have

$$0 \leq S_h + E_h + A_h + I_h + T_h + R_h \leq \frac{\Lambda_h}{\mu_h}. \tag{6.4}$$

Similarly, by adding the last two equations of model (6.1), we obtain the total dynamics of the mosquitoes at time t, given by

$$\frac{dN_m}{dt} = \Lambda_m - (\gamma + \mu_m)N_m \tag{6.5}$$

$$\frac{dN_m}{dt} \leq \Lambda_m - \mu_m N_m. \tag{6.6}$$

Solving differential inequality (6.6), we deduce that

$$\limsup_{t\to\infty} N_m(t) \leq \frac{\Lambda_m}{\mu_m}.$$

Thus, we have

$$0 \leq S_m + I_m \leq \frac{\Lambda_m}{\mu_m}. \tag{6.7}$$

□

Regarding equations (6.4) and (6.7) the set Ω is positively invariant. Thus, analyzing the system dynamics of model (6.1) within invariant set Ω ensures both biological relevance and mathematical well-posedness of model (6.1). Therefore, any solution from the system (6.1) with an initial data in (6.2) remain within Ω, $\forall t > 0$.

6.2.2 Malaria-free equilibrium point and reproduction number

Malaria-free equilibrium

A malaria-free equilibrium (MFE) point is defined as a state in which malaria is absent from the population. To determine the MFE, denoted by $\mathcal{E}_0$, we set the values $E_h = A_h = I_h = I_m = 0$ in the model described by (6.1). By solving the resulting system of equations, we determine

$$\mathcal{E}_0 = \Big(\frac{\Lambda_h}{\mu_h}, 0, 0, 0, 0, 0, \frac{\Lambda_m}{\gamma + \mu_m}, 0\Big), \tag{6.8}$$

Basic reproduction number

In the study of infectious disease models, the basic reproduction number, denoted as $\mathfrak{R}_0$, refers to the expected number of new cases generated by a single infectious individual in a completely susceptible population (Diekmann et al., 1990). If $\mathfrak{R}_0 < 1$, the disease will decline, as each infected individual generates fewer than one new case. Conversely, if $\mathfrak{R}_0 > 1$, the infection can spread, with each infected individual producing more than one new infection. To compute the reproduction number, $\mathfrak{R}_0$ of model (6.1), we employ the next generation matrix approach, as outlined in (Van den Driessche & Watmough, 2002). Accordingly, the malarial states are E_h, A_h, I_h, and I_m. Thus, the computation for $\mathfrak{R}_0$ starts with rewriting the malarial compartments of the model (6.1) in the form of:

$$\frac{dX}{dt} = \mathcal{F} - \mathcal{V},$$

where X represents the state variables defined as $X = \left(S_h, E_h, A_h, I_h, T_h, R_h, S_m, I_m\right)$, the secondary infection vectors $\mathcal{F}$ and the transition vectors $\mathcal{V}$ are defined as follows:

$$\mathcal{F} = \begin{pmatrix} \frac{\beta_1 S_h I_m}{N_h} \\ 0 \\ 0 \\ \frac{\beta_2 S_m A_h}{N_h} + \frac{\beta_3 S_m I_h}{N_h} \end{pmatrix}, \mathcal{V} = \begin{pmatrix} (r+\mu_h)E_h \\ (\phi+\mu_h)A_h - \sigma r E_h \\ (\delta+\eta+\mu_h)I_h - (1-\sigma)rE_h - q\phi A_h \\ (\gamma+\mu_m)I_m \end{pmatrix}. \tag{6.9}$$

Then the corresponding Jacobin matrices of $\mathcal{F}$ and $\mathcal{V}$ at the MFE $\mathcal{E}_0$ are, respectively,

$$F = \begin{pmatrix} 0 & 0 & 0 & \beta_1 \\ 0 & 0 & 0 & 0 \\ 0 & 0 & 0 & 0 \\ 0 & \frac{\beta_2\mu_h}{\gamma+\mu_m} & \frac{\beta_3\mu_h}{\gamma+\mu_m} & 0 \end{pmatrix}, V = \begin{pmatrix} r+\mu_h & 0 & 0 & 0 \\ -r\sigma & \phi+\mu_h & 0 & 0 \\ -r(1-\sigma) & -q\phi & \delta+\eta+\mu_h & 0 \\ 0 & 0 & 0 & \gamma+\mu_m \end{pmatrix}. \tag{6.10}$$

Now the matrix FV^{-1} is given by

$$F = \begin{pmatrix} 0 & 0 & 0 & \frac{\beta_1}{\gamma+\mu_m} \\ 0 & 0 & 0 & 0 \\ 0 & 0 & 0 & 0 \\ \frac{\sigma r\beta_2 B_0}{(r+\mu_h)(\phi+\mu_h)} + \frac{B_0\beta_3(\sigma qr\phi+(1-\sigma)(\phi+\mu_h)r)}{(\delta+\eta+\mu_h)(r+\mu_h)(\phi+\mu_h)} & \frac{B_0\beta_2}{\phi+\mu_h} + \frac{B_0 q\phi\beta_3(r+\mu_h)}{(\delta+\eta+\mu_h)(r+\mu_h)(\phi+\mu_h)} & \frac{B_0\beta_3}{(\delta+\eta+\mu_h)} & 0 \end{pmatrix},$$

where $B_0 = \frac{\Lambda_m\mu_h}{\Lambda_h(\gamma+\mu_m)}$. The reproductive number $\mathfrak{R}_0$ for model (6.1) is defined as the spectral radius of the matrix FV^{-1}, given by

$$\mathfrak{R}_0 = \sqrt{\frac{B_0\beta_1 r}{\gamma+\mu_m}\left(\frac{\sigma\beta_2}{(\phi+\mu_h)(r+\mu_h)} + \frac{(1-\sigma)\beta_3}{(\eta+\delta+\mu_h)(r+\mu_h)}\right)} = \sqrt{\mathfrak{R}_{I_m}\left(\mathfrak{R}_{A_h} + \mathfrak{R}_{I_h}\right)} \tag{6.11}$$

where $\mathfrak{R}_{I_m} = \frac{B_0\mu_h r\beta_1 r}{\gamma+\mu_m}$, $\mathfrak{R}_{A_h} = \frac{\sigma\beta_2}{(\phi+\mu_h)(r+\mu_h)}$, and $\mathfrak{R}_{I_h} = \frac{(1-\sigma)\beta_3}{(\eta+\delta+\mu_h)(r+\mu_h)}$. In this, each expression $\mathfrak{R}_{I_h}$, $\mathfrak{R}_{I_A}$, and $\mathfrak{R}_{I_m}$ carries its biological interpretations. The term $\mathfrak{R}_{I_m}$ implies the expected number of susceptible humans that a single infectious mosquito infects in its infectious period, where $\frac{1}{\gamma+\mu_m}$ determines the infectious period of mosquitoes. In addition, $B_0\mu_h\beta_1$ determines the amount of susceptible humans that infected mosquitoes infect per a unit time. On the contrary, the term $\mathfrak{R}_{A_h}/\mathfrak{R}_{A_h}$ determines an expected number of susceptible mosquitoes that a single asymptomatic/symptomatic infected human infects in its infectious period. In this context, the asymptomatic/symptomatic infected human stays in that class with an average infectious period of $\frac{1}{(\phi+\mu_h)(r+\mu_h)}/\frac{1}{(\phi+\mu_h)(\eta+\delta+\mu_h)(r+\mu_h)}$. During this period, the asymptomatic/symptomatic person infects $\sigma\beta_2/((1-\sigma)\beta_3$ mosquitoes per a unit time.

6.2.3 Local Stability of the malaria-free equilibrium point

Theorem 6.2.3. *The MFE, $\mathcal{E}_0$, of model (6.1) is locally asymptotically stable if $\mathfrak{R}_0 < 1$.*

Proof. We open the proof by evaluating the Jacobian matrix $\mathfrak{J}(\mathcal{E}_0)$ of model (6.1) at MFE $\mathcal{E}_0$, that is

$$\mathfrak{J}(\mathcal{E}_0) = \begin{pmatrix} -\mu_h & 0 & 0 & 0 & 0 & \varepsilon & 0 & -\beta_1 \\ 0 & -r-\mu_h & 0 & 0 & 0 & 0 & 0 & \beta_1 \\ 0 & r\sigma & -\phi-\mu_h & 0 & 0 & 0 & 0 & 0 \\ 0 & r(1-\sigma) & q\phi & -\delta-\eta-\mu_h & 0 & 0 & 0 & 0 \\ 0 & 0 & 0 & \eta & -\rho-\varphi-\mu_h & 0 & 0 & 0 \\ 0 & 0 & (1-q)\phi & 0 & \rho & -\varepsilon-\mu_h & 0 & 0 \\ 0 & 0 & -B_0\beta_2 & -B_0\beta_3 & 0 & 0 & -\gamma-\mu_m & 0 \\ 0 & 0 & B_0\beta_2 & B_0\beta_3 & 0 & 0 & 0 & -\gamma-\mu_m \end{pmatrix}$$

It is evident that the matrix $\mathfrak{J}(\mathcal{E}_0)$ is a block diagonal matrix. The first and fourth block sub-matrices constitute its eigenvalues. From the first block, denoted as $\mathfrak{J}(\mathcal{E}_0)$, we find that $\lambda_1 = -\mu_h$. The remaining eigenvalues, λ_i for $i = 2,3,4,5,6,7,8$, are determined from the fourth sub-block matrix, denoted as $\mathfrak{J}_4(\mathcal{E}_0)$, of the matrix $\mathfrak{J}(\mathcal{E}_0)$. Thus, we have

$$\mathfrak{J}_4(\mathcal{E}_0) = \begin{pmatrix} -r-\mu_h & 0 & 0 & 0 & 0 & 0 & \beta_1 \\ r\sigma & -\phi-\mu_h & 0 & 0 & 0 & 0 & 0 \\ r(1-\sigma) & q\phi & -\delta-\eta-\mu_h & 0 & 0 & 0 & 0 \\ 0 & 0 & \eta & -\rho-\varphi-\mu_h & 0 & 0 & 0 \\ 0 & (1-q)\phi & 0 & \rho & -\varepsilon-\mu_h & 0 & 0 \\ 0 & -B_0\beta_2 & -B_0\beta_3 & 0 & 0 & -\gamma-\mu_m & 0 \\ 0 & B_0\beta_2 & B_0\beta_3 & 0 & 0 & 0 & -\gamma-\mu_m \end{pmatrix}. \tag{6.12}$$

By expanding the determinant $|\mathfrak{J}_4(\mathcal{E}_0) - \lambda I| = 0$, we obtain the characteristic equation of degree seven

$$\left(\lambda^4 + \alpha_1\lambda^3 + \alpha_2\lambda^2 + \alpha_3\lambda + \alpha_4\right)(\lambda+\rho+\varphi+\mu_h)(\lambda+\varepsilon+\mu_h)(\lambda+\gamma+\mu_m) = 0. \tag{6.13}$$

From the characteristic equation (6.13), we obtain three eigen values: namely $\lambda_5 = -(\rho+\varphi+$

$\mu_h)$, $\lambda_6 = -(\varepsilon+\mu_h)$ and $\lambda_7 = -(\gamma+\mu_m)$. The remaining four eigenvalues: $\lambda_2, \lambda_3, \lambda_4$ and λ_8 are obtained from the characteristic equation

$$\lambda^4 + \alpha_1\lambda^3 + \alpha_2\lambda^2 + \alpha_3\lambda + \alpha_4 = 0, \text{ where} \tag{6.14}$$

$$\begin{aligned}
\alpha_1 &= (\eta+\delta+\mu_h)+(\gamma+\mu_m)+(r+\mu_h)+(\phi+\mu_h)\\
\alpha_2 &= (r+\eta+\phi+\delta+3\mu_h)(\gamma+2\mu_h+\mu_m)+\phi(\eta+\delta)+r(\eta+\phi+\delta)\\
\alpha_3 &= (\gamma+\mu_m)(\delta+\eta+\mu_h)(\phi+\mu_h)(r+\mu_h)(1-\mathfrak{R}_0)\\
&\quad + rB_0\beta_3\big((\eta+\delta+\mu_h)^2+(\gamma+\mu_m)^2+(r+\mu_h)^2+(\phi+\mu_h)^2\big)\\
\alpha_4 &= (\eta+\delta+\mu_h)(r+\mu_h)(\phi+\mu_h)(\gamma+\mu_m)\big(1-\mathfrak{R}_0\big).
\end{aligned}$$

The coefficients α_1 and α_2 are positive, and when $\mathfrak{R}_0 < 1$, the coefficients α_3 and α_4 are also positive. Consequently, all roots of the equation (6.14) have negative real parts. This implies that the eigenvalues $\lambda_2, \lambda_3, \lambda_4$, and λ_8 are all negative. Therefore, the MFE $\mathcal{E}_0$ is locally asymptotically stable within the region Ω when $\mathfrak{R}_0 < 1$. □

6.2.4 Global stability of MFE

In this subsection, we adopt the approach described by Castillo-Chavez & Song (2004) to show MFE is global asymptotically stable. The model (6.1) can be rewritten as follows:

$$\begin{cases} \frac{dZ_1}{dt} = F(Z_1, Z_2) \\ \frac{dZ_2}{dt} = G(Z_1, Z_2), \quad G(Z_1, 0) = 0, \end{cases} \tag{6.15}$$

where $Z_1 = (S_h, R_h, S_m)$ and $Z_2 = (E_h, A_h, I_h, T_h, I_m)$ stand for non-infected and infected compartments, respectively. Additionally, the MFE of the new system is denoted by $\mathcal{E}_0 = (Z_1^0, 0) = \left(\frac{\Lambda_h}{\mu_h}, 0, 0, 0, 0, 0, \frac{\Lambda_m}{\gamma+\mu_m}, 0\right)$ representing the malaria-free state of the new system. Assume that

(A_1) $\frac{dZ_1}{dt} = F(Z_1, 0)$, $\quad Z_1^0$ is globally asymptotically stable.

(A_2) $G(Z_1, Z_2) = AZ_2^T - \hat{G}(Z_1, Z_2)$, $\quad \hat{G}(Z_1, Z_2) \geq 0$ for all $(Z_1, Z_2) \in \Omega$ where matrix A is a Metzle-matrix in which the model makes biologically meaningful in Ω defined earlier. Then $\mathcal{E}_0$ is globally asymptotically stable such that $\mathfrak{R}_0 < 1$.

Having the aforementioned results, we can state the following theorem pertaining to model (6.1).

Theorem 6.2.4. *The MFE of model (6.1) is a globally asymptotic stable (G.A.S.) when* $\mathfrak{R}_0 < 1$ *and the assumptions* (A_1) *and* (A_2) *hold true.*

Proof. Now, we needed to confirm that conditions A_1 and A_2 hold true to prove that the MFE $\mathcal{E}_0$ is globally asymptotically stable (GAS) when $\mathfrak{R}_0 < 1$. Now the two vector-valued functions

$F(Z_1,Z_2)$ and $G(Z_1,Z_1)$ are given as:

$$F(Z_1,Z_2)=\begin{pmatrix}\Lambda_h-\frac{\beta_1 S_h I_m}{N_h}+\varepsilon R_h-\mu_h S_h\\(1-q)\phi A_h+\rho T_h-(\varepsilon+\mu_h)R_h\\\Lambda_m-\frac{\beta_2 S_m A_h}{N_h}-\frac{\beta_3 S_m I_h}{N_h}-(\gamma+\mu_m)S_m\end{pmatrix},\ G(Z_1,Z_2)=\begin{pmatrix}\frac{\beta_1 S_h I_m}{N_h}-(r+\mu_h)E_h\\\sigma r E_h-(\phi+\mu_h)A_h\\(1-\sigma)rE_h+q\phi A_h-(\eta+\delta+\mu_h)I_h\\\eta I_h-(\rho+\varphi+\mu_h)T_h\\\frac{\beta_2 S_m A_h}{N_h}+\frac{\beta_3 S_m I_h}{N_h}-(\gamma+\mu_m)I_m\end{pmatrix}.$$

Now we deal with the simplified systems to condition (A_1)

$$\frac{dZ_1}{dt}=F(Z_1,0)\iff\begin{cases}\dot{S_h}=\Lambda_h+\varepsilon R_h-\mu_h S_h\\\dot{R_h}=-(\varepsilon+\mu_h)R_h\\\dot{S_M}=\Lambda_m-(\gamma+\mu_m)S_m.\end{cases}\tag{6.16}$$

Clearly, the system (6.16) possesses a unique equilibrium point given by $Z_1^0=\left(\frac{\Lambda_h}{\mu_h},0,\frac{\Lambda_m}{\gamma+\mu_m}\right)$. Since the second and third equations of the system (6.16) are linear and also coupled with the first equation, we obtain solutions.

$$\begin{cases}S_h(t)=\frac{\Lambda_h}{\mu_h}+e^{-\mu_h t}\big(S_h(0)+R_h(0)-1\big)-R_h(0)e^{-(\varepsilon+\mu_h)t}\\R_h(t)=R_h(0)e^{-(\mu_h+\varepsilon)t}\\S_m(t)=S_m(0)e^{-(\gamma+\mu_m)t}+\frac{\Lambda_m}{\gamma+\mu_m}\big(1-e^{-(\gamma+\mu_m)t}\big)\end{cases}\tag{6.17}$$

It is evident that the solutions $\big(S_h(t),R_h(t),S_m(t)\big)\to\big(\frac{\Lambda_h}{\mu_h},0,\frac{\Lambda_m}{\gamma+\mu_m}\big)=Z_1^0$ as $t\to\infty$. Thus, Z_1^0 is globally asymptotically stable implying condition (A_1) holds true. Now we needed to determine $G(Z_1,Z_2)=AZ_2^T-\hat{G}(Z_1,Z_2)$, to ensure vector $\hat{G}(Z_1,Z_2)\geq 0$. Thus,

$$A=\frac{\partial G(Z_2^0,0)}{\partial Z_2}=\begin{pmatrix}-r-\mu_h & 0 & 0 & 0 & \beta_1\\r\sigma & -\phi-\mu_h & 0 & 0 & 0\\r(1-\sigma) & q\phi & -\delta-\eta-\mu_h & 0 & 0\\0 & 0 & \eta & -\rho-\varphi-\mu_h & 0\\0 & B_0\beta_2 & B_0\beta_3 & 0 & -\gamma-\mu_m\end{pmatrix},\text{ and}$$

$$\hat{G}(H,Z)=\begin{pmatrix}\beta_1 I_m\big(1-\frac{S_h}{N_h}\big)\\0\\0\\0\\\beta_2 B_0\big(1-\frac{S_m}{B_0 N_h}\big)+\beta_3 B_0\big(1-\frac{S_m}{B_0 N_h}\big)\end{pmatrix}.\tag{6.18}$$

Vector $\hat{G}(Z_1,Z_2)\geq 0$ if $1-\frac{S_m}{B_0 N_h}\geq 0$. As a result, the MFE $\mathcal{E}_0$ of model (6.1) is the GAS equilibrium whenever $\mathfrak{R}_0<1$ and hence Theorem 6.2.4 holds true. □

6.2.5 Existence of malaria equilibrium point

The Malaria Equilibrium Point (MEP) represents a steady-state solution in which malaria is sustained within the population. The MEP of model (6.1), denoted as $\mathcal{E}_1$, is expressed as:

$$\mathcal{E}_1 = (S_h^*, E_h^*, A_h^*, I_h^*, T_h^*, R_h^*, S_m^*, I_m^*)$$

It is obtained by equating the system in (6.1) to zero and solving for the state variables in terms of E_h.

$$\begin{aligned} &S_h^* = \xi_1 + \xi_3 E_h,\ A_h^* = \frac{\omega_1}{\omega_2} E_h,\ I_h^* = \frac{\omega_2\omega_3 + \omega_1\omega_4}{\omega_2\omega_5} E_h,\ T_h^* = \frac{\eta(\omega_2\omega_3 + \omega_1\omega_4)}{\omega_2\omega_5\omega_6} E_h, \\ &R_h^* = \frac{\eta\rho(\omega_2\omega_3 + \omega_1\omega_4) + \omega_1\omega_5\omega_6\omega_7}{\omega_2\omega_5\omega_6\omega_8} E_h, S_m^* = \omega_9 - \frac{\omega_0 N_h^*}{\beta_1(\xi_1 + \xi_3 E_h)} E_h, I_m^* = \frac{\omega_0 N_h^*}{\beta_1(\xi_1 + \xi_3 E_h)} E_h, \end{aligned} \tag{6.19}$$

where

$$\begin{aligned} &\omega_0 = r + \mu_h,\ \omega_1 = \sigma r,\ \omega_2 = \phi + \mu_h,\ \omega_3 = (1-\sigma)r,\ \omega_4 = q\phi,\ \omega_5 = \eta + \delta + \mu_h, \\ &\omega_6 = \rho + \varphi + \mu_h,\ \omega_7 = (1-q)\phi,\ \omega_8 = \varepsilon + \mu_h,\ \omega_9 = \frac{\Lambda_m}{\gamma + \mu_m},\ \xi_0 = \gamma + \mu_m,\ \xi_1 = \frac{\Lambda_h}{\mu_h}, \\ &\xi_3 = \frac{\varepsilon\eta\rho\omega_2\omega_3 + \varepsilon\eta\rho\omega_1\omega_4 + \varepsilon\omega_1\omega_5\omega_6\omega_7 + \omega_0\omega_2\omega_5\omega_6\omega_8}{\omega_8\omega_5\omega_6\omega_8\mu_h}. \end{aligned}$$

Plugging equation (6.19) into the last equation of system (6.1), it can be revealed that E_h satisfies the following equation:

$$E_h^*\left(A_0 E_h^{*2} + A_1 E_h^* + A_2\right) = 0, \tag{6.20}$$

where

$$\begin{aligned} A_0 =& \omega_0\left(\omega_1\left(\left(1+\xi_2\right)\omega_5\omega_6\omega_8 + \omega_3\left(\eta\rho + \left(\eta+\omega_6\right)\omega_8\right)\right) + \omega_1\left(\omega_5\omega_6\left(\omega_7+\omega_8\right) + \omega_4\left(\eta\rho + \left(\eta+\omega_6\right)\omega_8\right)\right)\right) \\ &\left(\beta_3\left(\omega_1\omega_3 + \omega_1\omega_4\right) + \beta_2\omega_1\omega_5\right)\omega_6\omega_8 + \xi_0\omega_1\left(\left(1+\xi_1\right)\omega_5\omega_6\omega_8 + \omega_3\left(\eta\rho + \left(\eta+\omega_6\right)\right)\right) \\ &\left(\left(\omega_8+\omega_1\right)\left(\omega_5\omega_6\left(\omega_7+\omega_8\right) + \omega_4\left(\eta\rho + \left(\eta+\omega_6\right)\omega_8\right)\right)\right), \\ A_1 =& \omega_2\omega_5\omega_6\omega_8(2\xi_0\xi_1\omega_0(\omega_1((1+\xi_1)\omega_5\omega_6\omega_8 + \omega_3(\eta\rho + (\eta+\omega_6)\omega_8)) + \omega_1(\omega_5\omega_6\omega_7 + \omega_8) \\ &+ \omega_4(\eta\rho + (\eta+\omega_6)\omega_8))) + (\beta_3(\omega_2\omega_3 + \omega_1\omega_4) + \beta_2\omega_1\omega_5)\omega_6\omega_8(\xi_1\omega_0 - \beta_1\xi_1\omega_9), \\ A_2 =& \xi_0\xi_1^2\omega_0\omega_2^2\omega_5^2\omega_6^2\omega_8^2(1 - \mathfrak{R}_0). \end{aligned}$$

The MFE, $\mathcal{E}_0$ is obtained when $E_h = 0$. In contrast, the MEP, $\mathcal{E}_1$ is determined from the equation

$$A_0 E_h^{*2} + A_1 E_h^* + A_2 = 0. \tag{6.21}$$

We observe that the coefficient A_0 is positive. Consequently, it is evident that the existence of all possible positive roots of E_h of the polynomial equation (6.21) depends on the signs of coefficients A_1 and A_2. To ascertain this, we apply Descartes rule of signs introduced in (Wang,

2004). Now, we present the possibilities for the existence of the positive malaria equilibrium point E_h in Table 6.2.

Table 6.2: Existence of possible positive roots of the polynomial equation. (6.21).

Case	A_0	A_1	A_2	$\mathfrak{R}_0$	Sign change	+Roots
(i)	+	+	+	$\mathfrak{R}_0 < 1$	0	0
(ii)	+	-	+	$\mathfrak{R}_0 < 1$	2	2
(iii)	+	+	-	$\mathfrak{R}_0 > 1$	1	1
(iv)	+	-	-	$\mathfrak{R}_0 > 1$	1	1

Thus, we can infer the following points from Table 6.2.

(i) There exist two MEP if $A_1 < 0$; $A_2 > 0$ and $A_1^2 - 4A_0A_2 > 0$;

(ii) There exist a unique MEP if $A_2 < 0$ (i.e., if $\mathfrak{R}_0 > 1$) regardless of the sign of A_1;

(iii) There exist a unique MEP if $A_1 < 0$ and $A_2 = 0$ or $A_1^2 - 4A_0A_2 = 0$;

(iv) There is no MEP if $A_1 > 0$ and $A_2 > 0$ or $A_1^2 - 4A_0A_2 < 0$.

Considering the conditions (i)-(iv), we can formulate the following theorem.

Theorem 6.2.5. *The malaria model (6.1) has*

1. *A unique MEP if*
   - $A_2 < 0$, *regardless of the sign of* A_1 *if and only if* $\mathfrak{R}_0 > 1$;
   - $A_1 < 0$ *and* $A_2 = 0$ *or* $A_1^2 - 4A_0A_2 = 0$;
2. *Two MEP if* $A_1 < 0$ *and* $A_2 > 0$;
3. *No MEP otherwise.*

In case 2, the model system (6.1) may have two malaria equilibrium when $\mathfrak{R}_0 < 1$, which can result in the occurrence of backward bifurcation. Thus, a bifurcation analysis is conducted in the next subsection to confirm this.

6.2.6 Bifurcation analysis

In this part, we apply the concepts of Centre Manifold Theory introduced in (Castillo-Chavez & Song, 2004), to investigate the stability of malaria equilibrium points. This theory elucidates the nature of both forward and backward bifurcations, providing valuable insights into the dynamic behaviour of these equilibria. A forward bifurcation indicates local asymptotic stability of the malaria-free equilibrium point when $\mathfrak{R}_0 < 1$ and of the malaria equilibrium point when $\mathfrak{R}_0 > 1$, suggesting potential global stability for these states. Conversely, a backward bifurcation arises when both malaria-free and endemic equilibria points coexist, even in the scenario where $\mathfrak{R}_0 < 1$. To explore dynamics of model (6.1), we transform the state variables as follows:

$S_h = x_1, E_h = x_2, A_h = x_3, I_h = x_4, T_h = x_5, R_h = x_6, S_m = x_7, I_m = x_8$. So that, $X_h = x_1 + x_2 + x_3 + x_4 + x_5 + x_6$. In vector representation, let $x = (x_1, x_2, x_3, x_4, x_5, x_6, x_7, x_8)^T$ and $F = (f_1, f_2, f_3, f_4, f_5, f_6, f_7, f_8)^T$. Then model (6.1) can be written compactly in the form

$$\frac{dx}{dt} = F(x), \tag{6.22}$$

where the function $F(x)$ represents the right hand side of (6.1). Thus, the model (6.1) is given by

$$\begin{cases} \frac{dx_1}{dt} = \Lambda_h - \frac{\beta_1 x_1 x_8}{X_h} + \varepsilon x_6 - \mu_h x_1 \\ \frac{dx_2}{dt} = \frac{\beta_1 x_1 x_8}{X_h} - (r + \mu_h) x_2 \\ \frac{dx_3}{dt} = \sigma r x_2 - (\phi + \mu_h) x_3 \\ \frac{dx_4}{dt} = (1-\sigma) r x_2 + q\phi x_3 - (\delta + \eta + \mu_h) x_4 \\ \frac{dx_5}{dt} = \eta x_4 - (\rho + \varphi + \mu_h) x_5 \\ \frac{dx_6}{dt} = (1-q)\phi x_3 + \rho x_5 - (\varepsilon + \mu_h) x_6 \\ \frac{dx_7}{dt} = \Lambda_m - \frac{\beta_2 x_7 x_3}{X_h} - \frac{\beta_3 x_7 x_4}{X_h} - (\gamma + \mu_m) x_7 \\ \frac{dx_8}{dt} = \frac{\beta_2 x_7 x_3}{X_h} + \frac{\beta_3 x_7 x_4}{X_h} - (\gamma + \mu_m) x_8 \end{cases} \tag{6.23}$$

Let the transmission rate $\beta_1^* = \beta_1$ be bifurcation parameter when $\Re_0 = 1$. Then β_1^* can be determined as

$$\beta_1^* = \frac{\Lambda_h (r + \mu_h)(\phi + \mu_h)(\eta + \delta + \mu_h)(\gamma + \mu_m)^2}{r \Lambda_m \mu_h (\sigma \beta_2 (\eta + \delta + \mu_h) + (1-\sigma)(\phi + \mu_h \beta_3))} \tag{6.24}$$

The Jacobian matrix $J(\mathcal{E}_0, \beta_1^*)$ for the transformed system (6.23), evaluated at $\mathcal{E}_0$ and β_1^*, is given by:

$$J(\mathcal{E}_0, \beta_1^*) = \begin{pmatrix} -\mu_h & 0 & 0 & 0 & 0 & \varepsilon & 0 & -\beta_1^* \\ 0 & -r - \mu_h & 0 & 0 & 0 & 0 & 0 & \beta_1^* \\ 0 & r\sigma & -\phi - \mu_h & 0 & 0 & 0 & 0 & 0 \\ 0 & r(1-\sigma) & q\phi & -\delta - \eta - \mu_h & 0 & 0 & 0 & 0 \\ 0 & 0 & 0 & \eta & -\rho - \varphi - \mu_h & 0 & 0 & 0 \\ 0 & 0 & (1-q)\phi & 0 & \rho & -\varepsilon - \mu_h & 0 & 0 \\ 0 & 0 & -B_0\beta_2 & -B_0\beta_3 & 0 & 0 & -\gamma - \mu_m & 0 \\ 0 & 0 & B_0\beta_2 & B_0\beta_3 & 0 & 0 & 0 & -\gamma - \mu_m \end{pmatrix} \tag{6.25}$$

Clearly, $J(\mathcal{E}_0, \beta_1^*)$ has one simple eigenvalue of zero, while the remaining eigenvalues are negative. The right eigenvector corresponding to this simple zero eigenvalue of the matrix $J(\mathcal{E}_0, \beta_1^*)$

is assumed to be: $u = (u_1, u_2, u_3, u_4, u_5, u_6, u_7, u_8)$, where

$$u_1 = \frac{-\varepsilon\eta\rho\beta_1^*(\omega_2\omega_3 + \omega_1\omega_4) + u_2\omega_0(\varepsilon\omega_1 - \omega_0\omega_2)\omega_5\omega_6}{\mu_h\omega_0\omega_2\omega_5\omega_6},\ u_2 = u_2 > 0,\ u_3 = \frac{\omega_1}{\omega_2}u_2,$$
$$u_4 = \frac{(\omega_2\omega_3 + \omega_1\omega_4)}{\omega_2\omega_5}u_2,\ u_5 = -\frac{\eta(\omega_2\omega_3 + \omega_1\omega_4)}{\omega_2\omega_5\omega_6}u_2,\ u_6 = \frac{u_2(\eta\rho\omega_2\omega_3 + \omega_1(\eta\rho\omega_4 - \omega_5\omega_6\omega_7))}{\omega_2\omega_5\omega_6\omega_8},$$
$$u_7 = \frac{\omega_0}{\beta_1^*}u_2,\ u_8 = -\frac{\omega_0}{\beta_1^*}u_2$$

In the same way the left eigenvector associated to a simple zero eigenvalue is given by $v = (v_1, v_2, v_3, v_4, v_5, v_6, v_7, v_8)$, where

$$v_1 = 0,\ v_2 = v_2 > 0,\ v_3 = \left(\frac{q\phi\xi_0 B_0\beta_3\beta_1^*}{\omega_2\omega_5\xi_0} + \frac{B_0\beta_2\beta_1^*}{\omega_2\xi_0}\right)v_2,\ v_4 = \frac{B_0\beta_3\beta_1^*}{\omega_5\xi_0}v_2,\ v_5 = 0,\ u_6 = 0,$$
$$u_7 = 0,\ v_8 = \frac{\beta_1^*}{\xi_0}v_2.$$

Now we utilize Theorem 4.1 stated by Castillo-Chavez & Song (2004) is to compute the bifurcation coefficients, a and b, of the model (6.1) where,

$$a = \sum_{k,i,j}^{8} v_k u_i u_j \frac{\partial^2 f_k}{\partial x_i \partial x_j}(\mathcal{E}_0, \beta_1^*) \tag{6.26}$$
$$b = \sum_{k,i}^{8} v_k u_i \frac{\partial^2 f_k}{\partial x_i \partial \beta_1^*}(\mathcal{E}_0, \beta_1^*).$$

Then by considering the non-zero second-order partial derivatives of $F(x)$ at the malaria-free equilibrium $\mathcal{E}_0$ and β_1^*

$$\frac{\partial^2 f_2}{\partial x_1\partial x_8} = \frac{\partial^2 f_2}{\partial x_8\partial x_1} = \frac{\beta_1(\xi_1 - 1)}{\xi_1^2},\ \frac{\partial^2 f_2}{\partial x_2\partial x_8} = \frac{\partial^2 f_2}{\partial x_8\partial x_2} = \frac{\partial^2 f_2}{\partial x_3\partial x_8} = \frac{\partial^2 f_2}{\partial x_8\partial x_3} = \frac{\partial^2 f_2}{\partial x_4\partial x_8} = \frac{\partial^2 f_2}{\partial x_8\partial x_4} = \frac{\partial^2 f_2}{\partial x_5\partial x_8}$$
$$= \frac{\partial^2 f_2}{\partial x_8\partial x_5} = \frac{\partial^2 f_2}{\partial x_6\partial x_8} = \frac{\partial^2 f_2}{\partial x_8\partial x_6} = \frac{\beta_1}{\xi_1},\ \frac{\partial^2 f_8}{\partial x_1\partial x_3} = \frac{\partial^2 f_8}{\partial x_3\partial x_1} = \frac{\partial^2 f_8}{\partial x_2\partial x_3} = \frac{\partial^2 f_8}{\partial x_3\partial x_2} = \frac{\partial^2 f_8}{\partial x_3\partial x_5} = \frac{\partial^2 f_8}{\partial x_5\partial x_3} = \frac{\partial^2 f_8}{\partial x_3\partial x_6}$$
$$= \frac{\partial^2 f_8}{\partial x_6\partial x_3} = -\frac{\beta_2}{B_0\xi_1},\ \frac{\partial^2 f_8}{\partial x_1\partial x_4} = \frac{\partial^2 f_8}{\partial x_4\partial x_1} = \frac{\partial^2 f_8}{\partial x_2\partial x_4} = \frac{\partial^2 f_8}{\partial x_4\partial x_2} = \frac{\partial^2 f_8}{\partial x_4\partial x_5} = \frac{\partial^2 f_8}{\partial x_5\partial x_4} = \frac{\partial^2 f_8}{\partial x_4\partial x_6} = \frac{\partial^2 f_8}{\partial x_6\partial x_4}$$
$$= -\frac{\beta_3}{B_0\xi_1},\ \frac{\partial^2 f_8}{\partial x_3\partial x_3} = -\frac{2\beta_2}{B_0\xi_1},\ \frac{\partial^2 f_8}{\partial x_3\partial x_4} = \frac{\partial^2 f_8}{\partial x_4\partial x_3} = -\frac{\beta_2 + \beta_3}{B_0\xi_1},\ \frac{\partial^2 f_8}{\partial x_3\partial x_7} = \frac{\partial^2 f_8}{\partial x_7\partial x_3} = \frac{\beta_2}{\xi_1},\ \frac{\partial^2 f_8}{\partial x_4\partial x_7}$$
$$= \frac{\partial^2 f_8}{\partial x_7\partial x_4} = \frac{\beta_3}{\xi_1},\ \frac{\partial^2 f_8}{\partial x_4\partial x_4} = -\frac{\beta_3}{B_0\xi_1},\ \frac{\partial^2 f_2}{\partial x_8\partial\beta_1^*} = 1,$$

we obtain the bifurcation parameters a and b respectively

$$a = -\left(\frac{d_0(\eta-(\rho+\varphi+\mu_h))}{\mu_h\xi_0^2} - d_1 + (\eta-(\rho+\varphi+\mu_h))\beta_1\omega_9(\omega_2+\eta\rho+\omega_8\omega_1)\right)\frac{2u_2^2v_2}{\omega_2^2\omega_5^2\omega_6\omega_8\xi_1^2}, \text{ where} \tag{6.27}$$

$$d_0 = \xi_1\xi_0\omega_0\omega_2\omega_5 + \beta_1\omega_9(\beta_3(\omega_2\omega_3+\omega_1\omega_4)+\beta_2\omega_1\omega_5),$$

$$d_1 = \varepsilon\xi_0(\eta\rho\omega_2\omega_3+\omega_1(\eta\rho\omega_4+\omega_5\omega_6\omega_7)) + \frac{\beta_1\omega_6\omega_8}{\omega_9}(\beta_3\xi_1(\omega_2\omega_3+\omega_1\omega_4+\beta_3\xi_1\omega_1\omega_5), \text{ and}$$

$$b = \frac{\omega_0}{\beta_1^*}u_2v_2 \tag{6.28}$$

The bifurcation coefficient b is always positive. Accordingly, whenever $a > 0$ for $\eta < \rho + \varphi + \mu_h$, backward bifurcation occurs. For this condition, the existence of backward bifurcation may depend on the parameters: drug treatment rate η, recovery rate of treated humans ρ, the rate of death due to treatment failure φ, rate of insecticides usage γ, and natural death rate of humans μ_h. In particular, we choosing $\gamma = 0.64$, $\varphi = 0.096$, and $\rho = 0.075$. Utilizing the parameter values from Table 5.1, we illustrate backward bifurcation as depicted in Figure (6.2a), which demonstrates the existence of two malaria equilibrium points for $\mathfrak{R}_0 = 0.84$. Notably from Figure (6.2a), varying these parameters under the condition $\eta < \rho + \varphi + \mu_h$, results in the emergence of two endemic equilibrium points for $\mathfrak{R}_0^* < \mathfrak{R}_0 < 1$. Among these equilibria, one point corresponds to a lower infection level and is unstable, while the other, associated with a higher infection level, is stable in conjunction with the stable MFE. Thus, reducing $\mathfrak{R}_0$ just below unity during an epidemic period can not be sufficient to eradicate the infection. Instead, malaria control strategies should be implemented to ensure that $\mathfrak{R}_0$ is significantly below unity.

Epidemiologically, the phenomena of backward bifurcation underscores the importance of maintaining balance between treatment capacity, recovery and over all mortality in humans. Thus, malaria intervention mechanisms may be needed to enhance drug treatment, refine the recovery outcomes and decrease malaria treatment failure induced death. Conversely, for the parameter values presented in Table 5.1, the bifurcation coefficient $a < 0$ satisfying the condition $\eta > \rho + \varphi + \mu_h$ indicates the occurrence of a forward bifurcation, as illustrated in Figure (6.2b). This forward bifurcation confirms the existence of a unique malaria equilibrium at $\mathfrak{R}_0 = 1.97$. In this scenario, malaria can only become endemic if $\mathfrak{R}_0 > 1$, resulting in a globally asymptotically stable malaria equilibrium point. Therefore, reducing $\mathfrak{R}_0$ just below unity can effectively suppress the spread of the disease within the framework of forward bifurcation.

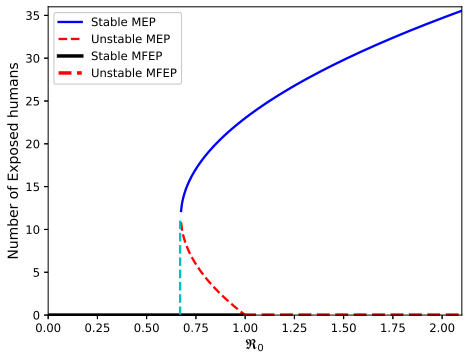

(a) Backward bifurcation for $\eta = 0.17, \gamma = 0.64, \varphi = 0.096, \rho = 0.075$ and the remaining parameters in Table 5.1 at $\mathfrak{R}_0 = 1$.

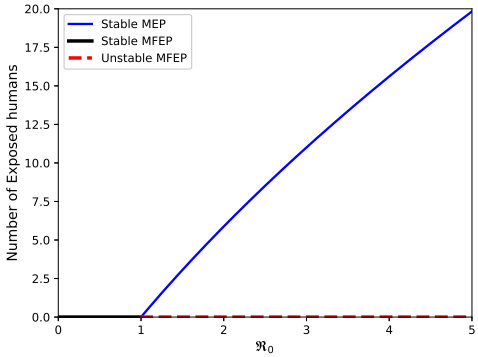

(b) Forward bifurcation for all parameters value specified in Table 5.1 at $\mathfrak{R}_0 = 1$.

Figure 6.2: Plot depicting both a backward and forward bifurcation for the model (6.1)

Considering the birth of backward-bifurcation, we prove the global stability of the unique *MEP* when $\mathfrak{R}_0 > 1$.

Due to the analytical complexity of our high-dimensional, nonlinear system, a rigorous proof of the global asymptotic stability of the malaria endemic equilibrium is not feasible. Therefore, for scenarios where the reproduction number exceeds unity $\mathfrak{R}_0 > 1$, we employ numerical simulations to investigate the system's long-term behavior. The results, detailed in Section 6.3.3, consistently show the convergence of all solutions toward the endemic equilibrium, providing strong numerical evidence for its global stability.

6.3 Numerical simulations

In this section we focus on parameter estimation, sensitivity analysis, model simulation, and exploring the effects of model-sensitive parameters. To investigate the parameter estimation and model simulation of the malaria model (6.1), we used $t = 50$ years based on the assertion of global malaria eradication by the year 2050 using values of parameters in Table 6.3a. Moreover, we used the following initial conditions for the populations of humans and mosquitoes: $S_h(0) = 564.23, E_h(0) = 100, A_h(0) = 0, I_h(0) = 322.7, T_h(0) = 10, R_h(0) = 3, S_m(0) = 800, I_m(0) = 200$.

6.3.1 Parameter estimation

In this section, we employ Ethiopian malaria incidence data to fit model (6.1) and estimate key parameters of malaria model (6.1). Since malaria has been endemic in Ethiopia for many years, the accurate estimation of model parameters is essential for predicting the course of an outbreak and evaluating the impact of interventions. Here, malaria incidence is defined as the number of new malaria cases per 1,000 individuals at risk in Ethiopia. The incidence data, sourced from the World Bank, ranges from the years 2000 to 2022 (WorldBank, 2024) and is illustrated in Figure (6.3a). For the model best-fit and parameters estimation, we employ the

least-squares fitting method. Thus, the model (6.1) can be written as follows:

$$\frac{dx}{dt} = F(t,x,\Theta),\ x(t_0) = x_0, \tag{6.29}$$

where x and Θ are the state variables and unknown parameters, respectively. Therefore, the sum of least-squares error is represented by

$$\Psi(\Theta) = \sum_{i=1}^{n} (x_i - \bar{x}_i)^2,$$

where $\bar{x}_i$ is the real data and $x_i = x(t_i,\Theta)$ is the solution of the model (6.1) and n denotes the number of the data. In order to obtain the parameter, the goal is to minimize the objective function.

$$\min_{\Theta} \Psi(\Theta),$$

subjected to equation (6.29).

The constant influx of malaria-prone humans Λ_h and the natural mortality rate of humans μ_h are estimated from Ethiopian demographic data. The value for μ_h is calculated by taking the reciprocal of the average life expectancy in Ethiopia, which is approximately 67.8 years WHO (2020a). Thus, we have $\mu_h = \frac{1}{67.8}$ deaths per year. To estimate annually constant influx of malaria-prone humans Λ_h, we explore a scenario introduced in Madueme & Chirove (2023) where the human population has reached a steady state $\Lambda_h = 1000 \times \mu_h$. For the constant influx of malaria-prone mosquitoes, we assume a hypothetical average population of 1,000, which satisfies the relationship $\frac{\Lambda_m}{\mu_m} = 1000$. This assumption is made due to the lack of quantified estimates for actual mosquito populations. The average lifespan of mosquitoes is calculated as $\mu_m = \frac{365}{21}\,\text{year}^{-1}$. In Ethiopia, the prevalence of asymptomatic malaria infections is lower compared to that of symptomatic infections Cherkos et al. (2024). This discrepancy leads to a higher chance of exposed individuals progressing to symptomatic malaria. Consequently, we assume a proportion $\sigma = 0.2$, indicating that the number of symptomatic infections exceeds that of asymptomatic carriers. Asymptomatic carriers who receive on-the-spot treatment after screening recover directly, while those without treatment may experience higher parasite loads and progress to symptomatic malaria Singh et al. (2022). The parameter φ is sourced from published literature, while parameters r and ϕ are reasonably assumed. The remaining parameters $\beta_1, \beta_2, \beta_3, \gamma, \eta, \rho, \delta$ and ε are obtained through a fitting process. The estimated parameters, specifically the transmission rates β_1, β_2, and β_3, are consistent with the empirical data reported by Xue et al. (2023). This alignment enhances the reliability of the inferred values, providing a robust foundation for subsequent analyses. The model-fit results, illustrated in Figure (6.3b), demonstrate that the model closely aligns with malaria incidence data in Ethiopia. The model-fit result is provided in Figure (6.3b) and it shows that the model best fits malaria incidence data in Ethiopia. The random fluctuations around zero, indicating an adequate model fit. However, the presence of clustered positive and negative residuals, variable amplitude over time, and occasional sharp deviations suggests underlying non-linear structure in the data that is currently not fully captured by the model. These patterns likely arise from the inherently non-linear and

variable nature of malaria transmission.

Remark 3. *The parameter values obtained from curve fitting, assumptions, and literature are presented in Table 5.1, with all values expressed in per year.*

Table 6.3: Parameters and their values.

Parameters	value	Reference
Λ_h	$\frac{1000}{67.8}$	Calculated
μ_h	$\frac{1}{67.8}$	WHO (2020a)
Λ_m	$\frac{1000\times 365}{21}$	Calculated
μ_m	$\frac{365}{21}$	Calculated
β_1	0.0047	Fitted
β_2	0.0344	Fitted
β_3	0.101	Fitted
ε	0.0055	Fitted
r	0.35	Assumed
ϕ	0.04	Assumed
ρ	0.00475	Fitted
δ	0.08	Fitted
η	0.17	Fitted
φ	0.006	fitted
γ	0.062	Fitted
σ	0.2	Assumed from 0 to 1
q	0.1	Assumed from 0 to 1

The outcomes of our model fitting are displayed in Figure (6.3b), demonstrating that our model aligns closely with the malaria incidence data in Ethiopia from 2000 to 2022.

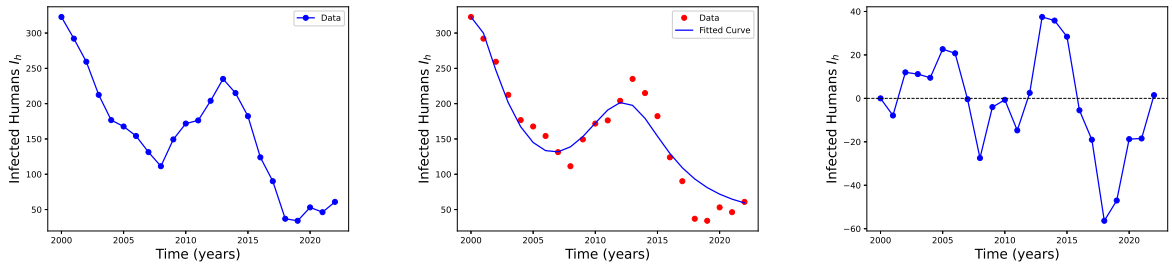

(a) Malaria prevalence **(b)** Curve fit **(c)** Residual plot

Figure 6.3: Plot showing malaria prevalence data, curve fit and residual plot

6.3.2 Sensitivity analysis

To identify the most dominant parameters of the model described in (6.1), we conduct a sensitivity analysis in terms of reproduction number $\mathfrak{R}_0$. This is achieved using the normalized

forward sensitivity index method.

The forward sensitivity index of the reproduction number $\mathfrak{R}_0$ in relation to model parameters $\beta_1, \Lambda_m, \Lambda_h, \gamma,$ and r is computed accordingly

$$\Upsilon_{\beta_1}^{\mathfrak{R}_0} = \Upsilon_{\Lambda_m}^{\mathfrak{R}_0} = 0.5, \Upsilon_{\Lambda_h}^{\mathfrak{R}_0} = -0.5, \Upsilon_{\gamma}^{\mathfrak{R}_0} = -\frac{\gamma}{\gamma+\mu_m}, \ \Upsilon_{r}^{\mathfrak{R}_0} = \frac{\mu_h}{2(r+\mu_h)}.$$

For the remaining model parameters, analytical sensitivity indices can be calculated using the same methodology. Moreover, Table 6.4 presents the numerical sensitivity indices of $\mathfrak{R}_0$, evaluated at the parameter values provided in Table 6.3. From Table 6.4, the positive sensitivity index

Table 6.4: Sensitivity index of $\mathfrak{R}_0$ calculated with parameters value in Table 6.3.

Parameters	Sensitivity indexes	Parameters	Sensitivity indexes
γ	-0.566	β_1	+0.5
Λ_h	-0.5	Λ_m	+0.5
μ_m	-0.434	μ_h	+0.4207
η	-0.227	β_3	+0.354
δ	-0.107	β_2	+0.146
ϕ	-0.106	r	+0.0202
σ	+0.057	q	+0.006

indicates that when a parameter value increases, so as the value of $\mathfrak{R}_0$. On the other hand, the negative sensitivity index indicates that the value of $\mathfrak{R}_0$ falls as the parameter value increases. Specifically, regarding $\Upsilon_{\Lambda_h}^{\mathfrak{R}_0} = -0.5$, increasing constant influx of malaria-prone humans Λ_h by 10%, raises $\mathfrak{R}_0$ by 10%. Contrarily, $\Upsilon_{\Lambda_m}^{\mathfrak{R}_0} = 0.5$, a 10% rise in the constant influx of malaria-prone mosquitoes Λ_m directs to a 10% lower in $\mathfrak{R}_0$. The same applies to the sensitivity indices of the remaining parameters. Parameters with high sensitivity indices should be carefully monitored, as small variations can lead to significant changes in $\mathfrak{R}_0$. As indicated in Table 6.4, parameters $\gamma, \Lambda_h, \eta, \phi, \beta_1, \Lambda_m, \beta_3, \beta_2$, and r have the most significant impact on the basic reproduction number, $\mathfrak{R}_0$. This suggests that increasing γ, Λ_h, η and ϕ reduces the spread of malaria within the population, while an increase in $\beta_1, \Lambda_m, \beta_3, \beta_2$and r enhances malaria transmission in the community.

6.3.3 Model simulation

In this, we present numerical solutions of model (6.1) to support the theoretical findings obtained from previous sections. We start with illustrations that reinforce the epidemiological concept of backward bifurcation, specifically when the basic reproduction number $\mathfrak{R}_0$ is below unity. To do this, we choose $\gamma = 0.64, \rho = 0.075,$ and $\varphi = 0.096$, with parameter values presented in Table 6.3. Upon substituting these values into equation (6.11), we found $\mathfrak{R}_0 = 0.84$. Thus, Figures (6.4a)-(6.4c) reveal that when the basic reproduction number, $\mathfrak{R}_0$, is below unity, the number of infectious individuals in each species becomes few, which does not guarantee the eradication of malaria as the result of the existence of backward bifurcation. In this scenario the transmission of the malaria becomes minimal, resulting in a small number of susceptible

humans becoming infected.

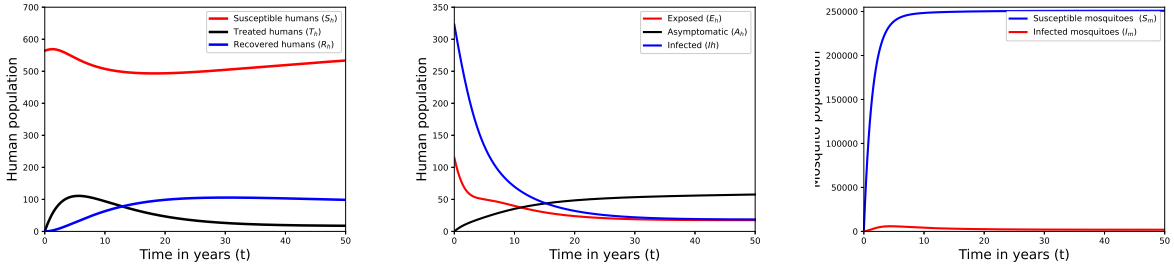

(a) The profile of susceptible, treated, and recovered humans when $\mathfrak{R}_0 = 0.84$.

(b) The profile of exposed, asymptomatic and symptomatic infected humans when $\mathfrak{R}_0 = 0.84$

(c) The profile of susceptible and infected mosquitoes when $\mathfrak{R}_0 = 0.84$

Figure 6.4: The profiles of human and mosquito populations when $\mathfrak{R}_0 < 1$.

Alternatively, by using the assertion in Table 6.3, we calculate $\mathfrak{R}_0 = 1.97$. This value brings the presence of a distinct positive malaria equilibrium point, which is globally asymptotically stable as depicted in Figure (6.5). Thus, this globally asymptotically stable malaria equilibrium point signifies a persistent state of infection in the population, where the dynamics eventually settle regardless of initial conditions. This concept is crucial for understanding how malaria dynamics behave in populations and for planning effective public health interventions.

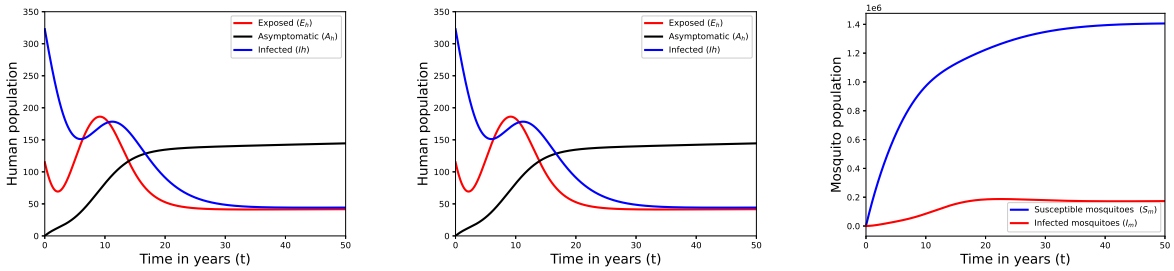

(a) The profiles of susceptible, treated, and recovered humans when $\mathfrak{R}_0 = 1.97$.

(b) The profiles of exposed,asymptomatic, and symptomatic infected humans when $\mathfrak{R}_0 = 1.97$.

(c) The profiles of susceptible and infected mosquitoes when $\mathfrak{R}_0 = 1.97$.

Figure 6.5: The profiles of humans and mosquitoes population when $\mathfrak{R}_0 > 1$.

6.3.4 The effect of model-sensitive parameters

Now, we explore the effect of model-sensitive parameters in the transmission dynamics of malaria. Thus, we vary parameters: the rate of insecticide usage γ, the rate of malaria treatment η, the rates of malaria transmission (β_1, β_2 and β_3), and the rate of recovery of treated humans ρ, while the remaining parameters are presented in Table 6.3. The primary aim of this analysis is to observe how these parameters influence the dynamics of malaria transmission in both human and mosquito populations.

The effect of of varying insecticide usage γ

Figure (6.6) illustrates the effects of insecticidal application on mosquito population while the model parameters in Table 6.3 are unvaried. Thus, Figures (6.6a)-(6.6c) illustrate that increasing insecticidal usage can significantly reduce the number of asymptomatic-carriers in humans and mosquito species.

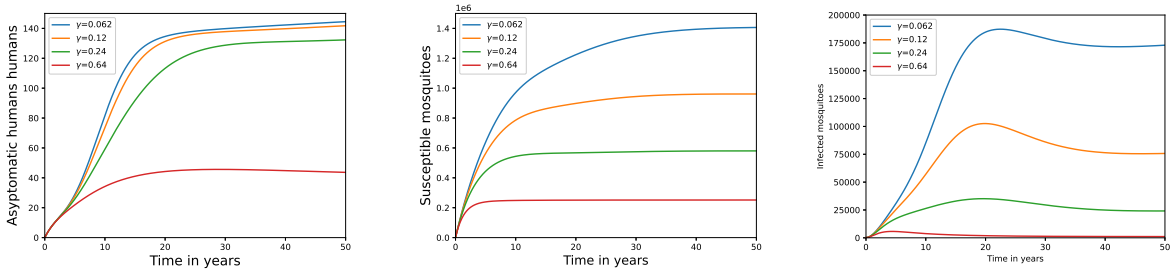

(a) Dynamics of A_h humans **(b)** Dynamics of S_m mosquitoes **(c)** Dynamics of I_m mosquitoes

Figure 6.6: The effect of varying insecticide usage γ

Effect of varying transmission rate β_1, β_2 and β_3

In this part, we examine variation in human and mosquito populations in response to variation in transmission rates $\beta_1, \beta_2,$ and β_3. Figures (6.7), (6.8), and (6.9) describe the effect of altering the transmission rates $\beta_1, \beta_2,$ and β_3, respectively, on the dynamics of the malaria model (6.1).

In particular, Figure (6.7a) reveals that the number of malaria-susceptible humans increases as the transmission rate β_1 value decreases and vice versa. Even so, from the Figures (6.7b) and (6.7c), it can be shown that when the transmission rate β_1 value increases, the number of asymptomatic humans and infected mosquitoes increases, and these values decrease as the transmission rate β_1 value decreases, but this is not continued over the simulation period for the infected mosquitoes class.

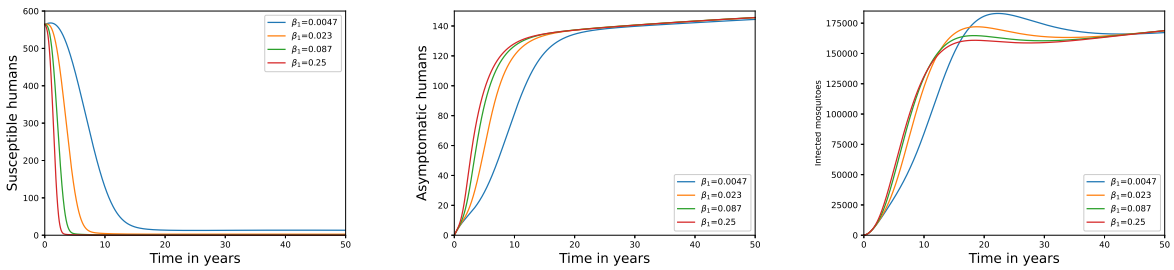

(a) Dynamics of S_h humans **(b)** Dynamics of A_h humans **(c)** Dynamics of I_m mosquitoes

Figure 6.7: The effect of varying transmission rate β_1

Figure (6.8) illustrates the effect of malaria transmission rate from asymptomatic infected humans to susceptible mosquitoes for different β_2 values. Notably, from Figures (6.8b) and (6.8c), it is evident that the endemicity of malaria increases in both asymptomatic infected human and infected mosquito populations as the β_2 value rises. However, Figure (6.8a) highlights that the number of susceptible humans decreases as the transmission rate β_2 increases, and vice versa.

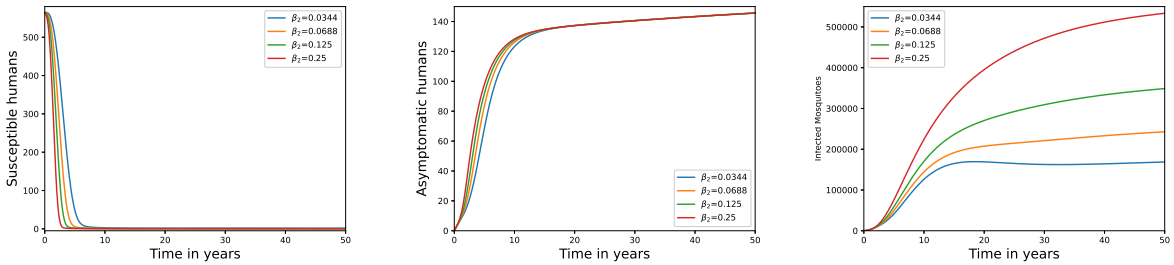

(a) Dynamics of S_h humans **(b)** Dynamics of A_h humans **(c)** Dynamics of I_m mosquitoes

Figure 6.8: The effect of varying transmission rate β_2

Figure (6.9) illustrates the effect of transmission rate from infected humans on susceptible mosquitoes for different β_3 values. From Figure (6.9c), it is evident that the number of infectious mosquitoes increase as the transmission rate β_3 increase and vice-versa. From the data in Figure (6.9b), it can be seen that, decrease in the malaria transmission rate leads to a increase in the number of infected human in class after 20 years of the outbreak. This epidemiological phenomena happen when the population quickly becomes asymptomatic infected and subsequently recovers or develops immunity, the number of new infections may decline despite a high initial transmission rate.

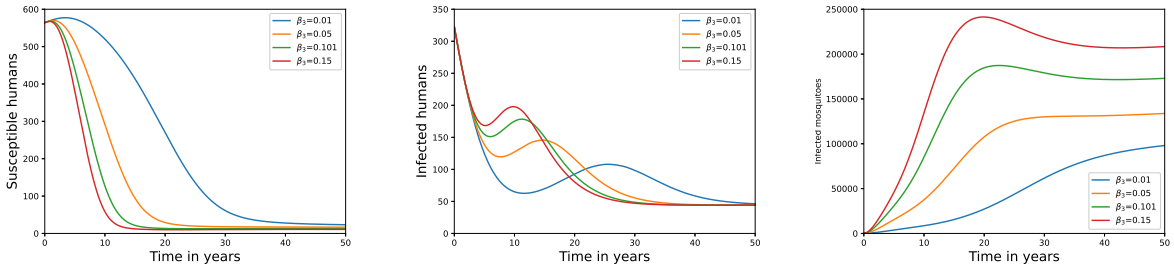

(a) Dynamics of S_h humans **(b)** Dynamics of I_h humans **(c)** Dynamics of I_m humans

Figure 6.9: The effect of varying transmission rate β_3

Effect of varying treatment rate η

Figure (6.10) illustrates the varying effect of malaria treatment rate on the human population while keeping all other parameters in Table 6.3 unvaried. Specifically, in Figures (6.10a)

and (6.10c), it is evident that both susceptible and treated humans increase as the treatment rate increases. Here, with increased malaria drug treatment, a greater number of individuals recover from the infection. However, these individuals may subsequently lose their natural immunity, leading to an increased susceptibility among those who have recovered. This phenomenon can be attributed to a loss of immunity rate of ε as discussed in Section (6.1).This dynamic behavior indicates that effective drug treatment alone does not guarantee the elimination of malaria. Therefore, it is essential to combine effective treatment with other recommended preventive measures to achieve comprehensive malaria elimination in the population. In contrast, Figure (6.10b) demonstrates a decrease in the number of infectious humans with the increasing malaria treatment rate.

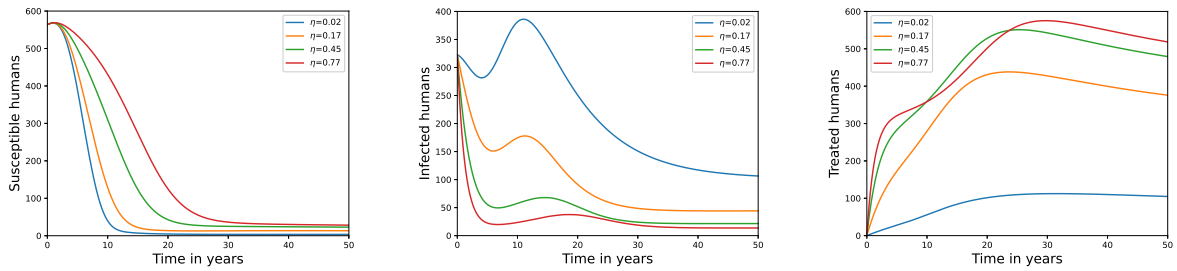

(a) Dynamics of S_h humans **(b)** Dynamics of I_h humans **(c)** Dynamics of T_h humans

Figure 6.10: The effect of varying treatment rate η

Effect of varying recovery rate ρ

Figure (6.11) illustrates the varying effect recovery rate in relation to model (6.1). Based on the graphical result in Figure (6.11c), it is observed that the number of recovered humans increases as the recovery rate ρ increases. However, from Figures (6.11a) and (6.11b), it can be seen that a decrease in the recovery rate leads to an increase in the number of susceptible and treated humans. This situation happens due to a prolonged infectious period, contributing to higher disease prevalence and preventing the transition of individuals from infectious to susceptible states. Understanding this epidemiological situation is important for control of malaria transmission.

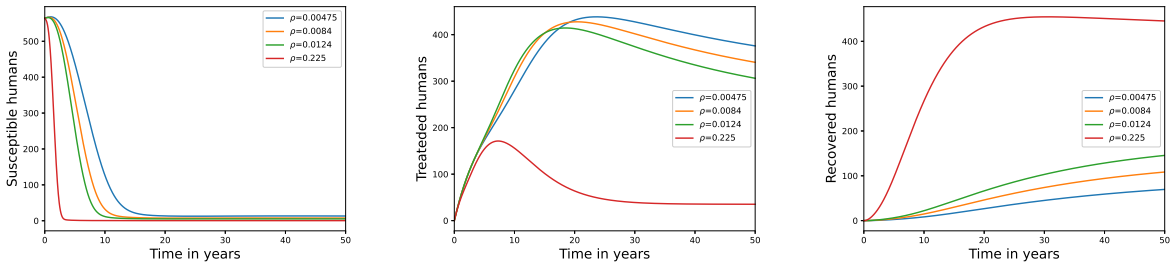

(a) Dynamics of S_h humans **(b)** Dynamics of T_h humans **(c)** Dynamics of R_h humans

Figure 6.11: The effect of varying insecticides usage ρ

Effect of varying progression rate ϕ

Figure (6.12) illustrates the impact of the asymptomatic malaria progression rate ϕ on the classes of asymptomatic humans A_h, symptomatic infectious humans I_h, and recovered humans R_h. Specifically, Figure (6.12a) highlights that a higher progression rate of asymptomatic infection correlates with an increased number of recoveries. In contrast, Figure (6.12c) indicates that there is no significant variation in the symptomatic infectious class I_h despite considerable changes in the progression rate ϕ.

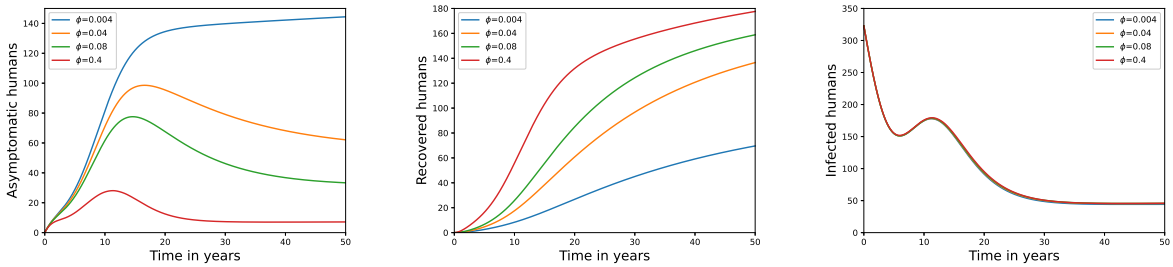

(a) Dynamics of A_h humans **(b)** Dynamics of R_h humans **(c)** Dynamics of I_h humans

Figure 6.12: The effect of varying progression rate ϕ

6.3.5 Dependency of asymptomatic infection on parameters

In this, we perform simulations to assess the dependency of asymptomatic prevalence of the malaria dynamics on insecticide usage rate γ, drug treatment rate η, progression rate of asymptomatic humans, and transmission rate β_1 on the equilibrium prevalence $A_h^* = \frac{\sigma r}{\phi+\mu_h} E_h$, where E_h is equilibrium prevalence of exposed class that can be computed from characteristic equation (6.21). Figure (6.13a) highlights the equilibrium prevalence of asymptomatic malaria as the function of insecticide usage rate γ and the rate of progression to class ϕ. The Figure reveals that the prevalence of asymptomatic infections decreases when both the insecticide usage rate and the progression rate from asymptomatic to either the recovery or infectious class increase. In this context, the population may face the highest disease burden due to an increase in reservoirs

within the infectious class. This has importance from an epidemiological perspective, informing public health strategies to control malaria in the community. Similarly, Figure (6.13b) illustrates the equilibrium prevalence of asymptomatic malaria A_h as a function of the drug treatment rate η and the progression rate ϕ. The data indicate that the equilibrium prevalence of asymptomatic humans A_h increases as η and ϕ values decrease, while it decreases when both parameters increase. Specifically, when the treatment of infected individuals rises and the recovery rates of asymptomatic individuals increase, the number of recoveries rises. This results in a considerable decrease in the prevalence of malaria by slowing the flow of asymptomatic patients to the symptomatic class. In contrast, Figure (6.13c) shows the equilibrium prevalence of asymptomatic infectious humans A_h as a function of β_1 and r. The prevalence is lowest when $\beta_1 = r = 0$, indicating that the asymptomatic class is nonexistent due to a lack of infection contributions, leading to its disappearance. Conversely, the prevalence of A_h is highest when $\beta_1 = r = 1$, suggesting that the asymptomatic class increases over time when both the transmission rate of mosquitoes β_1 and the progression rate of the exposed class r are elevated, allowing it to persist and potentially grow.

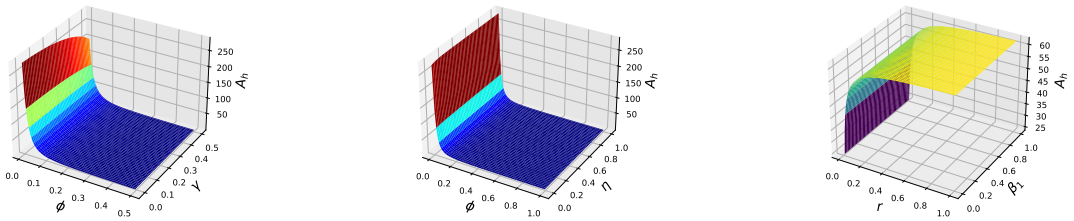

(a) **(b)** **(c)**

Figure 6.13: 3D plots depicting dependence of equilibrium prevalence A_h on parameters: (ϕ, γ) in Figure (6.13a), (ϕ, η) in Figure (6.13b) , and (r, β_1) in Figure (6.13c).

6.3.6 Asymptomatic infection contribution on $\mathfrak{R}_0$

The expression for $\mathfrak{R}_0$ accounts for contributions from both asymptomatic and symptomatic infections, highlighting the significant role of asymptomatic cases in malaria dynamics. In addition, accounting asymptomatic case generate backward bifurcation, a phenomenon not present in our standard S-I-T-R-S model. The expression for $\mathfrak{R}_0$ accounts for contributions from both asymptomatic and symptomatic infections, highlighting the significant role of asymptomatic cases in malaria dynamics. The average infection contributions from asymptomatic and symptomatic individuals can be expressed as $\mathfrak{R}_{I_m}\mathfrak{R}_{A_h}$ and $\mathfrak{R}_{I_m}\mathfrak{R}_{I_h}$, respectively. Having the estimated parameters provided in Table 6.3, we find that the asymptomatic class contributes approximately 29.8%, while the symptomatic class accounts for 70.2% of the basic reproduction number. This indicates that asymptomatic individuals represent about one-third of total infections in the community. Thus, to effectively control the malaria, it is essential to minimize the number of asymptomatic individuals through extensive vector control strategies and increasing transition them into the either infectious or recovery compartment for appropriate management.

CHAPTER 7

AGE-STRUCTURE VACCINATION STRATEGIES IN MATHEMATICAL MODELING OF MALARIA TRANSMISSION

7.1 Model formulation

Age is a key determinant of human susceptibility and infectivity in malaria transmission, reflecting differences in acquired and waning immunity (Gardner, 1980). Individuals without prior exposure are at substantially higher risk, which largely explains the high morbidity and mortality among children under five in endemic regions. Hence, age structuring is essential for realistic transmission modeling and effective control design (Ranjha et al., 2023). Motivated by this, we extend the two-group malaria model of (Tchoumi, Dongmo, et al., 2022) by incorporating age-specific vaccination for children under five, treatment and recovery with waning immunity, and insecticide-based mosquito control. The human population is divided into two age groups: children under five, who are highly vulnerable due to low acquired immunity, and individuals aged five and above, who are relatively less susceptible. Children under five are subdivided into five epidemiological compartments: susceptible (S_c), vaccinated (V_c), infected (I_c), treated (T_c), and recovered (R_c). Susceptible children are recruited at rate Π_c, mature at rate θ_c, increase due to waning immunity at rate ε_c, and decrease through vaccination at rate ν_c or infection with force of infection λ_c. Infected children transition to treatment at rate ρ_c, recover at rate η_c, or die from disease at rate δ_c. Vaccinated children may lose protection and return to the susceptible class at rate h. Treated individuals recover at rate η_c or die due to treatment failure at rate φ_c, while recovered children lose immunity at rate ε_c.

Analogously, individuals aged five and above are classified into susceptible (S_a), infected (I_a), treated (T_a), and recovered (R_a) compartments. The susceptible class increases through maturation from S_c at rate θ_c and waning immunity from R_a at rate ε_a, and decreases via infection with force of infection λ_a. Infected individuals transition to treatment at rate ρ_a or die from disease-induced mortality at rate δ_a. Treated individuals recover at rate η_a or die due to treatment failure at rate φ_a. Recovered individuals lose immunity and return to the susceptible class at rate ε_a. All adult compartments experience natural mortality at rate μ_h.

The total human population in the model is denoted by N_h is given by

$$N_h = S_c + V_c + I_c + T_c + R_c + S_a + I_a + T_a + R_a.$$

For analytical simplicity, we assume a constant recruitment rate Π_m for the susceptible mosquito population. The mosquito force of infection λ_m depends on the proportion of infected humans $(I_c + I_a)/N_h$, reflecting transmission driven by human-mosquito contacts rather than mosquito density. The mosquito population is assumed sufficiently large relative to humans, so its total size does not constrain transmission. Mosquitoes do not recover from infection and die either due to insecticide application at rate γ_m or natural mortality at rate μ_m. The total mosquito population, denoted as N_m is expressed as $N_m = S_m + I_m$. Figure 7.1 illustrates the interaction

between human and mosquito populations.

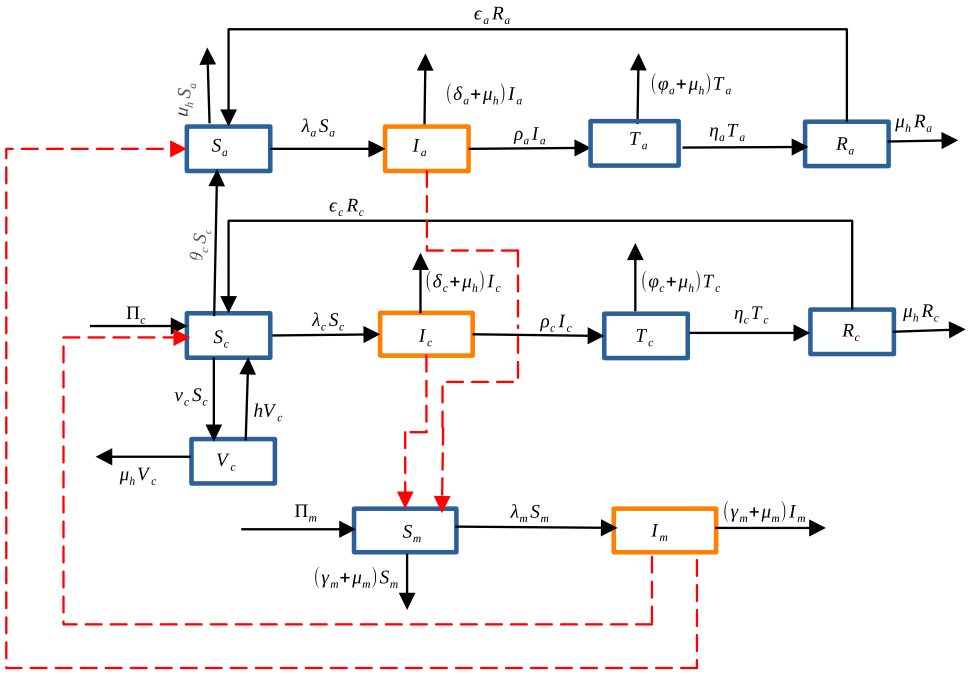

Figure 7.1: Schematic diagram showing dynamic transmission of malaria infection

Based on the model description and assumptions, we derive the following system of nonlinear ODEs.

$$\begin{cases} S_c'(t) = \Pi_c + hV_c + \varepsilon_c R_c - \lambda_c S_c - (\nu_c + \theta_c + \mu_h) S_c \\ V_c'(t) = \nu_c S_c - (h + \mu_h) V_c \\ I_c'(t) = \lambda_c S_c - (\rho_c + \delta_c + \mu_h) I_c \\ T_c' = \rho_c I_c - (\eta_c + \varphi_c + \mu_h) T_c \\ R_c' = \eta_c T_c - (\varepsilon_c + \mu_h) R_c \\ S_a' = \theta_c S_c + \varepsilon_a R_a - (\lambda_a + \mu_h) S_a \\ I_a' = \lambda_a S_a - (\rho_a + \delta_a + \mu_h) I_a \\ T_a' = \rho_a I_a - (\eta_a + \varphi_a + \mu_h) T_a \\ R_a' = \eta_a T_a - (\varepsilon_a + \mu_h) R_a \\ S_m' = \Pi_m - \lambda_m S_m - (\gamma_m + \mu_m) S_m \\ I_m' = \lambda_m S_m - (\gamma_m + \mu_m) I_m \end{cases} \tag{7.1}$$

subjected to initial conditions,

$$\begin{aligned} &S_c(0) > 0, V_c(0) \geq 0, I_c(0) \geq 0, T_c(0) \geq 0, R_c(0) \geq 0, S_a(0) > 0, \\ &I_a(0) \geq 0, T_a(0) \geq 0, R_a(0) \geq 0, S_m(0) \geq 0, I_m(0) \geq 0, \end{aligned} \tag{7.2}$$

where the forces of infection are defined as follows:

$$\lambda_c = \frac{\beta_1 I_m}{N_h},\ \lambda_a = \frac{\beta_2 I_m}{N_h},\ \lambda_m = \frac{\beta_3 I_c + \beta_4 I_a}{N_h}.$$

The model variables and parameters are summarized in Table 7.1.

Table 7.1: Description of the parameters of malaria model (7.1).

Parameters	Descriptions
Π_c	Recruitment rate of susceptible humans under 5 years old by birth
$\varepsilon_c, \varepsilon_a$	Waning immunity rates for humans aged <5 years and ≥ 5 years, respectively
ρ_c, ρ_a	Treatment rates for treated humans aged <5 years and ≥ 5 years, respectively
δ_c, δ_a	Malaria-induced death rates for infected humans aged <5 years and ≥ 5 years, respectively
η_c, η_a	Recovery rates for infected humans aged <5 years and ≥ 5 years, respectively
φ_c, φ_a	Treatment failure induced death rates for humans aged <5 years and ≥ 5 years, respectively
h	Rate of loss of vaccine efficacy
ν_c	Vaccination rate of susceptible humans aged <5 years
θ_c	Maturation rate of humans aged <5 years
β_1	Transmission rate from I_m to S_a class
β_2	Transmission rate from I_m to S_c class
β_3	Transmission rate from I_c to S_m class
β_4	Transmission rate from I_a to S_m class
μ_h	Natural mortality rate for humans
Π_m	Recruitment of susceptible mosquitoes
μ_m	Natural mortality rate for mosquitoes
γ_m	Rate of insecticides application

7.2 Model analysis

This section outlines the fundamental properties of the model (7.1), including positivity, boundedness, existence of solutions, and stability of equilibrium points. To simplify the expressions, we set

$$k_1 = \nu_c + \theta_c + \mu_h, k_2 = h + \mu_h, k_3 = \rho_c + \delta_c + \mu_h, k_4 = \eta_c + \varphi_c + \mu_h, k_5 = \varepsilon_c + \mu_h,$$
$$k_6 = \rho_a + \delta_a + \mu_h, k_7 = \eta_a + \varphi_a + \mu_h, k_8 = \varepsilon_a + \mu_h, k_9 = \gamma_m + \mu_m.$$

7.2.1 Positivity and boundedness of solutions

Theorem 7.2.1. *Given the initial condition (7.2) solutions* $(S_c(t), V_c(t), I_c(t), T_c(t), R_c(t), S_a(t), I_a(t), T_a(t), R_a(t), S_m(t), I_m(t))$ *of the system (7.1) remains nonnegative for all* $t \geq 0$.

Proof. Assume that there exists a time t_1 such that $S_c(t_1) = 0, S_c'(t_1) < 0, V_c(t) > 0, I_c(t) > 0, T_c(t) > 0, R_c(t) > 0, S_a(t) > 0, I_a(t) > 0, T_a(t) > 0, R_a(t) > 0, S_m(t) > 0, I_m(t) > 0$ for $0 < t < t_1$. From the first equation of model (7.1), we have

$$S_c'(t_1) = \Pi_c + \varepsilon_c R_c > 0.$$

This contradicts the assumption that $S_c'(t_1) < 0$. Therefore, we conclude that $S(t)$ is positive for all t in the specified interval $0 < t < t_1$.
Similarly, the solutions $V_c(t)$, $I_c(t)$, $T_c(t)$, $R_c(t)$, $S_a(t)$, $I_a(t)$, $T_a(t)$, $R_a(t)$, $S_m(t)$, $I_m(t)$ are all non-negative for $t \geq 0$. □

Theorem 7.2.2. *Every solution of the model (7.1) is bounded in the invariant region*

$$\Omega = \Big\{ \big(S_c(t),\, V_c(t),\, I_c(t),\, T_c(t),\, R_c(t),\, S_a(t),\, I_a(t),\, T_a(t), R_a(t),\, S_m(t),\, I_m(t)\big) \in \mathbb{R}_+^{11} : N_h(t) \leq \frac{\Pi_c}{\mu_h},\, N_m(t) \leq \frac{\Pi_m}{\mu_m} \Big\}.$$

Proof. Summing the first nine equations of model (7.1) provides the overall dynamics of the human population:

$$\frac{dN_h}{dt} = \Pi_c - \mu_h N_h - \delta_c I_c - \varphi_c T_c - \delta_a I_a - \varphi_a T_a \leq \Pi_c - \mu_h N_h. \tag{7.3}$$

By solving differential inequality in (7.3), we get

$$N_h(t) \leq \frac{\Pi_c}{\mu_h} + \big(N_h(0) - \frac{\Pi_c}{\mu_h}\big) e^{-\mu_h t}.$$

At $t = 0$, $N_h(0) \leq \frac{\Pi_c}{\mu_h} > 0$. For all $t > 0$, it follows that $N_h(t) \leq \frac{\Pi_c}{\mu_h}$. Thus, if $N_h(0) \in \Omega$, then $N_h(t) \in \Omega$ for all $t > 0$. Therefore, we have:

$$0 \leq S_c + V_c + I_c + T_c + R_c + S_a + I_a + T_a + R_a \leq \frac{\Pi_c}{\mu_h}. \tag{7.4}$$

Similarly, the total dynamics of the mosquito population at time t is given by

$$\frac{dN_m}{dt} = \Pi_m - (\gamma_m + \mu_m) N_m \leq \Pi_m - \mu_m N_m. \tag{7.5}$$

By solving differential inequality in (7.5), we deduce that

$$\limsup_{t \to \infty} N_m(t) \leq \frac{\Pi_m}{\mu_m}.$$

Then, we have

$$0 \leq S_m + I_m \leq \frac{\Pi_m}{\mu_m}. \tag{7.6}$$

From (7.4) and (7.6), we can conclude that the set Ω is positively invariant. Therefore, it is

adequate to contemplate the dynamics of system (7.1) in region Ω. In this region, the model is mathematically well-posed and biologically relevant. Moreover, each solution of the model (7.1) with initial condition (7.2) that starts in Ω remains in Ω for all $t > 0$. □

7.2.2 Malaria-free equilibrium (MFE) point

The malaria-free equilibrium (MFE), denoted as $\mathcal{E}_0$, is obtained by setting $I_c = 0, I_a = 0$, and $I_m = 0$ in the model (7.1). Thus, the MFE of the model is given by:

$$\begin{aligned}\mathcal{E}_0 &= \left(S_c^0, V_c^0, I_c^0, T_c^0, R_c^0, S_a^0, I_a^0, T_a^0, R_a^0, S_m^0, I_m^0\right) \\ &= \left(\frac{k_2\Pi_c}{h(\theta_c+\mu_h)+\mu_h k_1}, \frac{\nu_c\Pi_c}{h(\theta_c+\mu_h)+\mu_h k_1}, 0, 0, 0, \frac{\theta_c k_2\Pi_c}{\mu_h\left(h(\theta_c+\mu_h)+\mu_h k_1\right)}, 0, 0, 0, \frac{\Pi_m}{k_9}, 0\right).\end{aligned} \tag{7.7}$$

7.2.3 Effective reproduction number $(\mathfrak{R}_e)$

The effective reproduction number $(\mathfrak{R}_e)$ is defined as the average number of secondary infections produced by a single infectious individual in a partially susceptible population. For the model (7.1), $\mathfrak{R}_e$ is determined as the dominant eigenvalue of the matrix FV^{-1}, using the next-generation matrix approach as outlined by Diekmann et al. (1990); Van den Driessche & Watmough (2002). To compute $\mathfrak{R}_e$ for the model, we categorize the infected individuals into compartments $\mathcal{F}$ and $\mathcal{V}$, where

$$\mathcal{F} = \begin{pmatrix} \lambda_c S_c \\ \lambda_a S_a \\ \lambda_m S_m \end{pmatrix}, \mathcal{V} = \begin{pmatrix} k_3 I_c \\ k_6 I_a \\ k_9 I_m \end{pmatrix}. \tag{7.8}$$

The corresponding Jacobin matrices of $\mathcal{F}$ and $\mathcal{V}$ at the $\mathcal{E}_0$ are, respectively,

$$F = \begin{pmatrix} 0 & 0 & \beta_1 D_0 \\ 0 & 0 & \beta_2 D_1 \\ \beta_3 D_2 & \beta_4 D_2 & 0 \end{pmatrix}, V = \begin{pmatrix} k_3 & 0 & 0 \\ 0 & k_6 & 0 \\ 0 & 0 & k_9 \end{pmatrix}, \text{ where} \tag{7.9}$$

$$D_0 = \frac{S_c^0}{S_c^0+V_c^0+S_a^0} = \frac{\mu_h k_2}{h(\theta_c+\mu_h)+\mu_h k_1}, \; D_1 = \frac{S_a^0}{S_c^0+V_c^0+S_a^0} = \frac{\theta_c k_2}{h(\theta_c+\mu_h)+\mu_h k_1},$$
$$D_2 = \frac{S_m^0}{S_c^0+V_c^0+S_a^0} = \frac{\mu_h \nu_c}{h(\theta_c+\mu_h)+\mu_h k_1}.$$

Now the matrix FV^{-1} is given by

$$FV^{-1} = \begin{pmatrix} 0 & 0 & \frac{\beta_1 D_0}{k_9} \\ 0 & 0 & \frac{\beta_2 D_1}{k_9} \\ \frac{\beta_3 D_2}{k_3} & \frac{\beta_4 D_2}{k_6} & 0 \end{pmatrix}.$$

The reproductive number $\mathfrak{R}_e$ is defined as the spectral radius of the matrix FV^{-1}, given by

$$\mathfrak{R}_e = \sqrt{\frac{\mu_h k_1 \Pi_m}{k_9^2 \Pi_c} \left(\frac{\beta_1 \beta_3 \mu_h}{[h(\theta_c + \mu_h) + \mu_h k_1] k_3} + \frac{\beta_2 \beta_4 \theta_c}{[h(\theta_c + \mu_h) + \mu_h k_1] k_6} \right)}. \tag{7.10}$$

In a similar vein, the basic reproduction number, denoted as $\mathfrak{R}_0$, is derived by setting vaccination rate $\nu_c = 0$ in the equation (7.10). This offers valuable insight into the potential spread of malaria in the absence of vaccination efforts. Consequently, the basic reproduction number $\mathfrak{R}_0$ when $\nu_c = 0$ is defined by

$$\mathfrak{R}_0 = \sqrt{\frac{\mu_h \Pi_m (\theta_c + \mu_h)}{k_9^2 k_2 \Pi_c} \left(\frac{\beta_1 \beta_3 \mu_h}{(\theta_c + \mu_h) k_3} + \frac{\beta_2 \beta_4 \theta_c k_3}{(\theta_c + \mu_h) k_6} \right)}. \tag{7.11}$$

This implies that $\mathfrak{R}_e < \mathfrak{R}_0$. When the basic reproduction number $\mathfrak{R}_0$ exceeds the effective reproduction number $\mathfrak{R}_e$, it signifies that each infected host can potentially transmit malaria to susceptible hosts in the absence of the proposed vaccination effort. In contrast, when the effective reproduction number $\mathfrak{R}_e$ is close to the basic reproduction number $\mathfrak{R}_0$, it implies that the transmission potential of malaria is not being sufficiently reduced by vaccination or other control measures. This gap underscores the difficulty of achieving herd immunity, particularly in vulnerable groups such as children under five. Furthermore, a high $\mathfrak{R}_0$ relative to $\mathfrak{R}_e$ indicates the necessity for enhanced vaccination efforts and additional public health interventions to control malaria infection. From malaria control perspective, the effective reproduction number $\mathfrak{R}_e$ is more significant, because it directly reflects the impact of current interventions and the remaining transmission potential in the population. Thus, focusing on reducing $\mathfrak{R}_e$ below 1 is critical for malaria elimination.

7.2.4 Local stability of MFE

This sub-section presents the conditions for local stability of the malaria-free equilibrium state.

Theorem 7.2.3. *The MFE, $\mathcal{E}_0$, is locally asymptotically stable when the effective reproduction number $\mathfrak{R}_e < 1$ and unstable when $\mathfrak{R}_e > 1$.*

Proof. The Jacobian matrix for the model (7.1) at MFE state $\mathcal{E}_0$ is given by

$$J(\mathcal{E}_0) = \begin{pmatrix} -k_1 & h & 0 & 0 & \varepsilon_c & 0 & 0 & 0 & 0 & 0 & -D_0\beta_1 \\ \nu_c & -k_2 & 0 & 0 & 0 & 0 & 0 & 0 & 0 & 0 & 0 \\ 0 & 0 & -k_3 & 0 & 0 & 0 & 0 & 0 & 0 & 0 & D_0\beta_1 \\ 0 & 0 & \rho_c & -k_4 & 0 & 0 & 0 & 0 & 0 & 0 & 0 \\ 0 & 0 & 0 & \eta_c & -k_5 & 0 & 0 & 0 & 0 & 0 & 0 \\ \theta_c & 0 & 0 & 0 & 0 & -\mu_h & 0 & 0 & \varepsilon_a & 0 & -D_1\beta_2 \\ 0 & 0 & 0 & 0 & 0 & 0 & -k_6 & 0 & 0 & 0 & D_1\beta_2 \\ 0 & 0 & 0 & 0 & 0 & 0 & \rho_a & -k_7 & 0 & 0 & 0 \\ 0 & 0 & 0 & 0 & 0 & 0 & 0 & \eta_a & -k_8 & 0 & 0 \\ 0 & 0 & D_2\beta_3 & 0 & 0 & 0 & D_2\beta_4 & 0 & 0 & -k_9 & 0 \\ 0 & 0 & D_2\beta_3 & 0 & 0 & 0 & D_2\beta_4 & 0 & 0 & 0 & -k_9 \end{pmatrix}. \tag{7.12}$$

We aim to demonstrate that each eigenvalue of the matrix $J(\mathcal{E}_0)$ is negative. Using direct inspection techniques, we obtain the eigenvalues $\lambda_6 = -\mu_h$, $\lambda_8 = -k_7$, $\lambda_9 = -k_8$, $\lambda_{10} = -k_9$, and the remaining eigenvalues are those derived from the matrix Q.

$$Q = \begin{pmatrix} -k_1 & h & 0 & 0 & \varepsilon_c & 0 & -D_0\beta_1 \\ \nu_c & -k_2 & 0 & 0 & 0 & 0 & 0 \\ 0 & 0 & -k_3 & 0 & 0 & 0 & D_0\beta_1 \\ 0 & 0 & \rho_c & -k_4 & 0 & 0 & 0 \\ 0 & 0 & 0 & \eta_c & -k_5 & 0 & 0 \\ 0 & 0 & 0 & 0 & 0 & -k_6 & D_1\beta_2 \\ 0 & 0 & D_2\beta_3 & 0 & 0 & D_2\beta_4 & -k_9 \end{pmatrix}. \tag{7.13}$$

The matrix Q is an upper triangular block diagonal matrix, and its eigenvalues are derived from the eigenvalues of its block sub-matrices. Specifically, the eigenvalues λ_1 and λ_2 correspond to the first block sub-matrix, denoted as Q_1, while the remaining eigenvalues $\lambda_i, i = 3,4,5,7,$ and 11 are obtained from the fourth block sub-matrix. Thus, we have $Q_1 = \begin{pmatrix} -k_1 & h \\ \nu_c & -k_2 \end{pmatrix}$. We have $\mathrm{Tr}(Q_1) = -k_1 - k_2 < 0$, and $\mathrm{Det}(Q_1) = (\theta_c + \mu_h)(h + \mu_h) + \nu_c\mu_h > 0$. Accordingly, the eigenvalues $\lambda_1 < 0$ and $\lambda_2 < 0$. From the sub-matrix Q_4, we find $\lambda_4 = -k_4 < 0$, and $\lambda_5 = -k_5$. The remaining eigenvalues λ_3, λ_7, and λ_{11} are obtained from the matrix Q_4, given by

$$Q_4 = \begin{pmatrix} -k_3 & 0 & D_0\beta_1 \\ 0 & -k_6 & D_1\beta_2 \\ D_2\beta_3 & D_2\beta_4 & -k_9. \end{pmatrix}. \tag{7.14}$$

By expanding the determinant $|Q_4 - \lambda.I| = 0$, we obtain a cubic characteristic equation. That is

$$c_0\lambda^3 + c_1\lambda^2 + c_2\lambda + c_3 = 0, \text{where} \tag{7.15}$$

$$c_0 = 1,\ c_1 = (k_3 + k_6 + k_9),$$
$$c_2 = k_3k_6 + k_3k_9\left(1 - \frac{\beta_1\beta_3\mu_h}{[h(\theta_c+\mu_h)+\mu_hk_1]k_3}\right) + k_6k_9\left(1 - \frac{\beta_2\beta_4\theta_c}{[h(\theta_c+\mu_h)+\mu_hk_1]k_6}\right),\ c_3 = k_3k_6k_9\left(1-\Re_e^2\right).$$

The coefficients c_0 and c_1 are always positive. Additionally, for $\Re_e < 1$, the coefficients c_2 and c_3 are also positive. Therefore, we conclude that $c_i > 0$ for $i = 0,1,2,3$. To ensure all roots of the polynomial given by (7.15) have negative real parts, we apply the Routh-Hurwitz conditions (Mahardika et al., 2019), which provide sufficient and necessary criteria based on the coefficients of the polynomial. The Routh-Hurwitz conditions for polynomial are $c_i > 0$ and,

$$H_1 = \left|\ c_1\ \right| > 0,\ H_2 = \begin{vmatrix} c_1 & c_0 \\ c_3 & c_2 \end{vmatrix} > 0,\ H_3 = \begin{vmatrix} c_1 & c_0 & 0 \\ c_3 & c_2 & c_1 \\ 0 & 0 & c_3 \end{vmatrix} = c_3H_2 > 0.$$

Since, $H_1 > 0$; hence we needed to show that $H_2 > 0$. That is

$$H_2 = (k_3 + k_6 + k_9)\left(k_3k_6 + k_3k_9(1-T_0) + k_6k_9(1-T_1)\right) - k_3k_6k_9\left(1-\Re_e^2\right) > 0 \tag{7.16}$$

Expanding followed by some simplifications, equation (7.16), becomes

$$H_2 = (k_3 + k_6 + k_9)k_3k_9 + k_3k_9(k_3+k_9)(1-T_0) + (k_6+k_9)k_6k_9(1-T_1) + k_3k_6k_9\left(1-\Re_e^2\right),$$

where $T_0 = \frac{\beta_1\beta_3\mu_h}{[h(\theta_c+\mu_h)+\mu_hk_1]k_3}$ and $T_1 = \frac{\beta_2\beta_4\theta_c}{[h(\theta_c+\mu_h)+\mu_hk_1]k_6}$. It is observed that $H_2 > 0$ when $\Re_e < 1$. Moreover, since $H_3 = c_3H_2 > 0$ with H_2 positive, all eigenvalues of the Jacobian matrix $J(\mathcal{E}_0)$ have negative real parts under this condition. Hence, all eigenvalues of the Jacobian matrix $J(\mathcal{E}_0)$ have negative real parts under this condition, which implies that the malaria-free equilibrium $\mathcal{E}_0$ is locally asymptotically stable. Conversely, when $\Re_e > 1$, the coefficient c_3 becomes negative, and c_2 may also be negative. Consequently, not all roots of the polynomial given by (7.15) can have negative real parts, leading to the instability of the malaria-free equilibrium point $\mathcal{E}_1$. □

7.2.5 Global stability of MFE

We use the method outlined by Castillo-Chavez & Song (2004) to demonstrate that the MFE $\mathcal{E}_0$ is globally asymptotically stable. The model given by (7.1) can be reformulated as follows:

$$\begin{cases} \frac{dH_1}{dt} = F(H_1,H_2) \\ \frac{dH_2}{dt} = G(H_1,H_2), \quad G(H_1,0) = 0, \end{cases} \tag{7.17}$$

where $H_1 = (S_c, V_c, R_c, S_a, R_a, S_m)$ and $H_2 = (I_c, T_c, I_a, T_a, I_m)$ stand for non-infected and infected compartments, respectively. Additionally, the MFE of the new system is denoted by

$$\mathcal{E}_0 = (H_1^0, 0) = \left(\frac{k_2\Pi_c}{h(\theta_c+\mu_h)+\mu_hk_1}, \frac{\nu_c\Pi_c}{h(\theta_c+\mu_h)+\mu_hk_1}, 0, \frac{\theta_ck_2\Pi_c}{\mu_h(h(\theta_c+\mu_h)+\mu_hk_1)}, 0, \frac{\Pi_m}{k_9}, 0,0,0,0,0\right).$$

Assume that

$(\mathcal{A}_1)$ $\frac{dH_1}{dt} = F(H_1,0)$, $\quad H_1^0$ is globally asymptotically stable.

$(\mathcal{A}_2)$ $G(H_1,H_2) = AH_2^T - \hat{G}(H_1,H_2)$, where $\hat{G}(H_1,H_2) \geq 0$ for all $(H_1,H_2) \in \Omega$. Here, $A = D_{H_2}G(\mathcal{E}_0,0)$ is a Metzler matrix, maintaining biological relevance in Ω.

Having the aforementioned results, we can state the following theorem about model (7.1).

Theorem 7.2.4. *The MFE of model (7.1) is a globally asymptotic stable (G.A.S.) when $\mathfrak{R}_e < 1$ and the assumptions $(\mathcal{A}_1)$ and $(\mathcal{A}_2)$ hold true.*

Proof. We must verify that conditions $\mathcal{A}_1$ and $\mathcal{A}_2$ are satisfied to prove that the MFE $\mathcal{E}_0$ is globally asymptotically stable (GAS) when $\mathfrak{R}_e < 1$. The two vector-valued functions $F(H_1,H_2)$ and $G(H_1,H_2)$ are defined as follows:

$$F(H_1,H_2) = \begin{pmatrix} \Pi_c + \varepsilon_c R_c + hV_c - \lambda_c S_c - k_1 S_c \\ \nu_c S_c - k_2 V_c \\ \eta_c T_c - k_5 R_c \\ \theta_c S_c + \varepsilon_a R_a - \lambda_a S_a - \mu_h S_a \\ \eta_a T_a - k_8 R_a \\ \Pi_m - \lambda_m S_m - k_9 S_m \end{pmatrix}, \; G(H_1,H_2) = \begin{pmatrix} \lambda_c S_c - k_3 I_c \\ \rho_c I_c - k_4 T_c \\ \lambda_a S_a - k_6 I_a \\ \rho_a I_a - k_7 T_a \\ \lambda_m S_m - k_9 I_m \end{pmatrix}.$$

Now we deal with the simplified systems to condition (A_1)

$$F(H_1,0) = \begin{cases} \dot{S_c} = \Pi_c + \varepsilon_c R_c + hV_c - k_1 S_c \\ \dot{V_c} = \nu_c S_c - k_2 V_c \\ \dot{R_c} = -k_5 R_c \\ \dot{S_a} = \theta_c S_c + \varepsilon_a R_a - \mu_h S_a \\ \dot{R_a} = -k_8 R_a \\ \dot{S_m} = \Pi_m - k_9 S_m. \end{cases} \tag{7.18}$$

Since the third, fifth, and sixth equations of the system (7.18) are linear and also coupled with the first, second, and fourth equation, the system solutions approaches to a steady state solution $(S_c(t),V_c(t),R_c(t),S_a(t),R_a(t),S_m(t)) \to \mathcal{E}_0$.

Thus, H_1^0 is globally asymptotically stable implying condition (A_1) holds true. Now we need to determine $G(H_1,H_2) = AZ_2^T - \hat{G}(H_1,H_2)$, to ensure vector $\hat{G}(H_1,H_2) \geq 0$. Thus,

$$A = \begin{pmatrix} -k_3 & 0 & 0 & 0 & \beta_1 D_0 \\ \rho_c & -k_4 & 0 & 0 & 0 \\ 0 & 0 & -k_6 & 0 & \beta_2 D_1 \\ 0 & 0 & \rho_c & -k_7 & 0 \\ \beta_3 D_2 & 0 & \beta_4 D_2 & 0 & -k_9 \end{pmatrix}, \text{ then } \hat{G}(H,Z) = \begin{pmatrix} \beta_1 D_0 I_m \left(1 - \frac{S_c}{D_0 N_h}\right) \\ 0 \\ \beta_2 D_1 I_m \left(1 - \frac{S_a}{D_1 N_h}\right) \\ 0 \\ \left(\beta_3 D_2 I_m + \beta_4 D_2 I_a\right)\left(1 - \frac{S_m}{D_2 N_h}\right) \end{pmatrix}.$$

In a malaria-free state, most of the population remains susceptible, causing the terms D_0, D_1, and D_2 to approach one and ensuring that the vector $\hat{G}(Z_1,Z_2) \geq 0$. Consequently, the malaria-free equilibrium (MFE) $\mathcal{E}_0$ of model (7.1) is a globally asymptotically stable (GAS) equilibrium point whenever $\mathfrak{R}_e < 1$, validating Theorem 7.2.4. □

7.2.6 Existence of malaria equilibrium point (MEP)

The MEE point denoted as $\mathcal{E}_1$ represents a steady state at which malaria persists in both human and mosquito populations. To determine this equilibrium, we set the model system (7.1) to zero and solve for the state variables. Consequently, the model (7.1) has endemic equilibrium $\mathcal{E}_1 = (S_c^*, V_c^*, I_c^*, T_c^*, R_c^*, S_a^*, I_a^*, T_a^*, R_a^*, S_m^*, I_m^*)$ in terms of λ_c, where

$$\begin{aligned}
&S_c^* = \frac{a_3 k_2}{a_1 + a_2 k_2 \lambda_c},\ V_c^* = -\frac{a_3 \nu_c}{a_1 - a_2 k_2 \lambda_c},\ I_c^* = \frac{a_4 \lambda_c}{a_1 + a_2 k_2 \lambda_c},\ T_c^* = \frac{b_3 \lambda_c}{a_1 + a_2 k_2 \lambda_c},\ R_c^* = \frac{a_7 \lambda_c}{a_1 - a_2 k_2 \lambda_c},\\
&S_a^* = \frac{a_3 b_2 k_6}{(a_5 (a_0 \lambda_c + \mu_h) - a_0 \lambda_c b_0)(a_1 + a_2 k_2 \lambda_c)},\ I_a^* = \frac{a_3 b_2 a_0 \lambda_c}{(a_5 (a_0 \lambda_c + \mu_h) - a_0 \lambda_c b_0)(a_1 + a_2 k_2 \lambda_c)},\\
&T_a^* = \frac{a_3 b_1 a_0 \lambda_c}{(a_5 (a_0 \lambda_c + \mu_h) - a_0 \lambda_c b_0)(a_1 + a_2 k_2 \lambda_c)},\ R_a^* = \frac{a_3 a_6 a_0 \lambda_c}{(a_5 (a_0 \lambda_c + \mu_h) - a_0 \lambda_c b_0)(a_1 + a_2 k_2 \lambda_c)},\\
&S_m^* = \frac{\Pi_m}{k_9 + \lambda_m},\ I_m^* = \frac{\lambda_m \Pi_m}{k_9 (k_9 + \lambda_m)},\ \text{where}
\end{aligned} \tag{7.19}$$

$a_0 = k_2 k_3 k_4 k_5,\ a_1 = k_1 k_2 k_3 k_4 k_5 - h k_3 k_4 k_5 \nu_c,\ a_2 = k_3 k_4 k_5 - \varepsilon_c \eta_c \rho_c,\ a_3 = k_3 k_4 k_5 \Pi_c,$
$a_4 = k_2 k_4 k_5 \Pi_c,\ a_5 = k_6 k_7 k_8,\ a_6 = k_2 \eta_a \theta_c \rho_a,\ a_7 = k_2 \eta_c \Pi_c \rho_c,\ b_0 = \varepsilon_a \eta_a \rho_a,\ b_1 = k_2 k_8 \theta_c \rho_a,$
$b_2 = k_2 k_7 k_8 \theta_c,\ b_3 = k_2 k_5 \Pi_c \rho_c$. By substituting the above equilibrium values into the force of infection λ_c, we obtain the polynomial equation of degree 2 which is given by

$$\lambda_c \left(d_0 \lambda_c^2 + d_1\right) = 0, \tag{7.20}$$

where the coefficients d_0 and d_1 expressions are given by

$$\begin{aligned}
d_0 &= 4\varepsilon_c \eta_c k_2^2 \Pi_c \rho_c \left(\delta_c k_5 k_4 + \mu_h (\mu_h + \rho_c) k_4 + \varepsilon_c (\eta_c \mu_h + (\mu_h + \rho_c)(\mu_h + \varphi_c))\right) > 0,\\
d_1 &= -4h k_2{}^2 \nu_c \left(\theta_c k_2 + \mu_h (k_2 + \nu_c)\right) \Pi_c k_3^2 k_4^2 < 0.
\end{aligned}$$

The case $\lambda_c = 0$ corresponds to the MFE $\mathcal{E}_0$. Now we are interested in analyzing the following quadratic equation for the existence of positive equilibria.

$$d_0 \lambda_c^2 + d_1 = 0. \tag{7.21}$$

Since the coefficients $d_0 > 0$ and $d_1 < 0$, we conclude that the quadratic equation (7.21) has a unique positive root. Consequently, the model (7.1) has a unique MEE point $\mathcal{E}_1$.

7.3 Parameter estimation and numerical investigation

This section covers parameter estimation, sensitivity analysis, model simulation, and assessing the effects of model-sensitive parameters of the model (7.1).

7.3.1 Parameter estimation

To enhance our understanding and prediction of malaria transmission dynamics in Ethiopia, we utilize Ethiopian national malaria incidence data to fit and validate model (7.1). Here, malaria incidence is defined as the number of new malaria cases per $1,000$ individuals at risk in Ethiopia.

The incidence data, sourced from the World Bank, ranges from the years 2000 to 2022 (World-Bank, 2024) and is illustrated in Figure (7.2). For model fitting and parameter estimation, we utilize the least-squares fitting method as described in (Johnson & Faunt, 1992). Consequently, the model (7.1) can be written as follows

$$\frac{dx}{dt} = F(t,x,p),\ x(t_0) = x_0, \tag{7.22}$$

where x and p are the state variables and unknown parameters, respectively. Therefore, the sum of least-squares error is represented by

$$\Psi(p) = \sum_{i=1}^{n} (x_i - \bar{x}_i)^2,$$

where $\bar{x}_i$ is the real data and $x_i = x(t_i, p)$ is the solution of the model (7.1) and n denotes the number of the data. In order to obtain the parameter, the goal is to minimize the objective function.

$$\min_p \Psi(p),$$

subjected to equation (7.22). Thus, by estimating the model's key parameters, we aim to capture the complex interactions driving malaria transmission, including vaccination rates, host transmission rates, insecticide application rates, and other intervention strategies. This calibrated model serves as a valuable tool for forecasting malaria trends, evaluating the impacts of control measures, and informing evidence-based policy decisions to combat malaria in Ethiopia. Parameters that are not derived from the fitting process are calculated based on Ethiopian demographic data per year, with their sources cited in Table 7.2. This approach ensures that the most relevant Ethiopian demographic parameters are accounted for to provide a comprehensive understanding of malaria dynamics in the country. Unfortunately, we lack specific malaria incidence data on the proportions of individuals aged 5 and older or below five, so the model fits the total infected human $I_c + I_a$. Moreover, we assumed the following initial human and mosquito populations based on incidence data from the World Bank, ranging from the years 2000 to 2022 (WorldBank, 2024): $S_c(0) = 120$, $V_c = 0$, $I_c = 22$, $T_c = 0$, $R_c = 0$, $S_a = 557.3$, $I_a = 300.7$, $T_a = 0$, $R_a = 0$, $S_m = 800$, $I_m = 200$. For the model's best fit and parameter estimation, we utilize the least-squares fitting method (Mehrkanoon et al., 2012). The constant influx of malaria-prone humans Π_c and the natural mortality rate in humans μ_h are estimated from Ethiopian demographic data. The value for μ_h is calculated by taking the reciprocal of the average life expectancy in Ethiopia, which is approximately 67.8 years (WHO, 2020a). Thus, we have $\mu_h = \frac{1}{67.8}$ deaths per year. To calculate the annual constant influx of malaria-susceptible humans and mosquitoes Π_c, we explore a scenario introduced in (Madueme & Chirove, 2023) where human population under age five has reached its steady state. Thus, we consider total malaria incidence in the country of about 1000 humans, such that $\Pi_c = 1000 \times \mu_h$. For the annual constant influx of malaria-susceptible mosquitoes, we assume a hypothetical average population of 1,000, leading to $\Pi_m = 1000 \times \mu_m$, where $\mu_m = \frac{365}{21}\,\text{year}^{-1}$ represents the average lifespan of mosquitoes. This assumption is necessary due to the absence of quantified estimates for the actual annual mosquito population. We assumed a treatment rate of $\rho_c = 0.27$ for children under five years,

Table 7.2: Parameters and their values.

Parameters	value	Source
Π_c	$1000/67.8$	Calculated
μ_h	$1/67.8$	WHO (2020a)
Π_m	$1000 \times 365/21$	Calculated
μ_m	$365/21$	Calculated
β_1	0.021	Fitted
β_2	0.03	Fitted
β_3	0.07	Fitted
β_4	0.00231	Fitted
ε_c	0.0033	Fitted
ε_a	0.0012	Fitted
h	0.00027	Fitted
θ_c	0.028	Assumed
ρ_c	0.27	Assumed
ρ_a	0.2107	Fitted
ν_c	0.0401	Fitted
ρ_a	0.2107	Fitted
δ_c, δ_a	0.08	Fitted
η_c, η_a	0.17	Fitted
φ_c, φ_a	0.006	Fitted
γ_m	0.062	Fitted

based on empirical data from a previous study (Jaleta et al., 2025). This rate indicates that young children are often prioritized in treatment protocols due to their vulnerability and elevated risk of morbidity. The parameters η_a, γ_m, φ_c, φ_a, δ_a, δ_c, and η_c were adopted from a recently published mathematical modeling study on malaria, which utilized the same dataset for parameter fitting. Given the relevance and reliability of this source, these parameters were used directly rather than re-estimated. The corresponding citations are provided appropriately and credibly in Table 7.2. Furthermore, parameters $\beta_1, \beta_2, \beta_3, \beta_4, h, \varepsilon_c, \varepsilon_a, \theta_c, \rho_a, \nu_c$ are accurately fitted and summarized in Table 7.2.

We found that the fitted parameters for insecticide usage rate and transmission rates closely align with the results obtained in Chapter 6. The fitted values for the rate of loss of vaccine efficacy are realistic when compared to similar analyses in (Tchoumi, Dongmo, et al., 2022). Additionally, the parameters for waning immunity closely match those highlighted in the analysis presented in (Tchoumi, Diagne, et al., 2022). This close alignment confirms that our fitted parameters exhibit biological realism and validity in relation to prior empirical studies. The model fit presented in Figure (7.2) shows good alignment between the malaria model and incidence data in Ethiopia over the past twenty-three years. This close correspondence underscores the robustness and accuracy of our model in capturing the trends and patterns of malaria incidence in the region.

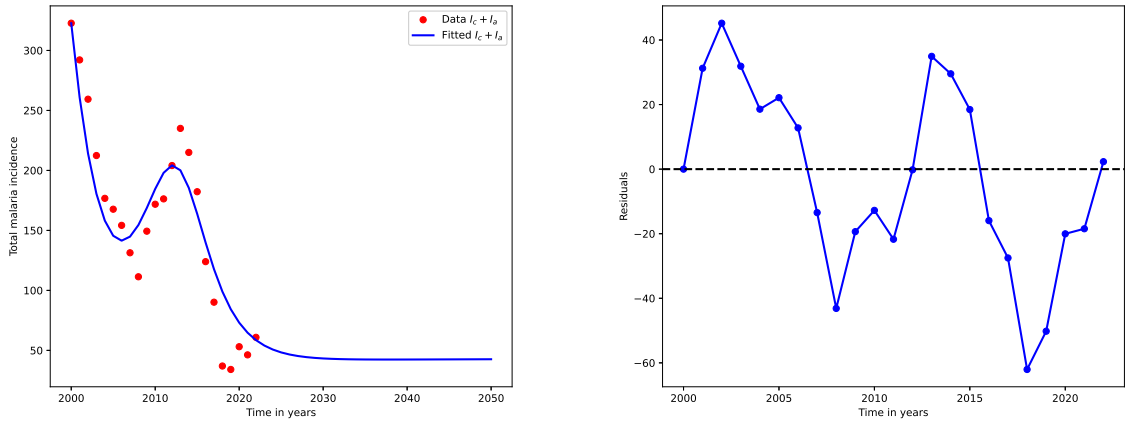

(a) Curve fit

(b) Residual plot

Figure 7.2: Plot showing curve fit and malaria prevalence data in Figure (7.2a) and residual plot in (7.2b)

7.3.2 Sensitivity analysis

To identify the most influential parameters in the malaria model (7.1), we conduct a sensitivity analysis focused on the effective reproduction number $\mathfrak{R}_e$. This analysis employs the normalized forward sensitivity index method, which quantifies the relative impact of each parameter on $\mathfrak{R}_e$, as outlined by Chitnis et al. (2008). Thus, the forward sensitivity index for a quantity $\mathfrak{R}_e$ in relation to a model parameter ψ is defined as:

$$\Upsilon_{\psi}^{\mathfrak{R}_e} = \frac{\partial \mathfrak{R}_e}{\partial \psi} \cdot \frac{\psi}{\mathfrak{R}_e} \tag{7.23}$$

This index measures the proportional change in $\mathfrak{R}_e$ resulting from a small variation in ψ. Parameters with higher sensitivity indices are considered more dominant, as they exert a greater influence on the transmission dynamics of the infection. By ranking the parameters based on their sensitivity indices, we can identify those that are most critical for controlling or mitigating the spread of the disease. The forward sensitivity index of the reproduction number $\mathfrak{R}_e$ in relation to model parameters $\Pi_c, \Pi_m, \gamma_m, \nu_c$ and μ_m is analytically computed accordingly

$$\Upsilon_{\Pi_m}^{\mathfrak{R}_e} = 0.5, \Upsilon_{\Pi_c}^{\mathfrak{R}_e} = -0.5, \Upsilon_{\gamma_m}^{\mathfrak{R}_e} = -\frac{\gamma_m}{\gamma_m + \mu_m}, \ \Upsilon_{\nu_c}^{\mathfrak{R}_e} = -\frac{\mu_h \nu_c}{2\left(h\left(\theta_c + \mu_h\right) + \mu_h k_1\right)}, \ \Upsilon_{\mu_m}^{\mathfrak{R}_e} = -\frac{\mu_m}{\gamma_m + \mu_m}$$

For the remaining model parameters, analytical sensitivity indices can be calculated using the same methodology. Moreover, Table 7.3 presents the numerical normalized forward sensitivity indices of $\mathfrak{R}_e$, evaluated at the parameter values provided in Table 7.2. From Table 7.3 and Figure (7.3) , the positive sensitivity index suggests that an increase in a parameter value leads to a corresponding increase in the value of $\mathfrak{R}_e$. Conversely, the negative sensitivity index indicates that as the parameter value increases, the value of $\mathfrak{R}_e$ decrease. Specifically, regarding $\Upsilon_{\gamma_m}^{\mathfrak{R}_e} = -0.565$, increasing the usage insecticides application (γ_m) by 10%, decrease $\mathfrak{R}_e$ by

Table 7.3: Sensitivity index of $\mathfrak{R}_e$ calculated with parameters value in Table 7.2.

Parameters	Sensitivity indexes	Parameters	Sensitivity indexes
γ_m	-0.565	β_3	+0.5
Π_c	-0.5	Π_m	+0.5
μ_m	-0.4344	β_1	+0.5
ρ_c	-0.349	μ_h	+0.34
ν_c	-0.3446	h	0.0061
δ_c	-0.109	β_4	+0.00053
θ_c	-0.024	β_2	+0.00053
ρ_a	-0.00036		
δ_a	-0.00013		

10%. Similarly, $\Upsilon_{\Pi_c}^{\mathfrak{R}_e} = -0.5$ indicates that a 5% increase in the constant influx of susceptible humans, (Π_c), results in a 10% decrease in $\mathfrak{R}_e$. Moreover, $\Upsilon_{\theta_c}^{\mathfrak{R}_e} = -0.024$ and $\Upsilon_{\nu_c}^{\mathfrak{R}_e} = -0.3446$ indicate that for every 10% increase in the vaccination rate of susceptible (ν_c), and the maturation rate (θ_c), the value of $\mathfrak{R}_e$ decrease by 4.34% and 0.24%, respectively. Conversely, $\Upsilon_{\Pi_m}^{\mathfrak{R}_e} = \Upsilon_{\beta_1}^{\mathfrak{R}_e} = \Upsilon_{\beta_3}^{\mathfrak{R}_e} = 0.5$ indicates that a 10% increase in the constant influx of malaria-prone mosquitoes (Π_m), and the transmission rates (β_1) and (β_3), lead to a 10% increase in $\mathfrak{R}_e$ individually. We can employ the same procedures for the sensitivity analysis of the other parameters influencing the reproduction number.

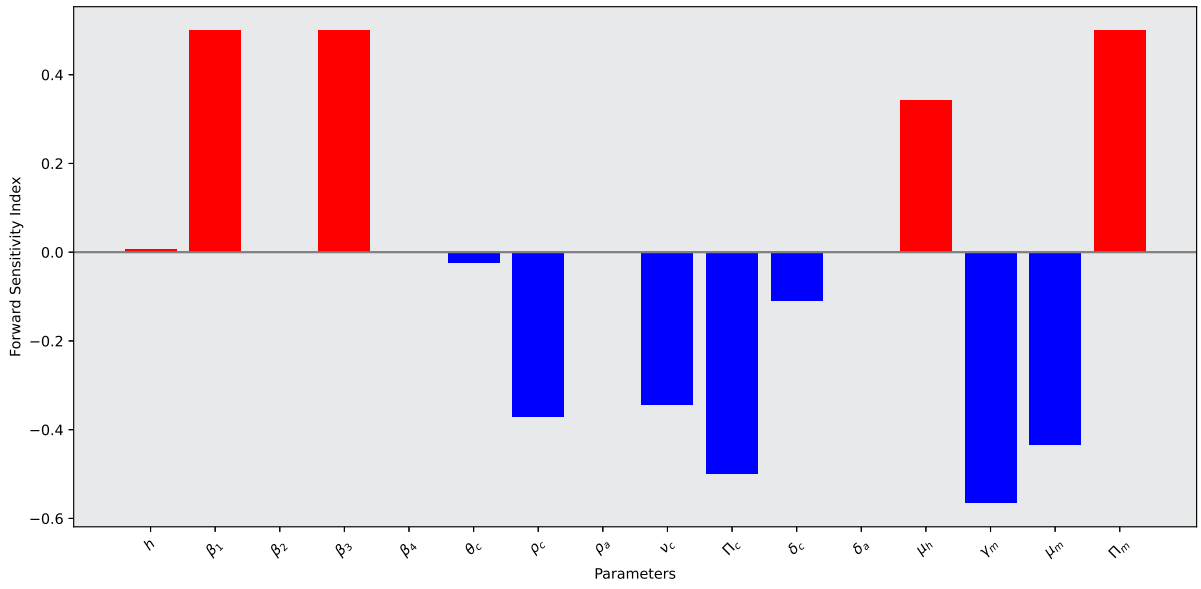

Figure 7.3: Bar plot showing forward sensitivity indices of $\mathfrak{R}_e$ with respect to certain parameters involved in the $\mathfrak{R}_e$

As shown in Table 7.3, the parameters γ_m, Π_c, ρ_c, ν_c, Π_m, β_1 and β_3 are most sensitive and epidemiologically relevant parameters influence on the effective reproduction number $(\mathfrak{R}_e)$.

This indicates that increases in γ_m, Π_c, ρ_c, and ν_c contribute to a reduction in the spread of malaria within the population. Conversely, increases in Π_m, β_1 and β_3 enhance malaria transmission within the community. Therefore, controls of these sensitive parameters can significantly affect public health strategies and resource allocation.

Contour plots

The contour plots depicting the influence of various parameters on the effective reproduction number $(\mathfrak{R}_e)$ are displayed in Figures (7.4) and (7.5). Figure (7.4) illustrates the effects of transmission rates (β_1, β_3), insecticide application rate (γ_m), vaccination rate (ν_c), maturation rate (θ_c), and treatment rate (ρ_c) on the effective reproduction number $(\mathfrak{R}_e)$. In the contour plot, each contour line represents a constant value of $(\mathfrak{R}_e)$, demonstrating that its values increase as both β_1 and β_3 rise. Closer contour lines indicate rapid changes in $\mathfrak{R}_e$ with small perturbations in these parameters, while more distant contour lines reflect more gradual changes. In particular, Figure (7.4a) illustrates the effective reproduction number $(\mathfrak{R}_e)$ as a function of two critical parameters: the transmission rates (β_1 and β_3). Figures (7.4b), (7.4c), and (7.4d) illustrate the critical roles of the parameter pairs (ν_c, γ_m), (θ_c, γ_m), and (ρ_c, ν_c) in influencing $\mathfrak{R}_e$. These figures demonstrate that as each parameter pair decreases (or increases), $\mathfrak{R}_e$ correspondingly increases (or decreases).

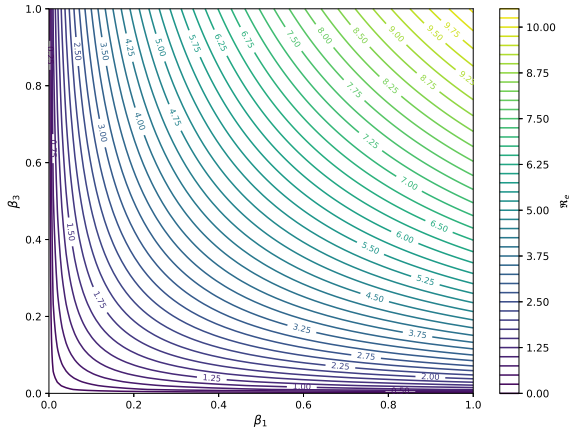

(a) Contour plot of $\mathfrak{R}_e$ with respect to β_1 and β_3

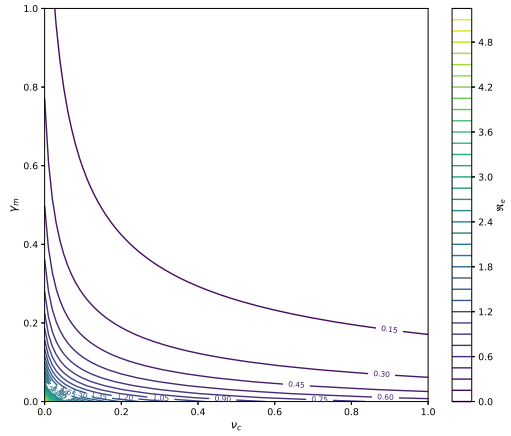

(b) Contour plot of $\mathfrak{R}_e$ with respect to ν_c and γ_m

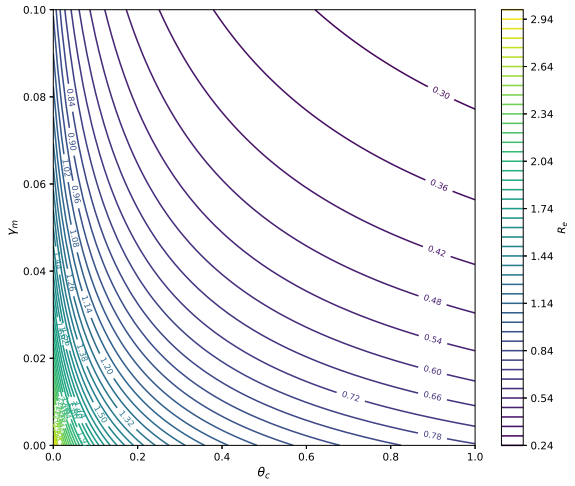

(c) Contour plot of $\mathfrak{R}_e$ with respect to θ_c and γ_m

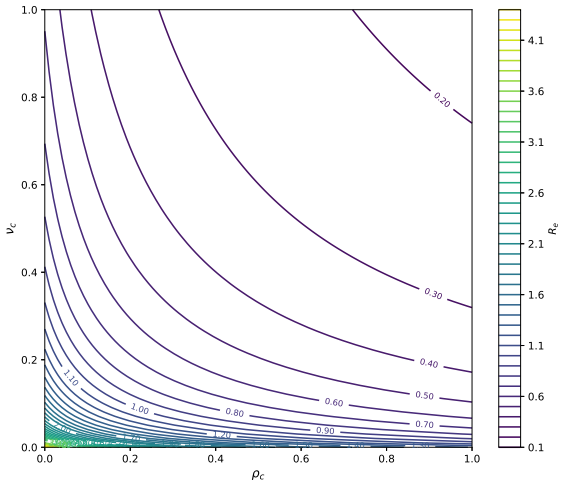

(d) Contour plot of $\mathfrak{R}_e$ with respect to ρ_c and ν_c

Figure 7.4: Effect of transmission rates (β_1, β_3), vaccination rate (ν_c), insecticide application rate (γ_m) maturation rate (θ_c), treatment rates (ρ_c) on effective reproduction number $(\mathfrak{R}_e)$.

Similarly, Figure (7.5) illustrates the multifaceted impact of various parameters on the effective reproduction number $(\mathfrak{R}_e)$. These parameters include the loss of vaccine efficacy rate (h), vaccination rate (ν_c), maturation rate (θ_c), transmission rates (β_1, β_3), and insecticide application rate (γ_m). Figure (7.5a) demonstrates the pivotal role of the malaria vaccination rate (ν_c) in mitigating $\mathfrak{R}_e$. The figure reveals that an increase in the vaccination rate substantially reduces $\mathfrak{R}_e$, even when confronted with a high loss of vaccine efficacy (h). This underscores the vaccination's dominant influence on controlling malaria transmission. Figure (7.5b) explores the intricate relationship between the loss of vaccine efficacy rate (h) and the maturation rate (θ_c). The analysis indicates that elevating the maturation rate proves more effective in diminishing $\mathfrak{R}_e$ when the loss of vaccine efficacy remains minimal to moderate. This suggests that optimizing the timing of interventions could enhance their impact on malaria control. Furthermore, Figures (7.5c) and (7.5d) delve into the combined effects of transmission rates (β_1) and (β_3) alongside the insecticide application rate (γ_m). The findings reveal that a strategic increase in the insecti-

cide application rate, coupled with a reduction in the malaria transmission rates (β_1) or (β_3), can significantly curtail $\mathfrak{R}_e$. This highlights the potential of integrated vector management strategies in curbing malaria spread. Collectively, these figures underscore the complex interplay of multiple factors in determining the effective reproduction number $\mathfrak{R}_e$ for malaria. The insights gleaned from these analyses can inform the design of more effective malaria control strategies, tailored to the specific epidemiological context.

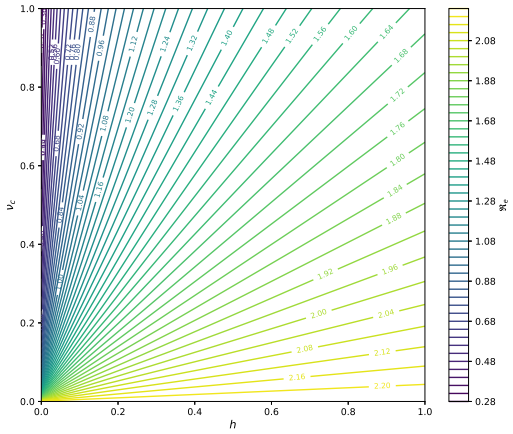

(a) Contour plot of $\mathfrak{R}_e$ with respect to h and ν_c

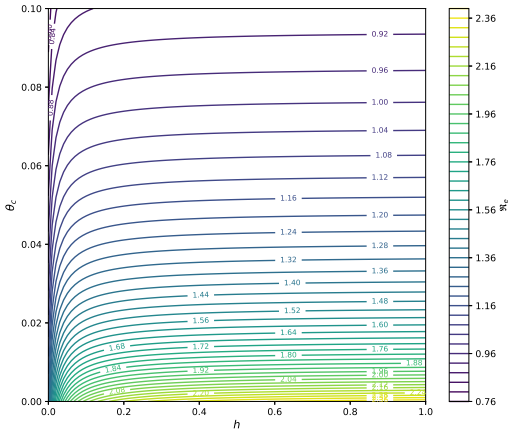

(b) Contour plot of $\mathfrak{R}_e$ with respect to h and θ_c

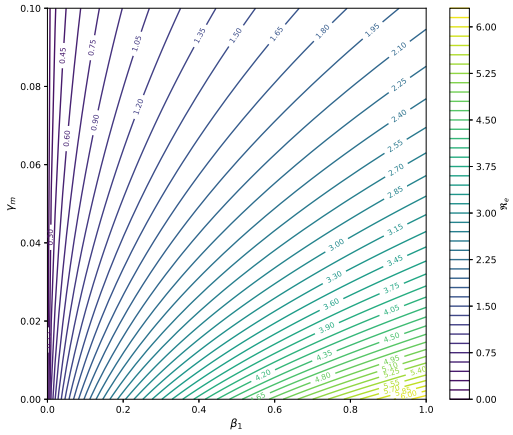

(c) Contour plot of $\mathfrak{R}_e$ with respect to β_1 and γ_m

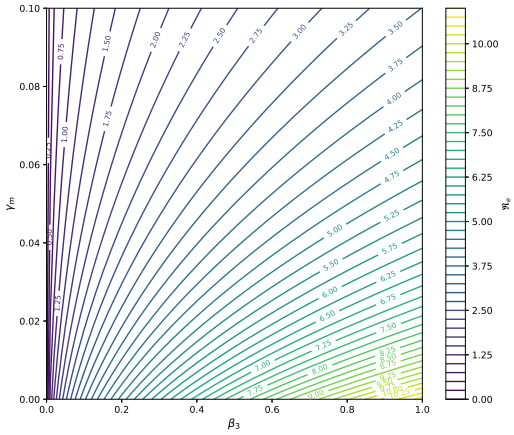

(d) Contour plot of $\mathfrak{R}_e$ with respect to β_3 and γ_m

Figure 7.5: Effect of loss of vaccine efficacy (h), vaccination rate (ν_c), maturation rate (θ_c), insecticide application rate (γ_m) transmission rates (β_1, β_3) on effective reproduction number $(\mathfrak{R}_e)$.

7.3.3 Model simulation

In this sub-section, we present numerical solutions of model (7.1) to support the theoretical findings obtained from previous sections. The simulations were executed using scipy.integrate.solve-ivp function, which is well-suited for solving ODEs in Python software. To illustrate the convergence of model equilibria, we aim to show that the solutions of the model approach a specific equilibrium point as time goes. Figures (7.6) and (7.7) depicts the time-course behavior of

the model solution for the cases when $\mathfrak{R}_e < 1$ and $\mathfrak{R}_e > 1$, respectively. To demonstrate convergence to $\mathcal{E}_0$, we used parameter values from Table 7.2 and set the transmission rate $\beta_1 = 0.0021$. Substituting these values into equation (7.10), we get $\mathfrak{R}_e = 0.415$. In this scenario, the model exhibits an MFE given by $\mathcal{E}_0 = (257,675,0,0,0,48,0,0,0,158557.8,0)$, which is globally asymptotically stable as depicted in Figure (7.6). In particular, the number of non-infected humans in Figure (7.6a) and non-infected mosquitoes in Figure (7.6d) continues to rise. This trend indicates that an increasing proportion of individuals in both species remain malaria-free, while the populations of infected and treated individuals decline. As a consequence, the human population of recovered individuals also decreases, as expected. This is further supported by the data presented in Figure (7.6b) and Figure (7.6c), which demonstrate that the number of infected and treated humans continue to diminish, approaching zero over time. This suggests that the disease eventually be brought under control when $\mathfrak{R}_e < 1$.

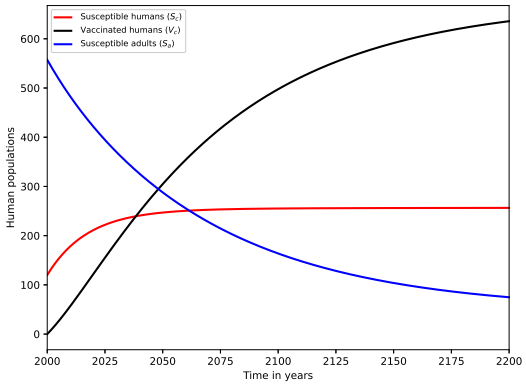

(a) Dynamics of S_c, V_c and S_a humans

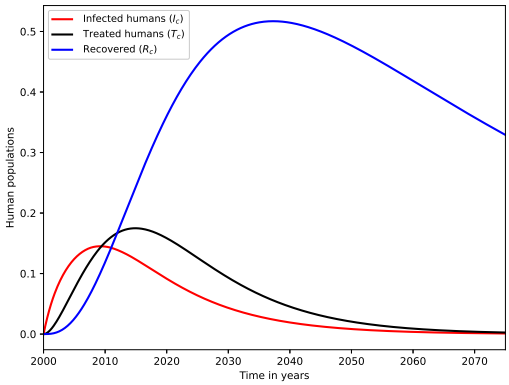

(b) Dynamics of I_c, T_c and R_c humans

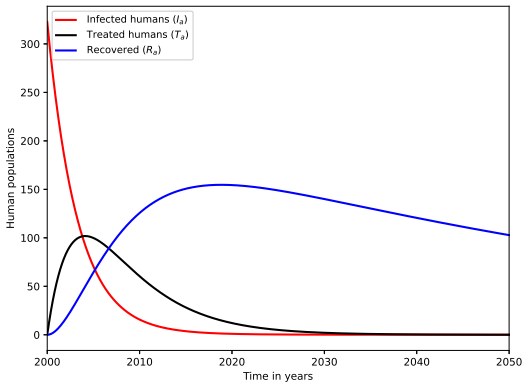

(c) Dynamics of I_a, T_a and R_a humans

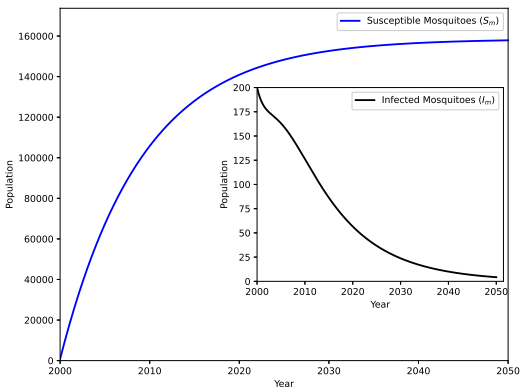

(d) Dynamics of S_m and I_m mosquitoes

Figure 7.6: The plot illustrating convergence of MFE, $\mathcal{E}_0$ when $\mathfrak{R}_e = 0.425$.

To illustrate the convergence of malaria equilibrium $(\mathcal{E}_1)$, we used the parameter values presented in Table 7.2. Substituting these values in (7.10), we determine $\mathfrak{R}_e = 1.25 > 1$ gives a

unique $\mathcal{E}_1$

$$\mathcal{E}_1 = (10.0, 42.0, 41.3, 58.2, 294.5, 2, 1.27, 2.0, 286.5, 152559.1, 5342.81)\,.$$

As shown in Figure 7.7a, the populations of susceptible humans under 5 years old (S_c), vaccinated humans in this age group (V_c), and susceptible humans aged 5 and older (S_a) converge to their respective malaria equilibrium values of 10, 42.0, and 2.0 beyond the year 2050. In Figure (7.7b) the solution trajectories of infected, treated, and recovered humans under age five ultimately rise and stabilize at equilibrium values of 41.3, 58.16, and 294.5, respectively. Conversely, Figure (7.7c) shows that the trajectories for infected, treated, and recovered humans aged five and older decline and converge to equilibrium values of 1.27, 2.0, and 286.5, respectively. Lastly, Figure (7.7d) indicates a significant decrease in the population of malaria-infected mosquitoes, which stabilizes at approximately 5342.81. However, the population of malaria-susceptible mosquitoes in Figure (7.7d) increase and converge to equilibrium value of 152559.1. The biological implication of the globally asymptotically stable equilibrium $\mathcal{E}_1$ is that malaria infection levels remain constant over time. This underscores the critical importance of maintaining effective control measures to prevent disruptions that could lead to an increase in transmission rate.

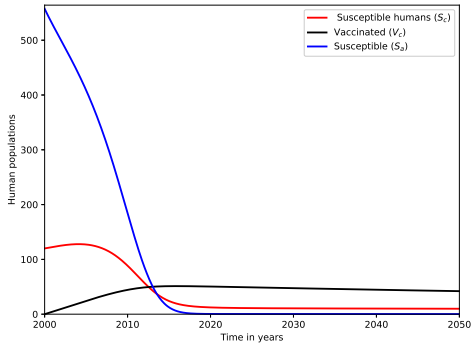

(a) Dynamics of S_c, V_c and S_a humans

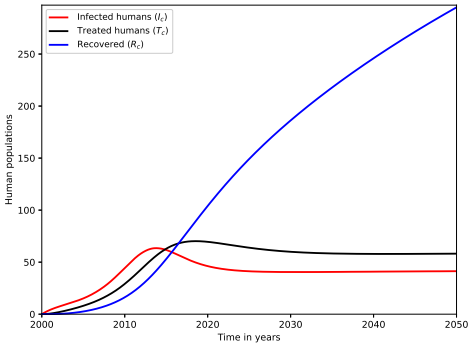

(b) Dynamics of I_c, T_c and R_c humans

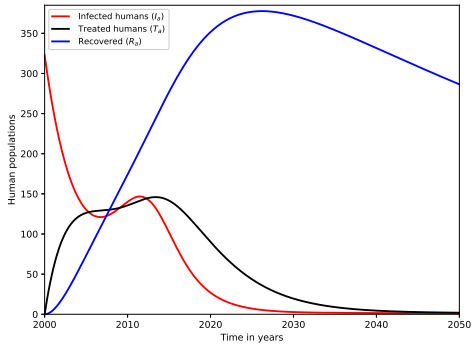

(c) Dynamics of I_a, T_a and R_a humans

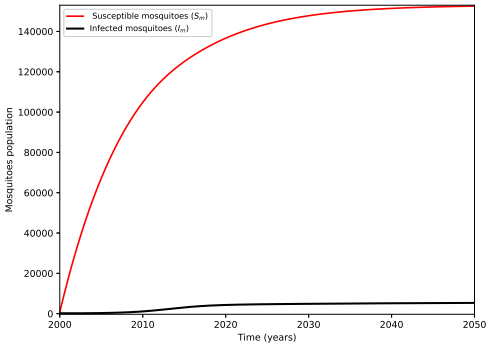

(d) Dynamics of $_m$ and I_m mosquitoes

Figure 7.7: Dynamics of human and mosquito populations when $\mathfrak{R}_e = 1.25$.

7.3.4 Impact of some model parameters

In this sub-section, we examine the dynamics of model solutions in relation to the maturation rate (ν_c) and the malaria vaccination rate (θ_c). In addition, we analyze the impact of model-sensitive parameters on malaria transmission dynamics.

Impact of maturation rate θ_c

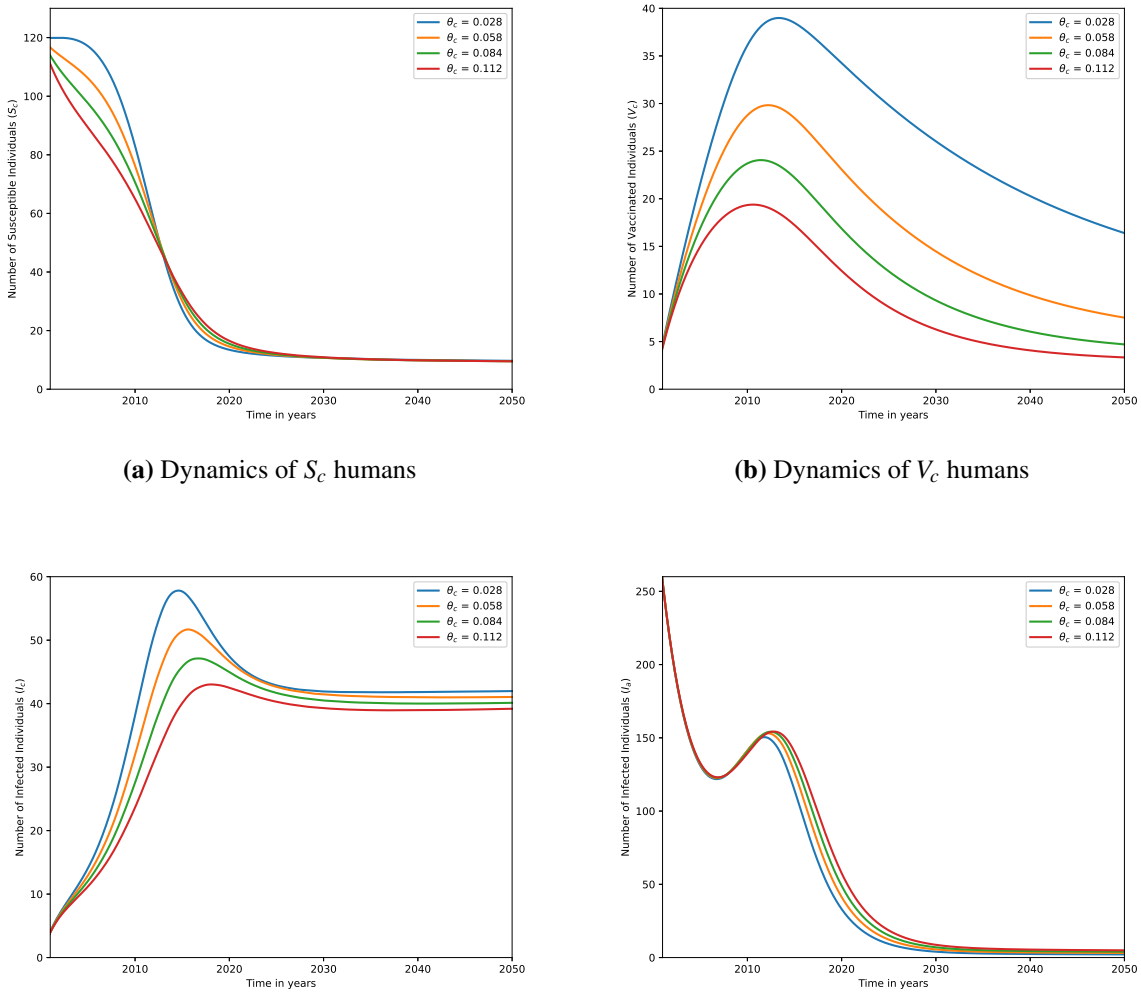

(a) Dynamics of S_c humans

(b) Dynamics of V_c humans

(c) Dynamics of I_c humans

(d) Dynamics of I_a humans

Figure 7.8: The plot illustrating the effect of vaccination rate θ_c

Figure 7.8 illustrates the impact of various maturation rates (θ_c), on malaria transmission dynamics over 50 years. Each sub-figure represents a distinct epidemiological class affected by the maturation (θ_c). Figure (7.8a) shows that higher maturation rates significantly reduce the

peak number of susceptible individuals in this age group, particularly during the initial ten years following the onset of the infection. Figure (7.8b) indicates that an increased maturation rate contributes to a decline in the number of individuals in the vaccinated class. Similarly, Figure (7.8c) reveals a downward trend in infectious class as maturation rates θ_c increase. Lastly, Figure (7.8d) demonstrates a significant decrease in the number of malaria-infected individuals within the I_a class as maturation rates θ_c rise.

Impact of vaccination rate ν_c

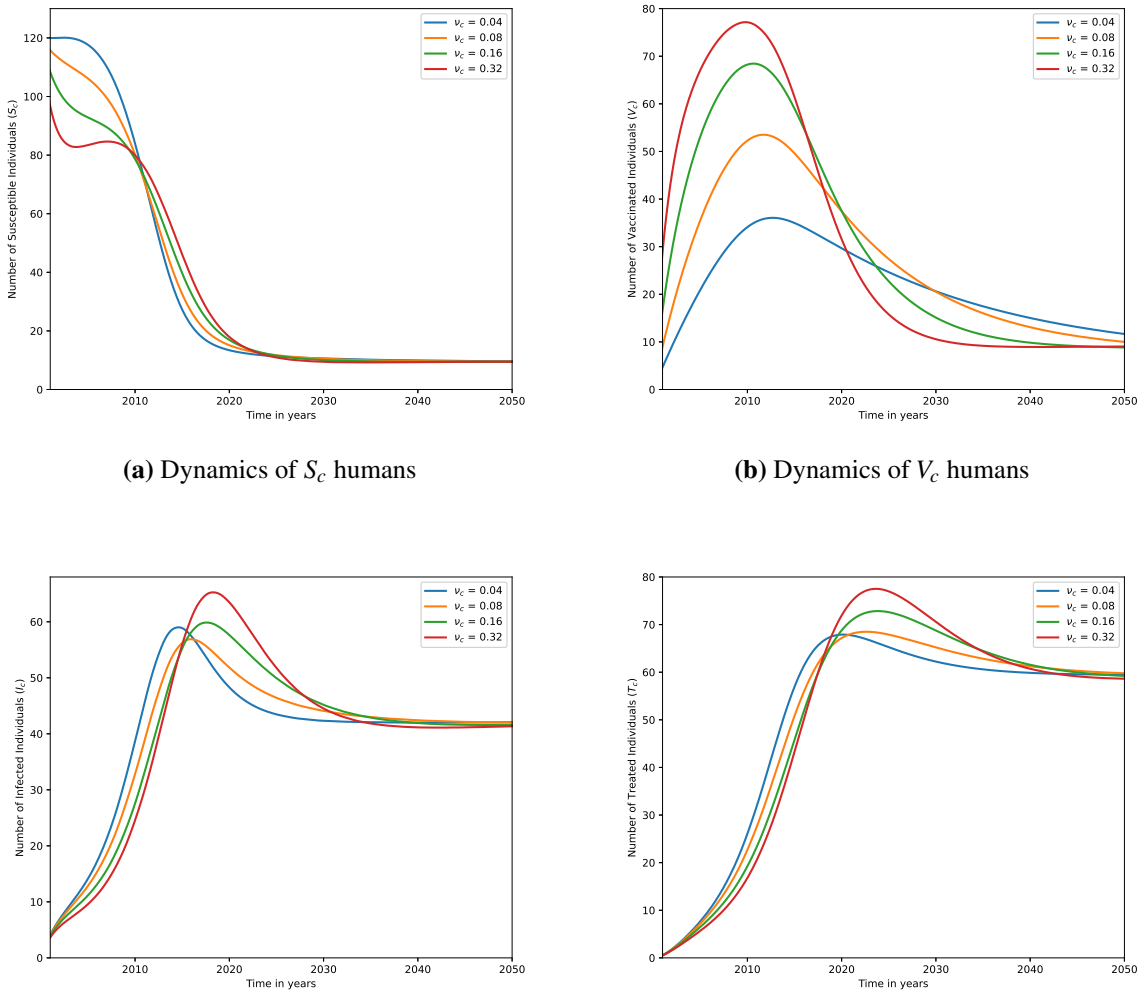

(a) Dynamics of S_c humans

(b) Dynamics of V_c humans

(c) Dynamics of I_c humans

(d) Dynamics of T_c humans

Figure 7.9: The plot illustrating the effect of vaccination rate ν_c

Figure 7.9 illustrates the impact of varying vaccination rates (ν_c) on malaria dynamics over 50 years. In Figure 7.9a, the effect on susceptible individuals S_c is shown, where higher vacci-

nation rates lead to lower peaks, indicating a reduction in the number of individuals entering the susceptible class as ν_c increases. Similarly, Figure 7.9c shows a decline in malaria-infected individuals I_c as vaccination rates rise. Lastly, Figure 7.9d illustrates a significant drop in the number of malaria-treated individuals T_c with increasing vaccination rates. However, Figure 7.9b depicts the vaccinated individuals V_c, demonstrating that greater vaccination rates significantly increase the number of vaccinated humans.

Impact of treatment rate ρ_c

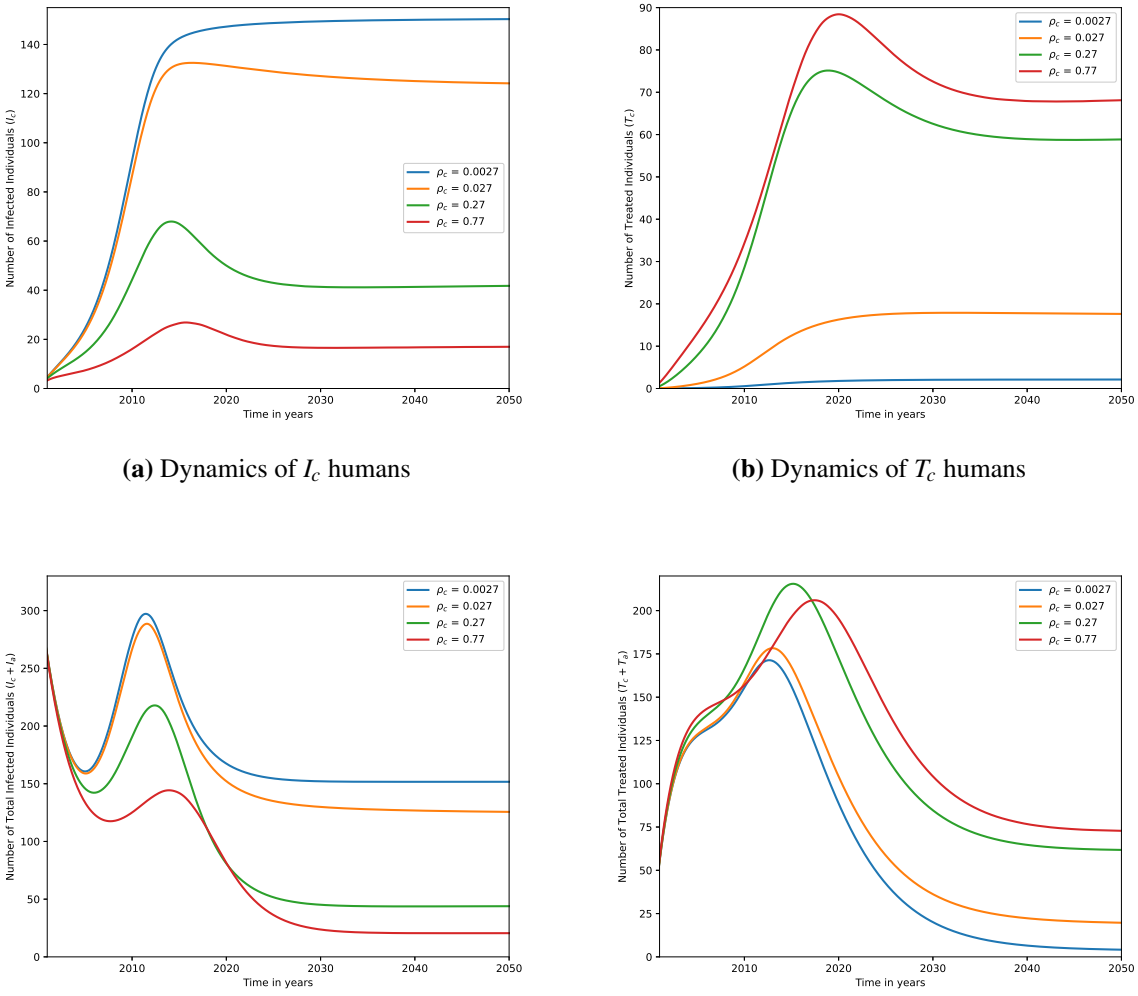

(a) Dynamics of I_c humans

(b) Dynamics of T_c humans

(c) Dynamics of $I_c + I_a$ humans

(d) Dynamics of $T_c + T_a$ humans

Figure 7.10: The plot illustrating the effect of treatment rate ρ_c

Figure (7.10) illustrates the influence of the treatment rate (ρ_c) on the malaria dynamics focusing on the infected and treated classes. As shown in Figures (7.10a) and (7.10c), both

the infected class I_c and the total number of infected individuals $I_c + I_a$ decrease as treatment rate increase. Conversely, Figures (7.10b) and 7.10d demonstrate that as the treatment rate increases, the number of treated individuals T_c and the total treated population $T_c + T_a$ also rise. This indicates that higher treatment rates effectively lift more individuals from the infected class to the treated class, thereby mitigating the spread of malaria over time.

Impact of insecticides application

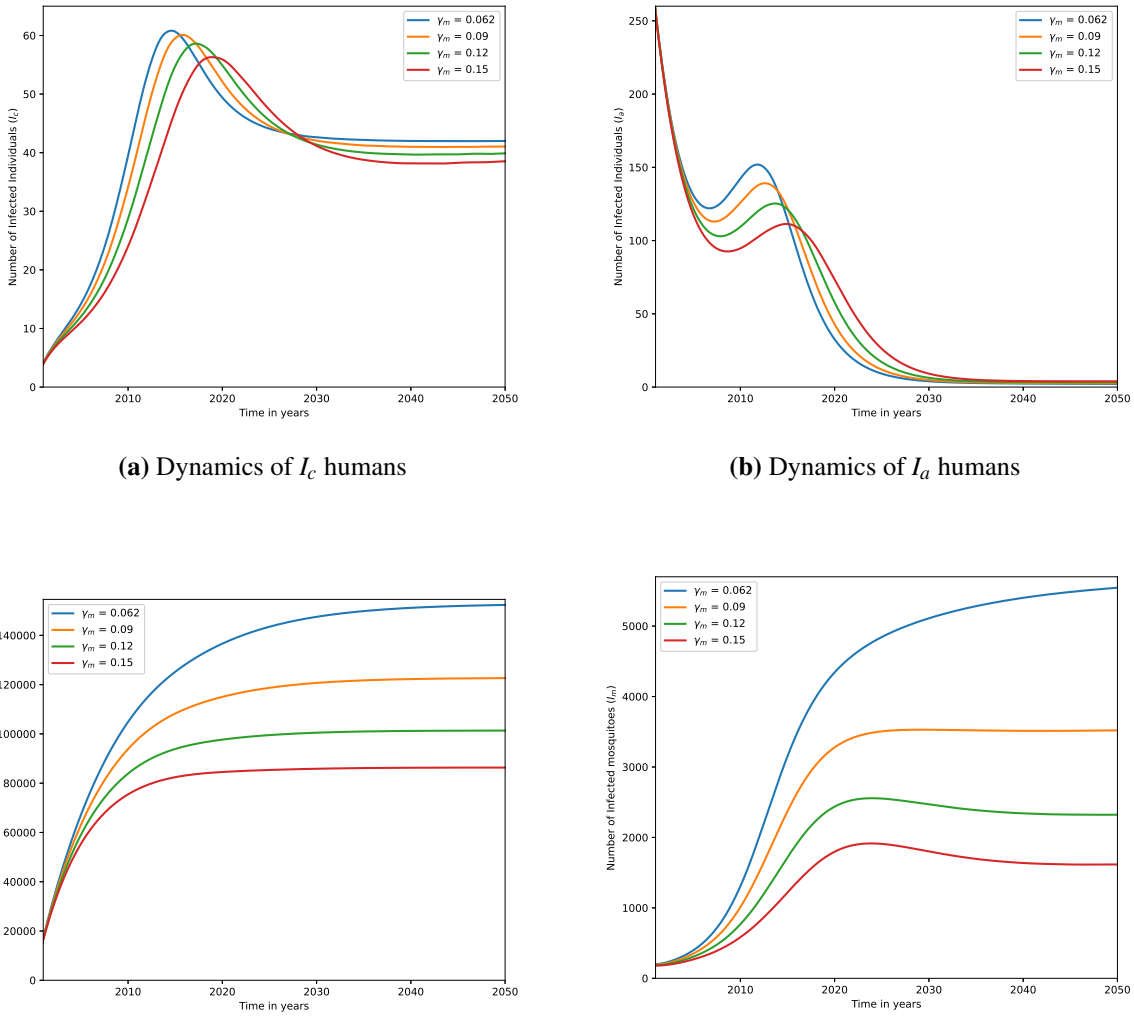

(a) Dynamics of I_c humans

(b) Dynamics of I_a humans

(c) Dynamics of S_m mosquitoes

(d) Dynamics of I_m humans

Figure 7.11: The plot illustrating the effect of vaccination rate ν_c

Figure (7.11) examines the effect of the insecticide application rate (γ_m) on minimizing the spread of malaria. Specifically, Figures (7.11a) and (7.11b) show that higher insecticide application rates result in a decrease in malaria-infected individuals in the I_c and I_a classes, respectively. Additionally, Figures (7.11c) and (7.11d) illustrate the significant impact of increased insecti-

cide usage on reducing both susceptible and infected mosquito populations. These observations emphasize the crucial role of heightened insecticide application in mitigating the transmission of malaria, affecting not only human cases but also targeting the mosquito population. This underscores the importance of comprehensive vector control strategies for effective malaria management.

Impact of transmission rates β_1

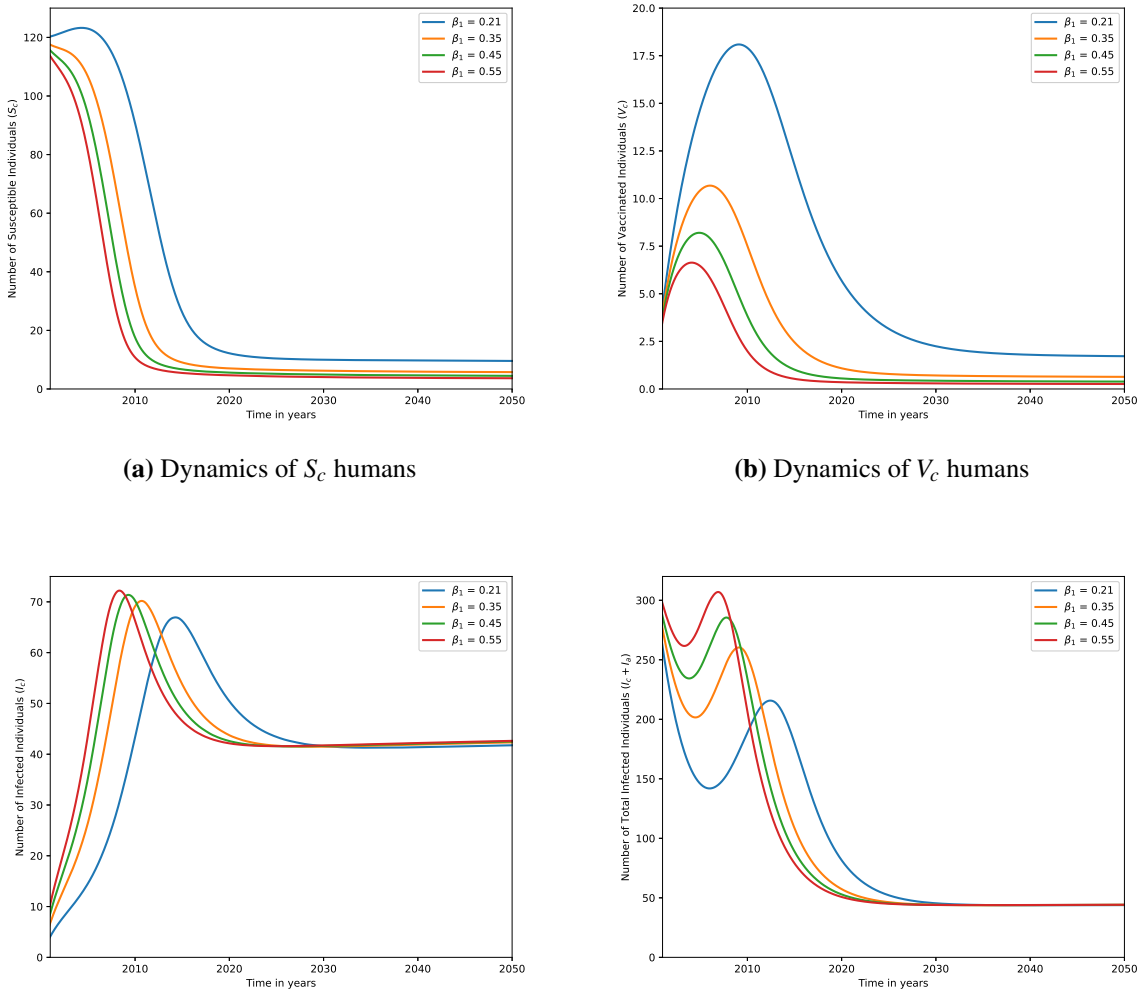

(a) Dynamics of S_c humans

(b) Dynamics of V_c humans

(c) Dynamics of I_c humans

(d) Dynamics of $I_c + I_a$ humans

Figure 7.12: The plot illustrating the effect of transmission rate β_1

Figure (7.12) illustrates the impact of the transmission rate (β_1) from infected mosquitoes to susceptible individuals for various values of β_1. In Figures (7.12a) and (7.12b), it is evident that the endemicity of malaria increases in both susceptible humans and vaccinated individuals

under five years of age as the β_1 value rises. However, Figures (7.12c) and (7.12d) highlight that the number of malaria-infectious individuals in both I_c and I_a classes increases as the contact rate β_1 decreases, and vice versa. Consequently, by minimizing the contact between susceptible humans and infected mosquitoes, the likelihood of humans transmitting malaria to mosquitoes is significantly reduced. This, in turn, leads to a decrease in malaria infection rates within the population.

Impact of transmission rates β_3

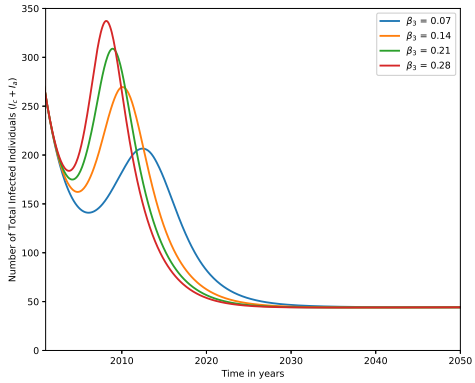

(a) Dynamics of $I_c + I_a$ humans

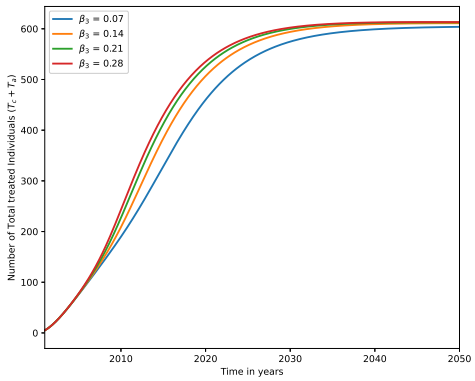

(b) Dynamics of $T_c + T_a$ humans

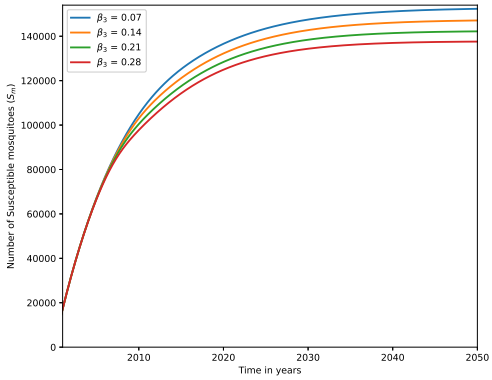

(c) Dynamics of S_m mosquitoes

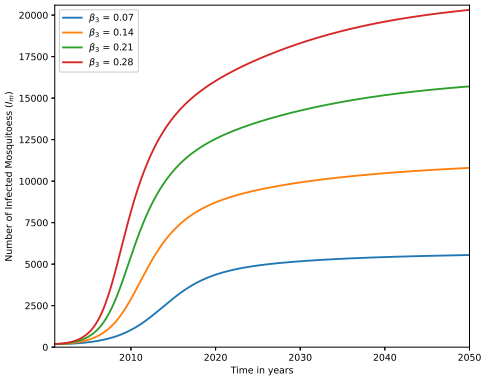

(d) Dynamics of S_m mosquitoes

Figure 7.13: The plot illustrating the effect of transmission rate β_3

Figure (7.13) shows the effect of the infection rate from infected humans I_c on susceptible mosquitoes S_m for varying values of β_3. As shown in Figures (7.13a) and (7.13b), the endemicity of malaria increases in both the total infected population $I_c + I_a$ and the total treated individuals $T_c + T_a$ with rising values of β_3. Likewise, data from Figure (7.13d) shows that the number of

malaria-infected mosquitoes increases as contact rate β_3 rises and decreases as this rate diminishes. On the other hand, the number of susceptible mosquitoes declines as the contact rate between malaria-infected humans I_c and susceptible mosquitoes S_m escalates as depicted in Figure (7.13c). Therefore, minimizing contact between infected humans and susceptible mosquitoes significantly lessens the likelihood of malaria transmission to others.

CHAPTER 8

SUMMARY, CONCLUSIONS AND RECOMMENDATIONS

This chapter offers a concise summary of the research findings, presents key conclusions, and proposes recommendations based on the study. It also discusses potential areas for future research to build upon the existing knowledge and address identified gaps.

8.1 Summary

In this dissertation, we developed compartmental mathematical models to describe the dynamics of malaria infection, incorporating media awareness, treatment interventions, asymptomatic infections, age-structured vaccination strategies, and optimal control and cost-effectiveness approaches. Thus, we first formulate a deterministic mathematical model of malaria transmission incorporating media-driven awareness and treatment interventions in Chapter 4. The model captures the effect of media-based campaigns on the effectiveness of insecticide application in malaria control. We examined the mathematical properties of the model, demonstrating its epidemiological relevance. The basic reproduction number, $\mathfrak{R}_0$, is computed using the next-generation matrix method. Stability analysis indicates that the malaria-free equilibrium is globally asymptotically stable when $\mathfrak{R}_0 < 1$ and unstable when $\mathfrak{R}_0 > 1$. The global stability of the endemic equilibrium for $\mathfrak{R}_0 > 1$ is established via a suitable quadratic Lyapunov function. The result from sensitivity analysis identified that insecticide usage rate (γ/γ_m), malaria treatment (ρ), and malaria transmission rates (β_1 and β_2) are the most influential parameters governing disease dynamics.

In Chapter 5, we investigated an optimal control and cost-effectiveness analysis incorporating three time-dependent intervention strategies: personal protective measures $u_1(t)$, improved treatment capability $u_2(t)$, and mosquito breeding site destruction $u_3(t)$ to reduce malaria infections. We extended the autonomous malaria model from Chapter 4 into an optimal control framework by incorporating time-dependent controls. Utilizing Pontryagin's Minimum Principle, we derived the necessary conditions for the optimal control model. To identify the most cost-effective intervention strategy, we computed the ACER and ICER. The numerical simulations were conducted using the Python Gekko optimization package, supporting our analytical findings. Results indicate that malaria can be effectively controlled using any of the proposed strategies; however, resource limitations may hinder their implementation. Our cost-effectiveness analysis suggests that the optimal combination of improved treatment capability and mosquito breeding site destruction is the most economically viable strategy for controlling malaria transmission compared to other combinations.

In Chapter 6, we formulated a mathematical model to investigate the impact of asymptomatic infections on malaria transmission. By analyzing key properties such as positivity, boundedness, and equilibrium stability, the model underscores the epidemiological significance of these silent carriers. The basic reproduction number $\mathfrak{R}_0$ was calculated using the next-generation matrix method, revealing critical dynamics, including backward bifurcation. Numerical simulations suggest that asymptomatic cases account for approximately 30% of all infections, highlighting

their crucial role in malaria transmission. These findings underscore the necessity for integrated control strategies that address both symptomatic and asymptomatic cases to effectively manage and reduce malaria transmission.

Lastly in Chapter 7, we investigated an age-structured vaccination model to analyze interactions between human and mosquito hosts. Key mathematical properties were established, and equilibrium stability was examined in relation to the effective reproduction number $\mathfrak{R}_e$. The system has two equilibrium points: a malaria-free equilibrium and a malaria equilibrium. Analytical results demonstrate that the malaria-free equilibrium is locally and globally asymptotically stable when $\mathfrak{R}_e < 1$, while the malaria equilibrium is globally asymptotically stable when $\mathfrak{R}_e > 1$. Numerical results support theoretical findings, indicating that effective vaccinations, treatments, and vector control could reduce malaria transmission to near-zero levels, facilitating potential eradication. This study highlights the importance of integrating vaccination with other malaria control strategies for sustainable public health planning in endemic regions.

8.2 Conclusion

Malaria is a severe infectious disease caused by *Plasmodium parasites*, which are transmitted to humans through the bites of infected *Anopheles* mosquitoes. It continues to be a significant global health burden, with substantial socioeconomic and health impacts Sub-Saharan Africa (SSA) regions particularly Ethiopia. In Ethiopia, malaria affects approximately 75% of the landmass and 69% of the population, accounting for about 20% of deaths among children under five. Despite existing interventions, including vector control strategies and antimalarial therapies, the disease burden persists. To address these ongoing challenges, we developed and analyzed mathematical model for malaria transmission incorporating different aspects. Thus, in Chapter 4, we formulated and analyzed a mathematical model incorporating media awareness and treatment interventions within an ODEs framework. The analysis of the proposed model demonstrates that media awareness and treatment interventions are critical for controlling disease dynamics. Stability analysis indicates that the malaria-free equilibrium is maintained when the basic reproduction number is below one, while the endemic equilibrium persists when it exceeds one, highlighting the threshold behavior of malaria transmission. Numerical results further show that combining awareness-driven vector control, effective treatment, and transmission-reduction strategies can substantially reduce infection prevalence and support eradication efforts. These findings emphasize the importance of integrating behavioral interventions with conventional control measures to achieve sustainable malaria management and long-term disease mitigation.

The optimal control and cost-effectiveness analysis studied in Chapter 5 highlights that integrating the time-dependent interventions can substantially reduce malaria burden and associated costs. Among the strategies evaluated, combining enhanced treatment capacity with mosquito breeding site destruction emerges as the most cost-effective approach. These results underscore that, while resource constraints may limit implementation, carefully targeted and economically efficient interventions can significantly improve malaria control outcomes.

In Chapter 6, we formulate and analyze a mathematical model that examines the impact of asymptomatic infections on malaria dynamics. The analysis of the malaria model highlights the critical role of asymptomatic infections in sustaining transmission dynamics. The occurrence of backward bifurcation indicates that reducing the basic reproduction number below one alone

is insufficient for eradication, emphasizing the need for comprehensive control strategies. Both symptomatic and asymptomatic infections significantly contribute to overall disease prevalence, necessitating interventions that target all infected individuals. Additionally, the model identifies human-mosquito contact and mosquito influx as key drivers of transmission, underscoring the importance of effective vector control. Consequently, maximizing insecticide-treated nets (ITNs) and indoor residual spraying (IRS) alongside treatment interventions is essential for substantially reducing malaria transmission and achieving sustainable disease control.

In Chapter 7, we formulate and analyze an age-structured mathematical model of malaria, incorporating vaccination strategies for children under five years of age. The model highlights the pivotal role of vaccination in controlling disease spread and achieving herd immunity, particularly when the basic reproduction number $\mathfrak{R}_0$ exceeds the effective reproduction number $\mathfrak{R}_e$. Analytical results, supported by numerical simulations, indicate that reducing transmission rates and minimizing vaccine efficacy loss are critical for mitigating infections, while increased insecticide use, treatment coverage, vaccination, and maturation rates effectively curb malaria transmission. These findings suggest that targeted vaccination of specific age cohorts, combined with complementary interventions, is essential for both immediate protection and long-term malaria elimination, thereby enhancing the effectiveness of public health strategies in endemic regions. Conversely, inadequate implementation results in an endemic equilibrium, emphasizing the need for robust public health policies, including targeted vaccination in high-burden regions such as Ethiopia.

In conclusion, this research has advanced the mathematical modeling of malaria transmission by progressively incorporating real-world complexities such as awareness driven behavior, optimal intervention strategies, asymptomatic infections, and age specific vaccination effects. The models developed not only provide theoretical insights into the dynamics of malaria but also offer practical guidance for designing cost effective, data driven public health policies. By grounding the analysis in the context of Ethiopia, a region heavily burdened by malaria, this work reveals the importance of tailoring intervention strategies to local epidemiological realities. Ultimately, the findings contribute to a deeper understanding of malaria dynamics and support global efforts toward effective and sustainable malaria control and eradication.

8.3 Recommendations

In this dissertation, we examine various aspect of malaria transmission dynamics to gain a comprehensive understanding of the underlying factors influencing its spread. Our analysis addresses the intended research objectives, providing valuable insights into the complexities of malaria epidemiology. To effectively translate our research findings into practical applications for policymakers, modelers, and public health practitioners, we recommend the following strategies.

- ◇ Our findings highlight the potential of combining awareness-based insecticide use with malaria treatment as an effective strategy for malaria eradication, offering significant implications for public health by identifying optimal scenarios to contain transmission within communities. We recommend enhancing insecticide use, strengthening treatment capacity, and promoting media-based awareness campaigns to collectively reduce malaria trans-

mission and burden in endemic areas.

- ◇ Existing literature indicates that asymptomatic malaria presents major challenges to control and elimination, as many carriers remain undiagnosed and untreated. Findings from quantitative analysis stressed that asymptomatic cases constitute a substantial proportion of total infections. Thus, policymakers and public health practitioners should prioritize effective control strategies centered on screening with immediate treatment in endemic areas, complemented by mass drug administration for high-risk groups, including children and pregnant women. Continued research and surveillance are essential to track prevalence, assess intervention impact, and advance progress toward malaria elimination.

- ◇ Analytical and numerical analysis of the age-structured vaccination model highlights the crucial role of malaria vaccination in achieving herd immunity. Yet, implementation for the proposed age cohort may be limited by financial constraints. We recommend that mathematical modelers and epidemiologists prioritize optimal, cost-effective strategies to deliver vaccination, aiming to disrupt transmission dynamics and support long-term eradication. Integrating this approach with existing control strategies align interventions with the epidemiological context of endemic regions such as Ethiopia and improve public health outcomes.

8.4 Future work

Although, this dissertation addressed the research objectives stated in Chapter 1, the models presented in this study lack some other important factors influencing the dynamics malaria transmission. Thus, The possible directions for extending the models presented in Chapter 4, Chapter 6 and Chapter 7 are as follows

- ◇ The model presented in Chapter 4 can be extended in several ways, including the integration of stochastic elements, time-varying mosquito recruitment, and environmental drivers. Incorporating these factors improve the model's accuracy and its capacity to simulate and predict malaria transmission under various intervention scenarios, thereby increasing its utility as a decision-making tool in malaria control strategies.

- ◇ Theoretical analyses often neglect malaria transmission models that include asymptomatic cases. To address this gap, the model in Chapter 6 can be extended by incorporating additional epidemiological compartments, environmental factors (e.g., temperature and rainfall), and time-varying mosquito recruitment. These extensions enhance realism, better capture human–vector dynamics, and improve predictive accuracy for effective malaria control.

- ◇ The model presented in Chapter 7 can be extended by introducing important epidemiological compartments for exposed and asymptomatic individuals. Furthermore, it can be enhanced by employing age-structured, specific real-world data for proportions of individuals aged five and older and those below five, rather than relying on implicit data. This approach will improve model validation and parameter estimation, providing better insights into future malaria dynamics and informing effective public health planning and intervention strategies.

CONTRIBUTION OF THE DISSERTATION

The dissertation reports original results that contribute knowledge to the scientific advancement in mathematics. All of the contributions were published in peer reviewed journals indexed in Scopus, PubMed and Web of Science.

1. *Haringo, Andualem Tekle, Legesse Lemecha Obsu, and Feyissa Kebede Bushu. "A mathematical model of malaria transmission with media-awareness and treatment interventions." Journal of Applied Mathematics and Computing 70.5 (2024): 4715-4753.* https://doi.org/10.1007/s12190-024-02154-9

2. *Haringo, Andualem Tekle, Legesse Lemecha Obsu, and Feyissa Kebede Bushu. "Optimal control and cost-effectiveness analysis of malaria transmission dynamics: AT Haringo et al." International Journal of Dynamics and Control 13.6 (2025): 230.* https://doi.org/10.1007/s40435-025-01719-1

3. *Haringo, Andualem Tekle, Legesse Lemecha Obsu, and Feyissa Kebede Bushu. "Impact of asymptomatic infections on malaria transmission dynamics." Infectious Disease Modelling (2025).* https://doi.org/10.1016/j.idm.2025.07.012

4. *Haringo, Andualem Tekle, Legesse Lemecha Obsu, and Feyissa Kebede Bushu. "Age-structured vaccination strategies in mathematical Modeling of malaria transmission." Journal of Current Research in Parasitology & Vector-Borne Diseases (2025).* https://doi.org/10.1016/j.crpvbd.2025.100328

Journal Reviewer Certificates

1. *Certificate awarded in recognition of commitment and service to* ***Sohag Journal of Mathematics*** *as a reviewer of this international journal*

2. *Certificate awarded in recognition of commitment and service to* ***Contemporary Mathematics*** *as a reviewer of this international journal*

APPENDIX A
MATHEMATICAL PRELIMINARIES

This Appendix introduces and explains some key definitions and theorems from existing literature. Moreover, we have discussed concepts related to stability analysis and optimal control.

A.1 Dynamical system of differential equations

Dynamics primarily studies how systems evolve over time. The mathematical framework describing such processes is known as a dynamical system (Broer & Takens, 2011). Generally, a system of n first-order differential equations in the space $\mathbb{R}^n$ is referred to as a dynamical system of dimension n, which governs the temporal behavior of evolutionary processes. In this context, a deterministic process uniquely determines its future and past states based on the present state, while nondeterministic processes do not. However, processes may be semi-deterministic, meaning they are determined but not uniquely (Brandon, 1991; Layek et al., 2015). The continuous-time processes are described using differential equations, while discrete-time processes are described by difference equations (or maps). Mathematically, continuous-time dynamical systems can be described as follows:

$$\dot{x}(t) = F(t,x), \tag{1}$$

where $F(t,x)$ is a smooth function defined on a subset $\Omega \subset \mathbb{R}^n \times \mathbb{R}$, and t represents time. If $F(t,x)$ is explicitly time-independent, then the system (1) is called **autonomous**; otherwise, it is (1) is **nonautonomous**. Generally, solving equation (1) is challenging or impossible for nonlinear $F(t,x)$, except in special cases.

A.2 Existence and uniqueness theorem

The equation (1) along with the initial condition $x(t_0) = x_0 \in \Omega \subset \mathbb{R}^n$, constitutes an autonomous system initial value problem (IVP), given as follows:

$$\begin{aligned} \dot{x}(t) &= F(t,x), \\ x(t_0) &= x_0 \end{aligned} \tag{2}$$

where $x(t) \in \mathbb{R}^n$ is a time dependent variable and $F(t,x) : \mathbb{R} \to \mathbb{R}^n$ is a bounded function in a neighborhood of the point x_0. We do not consider non-autonomous equations because in epidemiological modeling the function $F(t,x)$ does not in general explicitly depend on t. Before one spends much time attempting to solve (2), it is wise to know that solutions actually exist. We may also want to know whether the solution is uniquely satisfy the equation with the given initial conditions. The basic existence and uniqueness theorem under the hypothesis that $F(t,x)$ is locally lipschitzian in x is usually referred to as the Picard-Lindelöf theorem. The following basic definitions and theorems are taken from Coddington et al. (1956); Hale (2009).

Definition A.2.1 *Suppose f is defined in a domain D of the (t,x) space. If there exists a constant $K>0$ such that for every (t,x) and (t,y) in D*

$$| f(t,x)-f(t,y) | \leq K | x-y |,$$

then f is said to satisfy a Lipschitz condition (with respect to x) in D, and this fact denoted by $f \in Lip$ in D. The constant K is called the Lipschitz constant. If, in addition $f \in C$ in D, one writes $f \in (C, Lip)$ in D.

Definition A.2.2 ***(Locally Lipschitzian function)*** *If f satisfies the Lipschitz condition and $f(t,x)$ has continuous first partial derivatives with respect to x in D, then $f(t,x)$ is locally lipschitzian in x.* Consider the region $\mathbb{R}$ defined by

$$R : | t-\tau | \leq a \qquad ||x-\xi|| \leq b$$

where (τ,ξ) is some point in the (t,x) space, and $a>0$, $b>0$. If $f \in C$ on R, then f is bounded there; let $\sup ||f|| = M$ on R, and, $\alpha = \min(a, b/M)$. Then we have the following theorem from Hale (2009).

Theorem A.2.1 *If $f(t,x)$ is continuous in $\mathbb{R}$ and locally lipschitzian with respect to x in R, then for any (t_0,x_0) in R, there exists a unique solution $x(t,t_0,x_0), x(t_0,t_0,x_0) = x_0$, of $\dot{x} = f(t,x)$ passing through (t_0,x_0).*

Definition A.2.3 *Let f be a real valued function defined on a domain D. The function f is said to be **bounded** on D if and only if there is a positive number M such that $|f(x,y)| \leq M$ for all $(x,y) \in D$.*

Definition A.2.4 ***(Positively invariant set)*** *A domain $\Omega \subseteq \mathbb{R}^n$ is said to be positively invariant for the system $\frac{dx}{dt} = f(x)$ if for all $x(t_0) \in \Omega$, then $x(t) \in \Omega$, for all $t \geq t_0$.*

A.3 Stability Analysis

By Considering the n dimensional initial value autonomous system (2). An equilibrium solution x^* (steady-state solution/fixed point or critical point) is a constant solution x following algebraic equation. The characteristic equation at x^* is given by:

$$p(\lambda) = \det(\lambda I - J(x^*)) = 0 \tag{3}$$

The stability of x^* is determined by the roots of (3).
More specifically

1. If all the roots of (3) have negative real parts, then x^* is locally asymptotically stable.
2. If at least one root of (3) has a positive real part, then x^* is unstable.

In order to derive sufficient conditions for the global stability and asymptotic stability of a rest point x^*, we apply the so called direct method of Lyapunov and Routh-Hurwitz Criteria. Routh-Hurwitz criteria provides a necessary and sufficient conditions for the existence of negative real eigen roots. In the following we state the theorem:

Theorem A.3.1 *Routh-Hurwitz Criteria (Allen, 2007). Consider the n^{th} degree polynomial with real constant coefficients given by:*

$$p(\lambda) = \lambda^n + a_1\lambda^{n-1} + a_2\lambda^{n-2} + ... + a_{n-1}\lambda + a_n = 0. \tag{4}$$

Using the coefficients $a_j, j = 1,2,...n$ of the characteristic polynomial, define n Hurwitz matrices:

$$H_1 = (a_1),\ H_2 = \begin{pmatrix} a_1 & 1 \\ a_3 & a_2 \end{pmatrix}, ..., H_n = \begin{pmatrix} a_1 & 1 & 0 & 0 & ... & 0 \\ a_3 & a_2 & a_1 & 1 & ... & 0 \\ a_5 & a_4 & a_3 & a_2 & ... & 0 \\ \vdots & \vdots & \vdots & \vdots & ... & \vdots \\ 0 & 0 & 0 & 0 & ... & a_n \end{pmatrix},$$

where $a_i = 0$ if $j > n$. All the roots of polynomial $p(\lambda)$ are negative or have negative real part iff the determinants of all Hurwitz matrices are positive:

$$det\ H_j > 0,\ j = 1,2,...,n.$$

When $n = 2$, the Routh-Hurwitz criteria simplify to $det\ H_1 = a_1 > 0$ and

$$det\ H_2 = det \begin{pmatrix} a_1 & 1 \\ 0 & a_2 \end{pmatrix} = a_1 a_2 > 0$$

or $a_1 > 0$ and $a_2 > 0$. For polynomials of degree $n = 2,3,4$ and 5, the Routh-Hurwitz citeria are summarized as follows.

$n = 2 : a_1 > 0$ and $a_2 > 0$.

$n = 3 : a_1 > 0, a_3 > 0$, and $a_1 a_2 > a_3$.

$n = 4 : a_1 > 0, a_3 > 0, a_4 > 0$, and $a_1 a_2 a_3 > a_3^2 + a_1^2 a_4$.

$n = 5 : a_i > 0; i = 1,2,3,4,5, a_1 a_2 a_3 > a_3^2 + a_1^2 a_4$, and $(a_1 a_4 - a_5)\ (a_1 a_2 a_3 - a_3^2 - a_1^2 a_4) > a_5 (a_1 a_2 a_3)^2 + a_1 a_5^2$.

Definition A.3.1 *(Allen, 2007) Let U be an open subset of $\mathbb{R}^2$ containing the origin. A real-valued $C^1(U)$ function, $V : U \to R$, $[(x,y) \in U, V(x,y) \in R]$ is said to be positive definite on the set U if the following two conditions hold.*

1. $V(0,0) = 0$
2. $V(x,y) > 0$ *for all* $(x,y) \in U$ *with* $(x,y) \neq 0$. *The function $V(x,y)$ is said to be negative definite if $-V(x,y)$ is positive definite.*

Definition A.3.2 *see (Jordan & Smith, 2007) $V(x)$ is said to be positive (negative) definite in a neighbourhood U of the origin if $V(x) > 0 (V(x) < 0)$ for all $x \neq 0$ in U , and $V(0) = 0$. $V(x)$*

is positive (negative) semi-definite in a neighbourhood U of the origin if $V(x) \geq 0 (V(x) \leq 0)$ for all $x \neq 0$ in U , and $V(0) = 0$.

Theorem A.3.2 *see (Jordan & Smith, 2007) Let $x^*(t) = 0$, $t \geq t_0$, be the zero solution of the regular system $x^{'} = x(t)$, where $x(0) = 0$. Then $x(t)$ is uniformly stable for $t \geq t\ 0$ if there exists $V(x)$ with the following properties in some neighborhood of $x = 0$:*

- *If $V(x)$ and its partial derivatives are continuous;*
- *If $V(x)$ is positive definite;*
- *If $V^{'}(x)$ is negative semi-definite.*

Theorem A.3.3 *Suppose that all the conditions of the Theorem (8.4) apply, except that condition three is replaced by negative definite. Then the zero solution is asymptotically stable (and such a function V is called a strong Lyapunov function for the system).*

Theorem A.3.4 ***(Lassalle's invariance principles)*** *Let $f(x)$ be a locally Lipschitz function defined over a domain $D \subset \mathbb{R}^n$ and $\Omega \subset D$ be a compact set that is positively invariant with respect to $\dot{x} = f(x)$. Let $V(x)$ be a continuously differentiable function defined over D such that $\dot{V}(x) \leq 0$ in Ω. Let E be the set of all points in Ω where $\dot{V}(x) = 0$, and M be the largest invariant set in E. Then every solution starting in Ω approaches M as $t \longrightarrow \infty$.*

A.4 Basic reproduction number

The basic reproduction number is defined as the number of secondary disease cases caused by introducing a single infective host into a fully susceptible population of both humans and mosquitoes. It is a positive dimensionless bifurcation parameter (Anderson & May, 1991; Brauer et al., 2008; O. Diekmann, 1996). This number measures the potential of disease spread within a population. If $\Re_0 < 1$, then on average an infected individual produces less than one new infected individual over the course of its infectious period, and the infection cannot grow. On the other hand, if $\Re_0 > 1$, then each infected individual produces, more than one new infection on average and the disease can invade the population. A lot of scholars use the words reproductive for reproduction and rate or ratio for number. Each combination can be supported by convincing arguments: $\Re_0$ can be specified as either a ratio of rates, or a number of secondary cases per index case. In the context of differential equation models (or, more generally, evolution equation models), $\Re_0$ arises through dimensional analysis as a dimensionless rate of transmission (Hethcote, 2000).

A.5 Next-Generation Matrix

The basic reproduction number $\Re_0$ is computed using the method of next-generation matrix (NGM) as presented in (Van den Driessche & Watmough, 2002). Suppose there are n disease compartments and m nondisease compartments, and let $x \in R^n$ and $y \in R^m$ be the sub-populations in each of these compartments. Further, denote by $\mathcal{F}_i$ the rate secondary infections increase the i^{th} disease compartment and by $\mathcal{V}_i$ the rate disease progression, death and recovery decrease the i^{th} compartment. The compartmental model can then be written in the following form:

$$\frac{dx}{dt} = \mathcal{F}_i(x,y) - \mathcal{V}_i(x,y) \quad , i = 1,2,...n \tag{5}$$
$$\frac{dy}{dt} = g_j(x,y), \quad j = 1,2,...n.$$

The existence of $\mathfrak{R}_0$ is established if the following conditions are satisfied:

1. $\mathcal{F}_i(0,y) = 0$ and $\mathcal{V}_i(0,y) = 0$ for all $y \geq 0$ and i = 1, ..., n (All new infections are secondary infections arising from infected host, there is no immigration of individuals into the disease compartments).

2. $\mathcal{F}_i(0,y) \geq 0$ for all non-negative x and y and i = 1, ..., n (The function F represents new infections and can not be negative).

3. $\mathcal{V}_i(0,y) \leq 0$ whenever $x_i = 0$, i = 1, ..., n (Each component, $\mathcal{V}_i$ represents a net outflow from compartment i and must be negative (inflow only) whenever the compartment is empty).

4. $\sum_{i=1}^{n} \mathcal{V}_i(x,y) \geq 0$ for all non-negative x and y (This sum represent the total outflow from all infected compartments. Terms in the model leading to increase in $\sum_{i=1}^{n} x_i$ are assumed to represent secondary infections and therefore belong in $\mathcal{F}_i$.

5. The malaria free system $\frac{dy}{dt} = g_i(0,y)$ has a unique equilibrium that is asymptotically stable. That is, all solution with initial conditions of the form $(0,y)$ approach a point $(0,y_0)$ as $t \to \infty$. This point is referred to as the malaria free equilibrium.

Now assuming that $\mathcal{F}_i$ and $\mathcal{V}_i$ meet the above conditions, we can form the next generation matrix FV^{-1} from matrices of partial derivatives of $\mathcal{F}_i$ and $\mathcal{V}_i$, with

$$F = [\frac{\partial \mathcal{F}_i(0,y_0)}{\partial x_j}]_{1 \leq i,j \leq m}$$

and

$$V = [\frac{\partial \mathcal{V}_i(0,y_0)}{\partial x_j}]_{1 \leq i,j \leq m},$$

and $(0,y_0)$ is the malaria free equilibrium. The entries of FV^{-1} give the rate at which infected individuals in x_j produce new infections in x_i, times the average length of time an individual spends in a single visit to compartment j. The basic reproduction number $\mathfrak{R}_0$ is the spectral radius (dominant eigenvalue) of the next generation matrix FV^{-1}, i.e.,

$$\mathfrak{R}_0 = \rho(FV^{-1}).$$

Remark 4. *A matrix $\rho(FV^{-1})$ is a square matrix of dimension n and λ_i, $i = 1,...n$, its eigenvalues, then the spectral radius of $\rho(FV^{-1})$ is the eigenvalue with largest value in modulus, i.e*

$$\rho(FV^{-1}) = \max_{1 \leq i \leq n} | \lambda_i | . \tag{6}$$

A.6 Sensitivity analysis

Sensitivity indices give us a way to measure the relative change in a variable that occurs when a parameter changes. If the model is easy, it might be possible to distinguish the outcome for each parameter individually. The derivatives represent the rate at which predictions vary in relation to the parameters. The normalized forward sensitivity index of a variable with respect to a parameter is the ratio of the relative change in the variable to the relative change in the parameter. When the variable is a differentiable function of the parameter, the sensitivity index may be alternatively defined using partial derivative (Chitnis et al., 2008; Edward & Nyerere, 2015). Our work use the normalized forward sensitivity index to carryout the sensitivity analysis. For instance, the normalized forward sensitivity index on $\mathfrak{R}_0$, which depends defferentially on a parameter p, is defined by

$$\gamma_p^{\mathfrak{R}_0} = \frac{\partial \mathfrak{R}_0}{\partial p} \times \frac{p}{\mathfrak{R}_0}.$$

A.7 Bifurcation

A bifurcation of a dynamical system occurs when the parameter value of a system changes such that it causes a sudden qualitative change in its behaviour. Bifurcations occur in both continuous systems and discrete systems providing insight into how small alterations can lead to significant shifts in system behavior (McCann, 2013). In recent years, the bifurcation theorem developed by Castillo-Chavez and Song has emerged as a valuable tool for assessing the direction of bifurcations, particularly at the equilibrium point where the basic reproduction number $\mathfrak{R}_0 = 1$. This theorem facilitates a deeper understanding of how changes in parameters can influence the stability and dynamics of epidemiological models and other complex dynamical systems. For the most part, in epidemic models, there are two distinct bifurcations at $\mathfrak{R}_0 = 1$ forward (supercritical) and backward (sub-critical) (Castillo-Chavez & Song, 2004). A forward bifurcation happens when $\mathfrak{R}_0$ crosses unity from below; a positive asymptotically stable equilibrium appears and the malaria-free equilibrium losses its stability. On the other hand, a backward bifurcation happens when $\mathfrak{R}_0$ is less than unity; a small positive unstable equilibrium appears while the malaria-free equilibrium and a larger positive equilibrium are locally asymptotically stable. Epidemiologically, a backward bifurcation "says" that it is not enough to only reduce the basic reproductive number to less than one to eliminate a disease and that when $\mathfrak{R}_0$ crosses unity, hysteresis takes place.

A.8 Castillo-Chavez and Song bifurcation theorem

Theorem A.8.1 *Consider the following general system of ODEs with a parameter* ϕ*:*

$$\frac{dx}{dt} = f(x,\phi), \quad f : \mathbb{R}^n \times \mathbb{R} \longrightarrow \mathbb{R}^n, \quad f \in C^2(\mathbb{R}^n \times \mathbb{R}), \tag{7}$$

where 0 *is an equilibrium point of the system, that is,* $f(0,\phi) \equiv 0$ *for all* ϕ*. Assume the following:*

A1. $A = D_x f(0,0) = \left(\frac{\partial f_i}{\partial x_j}(0,0)\right)$ *is the linearization matrix of system (7) around the equilibrium* 0 *with* ϕ *evaluated at* 0*. Zero is a simple eigenvalue of A , and other eigenvalues have negative real parts.*

A2. *The matrix A has a non-negative right eigenvector w and a left eigenvector v each corresponding to the zero eigenvalue.*

Let f_k *be the* k^{th} *component of f and*

$$a = \sum_{k,i,j=1}^{n} v_k w_i w_j \frac{\partial^2 f_k}{\partial x_i \partial x_j}(0,0)$$

$$b = \sum_{k,i=1}^{n} v_k w_i \frac{\partial^2 f_k}{\partial x_i \partial \phi}(0,0).$$

The local dynamics of the system around 0 *are completely determined by the signs of a and b:*

i. $a > 0$, $b > 0$. *When* $\phi < 0$ *with* $|\phi| \ll 1$, 0 *is locally asymptotically stable, and there exists a positive unstable equilibrium; when* $0 < \phi \ll 1$, 0 *is unstable, and there exists a negative and locally asymptotically stable equilibrium.*

ii. $a < 0$, $b < 0$. *When* $\phi < 0$ *with* $|\phi| \ll 1$, 0 *is unstable; when* $0 < \phi \ll 1$, 0 *is locally asymptotically stable, and there exists a positive unstable equilibrium;*

iii. $a > 0$, $b < 0$. *When* $\phi < 0$ *with* $|\phi| \ll 1$, 0 *is unstable, and there exists a locally asymptotically stable negative equilibrium; when* $0 < \phi \ll 1$, 0 *is stable, and a positive unstable equilibrium appears;*

iv. $a < 0$, $b > 0$. *When* ϕ *changes from negative to positive,* 0 *changes its stability from stable to unstable. Correspondingly, a negative unstable equilibrium becomes positive and locally asymptotically stable.*

Particularly, if $a > 0$ *and* $b > 0$*, then a backward bifurcation occurs at* $\phi = 0$.

A.9 General optimal control method

Optimal control theory has been used as a very powerful mathematical tool to make decisions involving complex biological situations and it has been derived from the calculus of variations. Optimal control techniques are of great use in developing optimal strategies to control various kinds of diseases. For instance in the book of (Lenhart & Workman, 2007) it has been applied that finding the percentage of the population that should be vaccinated as time evolves in a given epidemic model to minimize the number of infected and the cost of implementing the vaccination strategy.
The behavior of a dynamic system is described by the state variable(s). We assume that there is a way to control the state variable(s) x, by acting upon it with a suitable control. We noticed that the dynamic system (state x) depends on the control u. The goal is to adjust the control u

in order to minimize or maximize a given objective functional, $J(u(t),x(t),t)$, that attains the desired goal, and the required costs to achieving it.
The optimal control is obtained when the desired goal is achieved with the least cost. The functional depends on the control and the state variables. There are a number of different methods for calculating the optimal control for a specific model. Pontryagin Maximum Principle for example allows the calculation of the optimal control for an ODEs model system with given constraints. For details See the books of Lenhart & Workman (2007); Pontryagin (1987). The principal technique for the optimal control problem is to solve a set of necessary conditions, that an optimal control and corresponding state must satisfy. It is important to understand the logical difference between necessary conditions and the sufficient conditions of solution sets.

A.10 Pontryagin's Maximum Principle

The Pontryagin's Maximum Principle converts the maximization or minimization of the objective functional J, coupled with the state variable into pointwise maximizing or minimizing of the Hamiltonian with respect to the control. The Hamiltonian $H(t,x,u,\lambda)$ is a function of four variables. Time t is the underlying variable for each of x,u and λ is a function of t, called the adjoint variable.
Let us considering the optimal control problem of the form:

$$J(x,u) = \min_{u}\left\{\int_0^T f(t,x(t),u(t))\right\} \tag{8}$$

where $x(t) \in R^n$ is state vector and $u \in R^m$ is the control vector. The state and the control variables are governed by the dynamics described by a set of first order differential equations:

$$x'(t) = f(t,x(t),u(t)), x(0) = x_0, \quad 0 \le t \le T \tag{9}$$

Theorem A.10.1 Lenhart & Workman (2007) If $u^*(t)$ and $x^*(t)$ are optimal for problem 8, then there exists a piecewise differential adjoint variable $\lambda(t)$ such that the following conditions hold for all t in the interval $[t_0,t(T)]$:

1. The optimality condition:
$$\frac{\partial H(t,x^*(t),u(t),\lambda(t))}{\partial u} = 0$$
2. The control system:
$$x'(t) = \frac{\partial H(t,x^*(t),u(t),\lambda(t))}{\partial \lambda} \tag{10}$$
3. Adjoint system
$$\lambda'(t) = -\frac{\partial H(t,x^*(t),u(t),\lambda(t))}{\partial x(t)}$$
where the Hamiltonian H is defined by: $H = f(t,x(t),u(t)) + \lambda(t)g(t,x(t),u(t))$
4. The universality condition $\lambda(T) = 0$

APPENDIX B
PYTHON CODES AND ALGORITHM

```
# L-BFGS-B Parameter Estimation Algorithm
# 1. Initialize
theta = theta0    # initial guess
bounds=[(theta_min[i], theta_max[i]) for i in range(n_params)]
t_obs = [...]  # observation times
Y_obs = [...]  # observed data (e.g., infected cases)

def loss(theta):
# a. Solve ODE: dX/dt = f(X, theta, t)
sol = solve_ivp(lambda t, X: f(t, X, theta), [t0, T], X0,
   t_eval=t_obs)
X_model = sol.y.T  # model states at t_obs

# b. Extract observable (e.g., I_h)
Y_model = H(X_model)  # H selects observed compartments

# c. Compute least-squares loss
return np.sum((Y_obs - Y_model)**2)

# 2. Optimize with L-BFGS-B
result = scipy.optimize.minimize(
loss,
theta,
method='L-BFGS-B',
bounds=bounds,
options={'disp': True}
)

# 3. Output
theta_opt = result.x
```

Listing 1: Python pseudocode for L-BFGS-B parameter estimation of ODE models

GEKKO ALGORITHM

```
START: Continuous OCP
|
v
[Discretize Time]
|
v
[Collocation: ODE -> Algebraic]
```

```
 |
 v
 [Add Constraints]{initial and boundary conditions}
 |
 v
 [Discretize Objective]
 |
 v
 [Form NLP: min J(z) s.t. c(z)=0]
 |
 v
 [Solve by NLP solver]
 |
 v
 [Recover Solution]
 |
 v
 [Error acceptable?] -> No -> [Refine mesh] -> Return to
    discretization
 |Yes
 v
 [Output Results]
```

Below are Python scripts for simulating a system of ODEs representing malaria transmission models

```
import numpy as np
import matplotlib.pyplot as plt
from scipy.integrate import odeint
#Parameters
b,kappa,d,beta1,beta2,beta3,epi=
   0.6,0.001,0.0005,0.019,0.02,0.25,0.005
muh,Caphih,rho,delta,eta,varphi
   =0.002,100,0.07,0.001,0,025,0.0006
Caphiv, gamma,muv,xi,vartheta=10000,0.9,0.05,0.03,0.01,0.016
#Initial epidemiological data
sa0_val = 8000
su0_val = 2000
ih0_val = 10
th0_val = 10
rh0_val = 0
sv0_val=10000
iv0_val=[10, 100, 200,300]
m0_val=3
#Defining functions
def odesystem(solution,t):
```

```
sa,su,ih,th,rh,sv,iv,m=solution
Nh=sa+su+ih+th+rh
dsadt=b*Caphih+kappa*su*m-(d*sa)/(1+m)-(beta1*sa*iv)/Nh+epi*rh-
   muh*sa
dsudt=(1-b)*Caphih-kappa*su*m+(d*sa)/(1+m)-(beta2*su*iv)/Nh-muh
   *su
dihdt=(beta1*sa*iv)/(sa+su+ih+th+rh)+(beta2*su*iv)/Nh-(rho+
   delta+muh)*ih
dthdt=rho*ih-(eta+varphi+muh)*th
drhdt=eta*th-(epi+muh)*rh
dsvdt=Caphiv-(beta3*sv*ih)/Nh-(gamma*sv+muv)*sv
divdt=(beta3*sv*ih)/Nh-(gamma*sv+muv)*iv
dmdt=phi+xi*ih-vartheta*m
return [dsadt,dsudt,dihdt,dthdt,drhdt,dsvdt,divdt,dmdt]
t=np.linspace(0,20,2001)
for iv0 in iv0_val:
initial_state=[sa0_val,su0_val,ih0_val,th0_val,rh0_val,sv0_val,
   iv0,m0_val]
solution=odeint(odesystem,initial_state,t)
#plt.plot(t,solution[:,5])
plt.plot(t,solution[:,6], label=f'$I_m(0)$={iv0}')
plt.savefig('DFEIV2.eps', format='eps', dpi=1200)
plt.ylabel('Infected mosquitoes')
plt.xlabel('Time in days')
plt.ylim(0,300)
plt.xlim(0,20)
plt.legend()
plt.show()
```

Listing 2: Python scripts for a malaria transmission model with media awareness and treatment interventions.

```
import numpy as np
import matplotlib.pyplot as plt
from scipy.integrate import odeint
from gekko import GEKKO
m = GEKKO(remote=False)
#Parameters
Caphih,ephib,kappa,d,beta1,beta2,beta3
   =15,0.1,0.07,0.6,0.02,0.124,0.129,0.189
muh,rho,delta,eta,varphi,Caphiv = 1/67.8,0.06,
   0.024,0.083,0.006,350
gamma,muv,phi,xi,p,a,vartheta
   =0.02,1/21,0.001,0.00003,0.25,0.25,0.016
#Time discritization
t=np.linspace(0,50,101)
```

```
#weight parameter values
A1,A2=1,1
K1,K2,K3=1,1,1
p = np.zeros(nt)
p[-1] = 1.0
final = m.Param(value=p)
# Initial values
sa=m.Var(value=8000)
su=m.Var(value=2000)
ih=m.Var(value=100)
th=m.Var(value=10)
rh=m.Var(value=0)
sv=m.Var(value=10000)
iv=m.Var(value=10)
ma=m.Var(value=3)
Nh=sa+su+ih+th+rh
u1=m.MV(value=0,ub=0.1,lb=0)
u2=m.MV(value=0.35,ub=0.35,lb=0)
u3=m.MV(value=0.1,ub=0.1,lb=0)
u=[u1, u2, u3]
#state variables
m.Equation(sa.dt()==b*Caphih+kappa*su*ma-(d*sa)/(1+ma)-(1-u1)*(
   beta1*sa*iv)/Nh+epi*rh-muh*sa)
m.Equation(su.dt()==(1-b)*Caphih-kappa*su*ma+(d*sa)/(1+ma)-(1-
   u1)*(beta2*su*iv)/Nh-muh*su)
m.Equation(ih.dt()==(1-u1)*(beta1*sa*iv)/Nh+(1-u1)*(beta2*su*iv
   )/Nh-(a*u2+rho+delta+muh)*ih)
m.Equation(th.dt()==(a*u2+rho)*ih-(eta+varphi+muh)*th)
m.Equation(rh.dt()==eta*th-(epi+muh)*rh)
m.Equation(sv.dt()==Caphiv-(1-u1)*(beta3*sv*ih)/Nh-(p*u3+gamma+
   muv)*sv)
m.Equation(iv.dt()==(1-u1)*(beta3*sv*ih)/Nh-(p*u3+gamma+muv)*iv
   )
m.Equation(ma.dt()==phi+xi*ih-vartheta*ma)
m.options.IMODE=6
u1.STATUS = 1
u1.DCOST=0.001
u2.STATUS = 1
u2.DCOST=0.001
u3.STATUS = 1
u3.DCOST=0.001
m.options.SOLVER = 3
m.options.TIME_SHIFT = 0
sa.value,su.value,ih.value = sa.value.value,su.value.value,ih.
   value.value
```

```
th.value,rh.value,sv.value = th.value.value, rh.value.value,sv.
   value.value
iv.value,ma.value = iv.value.value,ma.value.value
obj=m.Intermediate(m.integral(A1*ih+A2*(sv+iv)+K1*(u1**2)/2+K2
   *(u2**2)/2+K3*(u3**2)/2))
m.Minimize(obj*final)
m.solve(disp=False)
plt.figure(figsize=(8, 6))
plt.plot(t,solution[:,2],lw=2.5, color='red',label='$u_{1}=u_
   {2}=u_{3}=0$')
plt.plot(t,ih.value,lw=2.5,color='blue', label='$u_{1}\\neq 0,
   u_{2}\\neq 0,u_{3}\\neq 0$')
plt.legend()
plt.ylabel('Infected humans')
plt.xlabel('Time (days)')
plt.show()

PYTHON CODE FOR PARAMETER ESTIMATION
import numpy as np
from scipy.integrate import odeint
from scipy.optimize import minimize
import matplotlib.pyplot as plt
# Define the system of differential equations
Pi_c, delta_a, delta_c = 1000*365/68.7, 0.08, 0.08
mu_h, eta_c, eta_a = 0.015, 0.17, 0.17
gamma_m, mu_m, Pi_m, varphi_c, varphi_a = 0.062, 1/21, 17381,
   0.006, 0.006
def model(y, t, params):
Sc, Vc, Ic, Tc, Rc, Sa, Ia, Ta, Ra, Sm, Im = y
h, b1, b2, b3, b4, epsilon_c, epsilon_a, theta_c, rho_c, rho_a,
    nu_c = params
Nh = Sc + Vc + Ic + Tc + Rc + Sa + Ia + Ta + Ra
lambda_c = b1 * Im / Nh
lambda_a = b1 * Im / Nh
lambda_m = b3 * Ic / Nh + b4 * Ia / Nh
# Define the equations
dSc_dt = Pi_c + epsilon_c * Rc + h * Vc - (lambda_c + nu_c +
   theta_c + mu_h) * Sc
dVc_dt = nu_c * Sc - (h + mu_h) * Vc
dIc_dt = lambda_c * Sc - (rho_c + delta_c + mu_h) * Ic
dTc_dt = rho_c * Ic - (eta_c + varphi_c + mu_h) * Tc
dRc_dt = eta_c * Tc - (epsilon_c + mu_h) * Rc
dSa_dt = theta_c * Sc + epsilon_a * Ra - (lambda_a + mu_h) * Sa
dIa_dt = lambda_a * Sa - (rho_a + delta_a + mu_h) * Ia
dTa_dt = rho_a * Ia - (eta_a + varphi_a + mu_h) * Ta
```

```
dRa_dt = eta_a * Ta - (epsilon_a + mu_h) * Ra
dSm_dt = Pi_m - lambda_m * Sm - (gamma_m + mu_m) * Sm
dIm_dt = lambda_m * Sm - (gamma_m + mu_m) * Im

return [dSc_dt, dVc_dt, dIc_dt, dTc_dt, dRc_dt, dSa_dt, dIa_dt,
    dTa_dt, dRa_dt, dSm_dt, dIm_dt]

# Define the objective function for parameter estimation
def objective(params):
# Initial conditions
y0 = [120, 0, 0, 0, 0, 557.3, 322.7, 0, 0, 800, 200]
# Time points
t = np.linspace(2000, 2022, len(I_data))
# Solve the ODE
solution = odeint(model, y0, t, args=(params,))
# Extract Ic and Ia values
Ic_predicted = solution[:, 2]
Ia_predicted = solution[:, 6]
# Calculate the sum of squared errors
error = np.sum((Ic_predicted + Ia_predicted - I_data) ** 2)
return error

# Observed data for I_c + I_a
I_data = np.array([322.7, 292.1, 259.36, 212.4, 176.716,
167.654, 154.2, 131.35, 111.35, 149.343,
171.8072, 176.268, 204.059, 235.024, 214.992,
182.25, 123.96, 90.16, 36.96, 34.087,
53.05, 46.26, 60.86])

# Initial guess for parameters
initial_params = [0.003, 0.2, 0.03, 0.003, 0.06, 0.0099, 0.01,
   0.01, 0.01, 0.0075, 0.0055]
bounds = [(0.00027,0.0033),(0,0.21),(0,0.05),(0,0.07)
   ,(0.0022,0.01),(0.0033,0.07),\
(0.0012,0.01),(0.0028,0.02),(0.0,0.27),(0.0,0.23),(0.0,0.06)]
# Perform the optimization
result = minimize(objective, initial_params, method='L-BFGS-B',
    bounds=bounds)

# Estimated parameters
estimated_params = result.x
print("Estimated parameters:", estimated_params)
# Time points for observed data
t_observed = np.linspace(2000, 2022, len(I_data))
# Get predicted values for observed time range
```

```
y0 = [120, 0, 0, 0, 0, 557.3, 322.7, 0, 0, 800, 200]
solution_observed = odeint(model, y0, t_observed, args=(
    estimated_params,))
# Extract predicted Ic and Ia
Ic_predicted_observed = solution_observed[:, 2]
Ia_predicted_observed = solution_observed[:, 6]
# Calculate total predicted infections for observed time range
total_predicted_observed = Ic_predicted_observed +
    Ia_predicted_observed
# Extend time to 2050 for future predictions
t_extended = np.linspace(2000, 2050, 51)  # 51 points from 2000
    to 2050
solution_extended = odeint(model, y0, t_extended, args=(
    estimated_params,))
# Extract predicted Ic and Ia for the extended time range
Ic_predicted_extended = solution_extended[:, 2]
Ia_predicted_extended = solution_extended[:, 6]
# Calculate total predicted infections for extended time range
total_predicted_extended = Ic_predicted_extended +
    Ia_predicted_extended
# Plot the results
plt.figure(figsize=(12, 5))
# Main plot
plt.subplot(1, 2, 1)  # Two rows, one column, first subplot
plt.plot(t_observed, I_data, 'ro', linewidth=2, label='Data
    $I_c + I_a$')
plt.plot(t_extended, total_predicted_extended,'b-',linewidth=2,
    label='Fitted $I_c + I_a$')
plt.xlabel('Time in years')
plt.ylabel('Total malaria incidence')
#plt.title('Infection Dynamics')
plt.legend()
plt.grid(True)
# Residual plot
plt.subplot(1, 2, 2)  # Second subplot
residuals = I_data - total_predicted_observed
plt.plot(t_observed, residuals, 'o-',linewidth=2,  color='blue'
    )
plt.axhline(0, color='black', linewidth=2, linestyle='--')
plt.xlabel('Time in years')
plt.ylabel('Residuals')
plt.tight_layout()
plt.show()
```

Listing 3: Python scripts for optimal control model

BIBLIOGRAPHY

Abioye, A. I., Ibrahim, M. O., Peter, O. J., & Ogunseye, H. A. (2020). Optimal control on a mathematical model of malaria. *Sci. Bull., Series A: Appl Math Phy*, *82*(3), 177–190.

Abubakar, S. F., & Ibrahim, M. (2022). Optimal control analysis of treatment strategies of the dynamics of cholera. *Journal of Optimization*, *2022*(1), 2314104.

Adamu, I. I., Usman, S., et al. (2018). Mathematical model for the dynamics of neisseria gonorrhea disease with natural immunity and treatment effects. *Journal of Mathematics Research*, *10*(2), 2018.

Adepoju, P. (2024). Q&a: Malaria fight needs whole-of-society approach. *SciDev. net-Health*.

Adugna, F., Wale, M., & Nibret, E. (2022). Prevalence of malaria and its risk factors in lake tana and surrounding areas, northwest ethiopia. *Malaria Journal*, *21*(1), 313.

Agaba, B. B., Rugera, S. P., Mpirirwe, R., Atekat, M., Okubal, S., Masereka, K., ... others (2022). Asymptomatic malaria infection, associated factors and accuracy of diagnostic tests in a historically high transmission setting in northern uganda. *Malaria Journal*, *21*(1), 392.

Aguilar, J. B., & Gutierrez, J. B. (2020). An epidemiological model of malaria accounting for asymptomatic carriers. *Bulletin of mathematical biology*, *82*(3), 42.

Agusto, F. B., Del Valle, S. Y., Blayneh, K. W., Ngonghala, C. N., Goncalves, M. J., Li, N., ... Gong, H. (2013). The impact of bed-net use on malaria prevalence. *Journal of theoretical biology*, *320*, 58–65.

Aldila, D., & Angelina, M. (2021). Optimal control problem and backward bifurcation on malaria transmission with vector bias. *Heliyon*, *7*(4).

Aldila, D., Shahzad, M., Khoshnaw, S. H., Ali, M., Sultan, F., Islamilova, A., ... Samiadji, B. M. (2022). Optimal control problem arising from covid-19 transmission model with rapid-test. *Results in Physics*, *37*, 105501.

Alghamdi, J. M., Al-Qahtani, A. A., Alhamlan, F. S., & Al-Qahtani, A. A. (2024). Recent advances in the treatment of malaria. *Pharmaceutics*, *16*(11), 1416.

Allen, L. (2007). An introduction to mathematical biology pearson prentice hall. *Upper Saddle River, New Jersey.[Google Scholar]*.

Alliance, A. L. M. (2024). *2024 africa malaria progress report.* Retrieved from https://alma2030.org/heads-of-state-and-government/african-union-malaria-progress-reports/2024-africa-malaria-progress-report/ (Accessed: 2024-06-15)

Alrabaiah, H., Safi, M. A., DarAssi, M. H., Al-Hdaibat, B., Ullah, S., Khan, M. A., & Shah, S. A. A. (2020). Optimal control analysis of hepatitis b virus with treatment and vaccination. *Results in Physics*, *19*, 103599.

Anderson, R. M., & May, R. M. (1991). *Infectious diseases of humans: dynamics and control*. Oxford university press.

Ankomah, A., Adebayo, S., Arogundade, E., Anyanti, J., Nwokolo, E., Inyang, U., ... Meremiku, M. (2014). The effect of mass media campaign on the use of insecticide-treated bed nets among pregnant women in nigeria. *Malaria research and treatment*, *2014*(1), 694863.

Arrow, K., Panosian, C., & Gelband, H. (2004). *Committee on the economics of antimalarial drugs.* National Academies Press (US).

Asante, K. P., Mathanga, D. P., Milligan, P., Akech, S., Oduro, A., Mwapasa, V., ... others (2024). Feasibility, safety, and impact of the rts, s/as01e malaria vaccine when implemented through national immunisation programmes: evaluation of cluster-randomised introduction of the vaccine in ghana, kenya, and malawi. *The Lancet*, *403*(10437), 1660–1670.

Ayobami, S. L. (2020). *Mathematical modelling of spread and control of the hepatitis c virus*. Unpublished master's thesis, Indiana University of Pennsylvania.

Bacaër. (2011a). Daniel bernoulli, d'alembert and the inoculation of smallpox (1760). *A short history of mathematical population dynamics*, 21–30.

Bacaër. (2011b). Ross and malaria (1911). In *A short history of mathematical population dynamics* (pp. 65–69). Springer.

Badmos, A., Alaran, A., Adebisi, Y., Bouaddi, O., Onibon, Z., Dada, A., et al. (2021). *What sub-saharan african countries can learn from malaria elimination in china* (Vol. 49) (No. 1). ([Internet]. 2021 Dec 24)

Bailey, N. T. (1975). *The mathematical theory of infectious diseases and its applications.*

Bakare, E., & Hoskova-Mayerova, S. (2023). Numerical treatment of optimal control theory applied to malaria transmission dynamic model. *Quality & Quantity*, *57*(Suppl 3), 409–431.

Balcha, F., Menna, T., & Lombamo, F. (2023). Prevalence of asymptomatic malaria and associated factors among pregnant women at boset district in east shoa zone, oromia region, ethiopia: a cross-sectional study. *Malaria Journal*, *22*(1), 28.

Bamou, R., Tchuinkam, T., Kopya, E., Awono-Ambene, P., Njiokou, F., Mwangangi, J., & Antonio-Nkondjio, C. (2022). Knowledge, attitudes, and practices regarding malaria control among communities living in the south cameroon forest region. *IJID regions*, *5*, 169–176.

Banasiak, J., Ouifki, R., & Tchoumi, S. (2023). The impact of demography in a model of malaria with transmission blocking drugs. *Authorea Preprints*.

Basir, & Abraha, T. (2023). Mathematical modelling and optimal control of malaria using awareness-based interventions. *Mathematics*, *11*(7), 1687.

Basir, Banerjee, A., & Ray, S. (2021). Exploring the effects of awareness and time delay in controlling malaria disease propagation. *International Journal of Nonlinear Sciences and Numerical Simulation*, *22*(6), 665–683.

Basir, Blyuss, K. B., & Ray, S. (2018). Modelling the effects of awareness-based interventions to control the mosaic disease of jatropha curcas. *Ecological complexity*, *36*, 92–100.

Bassinga, H., Ouedraogo, M., Cisse, K., Yira, P., Ouedraogo, S. C., Nombré, A., ... Rouamba, T. (2024). Prevalence of asymptomatic malaria at the communal level in burkina faso: an application of the small area estimation approach. *Population Health Metrics*, *22*(1), 21.

Basu, S., & Sahi, P. K. (2017). Malaria: an update. *The Indian Journal of Pediatrics*, *84*, 521–528.

Batu, T. D., & Obsu, L. L. (2025). Co-dynamics of covid-19, hiv and tb with information-dependent vaccination behavior and waning immunity. *Scientific African*, *28*, e02680.

Bauch, J. A., Gu, J. J., Msellem, M., Mårtensson, A., Ali, A. S., Gosling, R., & Baltzell, K. A. (2013). Perception of malaria risk in a setting of reduced malaria transmission: a qualitative study in zanzibar. *Malaria journal*, *12*(1), 75.

Beal, L. D., Hill, D. C., Martin, R. A., & Hedengren, J. D. (2018). Gekko optimization suite. *Processes*, *6*(8), 106.

Becker, N. (1979). The uses of epidemic models. *Biometrics*, 295–305.

Berhe, H. W., Makinde, O. D., & Theuri, D. M. (2018). Optimal control and cost-effectiveness analysis for dysentery epidemic model. *Applied Mathematics & Information Sciences*, *12*(6), 1183–1195.

Bernoulli, D., & Chapelle, D. (2023). Essai d'une nouvelle analyse de la mortalité causée par la petite vérole, et des avantages de l'inoculation pour la prévenir.

Bonds, J., Sawadogo, S., Niang, A., Diabete, A., & Latham, M. (2018). Characterization of targeted swarm spraying with refillable aerosol cans compared to broadcast space-spray applications via a backpack sprayer.

Bonyah, E., Badu, K., & Asiedu-Addo, S. K. (2016). Optimal control application to an ebola model. *Asian Pacific Journal of Tropical Biomedicine*, *6*(4), 283–289.

Bozkurt, F., & Peker, F. (2014). Mathematical modelling of hiv epidemic and stability analysis. *Advances in Difference Equations*, *2014*(1), 95.

Brandon, J. (1991). Introduction to applied nonlinear dynamical systems and chaos, by s wiggins. pp 672. dm98. 00. 1990. isbn 3-540-9703-7 (springer). *The Mathematical Gazette*, *75*(472), 255–255.

Brauer, F., Castillo-Chavez, C., & Castillo-Chavez, C. (2012). *Mathematical models in population biology and epidemiology* (Vol. 2) (No. 10). Springer.

Brauer, F., Van den Driessche, P., Wu, J., & Allen, L. J. (2008). *Mathematical epidemiology* (Vol. 1945). Springer.

Broer, H. W., & Takens, F. (2011). *Dynamical systems and chaos* (Vol. 172). Springer.

Burnet, M., & White, D. O. (1972). *Natural history of infectious disease*. Cambridge University Press.

Cai, L., Li, X., Tuncer, N., Martcheva, M., & Lashari, A. A. (2017). Optimal control of a malaria model with asymptomatic class and superinfection. *Mathematical biosciences*, *288*, 94–108.

Cassels, S., Clark, S. J., & Morris, M. (2008). Mathematical models for hiv transmission dynamics: tools for social and behavioral science research. *JAIDS Journal of Acquired Immune Deficiency Syndromes*, *47*, S34–S39.

Castillo-Chavez, C., & Song, B. (2004). Dynamical models of tuberculosis and their applications. *Mathematical Biosciences & Engineering*, *1*(2), 361–404.

CDC. (2024a, June). *Clinical guidance: Malaria diagnosis & treatment in the u.s.* Retrieved from https://www.cdc.gov/malaria/hcp/clinical-guidance/index.html

CDC. (2024b). *Insecticide-treated nets.* https://www.cdc.gov/malaria/php/public-health-strategy/insecticide-treated-nets.html?CDC_AAref_Val=https://www.cdc.gov/malaria/malaria_worldwide/reduction/itn.html. (Accessed: 2024-04-02)

CDC. (2024). *Malaria surveillance, united states 2019 – 2020.* Retrieved from https://www.cdc.gov/malaria/php/surveillance-report/index.html (Accessed: 2025-06-16)

Celebi, M. E., Celiker, F., & Kingravi, H. A. (2011). On euclidean norm approximations. *Pattern Recognition*, *44*(2), 278–283.

Chambers, M. (1965). The mathematical theory of optimal processes. *Journal of the Operational Research Society*, *16*(4), 493–494.

Cheneke, K. R. (2023). Optimal control and bifurcation analysis of hiv model. *Computational and Mathematical Methods in Medicine*, *2023*(1), 4754426.

Cherkos, T., Derso, A., Lemma, W., Abere, A., Deress, T., Tegegne, B., ... Tegegne, Y. (2024). Microscopic prevalence and risk factors of asymptomatic malaria in gorgora, western dembia, northwest ethiopia: exploring hidden threats during minor transmission season. *Malaria Journal*, *23*(1), 375.

Chitnis, N., Hyman, J. M., & Cushing, J. M. (2008). Determining important parameters in the spread of malaria through the sensitivity analysis of a mathematical model. *Bulletin of mathematical biology*, *70*, 1272–1296.

Coddington, E. A., Levinson, N., & Teichmann, T. (1956). *Theory of ordinary differential equations.* American Institute of Physics.

Collins, O., & Duffy, K. (2022). A mathematical model for the dynamics and control of malaria in nigeria. *Infectious disease modelling*, *7*(4), 728–741.

Consortium, M. (2007). *Malaria and poverty.* Retrieved from https://www.malariaconsortium.org/userfiles/file/Past%20events/factsheet2%20-%20malaria%20and%20poverty.pdf (Accessed: 2025-08-26)

David, J. F., Iyaniwura, S. A., Ward, M. J., & Brauer, F. (2020). A novel approach to modelling the spatial spread of airborne diseases: an epidemic model with indirect transmission. *Mathematical Biosciences and Engineering*, *17*(4), 3294–3328.

Diekmann, Heesterbeek, J. A. P., & Metz, J. A. J. (1990). On the definition and the computation of the basic reproduction ratio r 0 in models for infectious diseases in heterogeneous populations. *Journal of mathematical biology*, *28*, 365–382.

Diekmann, O. (1996). Mathematical epidemiology of infectious diseases.

Diekmann, O., & Heesterbeek, J. A. P. (2000). *Mathematical epidemiology of infectious diseases: model building, analysis and interpretation* (Vol. 5). John Wiley & Sons.

Ducrot, A., Sirima, S., Some, B., & Zongo, P. (2009). A mathematical model for malaria involving differential susceptibility, exposedness and infectivity of human host. *Journal of biological dynamics*, *3*(6), 574–598.

Edward, S., & Nyerere, N. (2015). A mathematical model for the dynamics of cholera with control measures. *Applied and computational Mathematics*, *4*(2), 53–63.

Edwards, A. J., Benson, L., Guo, Z., López-García, M., Noakes, C. J., Peckham, D., & King, M.-F. (2023). A mathematical model for assessing transient airborne infection risks in a multi-zone hospital ward. *Building and Environment*, *238*, 110344.

Egwu, C. O., Aloke, C., Chukwu, J., Nwankwo, J. C., Irem, C., Nwagu, K. E., ... others (2023). Assessment of the antimalarial treatment failure in ebonyi state, southeast nigeria. *Journal of Xenobiotics*, *13*(1), 16–26.

Elzubier, A. G., Ansari, E. H. H., El Nour, M. H., & Bella, H. (1997). Knowledge and misconceptions about malaria among secondary school students and teachers in kassala, eastern sudan. *Journal of the Royal Society of Health*, *117*(6), 381–385.

Engida, H. A., Gathungu, D. K., Ferede, M. M., Belay, M. A., Kawe, P. C., & Mataru, B. (2024). Optimal control and cost-effectiveness analysis for the human melioidosis model. *Heliyon*, *10*(4).

Ermert, V. (2010). *Risk assessment with regard to the occurrence of malaria in africa under the influence of observed and projected climate change*. Unpublished doctoral dissertation, Universität zu Köln.

Feachem, R. (2014). Malaria 2050: from science to strategy; from evidence to eradication. *Malaria Journal*, *13*(Suppl 1), O9.

Febiriana, I. H., Hassan, A. H., & Aldila, D. (2024). Enhancing malaria control strategy: Optimal control and cost-effectiveness analysis on the impact of vector bias on the efficacy of mosquito repellent and hospitalization. *Journal of Applied Mathematics*, *2024*(1), 9943698.

Feeney, M. E. (2020). The immune response to malaria in utero. *Immunological reviews*, *293*(1), 216–229.

Fillinger, U., & Lindsay, S. W. (2011). Larval source management for malaria control in africa: myths and reality. *Malaria journal*, *10*(1), 353.

Fleming, W. H., & Rishel, R. W. (2012). *Deterministic and stochastic optimal control* (Vol. 1). Springer Science & Business Media.

Foppa, I. (2017). Bernoulli: A pioneer of epidemiologic modeling (1760). *A Historical Introduction to Mathematical Modeling of Infectious Diseases*, 1–20.

Forouzannia, F., & Gumel, A. B. (2014). Mathematical analysis of an age-structured model for malaria transmission dynamics. *Mathematical biosciences*, *247*, 80–94.

Gardner, I. D. (1980). The effect of aging on susceptibility to infection. *Reviews of infectious diseases*, 801–810.

Gavi, t. V. A. (2023, April). *Malaria vaccine market shaping roadmap*. Retrieved from https://www.gavi.org/sites/default/files/white-paper/WPaper_malaria-roadmap.pdf (Accessed: 2025-06-06)

Glèlè Kakaï, R., & Djomatin, L. C. (2025). An age-structured mathematical model to assess the combined effects of vaccine and non-vaccine interventions on malaria transmission and burden. *Available at SSRN 5254469*.

Gupta, S., Snow, R. W., Donnelly, C. A., Marsh, K., & Newbold, C. (1999). Immunity to non-cerebral severe malaria is acquired after one or two infections. *Nature medicine*, *5*(3), 340–343.

Haile, G. T., Koya, P. R., & Mosisa Legesse, F. (2025). Sensitivity analysis of a mathematical model for malaria transmission accounting for infected ignorant humans and relapse dynamics. *Frontiers in Applied Mathematics and Statistics*, *10*, 1487291.

Hale, J. K. (2009). *Ordinary differential equations*. Courier Corporation.

Heesterbeek, J., & Dietz, K. (1996). The concept of ro in epidemic theory. *Statistica neerlandica*, *50*(1), 89–110.

Heffernan, J. M., Smith, R. J., & Wahl, L. M. (2005). Perspectives on the basic reproductive ratio. *Journal of the Royal Society Interface*, *2*(4), 281–293.

Hemingway, J., Ranson, H., Magill, A., Kolaczinski, J., Fornadel, C., Gimnig, J., ... others (2016). Averting a malaria disaster: will insecticide resistance derail malaria control? *The Lancet*, *387*(10029), 1785–1788.

Herdicho, F. F., Chukwu, W., Tasman, H., et al. (2021). An optimal control of malaria transmission model with mosquito seasonal factor. *Results in physics*, *25*, 104238.

Hethcote, H. W. (2000). The mathematics of infectious diseases. *SIAM review*, *42*(4), 599–653.

Hirsch, M. W. (1974). Differential equations, dynamical systems, and linear algebra.

Ibrahim, Bello, I. S., Ajetunmobi, A. O., Ayodapo, A., Afolabi, B. A., & Adeniyi, M. A. (2023). Prevalence of asymptomatic malaria infection by microscopy and its determinants among residents of ido-ekiti, southwestern nigeria. *PLoS One*, *18*(2), e0280981.

Ibrahim, Kamran, M. A., Naeem Mannan, M. M., Kim, S., & Jung, I. H. (2020). Impact of awareness to control malaria disease: A mathematical modeling approach. *Complexity*, *2020*(1), 8657410.

Igoe, M., Casagrandi, R., Gatto, M., Hoover, C. M., Mari, L., Ngonghala, C. N., ... others (2023). Reframing optimal control problems for infectious disease management in low-income countries. *Bulletin of mathematical biology*, *85*(4), 31.

Irish, S. R., Nimmo, D., Bharmel, J., Tripet, F., Müller, P., Manrique-Saide, P., & Moore, S. J. (2024). A review of selective indoor residual spraying for malaria control. *Malaria Journal*, *23*(1), 252.

Jaleta, S. F., Duressa, G. F., & Deressa, C. T. (2025). A novel abc fractional-order mathematical model for malaria transmission dynamics incorporating treatment-seeking behavior. *PLoS One*, *20*(6), e0319166.

Jarcho, S. (1970). A cartographic and literary study of the word malaria. *Journal of the History of Medicine and Allied Sciences*, *25*(1), 31–39.

Johnson, M. L., & Faunt, L. M. (1992). [1] parameter estimation by least-squares methods. In *Methods in enzymology* (Vol. 210, pp. 1–37). Elsevier.

Joi, P. (2024, January 23). *Vaccine profiles: malaria.* Retrieved from https://www.gavi.org/vaccineswork/vaccine-profiles-malaria (Accessed: 2024-01-23)

Jones, W. H. S. (1907). Malaria and history. *Annals of Tropical Medicine & Parasitology*, *1*(1-5), 528–546.

Jordan, D., & Smith, P. (2007). *Nonlinear ordinary differential equations: an introduction for scientists and engineers*. OUP Oxford.

Kaghou, M. M., Metoh, T. N., Fru, C. T., Berinyui, S., Bindamu, M., Chi, A., & Pieme, C. A. (2024). High prevalence and risk factors associated with asymptomatic malaria among children in nkwen village, northwest region, cameroon. *Malaria Journal*, *23*(1), 243.

Kanyi, E., Afolabi, A. S., & Onyango, N. O. (2021). Mathematical modeling and analysis of transmission dynamics and control of schistosomiasis. *Journal of Applied Mathematics*, *2021*(1), 6653796.

Kassie, G. A., Azeze, G. A., Gebrekidan, A. Y., Lombebo, A. A., Adella, G. A., Haile, K. E., ... Asgedom, Y. S. (2024). Asymptomatic malaria infection and its associated factors among pregnant women in ethiopia; a systematic review and meta-analysis. *Parasite Epidemiology and Control*, e00339.

Keno, T. D., Obsu, L. L., & Makinde, O. D. (2022). Modeling and optimal control analysis of malaria epidemic in the presence of temperature variability. *Asian-European Journal of Mathematics*, *15*(01), 2250005.

Kermack, W. O., & McKendrick, A. G. (1927). A contribution to the mathematical theory of epidemics. *Proceedings of the royal society of london. Series A, Containing papers of a mathematical and physical character*, *115*(772), 700–721.

Kifle, Z. S., & Obsu, L. L. (2022). Mathematical modeling for covid-19 transmission dynamics: a case study in ethiopia. *Results in Physics*, *34*, 105191.

Kopp, R. E. (1962). Pontryagin maximum principle. In *Mathematics in science and engineering* (Vol. 5, pp. 255–279). Elsevier.

Layek, G., et al. (2015). *An introduction to dynamical systems and chaos* (Vol. 1). Springer.

Lengeler, C. (2004). Insecticide-treated bed nets and curtains for preventing malaria. *Cochrane database of systematic reviews*(2).

Lenhart, S., & Workman, J. T. (2007). *Optimal control applied to biological models*. CRC press.

MacDonald, G. (1957). *The epidemiology and control of malaria. london: Oxford univ. pr.* Oxford.

Madueme, P.-G. U., & Chirove, F. (2023). Understanding the transmission pathways of lassa fever: A mathematical modeling approach. *Infectious disease modelling*, *8*(1), 27–57.

Mahardika, R., Widowati, & Sumanto, Y. (2019). Routh-hurwitz criterion and bifurcation method for stability analysis of tuberculosis transmission model. In *Journal of physics: Conference series* (Vol. 1217, p. 012056).

Mahase, E. (2019). *Malaria could be eradicated by 2050, say global experts.* British Medical Journal Publishing Group.

Malaria, E. (2020). *Zero malaria - the malaria dividend.* Retrieved from https://endmalaria.org/sites/default/files/Zero%20Malaria%20-%20The%20Malaria%20Dividend%20ONLINE%20FINAL.pdf (Accessed: 2023-10-17)

malERA. (2011). A research agenda for malaria eradication: modeling. *PLoS medicine*, *8*(1), e1000403.

Mandal, S., Sarkar, R. R., & Sinha, S. (2011). Mathematical models of malaria-a review. *Malaria journal*, *10*, 1–19.

Marcombe, S., Thammavong, P., Grandadam, M., & Brey, P. (2020). Auto-dissemination strategy for larval control of the insecticide-resistant dengue vector aedes aegypti in lao pdr. *International Journal of Infectious Diseases*, *101*, 490.

Mboera, L. E., Makundi, E. A., & Kitua, A. Y. (2007). Uncertainty in malaria control in tanzania: crossroads and challenges for future interventions. *Defining and Defeating the Intolerable Burden of Malaria III: Progress and Perspectives: Supplement to Volume 77 (6) of American Journal of Tropical Medicine and Hygiene*.

McCann, C. (2013). Bifurcation analysis of non-linear differential equations. *The University of Liverpool*.

McKenzie, F. E., Smith, D. L., O'Meara, W. P., & Riley, E. M. (2008). Strain theory of malaria: the first 50 years. *Advances in parasitology*, *66*, 1–46.

Mehrkanoon, S., Falck, T., & Suykens, J. A. (2012). Parameter estimation for time varying dynamical systems using least squares support vector machines. *IFAC Proceedings Volumes*, *45*(16), 1300–1305.

Mensah, E. A., Duah, H. O., Olomofe, C., & Quinn, M. (2024). Mass media exposure and sociodemographic factors associated with malaria vaccine awareness among women of childbearing age in ghana. *Discover Public Health*, *21*(1), 56.

MESA. (2023). *Age-dependent diversity of innate immune responses in malaria.* Retrieved from https://mesamalaria.org/mesa-track/age-dependent-diversity-innate-immune-responses-malaria/ (Accessed: 2023-06-14)

Milligan, P., & Fogelson, A. (2024). *Statistical report, malaria vaccine pilot evaluation (mvpe), analysis of data to month 46.* Retrieved from https://cdn.who.int/media/docs/default-source/immunization/sage/vpp-background-documents/malaria/mvip_statistical_report_4feb2024.pdf?sfvrsn=7858b456_1&download=true (Accessed: 2024-02-04)

Mojeeb, A., Rahman, E., Nor Osman, A. E., & Isack, E. K. (2018). Mathematical model for malaria transmission with optimal control strategies and their effects. *Journal of Scientific Research and Reports*, *20*(3), 1–16.

Moturi, A. K., Jalang'o, R., Cherono, A., Muchiri, S. K., Snow, R. W., & Okiro, E. A. (2023). Malaria vaccine coverage estimation using age-eligible populations and service user denominators in kenya. *Malaria Journal*, *22*(1), 287.

Mukala, J., Mogere, D., Kirira, P., Kanoi, B. N., Akisa, V., Kobia, F., ... Gitaka, J. (2024). Predictors of birth weight in pregnant women with malaria: a prospective cohort facility-based study in webuye-kenya. *BMC Pregnancy and Childbirth*, *24*(1), 187.

Mwebesa, E., Awor, S., Natuhamya, C., Dricile, R., Legason, I. D., Okimait, D., ... Tumwesigye, N. M. (2024). Impact of mass media campaigns on knowledge of malaria prevention measures among pregnant mothers in uganda: a propensity score-matched analysis. *Malaria Journal*, *23*(1), 256.

Ngonghala, C. N., Wairimu, J., Adamski, J., & Desai, H. (2020). Impact of adaptive mosquito behavior and insecticide-treated nets on malaria prevalence. *Journal of Biological Systems*, *28*(02), 515–542.

Niculescu, C., & Persson, L.-E. (2006). *Convex functions and their applications* (Vol. 23). Springer.

Oke, S. I., Matadi, M. B., & Xulu, S. S. (2018). Optimal control analysis of a mathematical model for breast cancer. *Mathematical and Computational Applications*, *23*(2), 21.

Okosun, K. O., & Makinde, O. D. (2014). Optimal control analysis of hepatitis c virus with acute and chronic stages in the presence of treatment and infected immigrants. *International journal of Biomathematics*, *7*(02), 1450019.

Okosun, K. O., Rachid, O., & Marcus, N. (2013). Optimal control strategies and cost-effectiveness analysis of a malaria model. *BioSystems*, *111*(2), 83–101.

Olaniyi, S., Falowo, O., Okosun, K., Mukamuri, M., Obabiyi, O., & Adepoju, O. (2023). Effect of saturated treatment on malaria spread with optimal intervention. *Alexandria Engineering Journal*, *65*, 443–459.

Olaniyi, S., Okosun, K., Adesanya, S., & Lebelo, R. (2020). Modelling malaria dynamics with partial immunity and protected travellers: optimal control and cost-effectiveness analysis. *Journal of Biological Dynamics*, *14*(1), 90–115.

Olaniyi, S., Okosun, K. O., Adesanya, S. O., & Areo, E. A. (2018). Global stability and optimal control analysis of malaria dynamics in the presence of human travelers. *The Open Infectious Diseases Journal*, *10*(1).

Olopade, I., Ajao, S., Akinwumi, T., Adeniran, G., Aderenle, R., & Adesanya, A. (2024). Mathematical modelling of the impacts of syphilis multi-stage treatments. *Modeling Earth Systems and Environment*, *10*(4), 5489–5502.

Olutimo, A., Mbah, N., Abass, F., & Adeyanju, A. (2024). Effect of environmental immunity on mathematical modeling of malaria transmission between vector and host population. *Journal of Applied Sciences and Environmental Management*, *28*(1), 205–212.

Omondi, E., Mbogo, R., & Luboobi, L. (2018). Mathematical modelling of the impact of testing, treatment and control of hiv transmission in kenya. *Cogent Mathematics & Statistics*, *5*(1), 1475590.

Oshagbemi, O. A., Lopez-Romero, P., Winnips, C., Csermak, K. R., Su, G., & Aubrun, E. (2023). Estimated distribution of malaria cases among children in sub-saharan africa by specified age categories using data from the global burden of diseases 2019. *Malaria journal*, *22*(1), 371.

Otieno, G., Koske, J. K., & Mutiso, J. M. (2016). Cost effectiveness analysis of optimal malaria control strategies in kenya. *Mathematics*, *4*(1), 14.

Pampana, E. (1963). A textbook of malaria eradication.

PATH. (2023). *Existing malaria vaccines.* Retrieved from https://www.malariavaccine.org/existing-vaccines (Accessed: 2025-06-06)

PATH. (2024, March). *Product information fact sheet: Rts,s and r21 malaria vaccines.* Retrieved from https://media.path.org/documents/Product_info_fact_sheet_RTSS-R21_March_2024.pdf (Accessed: 2025-06-06)

Pierre-Louis, A.-M., Qamruddin, J., Espinosa, I., & Challa, S. (2010). The malaria control success story. *Yes Africa Can: Success Stories from a Dynamic Continent*, 417–432.

Poirot, E., Skarbinski, J., Sinclair, D., Kachur, S. P., Slutsker, L., & Hwang, J. (2013). Mass drug administration for malaria. *Cochrane Database of Systematic Reviews*(12).

Pontryagin, L. S. (1987). *Mathematical theory of optimal processes*. CRC press.

Ranjha, R., Singh, K., Baharia, R. K., Mohan, M., Anvikar, A. R., & Bharti, P. K. (2023). Age-specific malaria vulnerability and transmission reservoir among children. *Global Pediatrics*, *6*, 100085.

Romero-Leiton, J. P., Montoya-Aguilar, J. M., & Ibargüen-Mondragón, E. (2018). An optimal control problem applied to malaria disease in colombia. *Applied mathematical sciences*, *12*(6), 279–292.

Ross, R. (1910). *The prevention of malaria*. J. Murray.

Roy, P. K., Roy, A. K., Khailov, E. N., Al Basir, F., & Grigorieva, E. V. (2020). A model of the optimal immunotherapy of psoriasis by introducing il-10 and il-22 inhibitors. *Journal of Biological Systems*, *28*(03), 609–639.

Sabbatani, S., Fiorino, S., & Manfredi, R. (2010). The emerging of the fifth malaria parasite (plasmodium knowlesi): a public health concern? *Brazilian Journal of Infectious Diseases*, *14*, 299–309.

Sabet, A., & Goddard, J. (2022). Promise or peril: using genetically modified mosquitoes in the fight against vector-borne disease. *The American Journal of Medicine*, *135*(3), 281–283.

Sahay, S. (2024). Empowering individuals and communities: The importance of health education and promotion in public health. *International Journal of Public Health & Safety*, *8*. Retrieved from https://www.hilarispublisher.com/open-access/empowering-individuals-and-communities-the-importance-of-health-education-and-promotion-in-public-health-98534.html#1 (Accessed: 2024-04-02)

Salle, J. P. (1966). *An invariance principle in the theory of stability* (Tech. Rep.).

Salpeter, E. E., & Salpeter, S. R. (1998). Mathematical model for the epidemiology of tuberculosis, with estimates of the reproductive number and infection-delay function. *American journal of epidemiology*, *147*(4), 398–406.

Samba, E. (2001). The malaria burden and africa. *Am J Trop Med Hyg*, *64*(1), ii.

Samsuzzoha, M., Singh, M., & Lucy, D. (2013). Uncertainty and sensitivity analysis of the basic reproduction number of a vaccinated epidemic model of influenza. *Applied Mathematical Modelling*, *37*(3), 903–915.

Sarma, N., Patouillard, E., Cibulskis, R. E., & Arcand, J.-L. (2019). The economic burden of malaria: revisiting the evidence. *The American journal of tropical medicine and hygiene*, *101*(6), 1405.

Sauboin, C. J., Van Bellinghen, L.-A., Van De Velde, N., & Van Vlaenderen, I. (2015). Potential public health impact of rts, s malaria candidate vaccine in sub-saharan africa: a modelling study. *Malaria Journal*, *14*, 1–17.

Savi, M. K. (2022). An overview of malaria transmission mechanisms, control, and modeling. *Medical Sciences*, *11*(1), 3.

Sharomi, O., & Malik, T. (2017). Optimal control in epidemiology. *Annals of Operations Research*, *251*(1), 55–71.

Shi, Y., Chen, F., Wang, L., & Zhang, X. (2024). Dynamics analysis of a reaction-diffusion malaria model accounting for asymptomatic carriers. *Zeitschrift für angewandte Mathematik und Physik*, *75*(2), 43.

Singh, A., Rajvanshi, H., Singh, M. P., Bhandari, S., Nisar, S., Poriya, R., ... others (2022). Mass screening and treatment (msat) for identifying and treating asymptomatic cases of malaria-malaria elimination demonstration project (medp), mandla, madhya pradesh. *Malaria journal*, *21*(1), 395.

Siriprapaiwan, S., Moore, E. J., & Koonprasert, S. (2018). Generalized reproduction numbers, sensitivity analysis and critical immunity levels of an seqijr disease model with immunization and varying total population size. *Mathematics and computers in simulation*, *146*, 70–89.

Smith Gueye, C., Newby, G., Gosling, R. D., Whittaker, M. A., Chandramohan, D., Slutsker, L., & Tanner, M. (2016). Strategies and approaches to vector control in nine malaria-eliminating countries: a cross-case study analysis. *Malaria journal*, *15*(1), 2.

Srivastav, A. K., & Ghosh, M. (2021). Modeling the transmission dynamics of malaria with saturated treatment: a case study of india. *Journal of Applied Mathematics and Computing*, *67*(1), 519–540.

Tchoumi, Diagne, Mamadou, Rwezaura, Juga, & Tchuenche. (2022). Optimal control of a two-group malaria transmission model with vaccination. *Network Modeling Analysis in Health Informatics and Bioinformatics*, *12*(1), 7.

Tchoumi, Diagne, M., Rwezaura, H., & Tchuenche, J. (2021). Malaria and covid-19 co-dynamics: A mathematical model and optimal control. *Applied mathematical modelling*, *99*, 294–327.

Tchoumi, Dongmo, E., Kamgang, J., & Tchuenche, J. (2022). Dynamics of a two-group structured malaria transmission model. *Informatics in Medicine Unlocked*, *29*, 100897.

Tefera, D. R., Sinkie, S. O., & Daka, D. W. (2020). Economic burden of malaria and associated factors among rural households in chewaka district, western ethiopia. *ClinicoEconomics and Outcomes Research*, 141–152.

Tilahun, G. T., & Alemneh, H. T. (2021). Mathematical modeling and optimal control analysis of covid-19 in ethiopia. *Journal of interdisciplinary mathematics*, *24*(8), 2101–2120.

UNICEF. (2024). Unicef data: Monitoring the situation of children and women. *UNICEF*. Retrieved from https://data.unicef.org/topic/child-health/malaria/ (Data generated on 31 October 2024)

Uwineza, M. A., Nzabanita, J., Ngaruye, I., & Sylla, M. B. (2024). A deterministic analysis of an age-sex-structured model for malaria transmission dynamics. *IJID regions*, *13*, 100478.

Van, M. A., Saint-luc, C., & Xu, X. (2017). Modelling plant disease epidemics modelling plant disease epidemics. 10.

Van den Driessche, P., & Watmough, J. (2002). Reproduction numbers and sub-threshold endemic equilibria for compartmental models of disease transmission. *Mathematical biosciences*, *180*(1-2), 29–48.

Wako, B. H., Dawed, M. Y., & Obsu, L. L. (2025). Optimal control analysis of malaria and its associated complications. *Scientific African*, e02932.

Waltman, P. (2013). *Deterministic threshold models in the theory of epidemics* (Vol. 1). Springer Science & Business Media.

Wang. (2004). A simple proof of descartes's rule of signs. *The American Mathematical Monthly*, *111*(6), 525–526.

Wang, & Cai, Y. (2025). Optimal control of an influenza model incorporating pharmacological and non-pharmacological interventions. *Advances in Continuous and Discrete Models*, *2025*(1), 17.

Wang, Chen, Y., & Liu, S. (2018). Dynamics of an age-structured host-vector model for malaria transmission. *Mathematical Methods in the Applied Sciences*, *41*(5), 1966–1987.

White, M. T., Verity, R., Churcher, T. S., & Ghani, A. C. (2015). Vaccine approaches to malaria control and elimination: Insights from mathematical models. *Vaccine*, *33*(52), 7544–7550.

WHO. (2013). Larval source management: a supplementary malaria vector control measure: an operational manual. In *Larval source management: a supplementary malaria vector control measure: an operational manual.*

WHO. (2015). *Global technical strategy for malaria 2016-2030*. World Health Organization.

WHO. (2020a). Life expectancy and healthy life expectancy, data by country. *World Health Organization*.

WHO. (2020b). *Malaria eradication: benefits, future scenarios and feasibility. a report of the strategic advisory group on malaria eradication*. Author.

WHO. (2022a). Malaria vaccines: preferred product characteristics and clinical development considerations.

WHO. (2022b). Malaria vaccine: Who position paper–march 2022. *Weekly Epidemiological Record*, *97*(9), 61–80.

WHO. (2023a). *Who malaria policy advisory group (mpag) meeting report, 18–20 april 2023*. World Health Organization.

WHO. (2023b). *World malaria report 2023*. World Health Organization.

WHO. (2023c, January). *World malaria report 2023*. Geneva: World Health Organization. Retrieved from https://www.who.int/teams/global-malaria-programme/reports/world-malaria-report-2023

WHO. (2024a). Disease outbreak news: Malaria - ethiopia. *WHO*. Retrieved from https://www.who.int/emergencies/disease-outbreak-news/item/2024-DON542 (Data generated on 31 October 2024)

WHO. (2024b, October). *Malaria - ethiopia*. Retrieved from https://www.who.int/emergencies/disease-outbreak-news/item/2024-DON542 (Accessed: 2025-08-26)

WHO. (2024a, October). *Malaria in ethiopia*. Retrieved from https://www.who.int/emergencies/disease-outbreak-news/item/2024-DON542 (Accessed: 2025-06-14)

WHO. (2024b). *World malaria report 2024: Regional data and trends briefing kit*. Retrieved from https://cdn.who.int/media/docs/default-source/malaria/world-malaria-reports/world-malaria-report-2024-regional-briefing-kit-eng.pdf?sfvrsn=bceac4ae_9&download=true (Accessed: 2024-12-11)

WHO, et al. (n.d.). *Disease outbreak news; malaria in ethiopia; 31 october 2024*.

WorldBank. (2024). *World health organization, world malaria report and global health observatory data repository/world health statistics*. Retrieved from https://data.worldbank.org/indicator/SH.MLR.INCD.P3 (Accessed: 2024-10-03)

Xue, L., Sun, L., & Guo, S. (2023). Dynamic effects of asymptomatic infections on malaria transmission. *Mathematics and Computers in Simulation*, *214*, 172–182.

Yaya, S., Uthman, O. A., Amouzou, A., & Bishwajit, G. (2018). Mass media exposure and its impact on malaria prevention behaviour among adult women in sub-saharan africa: results from malaria indicator surveys. *Global health research and policy*, *3*(1), 20.

Yirsaw, A. N., Gebremariam, R. B., Getnet, W. A., & Mihret, M. S. (2021). Insecticide-treated net utilization and associated factors among pregnant women and under-five children in east belessa district, northwest ethiopia: using the health belief model. *Malaria Journal*, *20*(1), 130.

Yue, Z., Zhang, Y., & Ji, X. (2025). Modelling, analysis and optimal control of zika virus transmission dynamics based on sterile insect technique. *Infectious Disease Modelling*.

Yusuf, T. T., & Abidemi, A. (2023). Effective strategies towards eradicating the tuberculosis epidemic: An optimal control theory alternative. *Healthcare analytics*, *3*, 100131.

Zahid, M. H., Van Wyk, H., Morrison, A. C., Coloma, J., Lee, G. O., Cevallos, V., ... Eisenberg, J. N. (2023). The biting rate of aedes aegypti and its variability: A systematic review (1970–2022). *PLoS neglected tropical diseases*, *17*(8), e0010831.

Zembere, K. (2024). The potential for attractive toxic sugar baits to complement core malaria interventions strategies: the need for more evidence. *Malaria Journal*, *23*(1), 356.

Zhao, & Mohammed-Awel. (2014). A mathematical model studying mosquito-stage transmission-blocking vaccines. *Mathematical Biosciences & Engineering*, *11*(5), 1229–1245.

Zhao, J. (2022). Optimal control and cost-effectiveness analysis of an echinococcosis transmission model with interventions. *Authorea Preprints*.

Zhao, S., Xu, Z., & Lu, Y. (2000). A mathematical model of hepatitis b virus transmission and its application for vaccination strategy in china. *International journal of epidemiology*, *29*(4), 744–752.